frontiers | Research Topics

Viruses in agricultural systems: Interactions with plants, insect pollinators and fungi

Edited by
Ken Komatsu, Sean Michael Prager and Beilei Wu

Published in
Frontiers in Microbiology

FRONTIERS EBOOK COPYRIGHT STATEMENT

The copyright in the text of individual articles in this ebook is the property of their respective authors or their respective institutions or funders. The copyright in graphics and images within each article may be subject to copyright of other parties. In both cases this is subject to a license granted to Frontiers.

The compilation of articles constituting this ebook is the property of Frontiers.

Each article within this ebook, and the ebook itself, are published under the most recent version of the Creative Commons CC-BY licence. The version current at the date of publication of this ebook is CC-BY 4.0. If the CC-BY licence is updated, the licence granted by Frontiers is automatically updated to the new version.

When exercising any right under the CC-BY licence, Frontiers must be attributed as the original publisher of the article or ebook, as applicable.

Authors have the responsibility of ensuring that any graphics or other materials which are the property of others may be included in the CC-BY licence, but this should be checked before relying on the CC-BY licence to reproduce those materials. Any copyright notices relating to those materials must be complied with.

Copyright and source acknowledgement notices may not be removed and must be displayed in any copy, derivative work or partial copy which includes the elements in question.

All copyright, and all rights therein, are protected by national and international copyright laws. The above represents a summary only. For further information please read Frontiers' Conditions for Website Use and Copyright Statement, and the applicable CC-BY licence.

ISSN 1664-8714
ISBN 978-2-83252-110-6
DOI 10.3389/978-2-83252-110-6

About Frontiers

Frontiers is more than just an open access publisher of scholarly articles: it is a pioneering approach to the world of academia, radically improving the way scholarly research is managed. The grand vision of Frontiers is a world where all people have an equal opportunity to seek, share and generate knowledge. Frontiers provides immediate and permanent online open access to all its publications, but this alone is not enough to realize our grand goals.

Frontiers journal series

The Frontiers journal series is a multi-tier and interdisciplinary set of open-access, online journals, promising a paradigm shift from the current review, selection and dissemination processes in academic publishing. All Frontiers journals are driven by researchers for researchers; therefore, they constitute a service to the scholarly community. At the same time, the *Frontiers journal series* operates on a revolutionary invention, the tiered publishing system, initially addressing specific communities of scholars, and gradually climbing up to broader public understanding, thus serving the interests of the lay society, too.

Dedication to quality

Each Frontiers article is a landmark of the highest quality, thanks to genuinely collaborative interactions between authors and review editors, who include some of the world's best academicians. Research must be certified by peers before entering a stream of knowledge that may eventually reach the public - and shape society; therefore, Frontiers only applies the most rigorous and unbiased reviews. Frontiers revolutionizes research publishing by freely delivering the most outstanding research, evaluated with no bias from both the academic and social point of view. By applying the most advanced information technologies, Frontiers is catapulting scholarly publishing into a new generation.

What are Frontiers Research Topics?

Frontiers Research Topics are very popular trademarks of the *Frontiers journals series*: they are collections of at least ten articles, all centered on a particular subject. With their unique mix of varied contributions from Original Research to Review Articles, Frontiers Research Topics unify the most influential researchers, the latest key findings and historical advances in a hot research area.

Find out more on how to host your own Frontiers Research Topic or contribute to one as an author by contacting the Frontiers editorial office: frontiersin.org/about/contact

Viruses in agricultural systems: Interactions with plants, insect pollinators and fungi

Topic editors

Ken Komatsu — Tokyo University of Agriculture and Technology, Japan
Sean Michael Prager — University of Saskatchewan, Canada
Beilei Wu — Institute of Plant Protection, Chinese Academy of Agricultural Sciences, China

Topic Coordinators

Islam Hamim — Bangladesh Agricultural University, Bangladesh

Citation

Komatsu, K., Prager, S. M., Wu, B., eds. (2023). *Viruses in agricultural systems: Interactions with plants, insect pollinators and fungi*. Lausanne: Frontiers Media SA. doi: 10.3389/978-2-83252-110-6

Table of contents

frontiers | Frontiers in Microbiology

TYPE Editorial
PUBLISHED 23 March 2023
DOI 10.3389/fmicb.2023.1170402

Check for updates

OPEN ACCESS

EDITED AND REVIEWED BY
Jesús Navas-Castillo,
IHSM La Mayora (CSIC), Spain

*CORRESPONDENCE
Islam Hamim
✉ hamimppath@bau.edu.bd

SPECIALTY SECTION
This article was submitted to Microbe and Virus Interactions with Plants, a section of the journal Frontiers in Microbiology

RECEIVED 20 February 2023
ACCEPTED 10 March 2023
PUBLISHED 23 March 2023

CITATION
Hamim I, Komatsu K, Prager SM and Wu B (2023) Editorial: Viruses in agricultural systems: Interactions with plants, insect pollinators and fungi. *Front. Microbiol.* 14:1170402. doi: 10.3389/fmicb.2023.1170402

COPYRIGHT
© 2023 Hamim, Komatsu, Prager and Wu. This is an open-access article distributed under the terms of the Creative Commons Attribution License (CC BY). The use, distribution or reproduction in other forums is permitted, provided the original author(s) and the copyright owner(s) are credited and that the original publication in this journal is cited, in accordance with accepted academic practice. No use, distribution or reproduction is permitted which does not comply with these terms.

Editorial: Viruses in agricultural systems: Interactions with plants, insect pollinators and fungi

Islam Hamim[1]*, Ken Komatsu[2], Sean Michael Prager[3] and Beilei Wu[4]

[1]Department of Plant Pathology, Faculty of Agriculture, Bangladesh Agricultural University, Mymensingh, Bangladesh, [2]Graduate School of Agriculture, Tokyo University of Agriculture and Technology, Fuchu, Tokyo, Japan, [3]Department of Plant Sciences, College of Agriculture and Bioresources, University of Saskatchewan, Saskatoon, SK, Canada, [4]Institute of Plant Protection, Chinese Academy of Agricultural Sciences, Beijing, China

KEYWORDS

food security, environment, agriculture, viruses, genomics, pathogenesis

Editorial on the Research Topic
Viruses in agricultural systems: Interactions with plants, insect pollinators and fungi

Plant pathogenic viruses in agricultural systems significantly reduce crop yields and pose a serious threat to global food security systems. However, the advent of "viromics" in biology has uncovered a plethora of viruses whose effects on ecosystems and food security have not been significantly studied. Studies on viruses are attracting increasing attention in agriculture because of their ability to directly infect crops and the wide-ranging ecological consequences they can have on agricultural ecosystems. Viruses can help plants survive biotic and abiotic stresses under certain conditions. In addition, viruses can interact with bacteria, weeds, pathogenic and symbiotic fungi, insect pollinators, and other species in ways that benefit or harm final crop production.

The Research Topic "*Viruses in agricultural systems: Interactions with plants, insect pollinators, and fungi*" was developed under the sections "Virology" and "Microbe and Virus Interactions with Plants," which belong to the journal "Frontiers in Microbiology." The distribution, diversity, transmission, pathogenesis, and control of viruses infecting plants, fungi, and insects in agricultural ecosystems were considered for this topic. However, the final article collection was expanded to include viruses infecting other host species in agroecosystems not listed in the title, considering host-shifting of viruses and phylogenetically related cross-kingdom viruses. This topic has accepted eight original research articles and one review article covering a range of topics related to viruses in agricultural systems. Of these, five of the original research articles focused on the molecular processes of viral infections in different hosts in agricultural systems.

In the work by Gong et al., it was shown that protein lysine acetylation (Kac), an essential post-translational modification in eukaryotes or prokaryotes, has a major impact on the tomato spotted wilt virus (TSWV) infection of *Nicotiana benthamiana*. Gong et al. discovered around three thousand sites linked to acetylated lysine in approximately two thousand proteins by analyzing the acetylation status of proteins in virus-free and TSWV-infected *N. benthamiana* leaves. They also found that after the viral infection, 408 sites on 294 proteins were positively regulated and 284 sites on 219 proteins were negatively

regulated. Altogether, 35 conserved motifs were recovered, and K*R was the most prevalent combination, accounting for 1,334 (31.63%) of the enriched motifs. According to their bioinformatics study, most proteins with lysine acetylation sites were found in the cytoplasm and chloroplast and were engaged in biological activities such as cellular and metabolic ones.

Chlorophyll a/b-binding protein of the light-harvesting complex II type 1 like (LHC II-1L), which largely controls the integrity of the electron transport system, is an essential component of photosynthesis. Xu et al. investigated the influence of the *Fragaria vesca* LHC II-1L protein (FvLHC II-1L) in strawberry vein banding virus (SVBV) infection. They found that the movement protein SVBV P1 interacted with FvLHC II-1L *in vitro* and *in vivo*. SVBV-infected epidermal cells of *N. benthamiana* leaves displayed co-localization of SVBV P1 and FvLHC II-1L; however, *F. vesca* had elevated FvLHC II-1L protein synthesis. Additionally, Xu et al. discovered that FvLHC II-1L efficiently boosted SVBV P1 to compensate for the intercellular movement of movement-deficient potato virus X (PVXΔP25) and the systemic movement of movement-deficient cucumber mosaic virus (CMVΔMP). Further, it was shown that the overexpression of FvLHC II-1L can enhance SVBV infection of *F. vesca via* interacting with the SVBV P1 protein.

The work by Sun et al. challenged the notion that virions of a virus that infects the host have the same viral genome and properties by examining the genetic variability of the virions of the white spot syndrome virus (WSSV), a DNA virus that affects crustaceans. They found that the WSSV population was made up of a 1:3 ratio of Type A (containing the WSSV lncRNA-24) and Type B (carrying the wsv195 gene), where there are two nucleotide changes between these two types. All virus-infected cells and tissues from different hosts showed a consistent 1:3 structure in viral populations. The study showed that type A WSSV virus infection was boosted by WSSV lncRNA-24 by interacting with WSSV miRNAs in shrimp, but type B WSSV required the wsv195 gene for viral infection. When Type A or Type B WSSV was eliminated from the WSSV population, the copy number of the virus decreased by 100 times in shrimp, and infection was prevented by the simultaneous elimination of both WSSV types. The complementary effects on the WSSV population and the accomplishment of the viral infection by two distinct WSSV types expressing various operational genes show the significance of complementarity between virus population components in viral infection.

Host adaptation causes significant genetic changes in symbiotic microorganisms in insects; however, it is still unknown how virus mutations in symbiotic hosts affect host adaptability to new environments and increase viral fitness in hosts. Acyrthosiphonpisum virus (APV), a symbiotic virus, has undergone genetic divergence in one location, and Lu et al. looked into the impact of this genetic differentiation on the ability of the aphid to respond to unfavorable plants. Single nucleotide polymorphism (SNP) sites in the APV genomes of the pea aphid colonies in *Vicia faba* and *Vicia villosa*, respectively, were discovered using a transcriptome investigation. When host aphids were switched from high-fitness plants *V. faba* to low-fitness plants *V. villosa* or *Medicago sativa*, the SNP at site 5,990, G5990A, located in the RNA-dependent RNA polymerase (RdRp) domain, showed a change from G to A. In RdRp, this SNP resulted in the asparagine (N) to serine (S) substitution at site 196. S196N was located at a random coil distance from the conserved active motifs, and the N196 type of RdRp's polymerase performed 44.5% better than the S196 type. The increased APV replication rate was caused by the enhanced enzymatic activity of RdRp positively impacted insects by lowering plant defenses against aphids, and it sheds light on a scenario in which a host can benefit from modifications of a symbiotic virus when the host adapts to the changed environmental conditions.

Bemisia tabaci (Hemiptera: Aleyrodidae) is a highly efficient vector for the spread of the chili leaf curl virus (ChiLCV, Begomovirus), which poses a considerable obstacle to the cultivation of chili in South Asia. Nekkanti et al. investigated the molecular processes driving interconnections between *B. tabaci* and ChiLCV transmission and found potential alternative candidates for the control of the *B. tabaci*-begomovirus complex. Transcriptome analysis of *B. tabaci* revealed 80 genes with distinct expression patterns after 6 h of ChiLCV intake, with 29 being positively regulated and 51 being negatively regulated. The Kyoto Encyclopedia of Genes and Genomes (KEGG) research of the differentially expressed genes (DEGs) revealed their role in metabolic activities, signaling channels, cellular processes, and organismal systems. Reverse transcription quantitative real-time PCR (RT-qPCR) was used to confirm the expression of positively regulated genes following the acquisition of ChiLCV. DEGs that were abundant in *B. tabaci* and promoted viral infection and circulation included replication factor A protein 1, fasciclin 2, inhibin beta chain, cytosolic carboxypeptidase 3, dual-specificity protein phosphatase 10, 15, dynein axonemal heavy chain 17, and Tob1.

Alternaria alternata apple pathotype is responsible for Alternaria leaf blotch, a serious fungal disease that reduces apple output worldwide. Interest in mycoviruses as a potential biocontrol agent has grown significantly due to their ability to impart hypovirulence on their hosts. Li et al. found that *A. alternata* f. sp. *mali* strain QY21 was coinfected with *A. alternata* chrysovirus 1 strain QY2 (AaCV1-QY2) and *A. alternata* magoulivirus 1 (AaMV1), which belong to the genera *Betachrysovirus* and *Magoulvirus*, respectively. Hypovirulence of *A. alternata* was associated with these two mycoviruses, with AaCV1-QY2 likely contributing significantly. AaCV1-QY2 can alone postpone development and lessen host virulence, as shown by the fact that the lack of AaMV1 in strain QY21 had no influence on the hypovirulence phenotype. Viruses also prevented strains of *A. alternata* from overproducing the mycotoxin alternariol. AaCV1-QY2/AaMV1 mycoviruses may infect diverse strains of *A. alternata*, which can increase the effectiveness of interspecific dissemination of AaCV1-QY2.

Two original research articles about the diagnosis and characterization of plant viruses are included in this Research Topic. In the first paper, Kumar et al. identified co-infections of tobamoviruses, frangipani mosaic virus (FrMV), and plumeria mosaic virus (PluMV), from the temple tree, or *Plumeria rubra* f. acutifolia. The existence of PluMV was also observed in association with the distinctive symptoms of *Gomphrena globosa*

(globe amaranth), a non-host of FrMV. To propagate PluMV, simple rub-inoculation was quite successful, and tobacco, globe amaranth, brinjal, datura, and chili were able to discriminate PluMV from FrMV in a host range assessment. The full genome sequence of PluMV was analyzed, revealing the genomic structure characteristics of tobamoviruses encoding four proteins: small replicase, large replicase, movement protein, and coat protein. The genome of PluMV was longer than that of FrMV; it shared significant sequence similarities with FrMV and other tobamoviruses, and it had a close but diverging evolutionary relationship with FrMV. RT-PCR assays confirmed the natural occurrence of PluMV in temple tree species in India, either alone or in combination with FrMV. In the second research article related to the diagnosis of viruses, Hamim et al. reported that virus-infected leaf samples stored in RNAlater® were acceptable for RT-PCR, PCR, Sanger sequencing, high-throughput sequencing (HTS), and enzyme-linked immunosorbent assay (ELISA)-based diagnostic tests. Agricultural productivity is significantly impacted by viral plant diseases, and accurate detection and characterization of viral infections are crucial for crop disease management. In order to carry out diagnostic tests using sensitive molecular techniques, intact nucleic acids present in plant tissue samples obtained from remote areas are required. RNAlater® offers effective, trustworthy sample preservation by preserving both RNA and DNA in plant tissue samples. Hamim et al. used leaf tissue samples from agricultural fields in Bangladesh that had viral symptoms to assess the viability of this method. Their research suggests that RNAlater® technology could be employed to characterize viruses in samples that have been kept for a long period and obtained from distant areas. This strategy will allow underdeveloped countries with limited laboratory facilities to greatly improve their capacity to identify and control viral infections in agricultural plants using cutting-edge analytical methods.

A comprehensive review article on this Research Topic contributes to our understanding of the biological roles of phosphorylation in the interactions between plants and viruses. One of the most well researched post-translational modifications, phosphorylation regulates multiple cell signaling pathways and is crucial for modulating the viral infection cycle in plants. The molecular mechanisms underlying the phosphorylation of plant virus proteins have been the subject of a considerable number of studies. Zhuang et al. analyzed these findings and classified the impacts on biological processes in accordance with the viral life cycle.

In conclusion, this Research Topic provides state-of-the-art research methods on virus interactions with different hosts in agricultural systems. We would like to take this opportunity to express our gratitude to each of the authors and reviewers, whose outstanding work enabled the publication of this Research Topic. We believe that this collection will increase knowledge, and awareness of the significance of viral diseases, enable better surveillance and potential control of emerging viral diseases in agricultural systems, and prevent epidemics in agricultural crops.

Author contributions

IH wrote the manuscript. All authors contributed to the article and approved the submitted version.

Acknowledgments

We would like to express our gratitude to each of the authors and reviewers, whose outstanding work enabled the publication of this Research Topic.

Conflict of interest

The authors declare that the research was conducted in the absence of any commercial or financial relationships that could be construed as a potential conflict of interest.

Publisher's note

All claims expressed in this article are solely those of the authors and do not necessarily represent those of their affiliated organizations, or those of the publisher, the editors and the reviewers. Any product that may be evaluated in this article, or claim that may be made by its manufacturer, is not guaranteed or endorsed by the publisher.

frontiers in Microbiology

ORIGINAL RESEARCH
published: 30 March 2022
doi: 10.3389/fmicb.2022.883436

Mutation in the RNA-Dependent RNA Polymerase of a Symbiotic Virus Is Associated With the Adaptability of the Viral Host

*Hong Lu[1], Jing Li[1], Pengcheng Yang[1], Fei Jiang[1], Hongran Liu[1,2] and Feng Cui[1,2]**

[1]State Key Laboratory of Integrated Management of Pest Insects and Rodents, Institute of Zoology, Chinese Academy of Sciences, Beijing, China, [2]CAS Center for Excellence in Biotic Interactions, University of Chinese Academy of Sciences, Beijing, China

Host adaptation has the potential to cause rapid genetic variation in symbiotic microorganisms in insects. How mutations in symbiotic viruses favor viral fitness in hosts and even influence host adaptability to new environments remains elusive. Here, we explored the role of genetic divergence at one site of a symbiotic virus, *Acyrthosiphon pisum* virus (APV), in the host aphid's adaptation to unfavorable plants. Based on the transcriptomes of the pea aphid *Vicia faba* colony and *Vicia villosa* colony, 46 single nucleotide polymorphism (SNP) sites were found in the APV genomes from the two aphid colonies. One SNP at site 5,990, G5990A, located at the RNA-dependent RNA polymerase (RdRp) domain, demonstrated a predominance from G to A when the host aphids were shifted from *V. faba* to the low-fitness plants *V. villosa* or *Medicago sativa*. This SNP resulted in a substitution from serine (S) to asparagine (N) at site 196 in RdRp. Although S196N was predicted to be located at a random coil far away from conserved functional motifs, the polymerase activity of the N196 type of RdRp was increased by 44.5% compared to that of the S196 type. The promoted enzymatic activity of RdRp was associated with a higher replication level of APV, which was beneficial for aphids as APV suppressed plant's resistance reactions toward aphids. The findings showed a novel case in which mutations selected in a symbiotic virus may confer a favor on the host as the host adapts to new environmental conditions.

Keywords: symbiotic virus, *Acyrthosiphon pisum* virus, RdRp, single nucleotide polymorphism, polymerase activity, pea aphid

OPEN ACCESS

Edited by:
Beilei Wu,
Institute of Plant Protection (CAAS), China

Reviewed by:
Jun-Min Li,
Ningbo University, China
Zhan Qi Wang,
Huzhou University, China

****Correspondence:***
Feng Cui
cuif@ioz.ac.cn

Specialty section:
This article was submitted to Virology, a section of the journal Frontiers in Microbiology

Received: *25 February 2022*
Accepted: *14 March 2022*
Published: *30 March 2022*

Citation:
Lu H, Li J, Yang P, Jiang F, Liu H and Cui F (2022) Mutation in the RNA-Dependent RNA Polymerase of a Symbiotic Virus Is Associated With the Adaptability of the Viral Host. Front. Microbiol. 13:883436. doi: 10.3389/fmicb.2022.883436

INTRODUCTION

RNA viruses are characterized by a high mutation rate due to the error-prone replication feature of the RNA-dependent RNA polymerase (RdRp; Elena and Sanjuan, 2005; Peck and Lauring, 2018). The mutation rate ranges from 10^{-6} to 10^{-4} substitutions per nucleotide per replication, and single-stranded RNA viruses mutate even faster (Duffy et al., 2008; Sanjuán et al., 2010). A high mutation rate and large viral population improves virus fitness for adapting to host conditions. The effects of mutations on viral pathogenicity in hosts

have been frequently reported in some notorious viruses, such as the H7N9 avian influenza virus and SARS-CoV-2 (Huang and Wang, 2020; Awadasseid et al., 2021). Symbiotic viruses usually do not induce obvious diseases in hosts. How mutations in symbiotic viruses may favor viral fitness in hosts and even host adaptability to new environments remains elusive.

Acyrthosiphon pisum virus (APV) is a symbiotic virus of the pea aphid *A. pisum*, belonging to unclassified picorna-like single-stranded RNA viruses (van den Heuvel et al., 1997). The approximately 10 kb genome contains two open reading frames (ORFs). The ORF1 product contains domains of helicase, chymotrypsin-like protease, and RdRp. APV capsids (CPs) are composed of a 34 kD of major protein encoded by ORF1 and two minor proteins of 66 kD, encoded by ORF1 and ORF2 in a translational frameshift, and 23/24 kD most likely arising from the proteolytic breakdown of the 34 kD protein (Van den Heuvel et al., 1997). Our previous study demonstrated that APV facilitated pea aphids in adapting to unsuitable plants such as *Medicago truncatula* and *Vicia villosa* once the aphids were shifted from *Vicia faba* to these undesirable plants (Lu et al., 2016, 2020). One of the key mechanisms is that APV suppresses the titer of the phytohormone jasmonic acid after it is horizontally transferred to plants with aphid feeding (Lu et al., 2020). Furthermore, we found that the amount of APV in the pea aphid *M. truncatula* colony or the *V. villosa* colony was significantly higher than that in the *V. faba* colony (Lu et al., 2020). However, the mechanism for the variation in viral load in aphids during the adaptation process of aphids to their plants is not clear.

In this study, we retrieved the genome sequences of APV from previously sequenced salivary gland transcriptomes of the pea aphid *V. faba* colony and the *V. villosa* colony (Lu et al., 2016) and analyzed the single nucleotide polymorphism (SNP) sites in APV genomes. One SNP leading to a nonsynonymous mutation in RdRp demonstrated a significantly large ratio divergence between the two colonies. Enzymatic activity measurement of the two genotypes of RdRp showed that this mutation had a considerable effect on RNA polymerase activity and may account for the promoted viral replication level in aphids on unsuitable plants.

MATERIALS AND METHODS

Aphids and Plants

The pea aphid *V. faba* colony, *V. villosa* colony, and APV-free *V. faba* colony were established as previously described (Wang et al., 2015; Lu et al., 2016, 2020) and raised in growth chambers at 21 ± 1°C, 60 ± 5% relative humidity, and a photoperiod of 16 h light:8 h dark. The field *M. sativa* colony was collected in Beijing in 2013.

SNP Analysis of the APV Genome

Transcriptomic reads of the *V. faba* colony, *V. villosa* colony and *M. truncatula* colony (Lu et al., 2016) were aligned to the APV reference sequence (AF024514.1) by tophat2 (Kim et al., 2013). SNP sites were identified by "samtools mpileup" (v0.1.19; Li et al., 2009). Allele frequency was extracted from the vcf file, and the sequence logo was generated using WebLogo 3.[1]

RNA Isolation and cDNA Synthesis

Total RNA was isolated from single aphids or five aphids using TRIzol Reagent (Invitrogen, Carlsbad, CA, United States) according to the manufacturers' protocols. After treatment with the TURBO DNA-free kit (Ambion, Austin, TX, United States) to remove genomic DNA contamination, RNA was reverse-transcribed to cDNA using the SuperScript™ III first-strand synthesis system (Invitrogen) and Oligo-dT primers (Promega, Madison, Wisconsin, United States) in accordance with the manufacturers' instructions.

Reverse Transcription-PCR and Sanger Sequencing

RNA of 20 individual aphids from the *V. faba* colony, *V. villosa* colony, and the *V. villosa* colony that was raised on *V. faba* for 1–5 months and 27 individual aphids from the *M. sativa* colony were extracted for cDNA synthesis. A 460 bp fragment encompassing site 5,990 was amplified using the primer pair G5990A-F/G5990A-R (**Supplementary Table S1**) on a Mastercycler thermal cycler (Eppendorf, Hamburg, Germany). The PCR protocol was as follows: 95°C for 5 min; 35 cycles of 95°C for 30 s, 55°C for 30 s, and 72°C for 30 s; and 72°C for 5 min. The PCR products were sequenced by Sanger sequencing technology in Invitrogen (Beijing, China).

RdRp Protein Sequence Alignment and *in silico* Structural Prediction

The amino acid sequences of APV RdRp were aligned with that of Kelp Fly virus RdRp using ClustalW at BioEdit.[2] The three-dimensional structures of APV RdRp were predicted using Robetta[3] and I-TASSER.[4] In the Robetta server, RoseTTAFold was used for automated modeling. The confidence for the prediction was evaluated by the lDDT value, which represents accurate predictions when it is above 0.75 (Baek et al., 2021). In the I-TASSER server, five models were generated, and the best model was selected based on the threading sequence identity and C-score, which is typically in the range from −5 to 2. The predicted structures were visualized using PyMOL software (DeLano Scientific, San Carlos, CA, United States).

RdRp Recombinant Protein Expression in *Escherichia Coli*

Two types of APV RdRp, S196, and N196, were subcloned into the pET28a vector to generate recombinant plasmids

[1]http://weblogo.threeplusone.com
[2]http://www.mbio.ncsu.edu/BioEdit/
[3]https://robetta.bakerlab.org/
[4]https://zhanggroup.org/I-TASSER/

with His-tags using the primer pair RdRp-his-F/RdRp-his-R (**Supplementary Table S1**). The recombinant plasmids were transformed into *E. coli* BL21 (DE3) cells for protein expression. After overnight induction with 0.5 mM isopropyl β-D-thiogalactoside (IPTG) at 16°C, the cells were pelleted by centrifugation and resuspended in lysis buffer (20 mM Tris–HCl, pH 8.0) for sonication in ice water. The supernatant was retained for the RdRp enzymatic assay.

RdRp Enzymatic Assay

A 101 bp fragment of APV *CP* containing a T7 RNA polymerase promoter at the 5′ terminus was amplified using cp101-T7F/cp101-R primers (**Supplementary Table S1**) and *in vitro* transcribed to *CP* RNA as an RNA template with T7 RNA polymerase (Promega) according to the manufacturer's instructions. The enzymatic assay was performed in a total volume of 25 μl containing 20 mM Tris–HCl (pH 8.0), 1.5 mM $MnCl_2$, 2 mM $MgCl_2$, 100 mM NaCl, 4 mM DTT, 10 U RNasin (Promega), 250 μM NTP (including a biotin-labeled UTP; Roche, Basel, Switzerland), 0.5 μl of RNA template (800 ng/μl) and 100 μg of crude RdRp-His protein. The reaction mixture was incubated at 25°C for 2 h, and then 30 μg of proteinase K (Ambion) was added to terminate the reaction. The RNA products were extracted with phenol/chloroform (1:1), precipitated overnight using 95% ethanol containing 0.3 M sodium acetate and dissolved in 10 μl of RNase-free water.

The biotin-labeled RNA product was detected *via* dot blot. The RNA products were first spotted onto a BrightStar™-Plus positively charged nylon membrane (Thermo Scientific, Waltham, MA, United States) and then placed in a UV crosslinker (Spectronics Corporation, Westbury, NY, United States) for 10 min. The biotin-labeled RNA products were detected with a Chemiluminescent Nucleic Acid Detection Module Kit (Thermo Scientific) according to the manufacturer's instructions. The RdRp-His protein in the crude extracts was measured by western blotting using an anti-His monoclonal antibody (CWBiotech, Beijing, China). The RdRp enzyme activity was represented by the relative intensity of biotin-labeled RNA products to RdRp-His, which was quantified with ImageJ software. The 1 mM and 0.1 mM biotin-16-UTP were used as positive controls. One hundred micrograms of crude protein from the cells transformed with pET28a vector and 20 mM Tris–HCl (pH 8.0) buffer were used as negative controls. Six replicates were prepared. Differences were analyzed using Student's *t* test with SPSS 17.0 software.

Quantification of APV Load by Real-Time Quantitative PCR

APV load in the following three groups of aphids was measured using qPCR: the third-instar nymphs of the *V. faba* colony and *V. villosa* colony; the APV-free third-instar nymphs that were fed on an artificial diet containing the APV crude preparations from the *V. faba* colony or *V. villosa* colony for 1 d (Lu et al., 2020) and then raised on *V. villosa* for 8 d; and the third-instar nymphs of the *V. villosa* colony that were raised on *V. faba* for 3, 4, and 5 months. Five to nine biological replicates with five aphids per replicate or from 13 to 19 individual aphids were prepared for RNA extraction. qPCR was applied to quantify the RNA level of APV *CP* with the primer pair cp-F/cp-R (**Supplementary Table S1**) on a Light Cycler 480 II instrument (Roche). The transcript level of ribosomal protein L27 (NM_001126221) was quantified with primer pair L27-F/L27-R (**Supplementary Table S1**) as an internal control. The thermal cycling conditions were 95°C for 2 min, 40 cycles of 95°C for 20 s, 55°C for 20 s, and 68°C for 20 s, followed by one cycle of 95°C for 30 s, 58°C for 30 s, and 95°C for 10 s to determine the melting curve. The relative RNA level of APV *CP* to the transcript level of *L27* is represented as the mean ± SE. Differences were analyzed using Student's *t* test for pairwise comparisons with SPSS 17.0 software.

RESULTS

Single Nucleotide Polymorphism Sites in APV Genomes From Two Pea Aphid Colonies

We assembled the APV genomes from the previously sequenced salivary gland transcriptomes of the pea aphid *V. faba* colony and *V. villosa* colony (Lu et al., 2016). The assembled APV genome (registration number of OM812681 in GenBank) had 10,019 nucleotides (nt), including a 249 nt 5′-untranslated sequence and a 240 nt 3′-untranslated sequence containing a polyadenine. Following alignment of the reference APV genome (van der Wilk et al., 1997), four domains were identified, i.e., helicase from 1,123 to 1,431 nt, chymotrypsin-like protease from 3,847 to 4,719 nt, RdRp from 5,404 to 6,273 nt, and CP from 7,468 to 8,819 nt (**Figure 1**).

A total of 46 SNP sites were found in the APV genomes from the *V. faba* colony and *V. villosa* colony (**Figure 1; Supplementary Table S2**). Five SNPs at nucleotides 388, 2,983, 5,135, 5,990, and 8,355 were supposed to change amino acids, and the remaining 41 SNPs were synonymous mutations. Among the five nonsynonymous SNPs, site 5,990 was located in the RdRp domain, and site 8,355 was in the CP domain. Furthermore, the predominant nucleotides at site 5,990 were significantly different between the APV genomes from the *V. faba* colony and the *V. villosa* colony, i.e., 84% of G in the *V. faba* colony and 87% of A in the *V. villosa* colony, leading to a change in amino acid residues from serine (S) to asparagine (N). In the APV genome from the *M. truncatula* colony, which was previously sequenced (Lu et al., 2016), the nucleotides at site 5,990 were 62% of G and 38% of A. On the other hand, the predominant nucleotides at site 8,355 were the same in the two colonies, i.e., 96% of A in the *V. faba* colony and 73% of A in the *V. villosa* colony. For the other three nonsynonymous SNPs at sites 388, 2,983, and 5,135, the ratios of predominant nucleotides were not as divergent as site 5,990 between the two colonies.

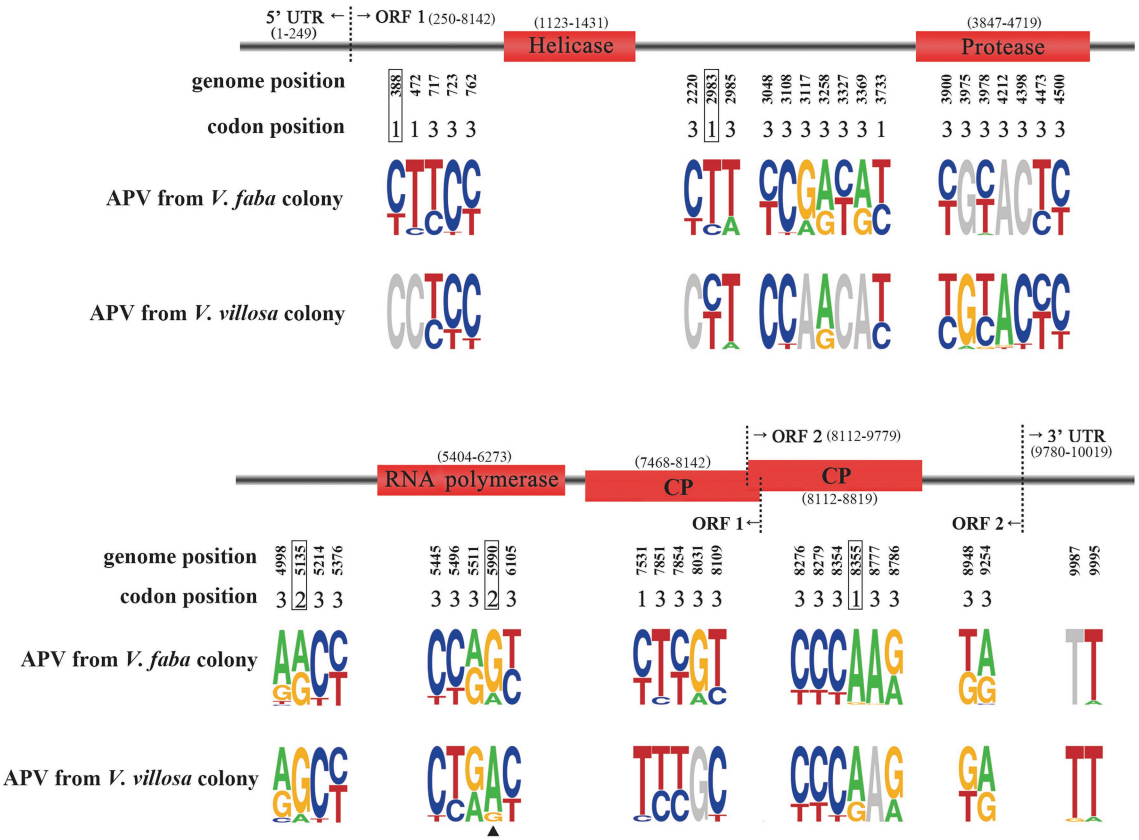

FIGURE 1 | Sequence logo showing allele frequencies at 46 SNP sites in APV genomes from the pea aphids *Vicia faba* colony and *Vicia villosa* colony. The genome position and corresponding codon position for each SNP are shown. Four domains are marked in red rectangles. Five SNPs resulting in nonsynonymous mutations are boxed. Site 5,990 is marked with a triangle. A logo represents each column of the alignment by a stack of letters, with the height of each letter proportional to the observed frequency of the corresponding nucleotide.

Divergence of SNP at Site 5,990 of APV in Different Colonies of Pea Aphids

To verify the different ratios of G or A at site 5,990 of APV in different colonies of pea aphids, we amplified and sequenced a 460 bp fragment encompassing site 5,990 with RT–PCR and Sanger sequencing in 20 individual pea aphids from both the *V. faba* colony and the *V. villosa* colony, which was acclimated 14 months after shifting from *V. faba*. In the *V. faba* colony, the ratio of G at site 5,990 was 92.26%, and the ratio of A was 4.99% (**Figure 2A**), while in the *V. villosa* colony, the ratio of G was 7.61%, and the ratio of A was 90.04% (**Figure 2B**). This result was consistent with that from the transcriptomes, suggesting that the predominant nucleotide at site 5,990 of APV was changed from G to A when the *V. faba* colony was shifted and adapted to the unsuitable *V. villosa*. However, when the *V. villosa* colony was transferred back to *V. faba* and raised for 5 months, the predominant nucleotide at site 5,990 of APV was still A, with a ratio no lower than 94% in 20 aphids sampled every month (**Figure 2C**). Furthermore, we sequenced the 460 bp fragment of APV from a field colony of pea aphids living on *Medicago sativa*, which is a low-fitness plant for pea aphids (Lu et al., 2016). In the 27 individuals, 62.07% of the nucleotides at site 5,990 of APV were A, and 28.25% were G (**Figure 2D**). Therefore, an obvious divergence in the predominant nucleotides at site 5,990 of APV occurred when the pea aphids adapted to different plants.

Location of Site 5,990 in the RdRp Structure

With alignment to the RdRp amino acid sequence of Kelp fly virus (YP_415507), which is also a picorna-like virus (Hartley et al., 2005), APV RdRp contained eight conserved motifs (I–VII, X; **Figure 3A**). The D-X (4 or 5)-D in motif IV and the GDD in motif VI bind the divalent cations Mg^{2+} and/or Mn^{2+}, and GDD also serve as crucial catalytic residues for RNA polymerase activity (Ng et al., 2002). Motif V determines the synthesis of RNA or DNA by discriminating NTPs from dNTPs (Gohara et al., 2000). The S or N at amino acid residue 196 of RdRp corresponding to genomic nucleotide site 5,990 was between motifs V and VI in the primary structure (**Figure 3A**). The three-dimensional structures of APV RdRp predicted *in silico* by the Robetta and I-TASSER servers were similar (**Figure 3B**), although the confidence levels were marginally acceptable, with a local distance difference test

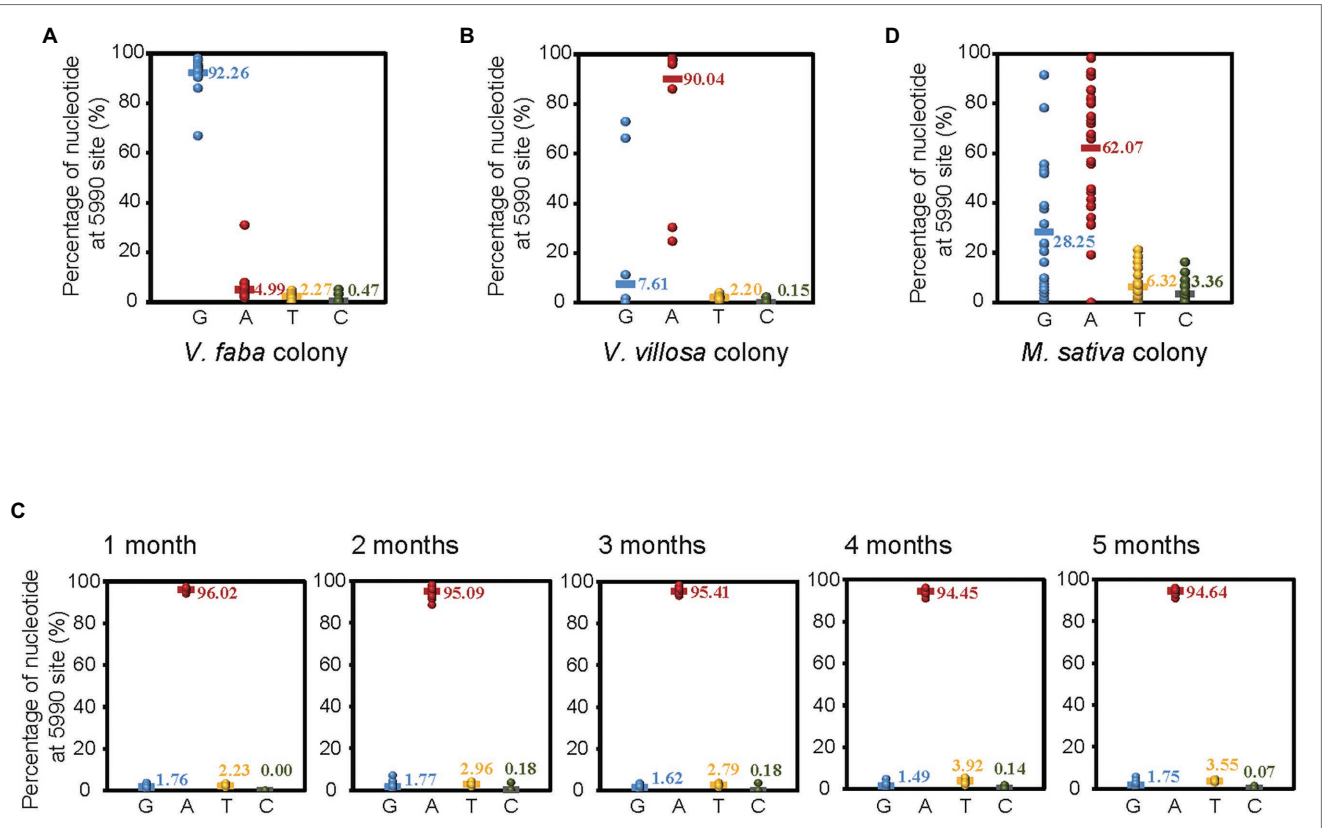

FIGURE 2 | Divergence of SNP at site 5,990 of APV in different colonies of pea aphids. **(A)** *Vicia faba* colony. **(B)** *Vicia villosa* colony. **(C)** *V. villosa* colony that was raised on *V. faba* for 1–5 months. **(D)** *Medicago sativa* colony. Twenty individual pea aphids were sequenced in **(A–C)**, and 27 individuals were sequenced in **(D)**.

(lDDT) value of 0.78 in the Robetta prediction and a C-score of 0.65 in the I-TASSER prediction. Site S196N was located at a random coil far away from the eight conserved motifs (**Figure 3B**).

Effects of SNP at Site 5,990 on the Enzymatic Activity of APV RdRp

To assess whether the substitution S196N at nucleotide site 5,990 affects enzymatic activity, two types of APV RdRp, S196 and N196, were recombinantly expressed in *E. coli* cells and used for enzymatic activity measurement with an RNA template and biotin-labeled NTP. The amounts of synthesized RNA products were compared between the two types of RdRp after normalization by the RdRp protein amounts. The results showed that the N196 type of RdRp produced more RNA products than the S196 type (**Figure 4A**), indicating that the substitution of G by A at site 5,990 increased the enzymatic activity of APV RdRp by 44.5% (**Figure 4B**).

Effects of SNP at Site 5,990 on Viral Replication Levels

The APV loads with different genotypes of RdRp were further explored in different aphid colonies using qPCR. The amount of APV in the *V. villosa* colony was approximately 3-fold that in the *V. faba* colony in terms of the RNA level of APV *CP* after 14 months of acclimation on *V. villosa* (**Figure 4C**). Even though the *V. villosa* colony was transferred back to *V. faba* and raised for 3–5 months, the predominant nucleotide at site 5,990 was still A (**Figure 2C**), and the amount of APV was significantly higher than that in the *V. faba* colony (**Figure 4D**). When the APV-free aphids were fed an artificial diet containing A5990-enriched APV from the *V. villosa* colony or G5990-enriched APV from the *V. faba* colony, a remarkably higher viral load was detected in the aphids 8 d post-infection with the A5990-enriched APV than that following infection with the G5990-enriched APV (**Figure 4E**). Considering the fact that the substitution of Ser by Asn (S196N) increased the enzymatic activity of RdRp, the higher replication level of the A5990-enriched APV could result from the promoted enzymatic activity of RdRp.

DISCUSSION

In this study, we found that a mutation in the RdRp of the symbiotic virus APV promoted polymerase activity, leading to an increased viral replication level in the host aphids. This mutation was preferred when aphids colonized unsuitable plants. The findings showed a novel case in which mutations selected

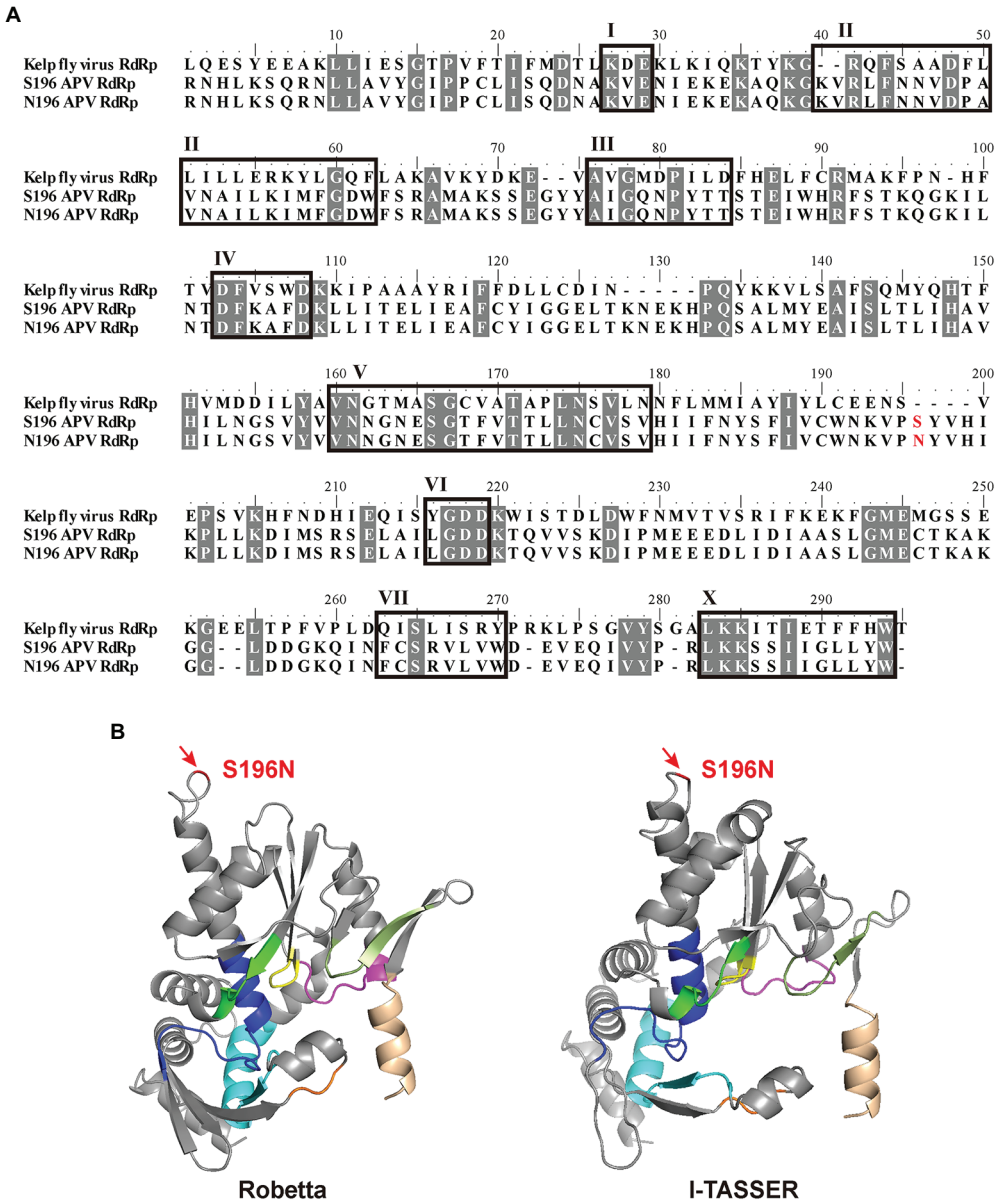

FIGURE 3 | Location of site 5,990 in the structure of RdRp. **(A)** Alignment of amino acid sequences among two types of APV RdRp and Kelp fly virus RdRp. Eight conserved motifs (I–VII, X) are boxed. The S or N at amino acid residue 196 is shown in red. Identical or similar amino acid residues among the three sequences are shaded in gray. **(B)** Three-dimensional structures of APV RdRp predicted *in silico* by the Robetta and I-TASSER servers. Motifs are shown in assorted colors: I, orange; II, cyan; III, magenta; IV, green; V, blue; VI, yellow; VII, smudge; X, wheat. Site S196N is marked in red.

in a symbiotic virus may confer a favor on the host as the host adapts to new environmental conditions.

The driving force for the S196N substitution in APV RdRp originated from the adaptation ability of host aphids to their plants. The S196N substitution enhanced APV replication in aphids so that more viruses were secreted to plants, which suppressed jasmonic acid-mediated resistance to aphids (Lu et al., 2020). This suggests that the symbiotic APV was in a similarly stressed situation as its host aphid during the aphid's adaptation to an unfamiliar environment, and the selection pressure on RdRp genotypes originated from the plants of host aphids. This case is different from the established theory of mutations in viral polymerases and surface glycoproteins, which are regarded as favorable for viral adaptability to new hosts. For example, nearly 80% of H5N1 influenza A virus isolates contain substitutions E627K, K526R, or D701N in the PB2 polymerase, leading to the enhancement of polymerase activity, virus replication and cross-species transmission (Hatta et al., 2001; Song et al., 2014). Similarly, the substitution D614G in the spike protein of SARS-CoV-2 increased viral transmission by 43–90% (Winger and Caspari, 2021), and the substitutions A226V in the envelope glycoprotein E1 and L210Q in E2

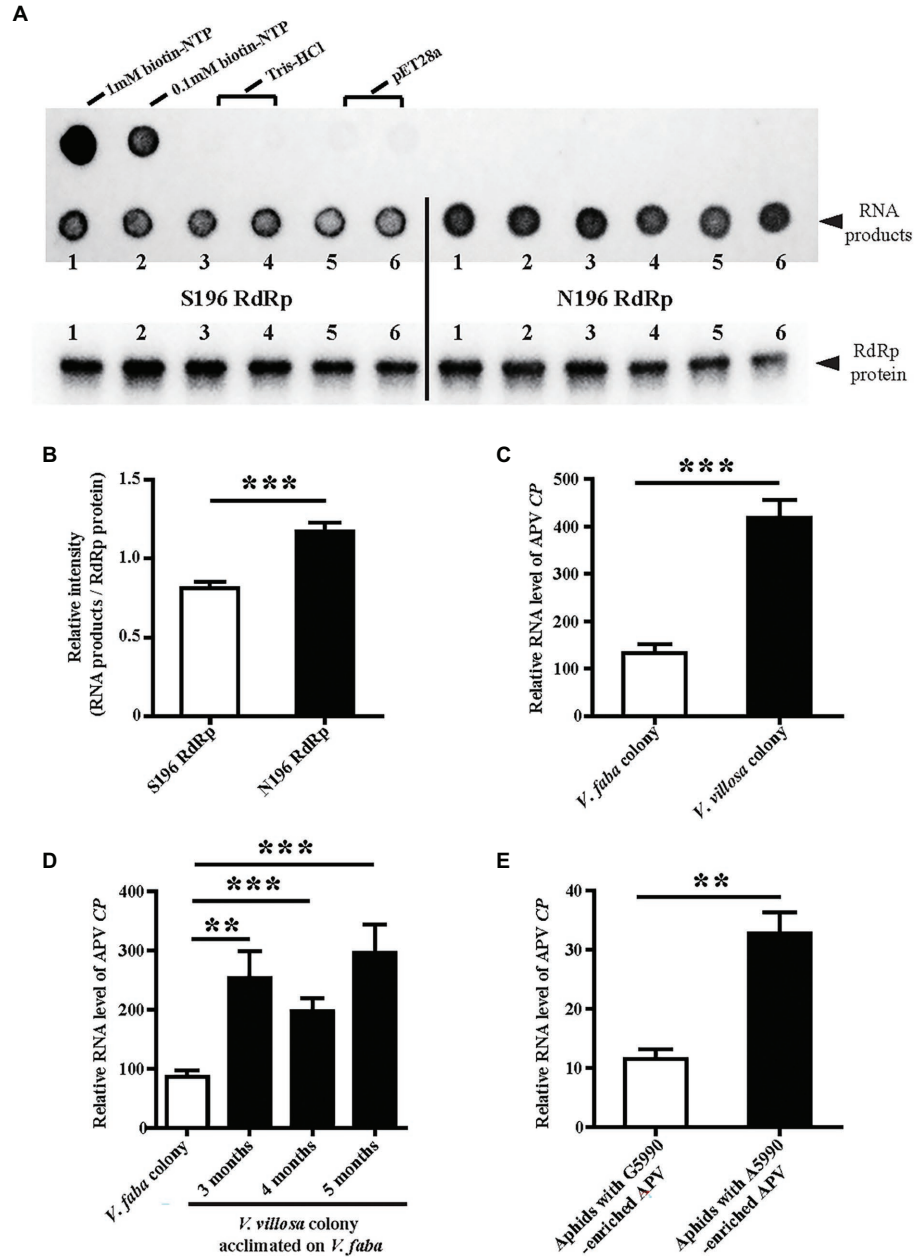

FIGURE 4 | Effects of SNP at site 5,990 on the enzymatic activity of APV RdRp and viral replication levels. **(A)** Dot blots showing the biotin-labeled RNA products synthesized by the recombinantly expressed S196-type RdRp-His and N196-type RdRp-His. The 1 and 0.1 mM biotin-NTP were used as positive controls. One hundred micrograms of crude protein from the cells transformed with pET28a vector and 20 mM Tris–HCl (pH 8.0) buffer were used as negative controls. The RdRp-His proteins used in the assays were measured by western blotting with an anti-His monoclonal antibody. Six replicates were prepared. **(B)** The relative intensity of synthesized RNA products to that of RdRp-His from **(A)** quantified with ImageJ software. The values represent the means ± SEs. **(C)** Comparison of the relative RNA levels of APV *CP* between the *V. faba* colony and *V. villosa* colony. Five to six biological replicates were prepared. **(D)** Comparison of the relative RNA levels of APV *CP* in the *V. villosa* colony that was acclimated on *V. faba* for 3–5 months. Thirteen to nineteen individual aphids were measured. **(E)** Comparison of the relative RNA levels of APV *CP* in the aphids 8 days post-infection with the A5990-enriched APV and the G5990-enriched APV. Nine biological replicates were prepared. The relative RNA level of APV *CP* to the transcript level of *L27* is represented as the mean ± SE. Differences were analyzed using Student's *t* test. $^{**}p < 0.01$; $^{***}p < 0.001$.

increased the infectivity of chikungunya virus in *Aedes albopictus* (Tsetsarkin et al., 2007; Tsetsarkin and Weaver, 2011).

The substitution at the S196N site had a profound influence on the enzymatic activity of APV RdRp. Viral RdRp usually contains palm, thumb and finger subdomains (Hansen et al., 1997). Motifs IV, V, and VI are localized in the palm subdomain and show unequivocal conservation throughout positive-stand RNA viruses (Poch et al., 1989; Koonin and

Dolja, 1993). *In vitro* mutations within the palm subdomain usually dramatically reduce or eliminate RdRp activity in viruses, such as encephalomyocarditis virus (Sankar and Porter, 1992), hepatitis C virus (Lohmann et al., 1997), Zika virus and Dengue virus (Xu et al., 2017). Alternatively, the substitution R345K enhances the RdRp activity of hepatitis C virus by approximately 50% (Lohmann et al., 1997). The S196N site is between motifs V and VI in the primary structure of APV RdRp but far away from the palm region viewed from the simulated three-dimensional structure. The inconsequential spatial location seems inadequate to explain the enhancement of RdRp activity with the S196N substitution unless the simulation was not sufficiently accurate considering the low conservation of the sequences in the region around the S196N site. Resolution of the genuine three-dimensional structure of APV RdRp would be enormously helpful in solving this puzzle.

CONCLUSION

The symbiotic virus APV changed as its host aphid acclimated to an unfavorable plant. The aphid's adaptation on unfavorable plants appears to have enhanced the selection of a mutation in viral RdRp that promoted APV replication, which may facilitate the aphid's adaptation process by suppressing the plant's resistance reaction toward aphids, representing a new evolutionary model of viruses in nature.

DATA AVAILABILITY STATEMENT

The original contributions presented in the study are included in the article/**Supplementary Material**, and further inquiries can be directed to the corresponding author.

AUTHOR CONTRIBUTIONS

HL did most experiments, wrote original draft, and predicted RdRp structure. JL and PY analyzed SNPs. FJ helped to measure RdRp activity. FC conceptualized and supervised the study and finalized the paper. All authors contributed to the article and approved the submitted version.

FUNDING

This work was supported by grants from the Strategic Priority Research Program of Chinese Academy of Sciences (no. XDA26050404) and the National Natural Science Foundation of China (no. 32102207).

SUPPLEMENTARY MATERIAL

The Supplementary Material for this article can be found online at: https://www.frontiersin.org/articles/10.3389/fmicb.2022.883436/full#supplementary-material

REFERENCES

Awadasseid, A., Wu, Y., Tanaka, Y., and Zhang, W. (2021). SARS-CoV-2 variants evolved during the early stage of the pandemic and effects of mutations on adaptation in Wuhan populations. *Int. J. Biol. Sci.* 17, 97–106. doi: 10.7150/ijbs.47827

Baek, M., DiMaio, F., Anishchenko, I., Dauparas, J., Ovchinnikov, S., Lee, G. R., et al. (2021). Accurate prediction of protein structures and interactions using a three-track neural network. *Science* 373, 871–876. doi: 10.1126/science.abj8754

Duffy, S., Shackelton, L. A., and Holmes, E. C. (2008). Rates of evolutionary change in viruses: patterns and determinants. *Nat. Rev. Genet.* 9, 267–276. doi: 10.1038/nrg2323

Elena, S. F., and Sanjuán, R. (2005). Adaptive value of high mutation rates of RNA viruses: separating causes from consequences. *J. Virol.* 79, 11555–11558. doi: 10.1128/JVI.79.18.11555-11558.2005

Gohara, D. W., Crotty, S., Arnold, J. J., Yoder, J. D., Andino, R., and Cameron, C. E. (2000). Poliovirus RNA-dependent RNA polymerase (3Dpol): structural, biochemical, and biological analysis of conserved structural motifs A and B. *J. Biol. Chem.* 275, 25523–25532. doi: 10.1074/jbc.M002671200

Hansen, J. L., Long, A. M., and Schultz, S. C. (1997). Structure of the RNA-dependent RNA polymerase of poliovirus. *Structure* 5, 1109–1122. doi: 10.1016/s0969-2126(97)00261-x

Hartley, C. J., Greenwood, D. R., Gilbert, R. J., Masoumi, A., Gordon, K. H., Hanzlik, T. N., et al. (2005). Kelp fly virus: a novel group of insect picorna-like viruses as defined by genome sequence analysis and a distinctive virion structure. *J. Virol.* 79, 13385–13398. doi: 10.1128/JVI.79.21.13385-13398.2005

Hatta, M., Gao, P., Halfmann, P., and Kawaoka, Y. (2001). Molecular basis for high virulence of Hong Kong H5N1 influenza A viruses. *Science* 293, 1840–1842. doi: 10.1126/science.1062882

Huang, S. W., and Wang, S. F. (2020). The effects of genetic variation on H7N9 avian influenza virus pathogenicity. *Viruses* 12:1220. doi: 10.3390/v12111220

Kim, D., Pertea, G., Trapnell, C., Pimentel, H., Kelley, R., and Salzberg, S. L. (2013). Top hat 2: accurate alignment of transcriptomes in the presence of insertions, deletions and gene fusions. *Genome Biol.* 14:R36. doi: 10.1186/gb-2013-14-4-r36

Koonin, E. V., and Dolja, V. V. (1993). Evolution and taxonomy of positive-strand RNA viruses: implications of comparative analysis of amino acid sequences. *Crit. Rev. Biochem. Mol. Biol.* 28, 375–430. doi: 10.3109/10409239309078440

Li, H., Handsaker, B., Wysoker, A., Fennell, T., Ruan, J., Homer, N., et al. (2009). The sequence alignment/map format and samtools. *Bioinformatics* 25, 2078–2079. doi: 10.1093/bioinformatics/btp352

Lohmann, V., Körner, F., Herian, U., and Bartenschlager, R. (1997). Biochemical properties of hepatitis C virus NS5B RNA-dependent RNA polymerase and identification of amino acid sequence motifs essential for enzymatic activity. *J. Virol.* 71, 8416–8428. doi: 10.1128/JVI.71.11.8416-8428.1997

Lu, H., Yang, P., Xu, Y., Luo, L., Zhu, J., Cui, N., et al. (2016). Performances of survival, feeding behavior, and gene expression in aphids reveal their different fitness to host alteration. *Sci. Rep.* 6:19344. doi: 10.1038/srep19344

Lu, H., Zhu, J., Yu, J., Chen, X., Kang, L., and Cui, F. (2020). A symbiotic virus facilitates aphid adaptation to host plants by suppressing jasmonic acid responses. *Mol. Plant-Microbe Interact.* 33, 55–65. doi: 10.1094/MPMI-01-19-0016-R

Ng, K. K., Cherney, M. M., Vazquez, A. L., Machin, A., Alonso, J. M., Parra, F., et al. (2002). Crystal structures of active and inactive conformations of a caliciviral RNA-dependent RNA polymerase. *J. Biol. Chem.* 277, 1381–1387. doi: 10.1074/jbc.M109261200

Peck, K. M., and Lauring, A. S. (2018). Complexities of viral mutation rates. *J. Virol.* 92, e01031–e01017. doi: 10.1128/JVI.01031-17

Poch, O., Sauvaget, I., Delarue, M., and Tordo, N. (1989). Identification of four conserved motifs among the RNA-dependent polymerase encoding elements. *EMBO J.* 8, 3867–3874. doi: 10.1002/j.1460-2075.1989.tb08565.x

Sanjuán, R., Nebot, M. R., Chirico, N., Mansky, L. M., and Belshaw, R. (2010). Viral mutation rates. *J. Virol.* 84, 9733–9748. doi: 10.1128/JVI.00694-10

Sankar, S., and Porter, A. G. (1992). Point mutations which drastically affect the polymerization activity of encephalomyocarditis virus RNA-dependent RNA polymerase correspond to the active site of *Escherichia coli* DNA polymerase I. *J. Biol. Chem.* 267, 10168–10176. doi: 10.1016/S0021-9258(19)50215-0

Song, W., Wang, P., Mok, B. W., Lau, S. Y., Huang, X., Wu, W. L., et al. (2014). The K526R substitution in viral protein PB2 enhances the effects of E627K on influenza virus replication. *Nat. Commun.* 5:5509. doi: 10.1038/ncomms6509

Tsetsarkin, K. A., Vanlandingham, D. L., McGee, C. E., and Higgs, S. (2007). A single mutation in chikungunya virus affects vector specificity and epidemic potential. *PLoS Pathog.* 3:e201. doi: 10.1371/journal.ppat.0030201

Tsetsarkin, K. A., and Weaver, S. C. (2011). Sequential adaptive mutations enhance efficient vector switching by Chikungunya virus and its epidemic emergence. *PLoS Pathog.* 7:e1002412. doi: 10.1371/journal.ppat.1002412

van den Heuvel, J. F., Hummelen, H., Verbeek, M., Dullemans, A. M., and van der Wilk, F. (1997). Characteristics of acyrthosiphon pisum virus, a newly identified virus infecting the pea aphid. *J. Invertebr. Pathol.* 70, 169–176. doi: 10.1006/jipa.1997.4691

van der Wilk, F., Dullemans, A. M., Verbeek, M., and van den Heuvel, J. F. (1997). Nucleotide sequence and genomic organization of Acyrthosiphon pisum virus. *Virology* 238, 353–362. doi: 10.1006/viro.1997.8835

Wang, W., Dai, H., Zhang, Y., Chandrasekar, R., Luo, L., Hiromasa, Y., et al. (2015). Armet is an effector protein mediating aphid-plant interactions. *FASEB J.* 29, 2032–2045. doi: 10.1096/fj.14-266023

Winger, A., and Caspari, T. (2021). The spike of concern-the novel variants of SARS-CoV-2. *Viruses* 13:1002. doi: 10.3390/v13061002

Xu, H. T., Hassounah, S. A., Colby-Germinario, S. P., Oliveira, M., Fogarty, C., Quan, Y., et al. (2017). Purification of Zika virus RNA-dependent RNA polymerase and its use to identify small-molecule Zika inhibitors. *J. Antimicrob. Chemother.* 72, dkw514–dkw734. doi: 10.1093/jac/dkw514

Conflict of Interest: The authors declare that the research was conducted in the absence of any commercial or financial relationships that could be construed as a potential conflict of interest.

Publisher's Note: All claims expressed in this article are solely those of the authors and do not necessarily represent those of their affiliated organizations, or those of the publisher, the editors and the reviewers. Any product that may be evaluated in this article, or claim that may be made by its manufacturer, is not guaranteed or endorsed by the publisher.

Copyright © 2022 Lu, Li, Yang, Jiang, Liu and Cui. This is an open-access article distributed under the terms of the Creative Commons Attribution License (CC BY). The use, distribution or reproduction in other forums is permitted, provided the original author(s) and the copyright owner(s) are credited and that the original publication in this journal is cited, in accordance with accepted academic practice. No use, distribution or reproduction is permitted which does not comply with these terms.

frontiers | Frontiers in Microbiology

ORIGINAL RESEARCH
published: 28 April 2022
doi: 10.3389/fmicb.2022.890807

Transcriptomic Changes of *Bemisia tabaci* Asia II 1 Induced by Chilli Leaf Curl Virus Trigger Infection and Circulation in Its Vector

Aarthi Nekkanti[1,2], Prosenjit Chakraborty[1], Amalendu Ghosh[1], Mir Asif Iquebal[3], Sarika Jaiswal[3] and Virendra Kumar Baranwal[1]*

[1] Advanced Centre for Plant Virology, Indian Agricultural Research Institute, New Delhi, India, [2] Division of Entomology, Indian Agricultural Research Institute, New Delhi, India, [3] Centre for Agricultural Bioinformatics, Indian Agricultural Statistics Research Institute, New Delhi, India

Bemisia tabaci (Hemiptera: Aleyrodidae) is a highly efficient vector in the spread of chilli leaf curl virus (ChiLCV, *Begomovirus*) which is a major constraint in the production of chilli in South Asia. Transcriptome analysis of *B. tabaci* post-6 h acquisition of ChiLCV showed differential expression of 80 (29 upregulated and 51 downregulated) genes. The maximum number of DEGs are categorized under the biological processes category followed by cellular components and molecular functions. KEGG analysis of DEGs showed that the genes are involved in the functions like metabolism, signaling pathways, cellular processes, and organismal systems. The expression of highly expressed 20 genes post-ChiLCV acquisition was validated in RT-qPCR. DEGs such as cytosolic carboxypeptidase 3, dual-specificity protein phosphatase 10, 15, dynein axonemal heavy chain 17, fasciclin 2, inhibin beta chain, replication factor A protein 1, and Tob1 were found enriched and favored the virus infection and circulation in *B. tabaci*. The present study provides an improved understanding of the networks of molecular interactions between *B. tabaci* and ChiLCV. The candidate genes of *B. tabaci* involved in ChiLCV transmission would be novel targets for the management of the *B. tabaci*-begomovirus complex.

Keywords: ChiLCV, silverleaf whitefly, RNA-Seq, transcriptome, RT-qPCR, virus-vector relationship

OPEN ACCESS

Edited by:
Sean Michael Prager, University of Saskatchewan, Canada

Reviewed by:
Susheel Kumar, National Botanical Research Institute (CSIR), India
Rajarshi Kumar Gaur, Deen Dayal Upadhyay Gorakhpur University, India

***Correspondence:**
Amalendu Ghosh
amal4ento@gmail.com; Amalendu.Ghosh@icar.gov.in
orcid.org/0000-0001-6634-5771

Specialty section:
This article was submitted to Virology, a section of the journal Frontiers in Microbiology

Received: *06 March 2022*
Accepted: *25 March 2022*
Published: *28 April 2022*

Citation:
Nekkanti A, Chakraborty P, Ghosh A, Iquebal MA, Jaiswal S and Baranwal VK (2022) Transcriptomic Changes of Bemisia tabaci Asia II 1 Induced by Chilli Leaf Curl Virus Trigger Infection and Circulation in Its Vector. Front. Microbiol. 13:890807. doi: 10.3389/fmicb.2022.890807

INTRODUCTION

Transmission of a plant virus within or between the fields is often dependent upon a mobile vector. Insects are the most efficient vectors of plant viruses because of their abundance and feeding behavior (Milenovic et al., 2019). About 70% of reported insect vectors are hemipterans (Fereres and Raccah, 2015). Silverleaf whitefly, *Bemisia tabaci* Gennadius (Hemiptera: Aleyrodidae) is an invasive insect pest and vector of several plant viruses (Legarrea et al., 2015). Transmission of several begomoviruses, carlaviruses, criniviruses, cytorhabdoviruses, ipomoviruses, poleroviruses, and torradoviruses by *B. tabaci* causes economic losses exceeding billions of US$ and threatens food security (Dasgupta et al., 2003; Jones, 2003; Navas-Castillo et al., 2011; Brown et al., 2015; Orfanidou et al., 2016; Saeed and Samad, 2017; Zanardo and Carvalho, 2017; Ghosh et al., 2019; Costa et al., 2020; Pinheiro-Lima et al., 2020; Cornejo-Franco et al., 2022).

The spectrum of diseases caused by begomoviruses is a continuing challenge to crop production worldwide (family: *Geminiviridae*) (Navas-Castillo et al., 2011). These diseases cause an estimated yield loss of 50–90% in tomatoes, chilli, and other crops including beans, cassava, cotton, cucurbits, eggplant, papaya, and potatoes (Briddon et al., 2010; Saeed and Samad, 2017). To date, 445 begomovirus species have been reported[1]. One of the begomoviruses, i.e., chilli leaf curl virus (ChiLCV) is a major threat to chilli production in tropical and sub-tropical countries (Senanayake et al., 2007, 2012; Menike and De Costa, 2017; Oraonand and Tarafdar, 2018; Thakur et al., 2018). ChiLCV has caused several epidemics in India and Sri Lanka (Senanayake et al., 2007, 2012). The disease is typically manifested in the infected plants as upward curling, puckering, and bunching of leaves. The leaves become smaller and severely affected plants produce fewer and deformed fruits. Yield loss of 20–50% has been recorded in chilli by ChiLCV (Thakur et al., 2018) which may rise to 100% with the infestation of thrips and mites (Menike and De Costa, 2017). Control options for *B. tabaci*-ChiLCV are very limited as insecticides continue to lose their efficacy due to the emergence of resistant *B. tabaci* populations (Barman et al., 2021). Additionally, insecticides adversely affect the environment and human health. Understanding the molecular interactions between *B. tabaci* and ChiLCV and interrupting the interrelationship is a promising approach to manage the virus-vector complex. The present understanding of *B. tabaci*-begomovirus interaction is largely based on the study of *B. tabaci* cryptic species MEAM1 and MED and tomato yellow leaf curl virus (TYLCV). Once ingested by *B. tabaci*, virus particles pass through the midgut, where they move across the midgut membrane into the hemolymph, possibly *via* receptor-mediated endocytosis, and circulate to the primary salivary glands, from where they are egested along with saliva during feeding (Czosnek and Ghanim, 2012). During the entire process, the viral proteins need to interact with several proteins in the midgut, hemolymph, and primary salivary glands (Wei et al., 2014). *B. tabaci* MEAM1 heat shock proteins (Hsp), cyclophilins, and peptidoglycan recognition protein interact with TYLCV coat protein (CP) for successful internalization (Götz et al., 2012; Kanakala and Ghanim, 2016; Wang et al., 2016). Silencing of *hsp70* in *B. tabaci* Asia II 1 inhibits transmission of ChiLCV (Chakraborty and Ghosh, 2022). A GroEL homolog produced by C-type endosymbionts in *B. tabaci* MEAM1 is known to transport TYLCV particles through the hemolymph of *B. tabaci* in coated vesicles (Bragard et al., 2013).

Over the past 5 years, transcriptomic analysis of *B. tabaci* has enabled us to study the differential expression of genes that are involved in virus transmission (Luan et al., 2011; Kaur et al., 2017; Xia et al., 2017; Hasegawa et al., 2018; Ding et al., 2019). However, these studies were limited to gene regulations in MEAM1 and MED cryptic species of *B. tabaci* in response to infection of TYLCV, tomato yellow leaf curl China virus (TYLCCV), and a crinivirus-tomato chlorosis virus (ToCV). To date, 46 morphologically indistinguishable cryptic species of *B. tabaci* are known (Rehman et al., 2021) that differ in genetic structure, chemical resistance, adaptability, and virus transmission (Brown, 2000; Gorman et al., 2010; Wang et al., 2010; Qin et al., 2016). The genes of *B. tabaci* involved in the transmission of begomoviruses are not conserved across all the *B. tabaci* cryptic species–begomovirus combinations. Also, little is known about the role of putative genes of *B. tabaci* Asia II 1 in response to ChiCLV transmission. The present study reports the candidate genes of *B. tabaci* Asia II 1 that are regulated at an early stage of ChiLCV infection. Identification of candidate genes involved in key physiological processes and ChiLCV infection would be novel targets for the management of the *B. tabaci*-ChiLCV complex.

[1]https://talk.ictvonline.org/taxonomy/

MATERIALS AND METHODS

Establishment of Isofemale Population of *Bemisia tabaci*

A homogeneous population of *B. tabaci* Asia II 1 maintained at Advanced Centre for Plant Virology, Indian Agricultural Research Institute (IARI), New Delhi since 2015 was used in the present study. The homogeneous population was developed from a single adult female on healthy eggplants. The cryptic identity of the *B. tabaci* was confirmed by PCR amplification of the mitochondrial cytochrome oxidase subunit I (mtCOI) using C1-J-2195 and L2-N-3014 primers (Simon et al., 1994; **Supplementary Table 1**) and sequencing. DNA was isolated from randomly collected adult flies from the homogeneous population using CTAB extraction buffer as described by Rehman et al. (2021). PCR was performed in a 25 μl reaction mixture comprised of 1x DreamTaq buffer, 0.1 mM dNTPs (Thermo Fisher Scientific, Waltham, MA, United States), 10 picomoles forward and reverse primers, 1.25 U DreamTaq DNA polymerase (Thermo Fisher Scientific, Waltham, MA, United States), and 50 ng of template DNA. Thermal cycling was followed as initial denaturation at 94°C for 2 min, 30 cycles of denaturation at 94°C for 30 s, annealing at 53°C for 30 s and polymerization at 72°C for 1 min, followed by final extension step at 72°C for 10 min. PCR products were visualized on 1% agarose gel stained with GoodView^{TM} (BR Biochem, New Delhi, India). The purified PCR products were sequenced bidirectionally. The sequences were processed by BioEdit and species homology was checked in BLASTn. A consensus sequence was submitted to GenBank. The genotype or cryptic species of the *B. tabaci* population was confirmed based on Bayesian Inference phylogeny considering a genetic divergence cutoff of 4% as described by Rehman et al. (2021). The population was maintained under controlled environmental conditions at 28 ± 2°C, 60 ± 10% relative humidity, and 16 h light- 8 h dark photoperiod.

Virus Isolate and Generation of ChiLCV-Exposed and Non-exposed *Bemisia tabaci*

A pure culture of ChiLCV maintained on chilli plant (var. Preeti, Nunhems, Haelen, Netherlands) by *B. tabaci* inoculation under insect-proof conditions was used in the study. ChiLCV

was confirmed by amplifying DNA-A using Begomo F and Begomo R primers (Akhter et al., 2009) (**Supplementary Table 1**) and nucleotide sequencing. To establish the ChiLCV-exposed and non-exposed *B. tabaci* populations, freshly emerged female adults were collected and released onto ChiLCV-infected and virus-free chilli plants at 4–6 leaf stage for 6 h in three biological replicates. A 6 h acquisition was found adequate for the successful transmission of ChiLCV by *B. tabaci* Asia II 1 (Senanayake et al., 2012; Roy et al., 2021). After 6 h of acquisition, ChiLCV-exposed (BtTrI1, BtTrI2, and BtTrI3) and non-exposed (BtTrH1, BtTrH2, and BtTrH3) *B. tabaci* adults were collected. ChiLCV infection in *B. tabaci* populations was confirmed by randomly collecting 10 flies from each population and testing in PCR using ChiLCV-specific primers (AG149F-AG150R) (Roy et al., 2021, **Supplementary Table 1**). Each population was divided into two parts. One part was utilized for RNA-Seq and another part was preserved in −80°C for gene expression analysis in a reverse transcription-quantitative polymerase chain reaction (RT-qPCR).

Total RNA Isolation

Total RNA was isolated from each ChiLCV-exposed (BtTrI1, BtTrI2, and BtTrI3) and non-exposed (BtTrH1, BtTrH2, and BtTrH3) *B. tabaci* populations using Trizol reagent (Invitrogen, Waltham, MA, United States) following manufacturer's protocol. In brief, 50 *B. tabaci* were crushed in 1 mL Trizol and kept at room temperature for 10 min. Two hundred microliter of chloroform was added to the mixture, vortexed for <10 s, and incubated at room temperature for 10 min. The mixture was then centrifuged at 16,000 x*g* for 10 min at 4°C. The upper aqueous phase was transferred to a fresh tube and 0.8 volume of ice-chilled isopropanol was added, mixed properly, and incubated at 4°C for 10 min. The mixture was again centrifuged at 16,000 x*g* for 10 min at 4°C and the supernatant was discarded. The pellet was finally washed with 70% ethanol, air-dried, and resuspended in 30 μl nuclease-free water. RNaseZAP (Thermo Fisher Scientific, Waltham, MA, United States) was used for decontamination, RNase-free tips, microfuge tubes, and water were used throughout the experiment. Total RNA quality was measured using RNA 6000 Nano Kit (Agilent Technologies, Santa Clara, CA, United States) on 2100 Bioanalyzer (Agilent Technologies) with a minimum RNA Integrity Number (RIN) value of 7. RNA concentrations were determined using a NanoDrop ND-8000 spectrophotometer (Thermo Fisher Scientific, Waltham, MA, United States).

Construction of cDNA Library and Sequencing of Transcripts

RNA-Seq libraries for all samples were prepared using NEBNext UltraII RNA library preparation kit for Illumina (New England Biolabs, Ipswich, MA, United States) following manufacturer's protocol and sequencing was done in a single HiSEQ 4000 (Illumina Inc., San Diego, CA, United States) lane using 150 bp paired-end chemistry. The library preparation and sequencing were done by commercial service providers (NxGenBio Life Sciences, Delhi, India). Briefly, mRNA was purified using oligo-dT beads. Magnetic beads were used for the second round of purification. During the second elution of the poly-A RNA, the RNA was also fragmented into short stretches of 200–500 bp at 94°C for 5 min using an ultrasonicator in presence of divalent cations. The cleaved RNA fragments were copied into first-strand cDNA using SuperScript-II reverse transcriptase (Thermo Fisher Scientific, Waltham, MA, United States) with random primers. After second-strand cDNA synthesis, fragments were end-repaired, A-tailed, and ligated to indexed adapters. The products were purified and enriched with PCR to create the final cDNA library. The tagged cDNA libraries were pooled in equal ratios and used for 2 × 150 bp paired-end sequencing on a single lane of the Illumina HiSEQ 4000. Illumina clusters were generated and were loaded onto Illumina Flow Cell and sequenced. After sequencing, the samples were demultiplexed and the indexed adapter sequences were trimmed using the CASAVA v1.8.2 software (Illumina Inc.).

Pre-processing of Raw Reads and Differential Gene Expression Analysis

The ambiguous "N" nucleotides with a ratio of "N" > 5%, reads with adaptor sequences, and low-quality reads with a quality score < 20% were removed by the Trim Galore v0.4.1 to get the high-quality reads. Reference genome index was established using BWAv0.7.5 and the clean reads were mapped to the reference genome of *B. tabaci* MEAM1 (Chen et al., 2016). Read numbers, mapped to every gene were counted using Samtools v0.1.19. Differential expression between the ChiLCV-exposed (BtTrI1, BtTrI2, and BtTrI3) and non-exposed (BtTrH1, BtTrH2, and BtTrH3) *B. tabaci* populations was analyzed using the DESeq R package[2]. Significant differential gene expression that was consistent among the biological replicates, was counted with $\geq \log_2$ 2-fold change and $p < 0.05$.

Annotation and Functional Enrichment Analysis of Differentially Expressed Genes

Gene annotations and functional enrichment analysis including Gene Ontology (GO) and Kyoto Encyclopedia of Genes and Genomes (KEGG) biological pathways were used to identify the differentially expressed genes (DEGs) that were significantly enriched in GO terms or biological pathways post-6 h of ChiLCV acquisition. Gene annotations against the Uniprot GO database[3] were performed by aligning DEGs to the NR database using the blast v 2.6.0+ programme. KEGG pathway enrichment analysis of DEGs was performed using the KEGG database resource[4] by KAAS (Moriya et al., 2007) to identify the pathways that were differentially regulated between ChiLCV-exposed and non-exposed *B. tabaci* with *p*-value < 0.05.

[2]http://www.bioconductor.org/packages/release/bioc/html/DESeq2.html

[3]http://geneontology.org/

[4]http://www.genome.jp/kegg

Relative Expression of Putative Genes in Reverse Transcription-Quantitative Polymerase Chain Reaction

To validate the RNA-Seq data, 20 putative genes of *B. tabaci* Asia II 1 with $\geq \log_2$ 2-fold change values were selected to assess the gene expression in RT-qPCR. Two sets of primers were designed for each of the target and endogenous control (β-actin) genes. The primer pairs were initially optimized in a gradient PCR. One set of primers for each target gene was selected based on the efficiency of PCR amplification at the same PCR conditions for the endogenous control primers. A part of the same ChiLCV-exposed and non-exposed *B. tabaci* populations used for RNA-Seq was preserved for RT-qPCR analysis. Total RNA was isolated from ChiLCV-exposed (BtTrI1, BtTrI2, and BtTrI3) and non-exposed (BtTrH1, BtTrH2, and BtTrH3) *B. tabaci* populations as described earlier. cDNA was synthesized using the FIREScript RT cDNA synthesis kit (Solis BioDyne, Estonia). The reaction mixture contained 1X RT reaction buffer, 1.0 μg template RNA, 5.0 μM oligo dT primer, 500 μM dNTP mix, 10-unit FIREScript RT, and 1-unit RiboGrip RNase inhibitor. The reverse transcription was carried out in a thermocycler (T100, Bio-Rad, Hercules, CA, United States) at 42°C for 60 min followed by enzyme inactivation at 85°C for 5 min.

The relative RT-qPCR was carried out in an InstaQ 48 real-time PCR (Himedia, Mumbai, India) with 20 μl reaction volume containing 10 μl of 2X Maxima SYBR green master mix, 10 μM ROX passive reference dye, 10 picomoles each forward and reverse primer (**Supplementary Table 1**), and 2 μl template cDNA. Thermal cycling was performed as initial denaturation at 94°C for 5 min, 30 cycles of 94°C for 30 sec, 56°C for 30 sec, and 72°C for 30 sec. The dissociation or melting stage was carried out after every reaction to determine the specificity of the amplicons in RT-qPCR using a computer interface programme for InstaQ 48M2 (Himedia). The RT-qPCR was performed with three biological and two technical replicates. The expression change of the target gene was normalized by excluding the changes in cycle threshold (C_T) value of endogenous control, β-actin. Log_2-fold change value was calculated and relative expression of mRNA was determined by normalizing the $\log_2$ values of the ChiLCV-exposed populations with non-exposed using the $2^{-\Delta\Delta\ C_T}$ method (Livak and Schmittgen, 2001) in Mircosoft Excel 2016.

RESULTS

Characterization of *Bemisia tabaci* and Begomovirus

An isofemale line of *B. tabaci* Asia II 1 (Accession No. MT920041), maintained on healthy eggplant at Advanced Centre for Plant Virology, IARI was used to generate ChiLCV-exposed and non-exposed *B. tabaci* populations. The identity of the *B. tabaci* cryptic species was confirmed by sequencing the mtCOI gene. PCR amplification of *B. tabaci* mtCOI with C1-J-2195 and L2-N-3014 primers showed an expected amplicon of ∼860 bp on an agarose gel. The nucleotide (nt) sequence showed 99.99% homology in BLASTn analysis with other *B. tabaci* sequences in NCBI. The sequence can be retrieved using the GenBank Accession No. MT920041. Bayesian Inference phylogeny considering genetic divergence cutoff of 4% revealed that the population belonged to the cryptic species *B. tabaci* Asia II 1 (data not shown).

PCR amplification of the DNA-A using Begomo F and Begomo R primer produced a 2.7 kb product as visualized on 1% agarose gel. Bidirectional sequencing of the cloned products produced an 1896 nt sequence, comprising complete AV1 and AV2 genes, and partial AC1, AC2, AC3, and AC4 genes, that was 100% similar to ChiLCV isolates upon BLASTn analysis. The sequence can be retrieved by GenBank Accession No. MW399222.

ChiLCV-Exposed and Non-exposed *Bemisia tabaci* Population

ChiLCV-exposed and non-exposed *B. tabaci* populations were developed by allowing the freshly emerged adult flies to feed on infected and healthy chilli plants for 6 h. A few randomly collected *B. tabaci* adults were tested in PCR with ChiLCV-specific primers, AG149F and AG150R (**Supplementary Table 1**). A product of 290 bp was visualized on agarose gel that confirmed the virus infection in ChiLCV-exposed *B. tabaci* adults. *B. tabaci* populations (BtTrH1, BtTrH2, and BtTrH3) that were exposed to healthy chilli plants did not produce any ChiLCV-specific amplification in PCR.

Illumina Sequencing and Assembly

Total RNA was extracted from three ChiLCV-exposed (BtTrI1, BtTrI2, and BtTrI3) and non-exposed (BtTrH1, BtTrH2, and BtTrH3) *B. tabaci* Asia II 1 populations. For RNA-Seq analysis of ChiLCV-exposed and non-exposed *B. tabaci*, a total of six cDNA libraries were constructed and used for 2 × 150 bp pair-end sequencing on a single HiSEQ4000 lane. About 26–33 million raw reads were generated from each library (**Table 1**). Of which, 99.58–99.70% reads were clean reads. The cleaned reads of all the six libraries were mapped with the reference genome of *B. tabaci* MEAM1 (Chen et al., 2016). The mapping percent for all six libraries ranged from 87.21 to 93.16% of clean reads.

General Pattern of *Bemisia tabaci* Gene Expression in Response to ChiLCV Infection

A total of 15,514 genes in adult *B. tabaci* Asia II 1 were found to be differentially expressed post 6 h of ChiLCV exposure. Out of which, 7,193 genes were upregulated and 8,321 genes were downregulated. However, only a total of 80 (0.52%) genes showed significant regulations with $\geq \log_2$ 2-fold change in expression level at a significant *p*-value of ≤ 0.05. Among the significant differentially expressed genes (DEGs), 29 genes were upregulated and 51 genes were downregulated in combined BtTrI as compared to BtTrH (**Figure 1**). The top upregulated and downregulated genes of *B. tabaci* in response to ChiLCV-infection are listed in **Table 2**. The DEGs of *B. tabaci* were

TABLE 1 | Summary of RNA-Seq data obtained from ChiLCV-exposed and non-exposed *B. tabaci* Asia II 1.

Sample		Raw reads	Filter reads	Clean reads (%)	% mapped with reference genome
ChiLCV non-exposed *B. tabaci*	BtTrH1	2,65,84,539	2,65,09,920	99.7	91.7
	BtTrH2	2,65,05,012	2,63,95,200	99.58	87.38
	BtTrH3	3,12,05,804	3,11,08,963	99.68	87.21
ChiLCV exposed *B. tabaci*	BtTrI1	3,31,48,645	3,30,35,921	99.65	93.16
	BtTrI2	2,97,68,269	2,96,75,113	99.68	88.01
	BtTrI3	2,67,77,701	2,66,83,511	99.64	90.03

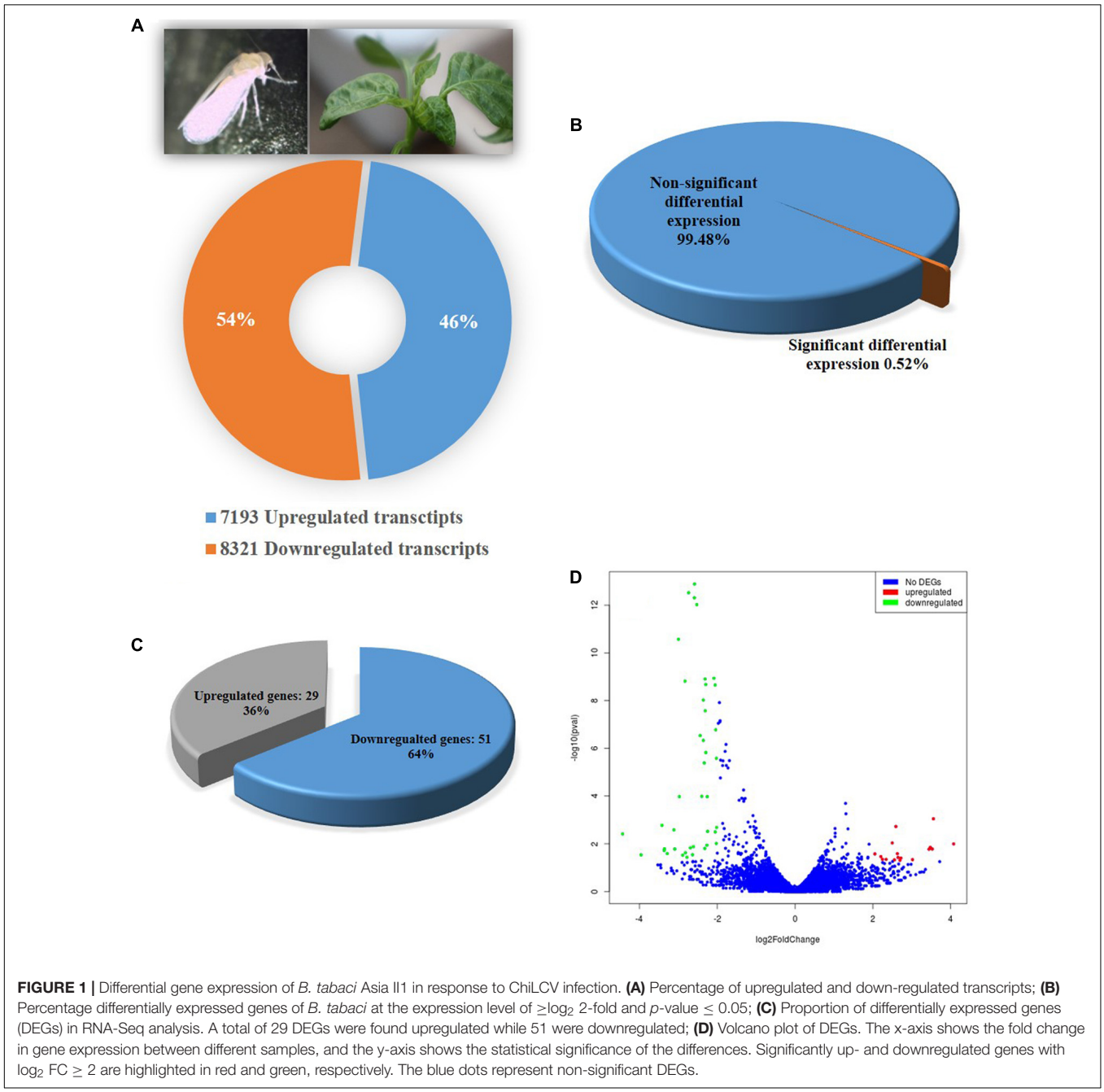

FIGURE 1 | Differential gene expression of *B. tabaci* Asia II1 in response to ChiLCV infection. **(A)** Percentage of upregulated and down-regulated transcripts; **(B)** Percentage differentially expressed genes of *B. tabaci* at the expression level of $\geq \log_2$ 2-fold and p-value ≤ 0.05; **(C)** Proportion of differentially expressed genes (DEGs) in RNA-Seq analysis. A total of 29 DEGs were found upregulated while 51 were downregulated; **(D)** Volcano plot of DEGs. The x-axis shows the fold change in gene expression between different samples, and the y-axis shows the statistical significance of the differences. Significantly up- and downregulated genes with $\log_2$ FC ≥ 2 are highlighted in red and green, respectively. The blue dots represent non-significant DEGs.

TABLE 2 | Differentially expressed upregulated and downregulated genes of *B. tabaci* Asia II 1 in response to ChiLCV infection.

Sl No.	Gene ID	Gene name	GO term	Log_2 fold change	*P*-value
Upregulated genes					
1	Bta12916	Toll receptor 3	Involved in control host immune response, activated by double-stranded RNA, a sign of viral infection	3.6	0.0009
2	Bta06925	Cytosolic carboxypeptidase 3	Catalyzes the deglutamylation of polyglutamate side chains generated by post-translational polyglutamylation in proteins such as tubulins	2.6	0.001
3	Bta15365	Dynein heavy chain	Involved in ATPase activity, plays a major role in sperm motility, implicated in sperm flagellar assembly and beating	4.1	0.01
4	Bta07280	Tob1	Plays an important role in controlling cell cycle progression, suppressing tumor development	3.4	0.01
5	Bta00655	GMP reductase	Functions in the conversion of nucleobase, nucleoside, and nucleotide derivatives of G to A nucleotides, and in maintaining the intracellular balance of A and G nucleotides	3.5	0.014
6	Bta13317	Replication factor A	Plays an essential role in DNA replication, recombination, and repair. Binds and stabilizes single-stranded DNA intermediates	3.5	0.016
7	Bta00469	Fasciclin 2	Homophilic cell adhesion *via* plasma membrane adhesion molecule, synapse organization	2.6	0.02
8	Bta06684	Estrogen sulfotransferase	Catalyzes the sulfate conjugation of many hormones, neurotransmitters, drugs, and xenobiotic compounds	2.3	0.04
9	Bta02631	Deoxyribonuclease I	Cleaves protein-free DNA, involved in cell death by apoptosis. Together with DNASE1L3, plays a key role in degrading neutrophil extracellular traps	2.2	0.04
10	Bta07061	Unknown protein	-	2.5	0.009
11	Bta03305	Unknown protein	-	2.1	0.02
12	Bta15645	Unknown protein	-	2.7	0.03
13	Bta12076	Unknown protein	-	2.6	0.03
14	Bta09526	Unknown protein	-	2.2	0.034
15	Bta08486	Unknown protein	-	3	0.04
16	Bta10794	Unknown protein	-	2.7	0.04
17	Bta11684	Unknown protein	-	2.6	0.04
Downregulated genes					
18	Bta00788	Protein argonaute 2	RNA interference (RNAi) pathway. A member of the RNA-induced transcriptional silencing (RITS) complex	−2.6	1.30E-13
19	Bta09958	Protein argonaute 2	Involved in RNA interference (RNAi) pathway. A member of the RNA-induced transcriptional silencing (RITS) complex	−3	2.70E-11
20	Bta07464	Pupal cuticle protein 36	Component of the pupal abdominal endocuticle. May have an important role in the larval and adult exoskeleton structure.	−2.6	2.54E-09
21	Bta05467	Major royal jelly protein	Induces the differentiation of honeybee larvae into queens through an Egfr-mediated signaling pathway	−3	0.0001
22	Bta10408	Prolyl 4-hydroxylase alpha-1 subunit	Iron ion binding, L-ascorbic acid-binding, procollagen proline 4 dioxygenase activity	−3.1	0.01
23	Bta13082	Endochitinase A	Involved in cortical microtubule organization	−2.6	0.013
24	Bta15272	Inhibin beta chain	Germ cell development and maturation, nerve cell survival, embryonic axial development	−2.7	0.014
25	Bta05443	T-box transcription factor TBX20	Acts as a transcriptional activator and repressor required for cardiac development and may have key roles in the maintenance of functional and structural phenotypes in adult heart	−3.4	0.016
26	Bta10856	Protein phosphatase 1L	Acts as a suppressor of the SAPK signaling pathways by associating with and dephosphorylating MAP3K7/TAK1 and MAP3K5, and by attenuating the association between MAP3K7/TAK1 and MAP2K4 or MAP2K6.	−3.4	0.019
27	Bta07414	Neurobeachin-like protein 1	Protein kinase binding and protein localization	−3.3	0.02
28	Bta01185	Anther-specific proline-rich protein	Serine type endopeptidase involved in inhibitor activity	−2.8	0.02
29	Bta03315	Adenosine deaminase	Plays an important role in purine metabolism and adenosine homeostasis	−2.6	0.028
30	Bta01284	AGAP004475-PA	Unreviewed	−4	0.029
31	Bta03804	AT-rich interactive domain-containing protein	Transcription factor which may be involved in the control of cell cycle progression by the RB1/E2F1 pathway and in B-cell differentiation	−2.9	0.03
32	Bta11712	Klingon	Axon guidance receptor activity, hemophilic cell adhesion *via* plasma membrane adhesion molecule	−2.8	0.03

(Continued)

TABLE 2 | (Continued)

Sl No.	Gene ID	Gene name	Go term	Log_2 fold change	*P*-value
33	Bta14472	Homeobox protein Hox-A2	Play a crucial role in several biological processes like control of cell identity, cell growth, and differentiation, cell to cell, and cell to extracellular matrix interactions	−2.2	0.01
34	Bta00780	Unknown protein	-	−2.7	3.02E-13
35	Bta04905	Unknown protein	-	−2.8	1.53E-09
36	Bta00785	Unknown protein	-	−3.4	0.001
37	Bta09990	Unknown protein	-	−4.4	0.003

involved in receptor binding, antigen binding, epithelial cell differentiation, extracellular matrix organization, cell-to-cell, and cell-surface receptor signaling. Besides, a large number of orphan genes were significantly regulated in *B. tabaci* post 6 h of ChiLCV acquisition.

Differentially Expressed Genes in *Bemisia tabaci* Post-ChiLCV Acquisition

A total of 16 known genes were found to be upregulated in adult *B. tabaci* at an early stage of ChiLCV infection. The key upregulated genes included dual-specificity protein phosphatase 10 (DUSP10)-like, dual-specificity protein phosphatase 15 (DUSP15)-like, estrogen sulfotransferase (Ste), cytosolic carboxypeptidase 3 (AGBL3)-like, fasciclin 2 (Fas2), Tob1, GMP reductase 1 (GMPR), dentin sialophosphoprotein (DSPP), toll receptor 3 (TLR3), dynein axonemal heavy chain 17 (DNAH17), ATP-dependent DNA helicase (DDX11), WAS/WASL-interacting protein family member 1 (WIPF1), proline-rich extensin protein EPR1 (EPR1), CG13607, and glutamyl-tRNA(Gln) amidotransferase subunit A (QRSL1).

Twenty-three genes were significantly downregulated in *B. tabaci* adults post 6 h of ChiLCV acquisition. Putative genes of *B. tabaci* such as nose resistant to fluoxetine protein 6 (nrf-6), protein masquerade (mas), protein argonaute 2 (AGO2), endochitinase A (CHIA), pupal cuticle protein 36 (PCP36), keratinocyte proline-rich protein (KPRP), adenylate cyclase, juvenile hormone acid O-methyltransferase (jhamt), T-box transcription factor TBX20 (TBX20), 1-acyl-sn-glycerol-3-phosphate acyltransferase (plsC), AGAP004475-PA, protein phosphatase 1L (PPM1L), neurobeachin-like protein 1 (NBEAL1), major royal jelly protein (MRJP), prolyl 4-hydroxylase alpha-1 subunit (P4HA1), AT-rich interactive domain-containing protein (ARID), Klingon (klg), inhibin beta chain (Actbeta), adenosine deaminase (ADA), chloroquine resistance marker protein, leptin receptor (LEPR), and homeobox protein Hox-A2 (HOXA2) could be seen significantly downregulated in response to ChiLCV infection.

Differentially Expressed Orphan Genes in *Bemisia tabaci* Post-ChiLCV Acquisition

Among the 80 differentially expressed transcripts, 50 (16 upregulated and 34 downregulated) transcripts could not be annotated based on nucleotide similarity against *B. tabaci* genome database[5]. When searched for nucleotide similarity at NCBI RefSeq non-redundant protein database, 43 (16 upregulated and 27 downregulated) transcripts did not show any similarity to known proteins. Out of the 16 upregulated genes, 9 genes showed similarity with unknown protein-coding genes. Whereas, 8 genes out of 27 downregulated genes showed similarity with unknown protein-coding genes. In common, 13 upregulated and 22 downregulated transcripts in adult *B. tabaci* could not be assigned any annotation. These genes were depicted as orphan genes that were differentially expressed in response to ChiLCV infection.

Functional Analysis of Differentially Expressed Genes

Based on the GO study, the DEGs were categorized into cellular components, biological processes, and molecular functions (**Figure 2**). A total of 38 genes were categorized under biological processes (47.5%) followed by cellular components (24 genes, 30%) and molecular functions (18 genes, 22.5%). In the biological processes, genes involved in the metabolic process (24%), cellular process (24%), biological regulation (16%), regulation of biological process (16%), signaling (8%), response to stimulus (8%), growth (2%), and cell proliferation (2%) were highly enriched. Similarly, genes associated with catalytic activity (28%), protein-containing complex (12%), organelle (12%), cell part (12%), cell (12%), membrane (6%), membrane part (6%), extracellular regions (6%), organelle part (3%), and extracellular region part (3%) were differentially enriched under cellular components category. In the molecular functions category, binding (67%), transcription regulator activity (22%), and molecular function regulator (11%) were enriched significantly.

Kyoto Encyclopedia of Genes and Genomes Pathway Analysis of Differentially Expressed Genes

KEGG pathway analysis of differentially expressed genes showed that a total of 17 DEGs in *B. tabaci* were involved in different functions like metabolism, signaling pathways, and cellular processes. The metabolic pathways that were majorly affected by the DEGs were metabolic pathways, TGF-beta signaling pathway, signaling pathways regulating pluripotency of stem

[5]http://www.whiteflygenomics.org/cgi-bin/bta/blast.cgi

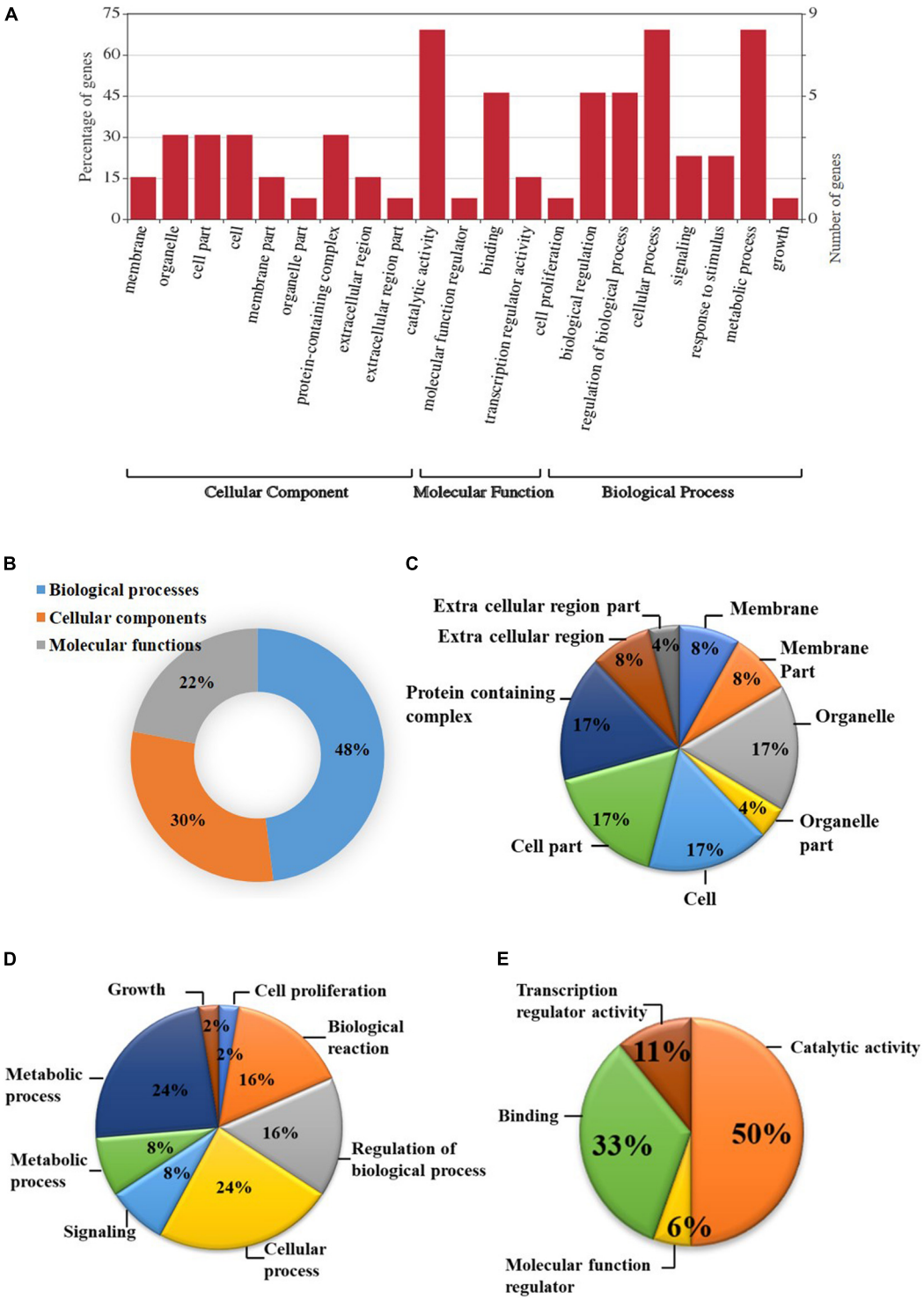

FIGURE 2 | Gene ontology (GO) enrichment analysis of differentially expressed genes (DEGs). **(A)** DEGs were characterized under the cellular components, molecular functions, and biological processes based on GO analysis; **(B)** Pie chart describing the Gene Ontology (GO) analysis of differentially expressed genes (DEGs) and their distribution under different GO terms. DEGs were categorized majorly under biological processes (48%) followed by cellular components (30%), and molecular functions (22%); **(C)** A major category of DEGs fall under cellular processes in which most of the DEGs belongs to cell, cell part, organelle, and protein-containing complex (17%) followed by membrane, membrane part, and extracellular region (8%); **(D)** In biological processes, cellular and metabolic processes (24%), regulation of biological process, and biological reaction (16%), etc. were enriched; **(E)** DEGS categorized under molecular functions were mainly distributed under catalytic activity (50%), binding (33%), transcription regulator activity (11%), and molecular function regulator (6%).

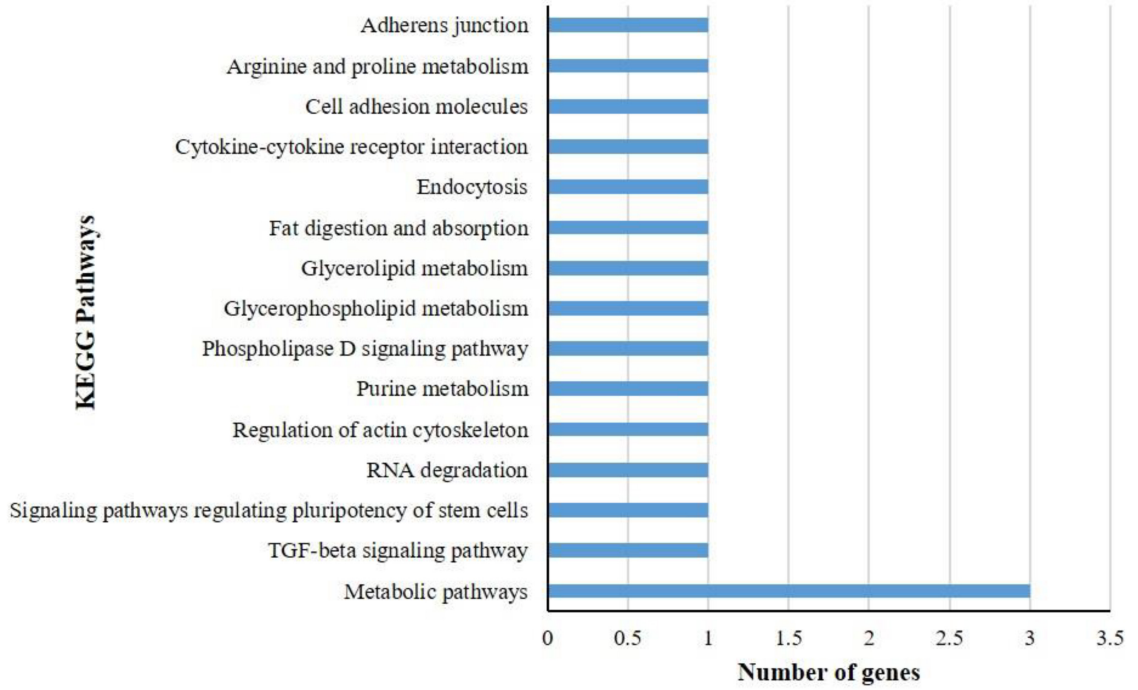

FIGURE 3 | KEGG pathway analysis of differentially expressed genes (DEGs) of *B. tabaci* Asia II 1 at an early stage of ChiLCV infection. KEGG pathway analysis of DEGs showed that the genes were involved in the functions like metabolic pathways, biosynthesis of secondary metabolites, signaling pathways, and actin cytoskeleton regulation in which mostly DEGs were involved in metabolic pathways.

cells, RNA degradation, regulation of actin cytoskeleton, purine metabolism, phospholipase D signaling pathway, glycerophospholipid metabolism, glycerolipid metabolism, fat digestion and absorption, endocytosis, cytokine-cytokine receptor interaction, cell adhesion molecules, arginine and proline metabolism, and adherens junction (**Figure 3**). The pathways identified in GO enrichment analysis were consistent with the findings of the KEGG pathway study.

Validation of Gene Expression in Reverse Transcription-Quantitative Polymerase Chain Reaction

To validate the differential expression of *B. tabaci* genes in response to ChiLCV infection, 20 highly regulated genes of *B. tabaci* were selected and mRNA expression levels were quantified in RT-qPCR. The primer pairs that produced a single sharp amplicon at the same PCR conditions for endogenous control (β-actin) primers were selected for RT-qPCR assay. Primer pair, AG177F and AG178R (**Supplementary Table 1**) specific to β-actin produced sharp bands at annealing temperatures of 54–59°C. The annealing temperature of target genes was standardized within the same temperature range. One primer pair for each of the target genes was optimized for RT-qPCR assay (**Supplementary Table 1**). The relative expression of a target gene was estimated using the $2^{-\Delta\Delta\ C_T}$ method (Roy et al., 2021). The C_T value of β-actin was used to normalize variation among biological replicates. Among the highly regulated genes that were selected for the RT-qPCR assay, the genes like Fas2-like (Bta00469) showed the highest regulation at an early stage of ChiLCV infection. The mRNA expression level of Fas2-like was upregulated by 4.518-fold in the RT-qPCR assay. TLR3 (Bta12916) was another upregulated gene with $\log_2$ 3.517-fold change in mRNA expression in response to ChiLCV infection. The mRNA expression of replication factor A protein 1 (RFA1) was upregulated by $\log_2$ 0.403-fold in ChiLCV-exposed *B. tabaci* adults in comparison to non-exposed adults. As a result of exposure to ChiLCV, the expression of GMPR of *B. tabaci* (Bta00655) was elevated by a factor of $\log_2$ 2.246-fold. Expression of protein Tob1 (Bta07280) was also augmented by $\log_2$ 1.34-fold at an early stage of ChiLCV infection. Likewise, the mRNA expression levels of a few other genes like AGBL3-like (Bta06925), DUSP10-like (Bta09526), QRSL1 (Bta13949) were elevated by $\log_2$ 0.168, 2.593, and 0.081-fold, respectively, in the RT-qPCR assay. An uncharacterized protein, CG13607 (Bta13910) was also upregulated by $\log_2$ 1.74-fold in the ChiLCV-exposed *B. tabaci* population in comparison to non-exposed populations.

Among the highly downregulated genes, expression of *B. tabaci* Actbeta (Bta15272) decreased by $\log_2$ 5.982-fold in the RT-qPCR assay at an early stage of ChiLCV infection. The next highly downregulated genes in RT-qPCR were TBX20 (Bta05443) and HOXA2 (Bta14472). Expression of TBX20 and HOXA2 declined by $\log_2$ 3.517, 2.378-fold, respectively in response to ChiLCV infection. The mRNA expression level of NBEAL1 (Bta07414) was also downregulated by $\log_2$ 1.146-fold in ChiLCV-exposed *B. tabaci* in comparison to non-exposed

populations. A $\log_2$ 0.793-fold downregulation for MRJP (Bta05465) was also recorded in response to ChiLCV infection. Few other genes of *B. tabaci* like ARID (Bta03804), anther specific protein (sf2)-like (Bta01185), plsC (Bta15094) showed significant downregulations by $\log_2$ 0.241, 0.036, and 1.687-fold, respectively, in RT-qPCR assay post-ChiLCV exposure.

All the primer pairs for the target and endogenous control genes produced single specific peaks without any secondary amplifications in the RT-qPCR melting curve analysis that indicated the specificity of the reactions. The melting temperatures of RT-qPCR amplicons were listed in **Supplementary Table 1**. The melt curve of each reaction has been provided as **Supplementary Figure 1**. The relative expression of selected *B. tabaci* genes in response to ChiLCV infection substantiated the RNA-Seq analysis (**Figure 4**).

DISCUSSION

The molecular interactions between *B. tabaci* cryptic species and begomoviruses are not universal (Czosnek et al., 2017) and not much is known about the interaction of ChiLCV with *B. tabaci*. For successful transmission, the begomovirus particles need to reach the salivary glands of *B. tabaci*. It takes 4–7 h after the onset of feeding to be circulated through hemolymph in coated vesicles and translocated into the primary salivary glands (Czosnek et al., 2002). In our recent study, ChiLCV copies were estimated in individual *B. tabaci* at different exposure of active acquisition feeding (Roy et al., 2021). A 6 h sacquisition was found adequate for the successful transmission of ChiLCV by *B. tabaci* Asia II 1 (Senanayake et al., 2012; Roy et al., 2021). About 7.86×10^{13} copies of ChiLCV can be acquired by an individual *B. tabaci* adult female during 6 h of feeding on an infected chilli leaf (Roy et al., 2021). Comparison between ChiLCV-exposed and non-exposed *B. tabaci* transcripts post-6 h of acquisition revealed differential expression of 80 DEGs involved in replication factor, cell adhesion receptor, and intracellular trafficking. GO analysis indicated the majority of the DEGs were involved in biological processes followed by cellular components and molecular functions. KEGG pathway analysis showed that the majority of the DEGs were involved in the metabolic pathways of *B. tabaci*.

The key upregulated genes included TLR3, Fas2, GMPR, RFA1, Tob 1, DUSP, DNAH17, AGBL3, and QRSL1. Several genes of *B. tabaci* that were related to immune response pathways such as TLR3, Fas2, RFA1, and GMPR were induced in response to ChiLCV infection. Toll receptors are important parts of the insect's innate immune system by triggering a cascade of signaling pathways. In mammals, it induces interferons to confer antiviral resistance (Ozato et al., 2002). Toll receptors might have a function in limiting the virus infection in vector and upregulation of TLR3 might be activated upon ChiLCV infection to preclude the adverse effect of the virus on the vector. Another component of *B. tabaci* immunoglobulin (Ig)-related superfamily, Fas2 was upregulated post-exposure to the ChiLCV in the present study. Fas2 belongs to the superfamily of cell adhesion receptors with structural similarity to the vertebrate receptor NCAM (Grenningloh et al., 1990; Brummendorf and Rathjen, 1993). NCAM molecules also have a role in viral attachment to promote virus penetration into the host cells but inhibit the replication of rabies virus *via* induction of interferon β (Hotta et al., 2007), which is mainly involved in innate immunity against viral infection. Silencing Fas 2 using dsRNA results in an increase of ChiLCV copies in *B. tabaci* Asia II 1 (Chakraborty and Ghosh, 2022). This suggests that upregulation of Fas2 transcripts in *B. tabaci* post-ChiLCV infection is due to the innate immune response against the virus infection. GMPR plays an important role in the purine salvage pathway and regulates intracellular purine nucleotides. Besides, it has a role in host innate immunity (Imamura et al., 2020). Upregulation of this gene after ChiLCV exposure indicated induction of defense in *B. tabaci* upon ChiLCV exposure. RFA1 is an ssDNA binding protein (Wold, 1997). Although replication factors play an important role in DNA replication, recombination, and repair (Vanoli et al., 2010; Yamamoto et al., 2019), ChiLCV-DNA does not replicate within the vector (Rosen et al., 2015; Ghosh et al., 2021). This rejected the possibility of involvement of RFA1 in virus multiplication in *B. tabaci*. Although not confirmed, upregulation of RFA1 the ChiLCV-exposure might be due to the employment of innate immune response by *B. tabaci* to protect itself from virus nuclease attack.

Some genes such as Tob1 and DUSP10 having a functional role in the virus lifecycle were also upregulated to favor virus transcription. Gene encoding Tob1 protein was found upregulated in *B. tabaci* post-ChiLCV exposure. Overexpression of Tob1 suppresses cell growth (Shan et al., 2009). The upregulation of this gene in the current study might lead to cellular dysfunction in *B. tabaci* to favor ChiLCV infection. DUSP10, also called MPK5 is involved in the regulation of mitogen-activated protein kinases. These proteins are the major modulators of critical signaling pathways that are dysregulated in various biotic stresses (Patterson et al., 2009). DUSP facilitates vaccinia virus transcription (Liu et al., 1995). Upregulation of this gene indicated the activation of signaling cascades in response to ChiLCV infection and functional role in the virus lifecycle in *B. tabaci*.

Expression of *B. tabaci* putative genes like DNAH17, AGBL3, and QRSL1 was manipulated by ChiLCV to facilitate its circulation within the vector. Several viruses access dynein to mediate the viral replication processes. Silencing of dynein reduced the infection of Murine leukemia virus (Valle-Tenney et al., 2016). Carboxypeptidases play an important role in the stimulation of slow migrating forms of cowpea mosaic virus (CPMV) to fast migrating CPMV leading to increased infectivity (Niblett and Semancik, 1969). Upregulation of DNAH17 and AGBL3 post-ChiLCV exposure in the present study might be due to the manipulation of *B. tabaci* genes by ChiLCV to facilitate the infection and circulation of the virus within the vector. QRSL1 is a highly conserved protein throughout eukaryotes and prokaryotes. This gene is essential for the proper translation of the proteins (Morris et al., 2008). Upregulation of this gene post-ChiLCV exposure might be due to the utilization of host translation apparatus by the virus.

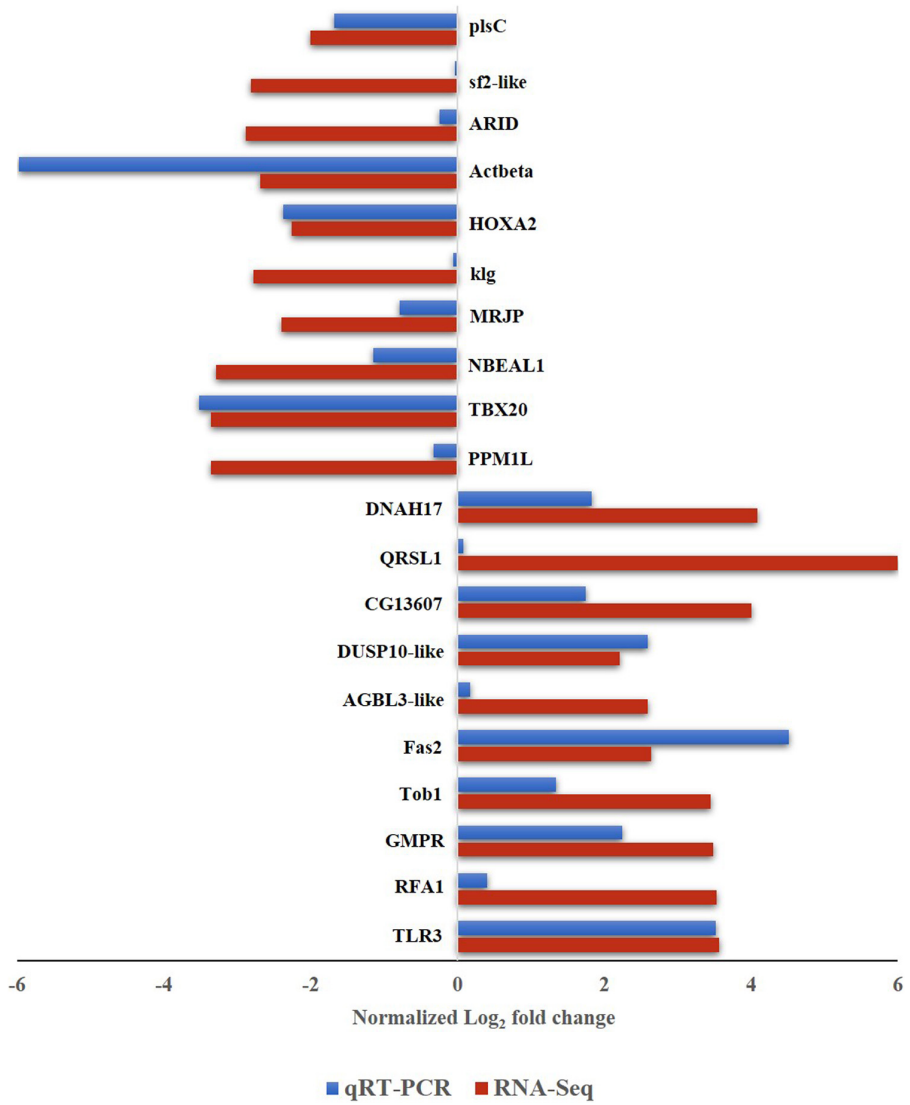

FIGURE 4 | Expression of *B. tabaci* Asia II 1 putative genes in response to ChiLCV infection in RNA-Seq and RT-qPCR. The values of log_2-fold changes calculated in RNA-Seq analysis were in accordance with the RT-qPCR fold change values.

Other than the above-mentioned upregulated genes, a few immune-associated genes like AGO2, PPM1L, NBEAL1, TBX20, and Actbeta were downregulated in *B. tabaci* upon ChiLCV exposure. AGO2 is a major component of the RNA-induced silencing complex (RISC). In *Drosophila*, loss of function of AGO2 leads to susceptibility against Drosophila C virus and Cricket paralysis virus (Van Rij et al., 2006). PPM1L is known to be associated with the replication of viruses like HIV-1, HIV-2, Ebola virus, papovavirus, adenovirus, and rift valley fever virus (Brown et al., 1994; Modrof et al., 2002; Nekhai et al., 2007; Zeng et al., 2009; Baer et al., 2016). Neurobeachin is a peripheral membrane protein of the BEACH domain protein family that is involved in the subcellular targeting of membrane proteins (De Lozanne, 2003). Increased expression of neurobeachin was recorded in stimulated immune cells (Wang et al., 2001, 2004). As an essential factor of autoimmunity, TBX20 produces IgG2a *via* activation of B cells during viral infection (Rubtsova et al., 2013). Inhibin plays an important function in immunological cell development (Licona-Limon and Soldevila, 2007). Lack of plsC activity increased the virulence and infectivity of coxsackievirus (Karlsson et al., 2009). Downregulation of these immune-associated genes in *B. tabaci* post-ChiLCV acquisition indicated a possibility of suppression of vector immune response by ChiLCV to become circulative in its vector.

Transcription regulatory genes like HOXA2, klg, and ARID were also downregulated to support ChiLCV entry and movement within *B. tabaci*. Homeobox proteins are transcriptional factors that regulate several genes in insects (Cillo et al., 2001). In tomatoes, homeobox protein was found to be involved in limiting programmed cell death that limits

pathogens (Mayda et al., 1999). In ChiLCV-exposed *B. tabaci*, downregulation of HOXA2 might be due to the suppression activity of ChiLCV that triggered the repression in *B. tabaci*. Klg is a CAM orthologue in insects that is required for photoreceptors and the prevention of excessive synapses (Shimozono et al., 2019). Upon infection of human cytomegalovirus (HCMV), klg is downregulated and causes increased adhesion of the virus to the tumor cells and transendothelial penetration (Blaheta et al., 2004). Downregulation of klg might help the binding and cellular entry of ChiLCV. ARID contains a DNA binding domain (Patsialou et al., 2005) and is an important factor for development, tissue-specific gene expression, and cell growth regulation (Kortschak et al., 2000; Wilsker et al., 2002). This gene is also involved in transcriptional activation and repression of genes through chromatin remodeling (Zhang et al., 2016). Repression of ARID in *B. tabaci* might favor ChiLCV entry and movement within the vector.

Putative genes that code for anther specific protein, major royal jelly protein, and CG13607 were also differentially expressed in *B. tabaci* at an early stage of ChiLCV infection. Although these genes have been characterized in other insects, their functions in *B. tabaci* and begomovirus transmission are yet to be explored. The expression of several orphan genes in *B. tabaci* Asia II 1 was also modulated upon ChiLCV exposure. Functional validation of these orphan genes in *B. tabaci* Asia II 1 and their role in virus transmission need further in-depth study.

CONCLUSION

In conclusion, we have assembled a whole-body transcriptome of *B. tabaci* Asia II 1. Several genes of *B. tabaci* associated with innate immune response, cell adhesion, and intracellular trafficking were regulated in response to ChiLCV infection to facilitate its survival and circulation within the vector, *B. tabaci*. The present study helps in understanding the network of molecular interactions between *B. tabaci* Asia II 1 and ChiLCV. Data generated in this study will enrich genomic information of whitefly and will enable future functional studies. The candidate genes of *B. tabaci* that are involved in key physiological processes and ChiLCV transmission would be novel targets for sustainable management of the whitefly-begomovirus complex.

DATA AVAILABILITY STATEMENT

The datasets generated during the current study are available in the NCBI with BioProject ID PRJNA759071.

AUTHOR CONTRIBUTIONS

AG conceived and designed the research and wrote and edited the final manuscript. AN and PC conducted the experiments, recorded the experimental data, and wrote the draft manuscript. AN, PC, MI, and SJ performed the analysis. AG and VB reviewed the data. All authors read and approved the manuscript.

FUNDING

The fellowship of AN was supported by Indian Council of Agricultural Research, New Delhi.

ACKNOWLEDGMENTS

The authors are thankful to Subhash Chander (NRCIPM) and Vinay Kalia (IARI) for their advisories. The support received from IARI, New Delhi is thankfully acknowledged.

SUPPLEMENTARY MATERIAL

The Supplementary Material for this article can be found online at: https://www.frontiersin.org/articles/10.3389/fmicb.2022.890807/full#supplementary-material

REFERENCES

Akhter, A., Qazi, J., Saeed, M., and Mansoor, S. (2009). A severe leaf curl disease on chilies in Pakistan is associated with multiple begomovirus components. *Plant Dis.* 93, 962–962. doi: 10.1094/PDIS-93-9-0962B

Baer, A., Shafagati, N., Benedict, A., Ammosova, T., Ivanov, A., Hakami, R. M., et al. (2016). Protein phosphatase-1 regulates Rift Valley fever virus replication. *Antiv. Res.* 127, 79–89. doi: 10.1016/j.antiviral.2016.01.007

Barman, M., Samanta, S., Thakur, H., Chakraborty, S., Samanta, A., Ghosh, A., et al. (2021). Effect of neonicotinoids on bacterial symbionts and insecticide-resistant gene in whitefly, *Bemisia tabaci*. *Insects* 12:742. doi: 10.3390/insects12080742

Blaheta, R. A., Beecken, W. D., Engl, T., Jonas, D., Oppermann, E., Hundemer, M., et al. (2004). Human cytomegalovirus infection of tumor cells downregulates NCAM (CD56): a novel mechanism for virus-induced tumor invasiveness. *Neoplasia* 6, 323–331. doi: 10.1593/neo.03418

Bragard, C., Caciagli, P., Lemaire, O., Lopez-Moya, J. J., MacFarlane, S., Peters, D., et al. (2013). Status and prospects of plant virus control through interference with vector transmission. *Annu. Rev. Phytopathol.* 51, 177–201. doi: 10.1146/annurev-phyto-082712-102346

Briddon, R. W., Patil, B. L., Bagewadi, B., Nawaz-ul-Rehman, M. S., and Fauquet, C. M. (2010). Distinct evolutionary histories of the DNA-A and DNA-B components of bipartite begomoviruses. *BMC Evol. Biol.* 10:97. doi: 10.1186/1471-2148-10-97

Brown, J. K. (2000). Molecular markers for the identification and global tracking of whitefly vector–Begomovirus complexes. *Virus Res.* 71, 233–260. doi: 10.1016/s0168-1702(00)00221-5

Brown, J. K., Zerbini, F. M., Navas-Castillo, J., Moriones, E., Ramos-Sobrinho, R., Silva, J. C., et al. (2015). Revision of begomovirus taxonomy based on pairwise sequence comparisons. *Arch. Virol.* 160, 1593–1619. doi: 10.1007/s00705-015-2398-y

Brown, S. M., Harland, J., MacLean, A. R., Podlech, J., and Clements, J. B. (1994). Cell type and cell state determine differential in vitro growth of non-neurovirulent ICP34. 5-negative herpes simplex virus types 1 and 2. *J. Gen. Virol.* 75, 2367–2377. doi: 10.1099/0022-1317-75-9-2367

Brummendorf, T., and Rathjen, F. G. (1993). Axonal glycoproteins with immunoglobulin—and fibronectin type III—related domains in vertebrates: structural features, binding activities, and signal transduction. *J. Neurochem.* 61, 1207–1219. doi: 10.1111/j.1471-4159.1993.tb13611.x

Chakraborty, P., and Ghosh, A. (2022). Topical spray of dsRNA induces mortality and inhibits chilli leaf curl virus transmission by *Bemisia tabaci* Asia II 1. *Cells* 11:833. doi: 10.3390/cells11050833

Chen, W., Hasegawa, D. K., Kaur, N., Kliot, A., Pinheiro, P. V., Luan, J., et al. (2016). The draft genome of whitefly *Bemisia tabaci* MEAM1, a global crop pest, provides novel insights into virus transmission, host adaptation, and insecticide resistance. *BMC Biol.* 14:110. doi: 10.1186/s12915-016-0321-y

Cillo, C., Cantile, M., Faiella, A., and Boncinelli, E. (2001). Homeobox genes in normal and malignant cells. *J. Cell. Physiol.* 188, 161–169. doi: 10.1002/jcp.1115

Cornejo-Franco, J. F., Reyes-Proaño, E. G., Mollov, D., Mowery, J., and Quito-Avila, D. F. (2022). Transmission and pathogenicity of papaya virus E: insights from an experimental papaya orchard. *Plant Dis.* 106:685–690. doi: 10.1094/PDIS-08-21-1785-RE

Costa, T. M., Inoue-Nagata, A. K., Vida, A. H., Ribeiro, S. G., and Nagata, T. (2020). The recombinant isolate of cucurbit aphid-borne yellows virus from Brazil is a polerovirus transmitted by whiteflies. *Plant Pathol.* 69, 1042–1050. doi: 10.1111/ppa.13186

Czosnek, H., and Ghanim, M. (2012). Back to basics: are begomoviruses whitefly pathogens. *J. Integr. Agric.* 11, 225–234. doi: 10.1016/S2095-3119(12)60007-0

Czosnek, H., Ghanim, M., and Ghanim, M. (2002). The circulative pathway of begomoviruses in the whitefly vector *Bemisia tabaci*-insights from studies with tomato yellow leaf curl virus. *Ann. Appl. Biol.* 140, 215–231. doi: 10.1111/j.1744-7348.2002.tb00175.x

Czosnek, H., Hariton-Shalev, A., Sobol, I., Gorovits, R., and Ghanim, M. (2017). The incredible journey of begomoviruses in their whitefly vector. *Viruses* 9:273. doi: 10.3390/v9100273

Dasgupta, I., Malathi, V. G., and Mukherjee, S. K. (2003). Genetic engineering for virus resistance. *Curr. Sci.* 84, 341–354.

De Lozanne, A. (2003). The role of BEACH proteins in *Dictyostelium*. *Traffic* 4, 6–12. doi: 10.1034/j.1600-0854.2003.40102.x

Ding, T. B., Li, J., Chen, E. H., Niu, J. Z., and Chu, D. (2019). Transcriptome profiling of the whitefly *Bemisia tabaci* MED in response to single infection of tomato yellow leaf curl virus, tomato chlorosis virus, and their co-infection. *Front. Physiol.* 10:302. doi: 10.3389/fphys.2019.00302

Fereres, A., and Raccah, B. (2015). *Plant Virus Transmission by Insects, eLS*. Chichester: John Wiley & Sons, doi: 10.1002/9780470015902.a0000760.pub3

Ghosh, A., Roy, B., Nekkanti, A., Dhar, S., and Mukherjee, S. (2021). Transovarial transmission of dolichos yellow mosaic virus by its vector, *Bemisia tabaci* Asia II 1. *Front. Microbiol.* 12:755155. doi: 10.3389/fmicb.2021.755155

Ghosh, S., Kanakala, S., Lebedev, G., Kontsedalov, S., Silverman, D., Alon, T., et al. (2019). Transmission of a new polerovirus infecting pepper by the whitefly *Bemisia tabaci*. *J. Virol.* 93:e00488-19. doi: 10.1128/JVI.00488-19

Gorman, K., Slater, R., Blande, J. D., Clarke, A., Wren, J., McCaffery, A., et al. (2010). Cross-resistance relationships between neonicotinoids and pymetrozine in *Bemisia tabaci* (Hemiptera: Aleyrodidae). *Pest Manage. Sci.* 66, 1186–1190. doi: 10.1002/ps.1989

Götz, M., Popovski, S., Kollenberg, M., Gorovits, R., Brown, J. K., Cicero, J. M., et al. (2012). Implication of *Bemisia tabaci* heat shock protein 70 in begomovirus-whitefly interactions. *J. Virol.* 86, 13241–13252. doi: 10.1128/JVI.00880-12

Grenningloh, G., Bieber, A. J., Rehm, E. J., Snow, P. M., Traquina, Z. R., Hortsch, M., et al. (1990). Molecular genetics of neuronal recognition in *Drosophila*: evolution and function of immunoglobulin superfamily cell adhesion molecules. *Cold Spring Harb. Symp. Quant. Biol.* 55, 327–340. doi: 10.1101/sqb.1990.055.01.034

Hasegawa, D. K., Chen, W., Zheng, Y., Kaur, N., Wintermantel, W. M., Simmons, A. M., et al. (2018). Comparative transcriptome analysis reveals networks of genes activated in the whitefly, *Bemisia tabaci* when fed on tomato plants infected with tomato yellow leaf curl virus. *Virology* 513, 52–64. doi: 10.1016/j.virol.2017.10.008

Hotta, K., Motoi, Y., Okutani, A., Kaku, Y., Noguchi, A., Inoue, S., et al. (2007). Role of GPI-anchored NCAM-120 in rabies virus infection. *Microbes Infect.* 9, 167–174. doi: 10.1016/j.micinf.2006.11.003

Imamura, A., Okada, T., Mase, H., Otani, T., Kobayashi, T., Tamura, M., et al. (2020). Allosteric regulation accompanied by oligomeric state changes of *Trypanosoma brucei* GMP reductase through cystathionine-β-synthase domain. *Nat. Commun.* 11:1837. doi: 10.1038/s41467-020-15611-3

Jones, D. R. (2003). Plant viruses transmitted by whiteflies. *Eur. J. Plant Pathol.* 109, 195–219.

Kanakala, S., and Ghanim, M. (2016). Implication of the whitefly *Bemisia tabaci* cyclophilin B protein in the transmission of tomato yellow leaf curl virus. *Front. Plant Sci.* 7:1702. doi: 10.3389/fpls.2016.01702

Karlsson, E. A., Wang, S., Shi, Q., Coleman, R. A., and Beck, M. A. (2009). Glycerol-3-phosphate acyltransferase 1 is essential for the immune response to infection with coxsackievirus B3 in mice. *J. Nutr.* 139, 779–783. doi: 10.3945/jn.108.101683

Kaur, N., Chen, W., Zheng, Y., Hasegawa, D. K., Ling, K. S., Fei, Z., et al. (2017). Transcriptome analysis of the whitefly, *Bemisia tabaci* MEAM1 during feeding on tomato infected with the crinivirus, *Tomato chlorosis virus*, identifies a temporal shift in gene expression and differential regulation of novel orphan genes. *BMC Genomics* 18:370. doi: 10.1186/s12864-017-3751-1

Kortschak, R. D., Tucker, P. W., and Saint, R. (2000). ARID proteins come in from the desert. *Trends Biochem. Sci.* 25, 294–299. doi: 10.1016/s0968-0004(00)01597-8

Legarrea, S., Barman, A., Marchant, W., Diffie, S., and Srinivasan, R. (2015). Temporal effects of a Begomovirus infection and host plant resistance on the preference and development of an insect vector, *Bemisia tabaci*, and implications for epidemics. *PLoS One* 10:e0142114. doi: 10.1371/journal.pone.0142114

Licona-Limon, P., and Soldevila, G. (2007). The role of TGF-β superfamily during T cell development: new insights. *Immun. Lett.* 109, 1–12. doi: 10.1016/j.imlet.2006.12.010

Liu, K., Lemon, B., and Traktman, P. (1995). The dual-specificity phosphatase encoded by vaccinia virus, VH1, is essential for viral transcription in vivo and in vitro. *J. Virol.* 69, 7823–7834. doi: 10.1128/JVI.69.12.7823-7834.1995

Livak, K. J., and Schmittgen, T. D. (2001). Analysis of relative gene expression data using real-time quantitative PCR and the 2- ΔΔCT method. *Methods* 25, 402–408. doi: 10.1006/meth.2001.1262

Luan, J. B., Li, J. M., Varela, N., Wang, Y. L., Li, F. F., Bao, Y. Y., et al. (2011). Global analysis of the transcriptional response of whitefly to tomato yellow leaf curl china virus reveals the relationship of coevolved adaptations. *J. Virol.* 85, 3330–3340. doi: 10.1128/JVI.02507-10

Mayda, E., Tornero, P., Conejero, V., and Vera, P. (1999). A tomato homeobox gene (HD−Zip) is involved in limiting the spread of programmed cell death. *Plant J.* 20, 591–600. doi: 10.1046/j.1365-313x.1999.00633.x

Menike, G. D. N., and De Costa, D. M. (2017). Variation of field symptoms and molecular diversity of the virus isolates associated with chilli leaf curl complex in different agroecological regions of Sri Lanka. *Trop. Agric. Res.* 28, 144–161. doi: 10.4038/tar.v28i2.8192

Milenovic, M., Wosula, E. N., Rapisarda, C., and Legg, J. P. (2019). Impact of host plant species and whitefly species on feeding behavior of *Bemisia tabaci*. *Front. Plant Sci.* 10:1. doi: 10.3389/fpls.2019.00001

Modrof, J., Mu, E., Klenk, H. D., and Becker, S. (2002). Phosphorylation of VP30 impairs Ebola virus transcription. *J. Biol. Chem.* 277, 33099–33104. doi: 10.1074/jbc.M203775200

Moriya, Y., Itoh, M., Okuda, S., Yoshizawa, A., and Kanehisa, M. (2007). KAAS: an automatic genome annotation and pathway reconstruction server. *Nucleic Acids Res.* 35, W182–W185. doi: 10.1093/nar/gkm321

Morris, J. Z., Bergman, L., Kruyer, A., Gertsberg, M., Guigova, A., Arias, R., et al. (2008). Mutations in the *Drosophila* mitochondrial tRNA amidotransferase, bene/gatA, cause growth defects in mitotic and endoreplicating tissues. *Genetics* 178, 979–987. doi: 10.1534/genetics.107.084376

Navas-Castillo, J., Fiallo-Olivé, E., and Sánchez-Campos, S. (2011). Emerging virus diseases transmitted by whiteflies. *Annu. Rev. Phytopathol.* 49, 219–248. doi: 10.1146/annurev-phyto-072910-095235

Nekhai, S., Jerebtsova, M., Jackson, A., and Southerland, W. (2007). Regulation of HIV-1 transcription by protein phosphatase 1. *Curr. HIV Res.* 5, 3–9. doi: 10.2174/157016207779316279

Niblett, C. L., and Semancik, J. S. (1969). Conversion of the electrophoretic forms of cowpea mosaic virus in vivo and in vitro. *Virology* 38, 685–693. doi: 10.1016/0042-6822(69)90187-1

Oraonand, U. B., and Tarafdar, J. (2018). Occurrence and distribution of chilli leaf curl complex disease in West Bengal. *Biomed. J. Sci. Tech. Res.* 3, 3515–3519. doi: 10.26717/BJSTR.2018.3.000948

Orfanidou, C. G., Pappi, P. G., Efthimiou, K. E., Katis, N. I., and Maliogka, V. I. (2016). Transmission of Tomato Chlorosis Virus (ToCV) by *Bemisia tabaci*

biotype Q and evaluation of four weed species as viral sources. *Plant Dis.* 100, 2043–2049. doi: 10.1094/PDIS-01-16-0054-RE

Ozato, K., Tsujimura, H., and Tamura, T. (2002). Toll-like receptor signaling and regulation of cytokine gene expression in the immune system. *Biotechniques* 33, S66–S75. doi: 10.2144/Oct0208

Patsialou, A., Wilsker, D., and Moran, E. (2005). DNA-binding properties of ARID family proteins. *Nucleic Acids Res.* 33, 66–80. doi: 10.1093/nar/gki145

Patterson, K. I., Brummer, T., O'brien, P. M., and Daly, R. J. (2009). Dual-specificity phosphatases: critical regulators with diverse cellular targets. *Biochem. J.* 418, 475–489. doi: 10.1042/bj20082234

Pinheiro-Lima, B., Pereira-Carvalho, R. C., Alves-Freitas, D. M. T., Kitajima, E. W., Vidal, A. H., Lacorte, C., et al. (2020). Transmission of the bean-associated cytorhabdovirus by the whitefly *Bemisia tabaci* MEAM1. *Viruses* 12:1028. doi: 10.3390/v12091028

Qin, L., Pan, L. L., and Liu, S. S. (2016). Further insight into reproductive incompatibility between putative cryptic species of the *Bemisia tabaci* whitefly complex. *Insect Sci.* 23, 215–224. doi: 10.1111/1744-7917.12296

Rehman, M., Chakraborty, P., Tanti, B., Mandal, B., and Ghosh, A. (2021). Occurrence of a new cryptic species of *Bemisia tabaci* (Hemiptera: Aleyrodidae): an updated record of cryptic diversity in India. *Phytoparasitica* 49, 869–882. doi: 10.1007/s12600-021-00909-9

Rosen, R., Kanakala, S., Kliot, A., Pakkianathan, B. C., Farich, B. A., Santana-Magal, N., et al. (2015). Persistent, circulative transmission of begomoviruses by whitefly vectors. *Curr. Opin. Virol.* 15, 1–8. doi: 10.1016/j.coviro.2015.06.008

Roy, B., Chakraborty, P., and Ghosh, A. (2021). How many begomovirus copies are acquired and inoculated by its vector, whitefly (*Bemisia tabaci*) during feeding? *PLoS One* 16:e0258933. doi: 10.1371/journal.pone.0258933

Rubtsova, K., Rubtsov, A. V., Van Dyk, L. F., Kappler, J. W., and Marrack, P. (2013). T-box transcription factor T-bet, a key player in a unique type of B-cell activation essential for effective viral clearance. *Proc. Natl. Acad. Sci.* 110, E3216–E3224. doi: 10.1073/pnas.1312348110

Saeed, S. T., and Samad, A. (2017). Emerging threats of begomoviruses to the cultivation of medicinal and aromatic crops and their management strategies. *Virusdisease* 28, 1–17. doi: 10.1007/s13337-016-0358-0

Senanayake, D. M. J. B., Mandal, B., Lodha, S., and Varma, A. (2007). First report of *Chilli leaf curl virus* affecting chilli in India. *Plant Pathol.* 56:343. doi: 10.1111/j.1365-3059.2007.01513.x

Senanayake, D. M. J. B., Varma, A., and Mandal, B. (2012). Virus–vector relationships, host range, detection and sequence comparison of chilli leaf curl virus associated with an epidemic of leaf curl disease of chilli in Jodhpur, India. *J. Phytopathol.* 160, 146–155. doi: 10.1111/j.1439-0434.2011.01876.x

Shan, J., Zhao, W., and Gu, W. (2009). Suppression of cancer cell growth by promoting cyclin D1 degradation. *Mol. Cell* 36, 469–476. doi: 10.1016/j.molcel.2009.10.018

Shimozono, M., Osaka, J., Kato, Y., Araki, T., Kawamura, H., Takechi, H., et al. (2019). Cell surface molecule, Klingon, mediates the refinement of synaptic specificity in the *Drosophila* visual system. *Genes Cells* 24, 496–510. doi: 10.1111/gtc.12703

Simon, C., Frati, F., Beckenbach, A., Crespi, B., Liu, H., and Flook, P. (1994). Evolution, weighting, and phylogenetic utility of mitochondrial gene sequences and a compilation of conserved polymerase chain reaction primers. *Ann. Entomol. Soc. Am.* 87, 651–701. doi: 10.1093/aesa/87.6.651

Thakur, H., Jindal, S. K., Sharma, A., and Dhaliwal, M. S. (2018). Chilli leaf curl virus disease: a serious threat for chilli cultivation. *J. Plant Dis. Protect.* 125, 239–249. doi: 10.1007/s41348-018-0146-8

Valle-Tenney, R., Opazo, T., Cancino, J., Goff, S. P., and Arriagada, G. (2016). Dynein regulators are important for ecotropic murine leukemia virus infection. *J. Virol.* 90, 6896–6905. doi: 10.1128/JVI.00863-16

Van Rij, R. P., Saleh, M. C., Berry, B., Foo, C., Houk, A., Antoniewski, C., et al. (2006). he RNA silencing endonuclease Argonaute 2 mediates specific antiviral immunity in *Drosophila melanogaster*. *Genes Dev.* 20, 2985–2995. doi: 10.1101/gad.1482006

Vanoli, F., Fumasoni, M., Szakal, B., Maloisel, L., and Branzei, D. (2010). Replication and recombination factors contributing to recombination-dependent bypass of DNA lesions by template switch. *PLoS Genetics* 6:e1001205. doi: 10.1371/journal.pgen.1001205

Wang, J. W., Gamsby, J. J., Highfill, S. L., Mora, L. B., Bloom, G. C., Yeatman, T. J., et al. (2004). Deregulated expression of LRBA facilitates cancer cell growth. *Oncogene* 23, 4089–4097. doi: 10.1038/sj.onc.1207567

Wang, J. W., Howson, J., Haller, E., and Kerr, W. G. (2001). Identification of a novel lipopolysaccharide-inducible gene with key features of both A kinase anchor proteins and chs1/beige proteins. *J. Immunol.* 166, 4586–4595. doi: 10.4049/jimmunol.166.7.4586

Wang, P., Ruan, Y. M., and Liu, S. S. (2010). Crossing experiments and behavioural observations reveal reproductive incompatibility among three putative species of the whitefly *Bemisia tabaci*. *Insect Sci.* 17, 508–516. doi: 10.1111/j.1744-7917.2010.01353.x

Wang, Z. Z., Shi, M., Huang, Y. C., Wang, X. W., Stanley, D., and Chen, X. X. (2016). A peptidoglycan recognition protein acts in whitefly (*Bemisia tabaci*) immunity and involves in *Begomovirus* acquisition. *Sci. Rep.* 6:37806. doi: 10.1038/srep37806

Wei, J., Zhao, J. J., Zhang, T., Li, F. F., Ghanim, M., Zhou, X. P., et al. (2014). Specific cells in the primary salivary glands of the whitefly *Bemisia tabaci* control retention and transmission of *Begomoviruses*. *J. Virol.* 88, 13460–13468. doi: 10.1128/JVI.02179-14

Wilsker, D., Patsialou, A., Dallas, P. B., and Moran, E. (2002). ARID proteins: a diverse family of DNA binding proteins implicated in the control of cell growth, differentiation, and development. *Cell Growth Differ.* 13, 95–106.

Wold, M. S. (1997). Replication protein A: a heterotrimeric, single-stranded DNA-binding protein required for eukaryotic DNA metabolism. *Ann. Rev. Biochem.* 66, 61–92. doi: 10.1146/annurev.biochem.66.1.61

Xia, W. Q., Wang, X. R., Liang, Y., Liu, S. S., and Wang, X. W. (2017). Transcriptome analyses suggest a novel hypothesis for whitefly adaptation to tobacco. *Sci. Rep.* 7, 1–10. doi: 10.1038/s41598-017-12387-3

Yamamoto, K., Haque, M. R., and Saruta, F. (2019). Identification and expression analysis of the replication factor C protein in the silkworm, *Bombyx mori*. *J. Insect Biotechnol. Sericol.* 88, 1017–1020. doi: 10.11416/jibs.88.1_017

Zanardo, L. G., and Carvalho, C. M. (2017). Cowpea mild mottle virus (Carlavirus, Betaflexiviridae): a review. *Trop. Plant Pathol.* 42, 417–430. doi: 10.1007/s40858-017-0168-y

Zeng, Q., Huang, Y., Zeng, L., Lan, X., Huang, Y., He, S., et al. (2009). Effect of IPP5, a novel inhibitor of PP1, on apoptosis and the underlying mechanisms involved. *Biotechnol. Appl. Biochem.* 54, 231–238. doi: 10.1042/BA20090168

Zhang, Q., Yan, H. B., Wang, J., Cui, S. J., Wang, X. Q., Jiang, Y. H., et al. (2016). Chromatin remodeling gene AT-rich interactive domain-containing protein 1A suppresses gastric cancer cell proliferation by targeting PIK3CA and PDK1. *Oncotarget* 7, 46127–461141. doi: 10.18632/oncotarget.10060

Conflict of Interest: The authors declare that the research was conducted in the absence of any commercial or financial relationships that could be construed as a potential conflict of interest.

Publisher's Note: All claims expressed in this article are solely those of the authors and do not necessarily represent those of their affiliated organizations, or those of the publisher, the editors and the reviewers. Any product that may be evaluated in this article, or claim that may be made by its manufacturer, is not guaranteed or endorsed by the publisher.

Copyright © 2022 Nekkanti, Chakraborty, Ghosh, Iquebal, Jaiswal and Baranwal. This is an open-access article distributed under the terms of the Creative Commons Attribution License (CC BY). The use, distribution or reproduction in other forums is permitted, provided the original author(s) and the copyright owner(s) are credited and that the original publication in this journal is cited, in accordance with accepted academic practice. No use, distribution or reproduction is permitted which does not comply with these terms.

frontiers | Frontiers in Microbiology

ORIGINAL RESEARCH
published: 13 May 2022
doi: 10.3389/fmicb.2022.877702

Complementary Effects of Virus Population Are Required for Efficient Virus Infection

*Yuechao Sun, Yu Zhang and Xiaobo Zhang**

College of Life Sciences and Southern Marine Science and Engineering Guangdong Laboratory (Zhuhai), Zhejiang University, Hangzhou, China

It is believed that the virions of a virus infecting a host may share the identical viral genome and characteristics. However, the role of genomic heterogeneity of the virions of a virus in virus infection has not been extensively explored. To address this issue, white spot syndrome virus (WSSV), a DNA virus infecting crustaceans, was characterized in the current study. In WSSV, differences in two nucleotides of the viral genome generated two types of WSSV, forming a virus population that consisted of Type A WSSV (encoding WSSV lncRNA-24) and Type B WSSV (encoding the wsv195 gene) at a ratio of 1:3. The virus populations in all virus-infected cells and tissues of different hosts exhibited a stable 1:3 structure. WSSV lncRNA-24 in Type A WSSV promoted virus infection by binding to shrimp and WSSV miRNAs, while the wsv195 gene in Type B WSSV played an essential role in virus infection. Loss of Type A WSSV or Type B WSSV in the WSSV population led to a 100-fold decrease in viral copy number in shrimp. Simultaneous loss of both types of WSSV prevented virus infection. These results indicated that the virus infection process was completed by two types of WSSV encoding different functional genes, revealing the complementary effects of WSSV population. Therefore, our study highlights the importance of the complementarity of virus population components in virus infection.

Keywords: virus population, complementary effect, virus infection, functional gene, lncRNA

OPEN ACCESS

Edited by:
Beilei Wu,
Institute of Plant Protection (CAAS), China

Reviewed by:
Felix Broecker,
Idorsia Pharmaceuticals Ltd., Switzerland
Qin Zhao,
Northwest A&F University, China

***Correspondence:**
Xiaobo Zhang
zxb0812@zju.edu.cn

Specialty section:
This article was submitted to Virology, a section of the journal Frontiers in Microbiology

Received: *17 February 2022*
Accepted: *07 March 2022*
Published: *13 May 2022*

Citation:
Sun Y, Zhang Y and Zhang X (2022) Complementary Effects of Virus Population Are Required for Efficient Virus Infection. Front. Microbiol. 13:877702. doi: 10.3389/fmicb.2022.877702

INTRODUCTION

There are about 10^{31} virus-like particles inhabiting our planet, which outnumber all cellular life forms on the earth (Suttle, 2005; Wigington et al., 2016). Despite the presence of viruses in astonishing number and the impact of viruses on the population dynamics and evolutionary trajectories of hosts, our knowledge about the genomic properties of viruses remains limited (Mahmoudabadi and Phillips, 2018). The genomic sequence of a virus is referred to as its "genomic fingerprint," which makes a virus unique (Lau et al., 2020). The large number of progeny (10^3–10^4) produced from an individual infected cell allows viruses to sample a large genetic space more rapidly than their hosts, helping them to evolve around adaptive and therapeutic defenses and to benefit from cooperative interactions among co-infecting quasispecies (Stray and Air, 2001; Chen et al., 2007). The remarkable capacity of viruses to adapt to new hosts and environments is highly dependent on their ability to generate *de novo* diversity in a short period of time (Sanjuán and Domingo-Calap, 2016). Rates of spontaneous mutations vary amply among viruses

(Sanjuán and Domingo-Calap, 2016). Viral mutation rates are modulated at different levels, including polymerase fidelity, sequence context, template secondary structure, cellular microenvironment, replication mechanisms, proofreading, and access to post-replicative repair (Sanjuán, 2012). The mutations of a viral genome, which occur naturally over time (Sun et al., 2020), generate different strains of a virus. It is popularly believed that a viral strain shares the same genomic sequence.

Groups of the same-species virus that share a set of genome mutations are referred to as a lineage, which includes some strains (Verhagen et al., 2021). Some lineages may have characteristics such as the ability to spread more quickly, or to cause more severe disease (Hufsky et al., 2019). These lineages are classified as variants of interest, variants being monitored, or variants of high concern. At present, the virulence and infectivity of viral strains are often well characterized. Nevertheless, the interactions between the viral strains are generally ignored (Mostafa et al., 2018). With the spread of the Coronavirus disease 2019 (COVID-19) pandemic to almost all nooks and corners of the world, the accepted view is that there are clear differences between different strains of the COVID-19 (Goel et al., 2020; Yamamoto and Bauer, 2020; Rangayasami et al., 2021). The differences in virulence and infectivity of different strains of COVID-19 have been identified (Jeyanathan et al., 2020; Seah and Agrawal, 2020). However, the interaction between COVID-19 strains is not explored. Hepatitis B virus (HBV) is a diverse double-stranded DNA virus with 9 genotypes (A–I) and a putative 10th genotype (J), being characterized thus far (McNaughton et al., 2020). In a genotype of HBV, the viral genome is generally consistent. During virus infection, viruses must navigate the complex and unpredictable environments inside and outside the host. The genetic variability of a virus is central to virus infection, as it helps the virus evades host immunity, withstands antiviral drugs, expands the host ranges, and adopts new routes of transmission. It is a popular phenomenon that a virus has multiple different viral strains, suggesting that a virus may exist as a viral population consisting of different strains. However, the genomic heterogeneity of a virus and its role and mechanism in virus-host interaction have not been intensively explored.

To address this issue, the virus population of white spot syndrome virus (WSSV), a DNA virus infecting crustaceans (Li et al., 2019), was explored in this study. Our results revealed the existence of a WSSV population consisting of two types of WSSV, Type A WSSV (encoding WSSV lncRNA-24) and Type B WSSV (encoding the wsv195 gene). Complementary effects of the two types of WSSV were required for virus infection.

RESULTS

Two Types of White Spot Syndrome Virus in the Virus Population in Infected Shrimp

To explore whether virus populations exist, WSSV, a DNA virus infecting crustaceans, was characterized. LncRNA sequencing of WSSV-infected *Marsupenaeus japonicus* haemocytes indicated that WSSV generated a total of 24 WSSV lncRNAs (**Figure 1A**). Among these lncRNAs, WSSV lncRNA-24 was a two-nucleotide deletion mutant of a WSSV mRNA (wsv195 mRNA) (**Figure 1B**). Therefore, WSSV lncRNA-24 (GenBank accession no. MN475881) was further investigated. RNA-seq data revealed that the ratio of WSSV lncRNA-24 to wsv195 mRNA contents was 1:3 (**Figure 1C**). To confirm the coexistence of WSSV lncRNA-24 and wsv195 mRNA, quantitative real-time PCR was conducted with a specific probe that could differentiate the two molecules. The results showed that WSSV lncRNA-24 and wsv195 mRNA coexisted in WSSV-infected shrimp at a ratio of 1:3 during virus infection (**Figure 1D**).

To determine whether WSSV lncRNA-24 was generated during post-transcriptional processing or existed in the viral genome, WSSV genomic DNA from individual WSSV-infected shrimp was tested for WSSV lncRNA-24 and wsv195 mRNA. The sequencing results revealed that there were two types of WSSV genomes: one encoding WSSV lncRNA-24 and another encoding wsv195 mRNA (**Figure 1E**), thus yielding two types of WSSV, Type A WSSV encoding WSSV lncRNA-24 and Type B WSSV encoding wsv195 mRNA. The ratio of Type A WSSV to Type B WSSV was approximately 1–3 (**Figure 1F**), which was consistent with the RNA-seq data. These results indicated that the change in two nucleotides of the viral genome formed a virus population consisting Type A WSSV and Type B WSSV.

Taken together, these findings showed that two types of WSSV simultaneously existed in individual WSSV-infected shrimp, suggesting that the population of the two types of WSSV was required for the WSSV infection.

Existence of Virus Populations in Situations Ranging From Single Virus-Infected Cells to Different Virus-Infected Hosts

To investigate whether the WSSV population containing Type A WSSV and Type B WSSV existed in single haemocytes, the single haemocytes were isolated from WSSV-infected shrimp haemolymph (**Figure 2A**). The results indicated that there were indeed two types of WSSV virions encoding WSSV lncRNA-24 (Type A WSSV) and wsv195 mRNA (Type B WSSV) in a single shrimp haemocyte (**Figure 2B**). The ratio of Type A WSSV to Type B WSSV was 1:3 (**Figure 2B**). These data confirmed that Type A WSSV and Type B WSSV formed a WSSV population in a single shrimp haemocyte. Viruses complete their life cycles in host cells. Therefore, our results suggest that virus populations in which the virions contain different genomes to execute different functions facilitate virus infection.

To explore the distribution of the WSSV population in different tissues or organs, the presence of Type A WSSV or Type B WSSV was examined in the shrimp lymphoid organ, haemolymph, gills, stomach and hepatopancreas, which can be infected by WSSV. The results showed that the types of WSSV existed in all examined tissues or organs at a ratio of 1:3 (Type A WSSV : Type B WSSV) (**Figure 2C**). The structures of the WSSV populations in different shrimp tissues and organs were

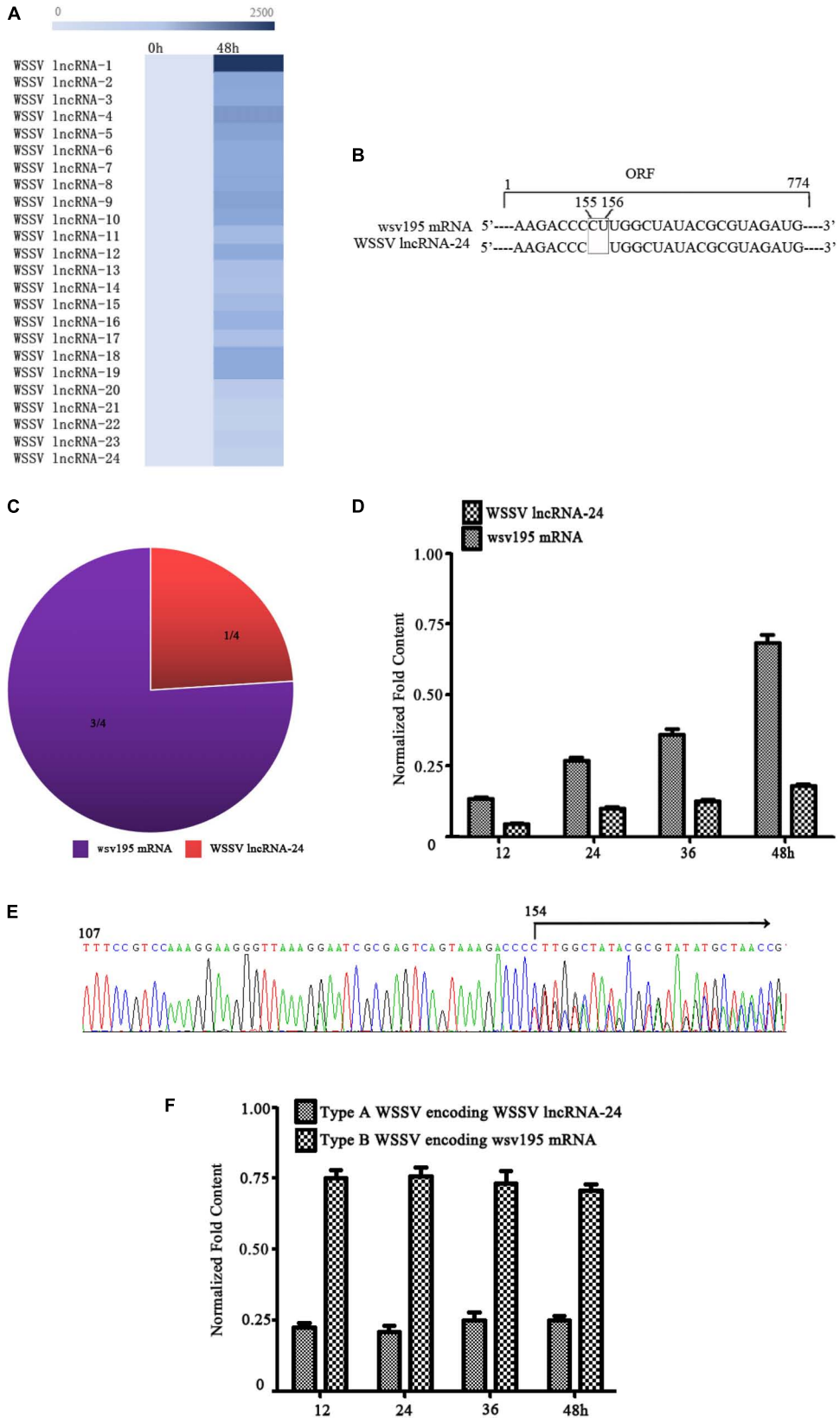

FIGURE 1 | (Continued)

FIGURE 1 | Two types of WSSV in the virus population in infected shrimp. **(A)** Heat map of WSSV lncRNA expression profiles in WSSV-challenged shrimp. The numbers indicate the time points post infection. **(B)** Sequence comparison of WSSV lncRNA-24 and wsv195 mRNA. The deletion sites are boxed. **(C)** Ratios of WSSV lncRNA-24 to wsv195 mRNA among the sequenced RNAs of WSSV-infected shrimp haemocytes. **(D)** Coexistence of WSSV lncRNA-24 and wsv195 mRNA in WSSV-infected shrimp. Shrimp were challenged with WSSV. At different time points post infection, the expression levels of WSSV lncRNA-24 and wsv195 mRNA were evaluated using quantitative real-time PCR with a specific probe differentiating wsv195 mRNA from WSSV lncRNA-24. U6 was used as the internal control. The experiment was biologically repeated for three times. **(E)** Genomic DNA sequencing of WSSV from individual virus-infected shrimp. The arrow indicates the distinguishing sites of wsv195 mRNA and WSSV lncRNA-24. **(F)** Examination of Type A WSSV encoding WSSV lncRNA-24 and Type B WSSV encoding wsv195 mRNA. The genomic DNA of WSSV was subjected to quantitative real-time PCR to detect the DNA encoding WSSV lncRNA-24 or wsv195 mRNA in WSSV-infected shrimp. The numbers indicate the times post infection. The assay was biologically repeated for three times.

identical to that in single shrimp haemocytes, indicating that the virus population consistently formed the stable 1:3 structure.

To further characterize the structure of the WSSV population in different hosts, Type A WSSV and Type B WSSV were examined in crayfish (*Procambarus clarkii*) and mud crabs (*Scylla paramamosain*). The results again revealed a 1:3 ratio (Type A WSSV : Type B WSSV) in different tissues or organs of virus-infected crayfish (**Figure 2D**). The analysis of the mud crabs generated essentially the same results (**Figure 2E**). These data showed that the structure of the WSSV population remained stable in different hosts.

Taken together, the above findings showed that the virus population existed in all virus-infected cells and tissues of different hosts and that its structure was stable with changing external stimuli.

Influence of Type A White Spot Syndrome Virus in the Virus Population on Virus Infection

To elucidate the role of Type A WSSV encoding WSSV lncRNA-24 in virus infection, the expression of WSSV lncRNA-24 was knocked down via injection of a sequence-specific siRNA (WSSV lncRNA-24-siRNA) into shrimp *in vivo* followed by evaluation of virus infection. The results indicated that WSSV lncRNA-24 was successfully silenced by WSSV lncRNA-24-siRNA in WSSV-infected shrimp (**Figure 3A**). The silencing significantly decreased the WSSV copy numbers (**Figure 3B**) and virus-infected shrimp mortality (**Figure 3C**) compared to those of the controls. The data showed that WSSV lncRNA-24 encoded by Type A WSSV exerted a positive effect on WSSV replication.

To explore the underlying mechanism of WSSV lncRNA-24, the protein and DNA molecules that interact with WSSV lncRNA-24 were screened, but no binding protein or DNA molecules were found. Thus, the miRNAs interacting with WSSV lncRNA-24 were characterized.

The prediction analysis showed that WSSV lncRNA-24 can target shrimp miRNAs (miR-2a, miR-9a and miR-184) and WSSV miRNAs (WSSV-miR-77, WSSV-miR-158, WSSV-miR-164, and WSSV-miR-212) (**Figure 3D**). To evaluate the interactions between WSSV lncRNA-24 and shrimp or WSSV miRNAs, the plasmid pIZ/EGFP-WSSV lncRNA-24 containing EGFP and WSSV lncRNA-24 was cotransfected with a miRNA into insect cells. The results indicated that the fluorescence intensity of the cells cotransfected with shrimp miR-2a or miR-184 and pIZ/EGFP-WSSV lncRNA-24 was significantly lower than that of the controls (**Figure 3E**). However, the fluorescence intensity of the cells cotransfected with miR-2a or miR-184 and EGFP-ΔWSSV lncRNA-24 was similar to that of the controls (**Figure 3E**). Treatment with shrimp miR-9a did not change the fluorescence intensity of the cells (**Figure 3E**). These data revealed that WSSV lncRNA-24 interacted with shrimp miR-2a and miR-184.

To characterize the interactions between WSSV lncRNA-24 and WSSV miRNAs, WSSV lncRNA-24 was cotransfected with WSSV-miR-77, WSSV-miR-158, WSSV-miR-164 or WSSV-miR-212 into insect cells. The data showed that WSSV lncRNA-24 interacted with WSSV-miR-77, WSSV-miR-158 and WSSV-miR-164 (**Figure 3F**).

To reveal the roles of miRNA interactions with WSSV lncRNA-24, the expression levels of miRNAs in the haemocytes of WSSV-infected shrimp were examined. Northern blots indicated that shrimp miR-2a, shrimp miR-184, WSSV-miR-77, WSSV-miR-158, and WSSV-miR-164 were significantly upregulated in shrimp in response to WSSV infection (**Figure 3G**), suggesting that these miRNAs were involved in the infection process. When the expression of miR-2a, miR-184, WSSV-miR-77, WSSV-miR-158, or WSSV-miR-164 was knocked down with a sequence-specific siRNA in WSSV-infected shrimp (**Figure 3H**), the WSSV copy numbers were significantly higher than those in the control group (**Figure 3I**), indicating the negative roles of shrimp miR-2a, shrimp miR-184, WSSV-miR-77, WSSV-miR-158, and WSSV-miR-164 in virus infection.

Taken together, the findings revealed that Type A WSSV in the virus population promoted virus infection by encoding WSSV lncRNA-24 to suppress the expressions of shrimp and WSSV miRNAs (**Figure 3J**).

Impact of Type B White Spot Syndrome Virus in the Virus Population on Virus Infection

To elucidate the role of Type B WSSV encoding wsv195 mRNA in virus infection, the expression of the wsv195 gene was knocked down by injecting a sequence-specific siRNA (wsv195-siRNA) into shrimp. The results confirmed that the expression of wsv195 was silenced by wsv195-siRNA in WSSV-infected shrimp compared with controls (**Figure 4A**). Western blot analysis generated similar results (**Figure 4B**).

The results showed that silencing wsv195 expression significantly decreased the WSSV copy numbers in WSSV-infected shrimp compared with controls (**Figure 4C**). In addition, wsv195 silencing led to a significant decrease in WSSV-infected shrimp mortality (**Figure 4D**). These

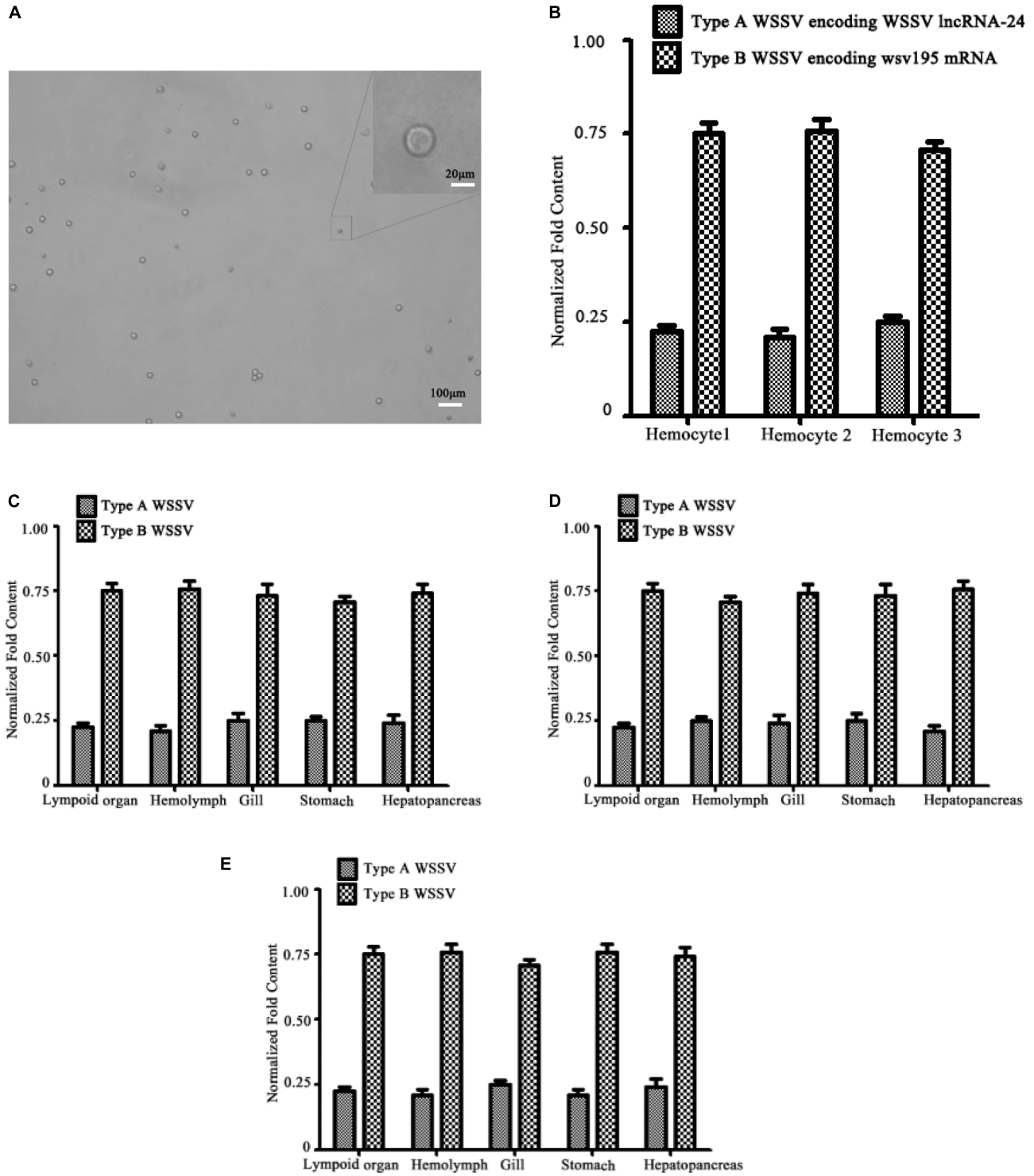

FIGURE 2 | Existence of virus populations in situations ranging from single virus-infected cells to different virus-infected hosts. **(A)** Isolation of single haemocytes from the haemolymph of WSSV-infected shrimp. **(B)** Existence of two types of WSSV genomes in single shrimp haemocytes. Single haemocytes from the haemolymph of WSSV-infected shrimp were subjected to quantitative real-time PCR to detect Type A WSSV and Type B WSSV. **(C)** Identification of viral genome heterogeneity in different tissues or organs of WSSV-infected shrimp. Shrimp were infected with WSSV. At 48 h post infection, the WSSV genome in different tissues or organs of shrimp was detected with quantitative real-time PCR. **(D)** Viral genome heterogeneity in different tissues or organs of WSSV-infected crayfish. **(E)** Distribution of two types of WSSV genomes in different tissues or organs of WSSV-infected mud crabs. All the experiments are biologically repeated for three times.

findings demonstrated that Type B WSSV exerted a positive effect on WSSV replication in shrimp via encoding wsv195 protein.

Complementary Effects of Type A White Spot Syndrome Virus and Type B White Spot Syndrome Virus in the Virus Population on Virus Infection

To further evaluate the role of the virus population in virus infection, the expression of WSSV lncRNA-24 encoded by Type A WSSV or/and the wsv195 gene encoded by Type B WSSV was silenced in WSSV-infected shrimp before examination of virus infection. Northern blots indicated that the expression of WSSV lncRNA-24 was completely silenced in the WSSV-infected shrimp (**Figure 5A**). The results showed that the depletion of Type A WSSV led to significant decreases of virus copies in shrimp (**Figure 5B**). At 48 h post-infection, the WSSV content in shrimp without Type A WSSV was 100-fold lower than that in the positive controls (WSSV) (**Figure 5B**). These data demonstrated the importance of Type A WSSV of virus population in virus infection.

To reveal the impact of Type B WSSV in virus population on virus infection, the expression of wsv195 was silenced in WSSV-infected shrimp. When Type B WSSV was completely depleted (**Figure 5C**), the WSSV copy numbers in shrimp hemocytes were significantly lower than those in the positive controls (infected with WSSV) (**Figure 5D**). At 48 h post-infection, the depletion of Type B WSSV led to a 100-fold decrease of WSSV copies in shrimp compared with the positive controls (**Figure 5D**), showing the importance of Type B WSSV for WSSV infection.

To further explore the impact of the simultaneous loss of Type A and Type B WSSVs on virus infection, the expressions of WSSV lncRNA-24 and wsv195 were simultaneously completely suppressed in shrimp (**Figure 5E**). The WSSV content in shrimp injected with WSSV lncRNA-24-siRNA and wsv195 mRNA was comparable with that in the negative controls (**Figures 5E,F**), showing that the simultaneous loss of Type A WSSV and Type B WSSV led to no virus infection in shrimp.

The above data demonstrated that the virus infection process was completed by different types of virus encoding different functional genes that exerted complementary effects in the virus population (**Figure 5G**).

DISCUSSION

Viruses have very small genomes, limiting the genes needed to complete their life cycle in host cells (Casey et al., 2018; Bao et al., 2019). In order to navigate complex and unpredictable environments inside and outside the host, viruses must make

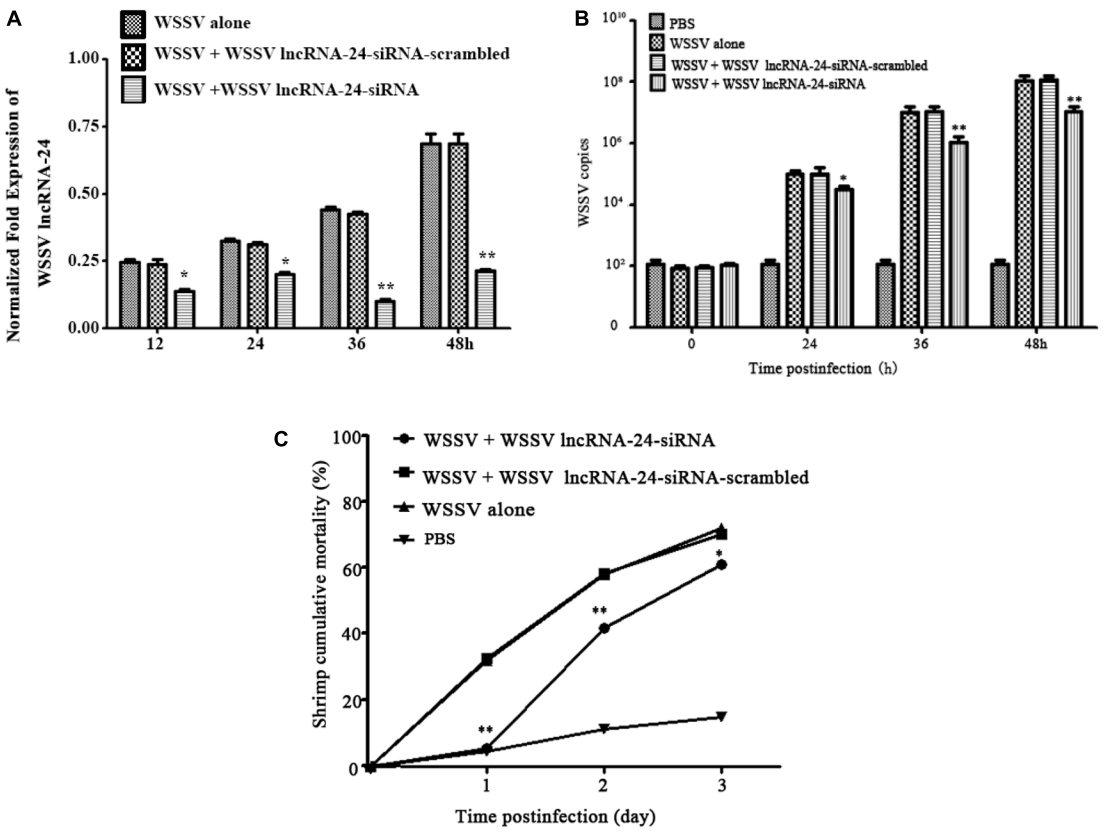

FIGURE 3 | (Continued)

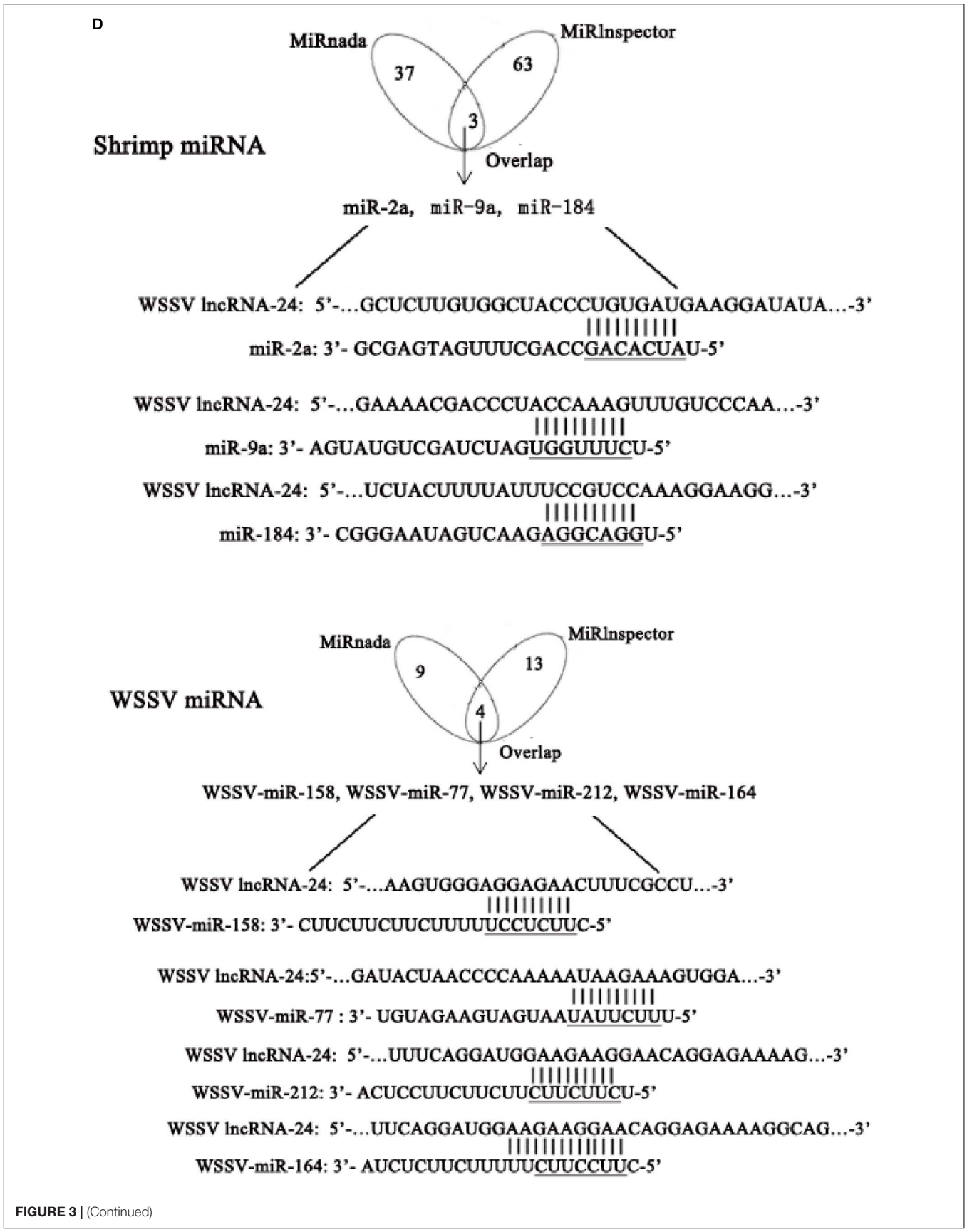

FIGURE 3 | (Continued)

full use of their viral genomes. Genetic variability within a viral genome is central for virus life cycle, helping the virus evade host immunity (Dingens et al., 2017; Schroeder et al., 2017), withstand antiviral drugs (Belshe et al., 1988), expand host range (Ma et al., 2016), and adopt new routes of transmission (Imai et al., 2012). It is well known that a virus can proliferate only in its host cells. In the process of virus infection, therefore, it can be inferred that a predictable result of genetic variability of a virus in single cells should be viral genome heterogeneity. Up to date, however, whether a virus functions as a virus population in single host cells and single hosts has not been extensively explored. In this study, the findings revealed that the differences in two nucleotides of the viral genome yielded two types of WSSV, forming a virus population that consisted of Type A WSSV and Type B WSSV at a ratio of 1:3. The structure of the WSSV populations in all virus-infected cells and tissues of different hosts were stable, indicating the importance of virus population in the process of virus invasion to its hosts. In the clinic, viruses are widely known to consist of a variety of viral strains with different viral genomes, suggesting the existence of virus populations. Therefore the concept of virus populations might be universal in animals for the efficient infection of viruses, which was an efficient strategy for a virus to make full use of the viral genome during the infection process.

In this study, the results demonstrated that the loss of Type A WSSV or Type B WSSV in the WSSV population resulted in a 100-fold decrease of viral copies in hosts. When both types of WSSV in the virus population were simultaneously depleted, the virus was not able to infect its hosts. Therefore there was a complementary effect between different viral types in the WSSV population, resulting from different functional genes encoded by different viral types. In the process of virus infection, the virions with varied viral genomes proliferated in the same host cells, thus benefiting from cooperative interactions among co-infecting virions with heterogeneous viral genomes. Every type of virions could function as a helper virus to the other types of virions of the virus based on the differences in their viral genomic sequences. The existence of virus population, which allowed permissive genomic mutations to reside in different virions, was indispensable for the propagation of the virus. The consequences of the complementary effect of virus population discussed here would not be exclusive to WSSV, raising the possibility that similar considerations existed in

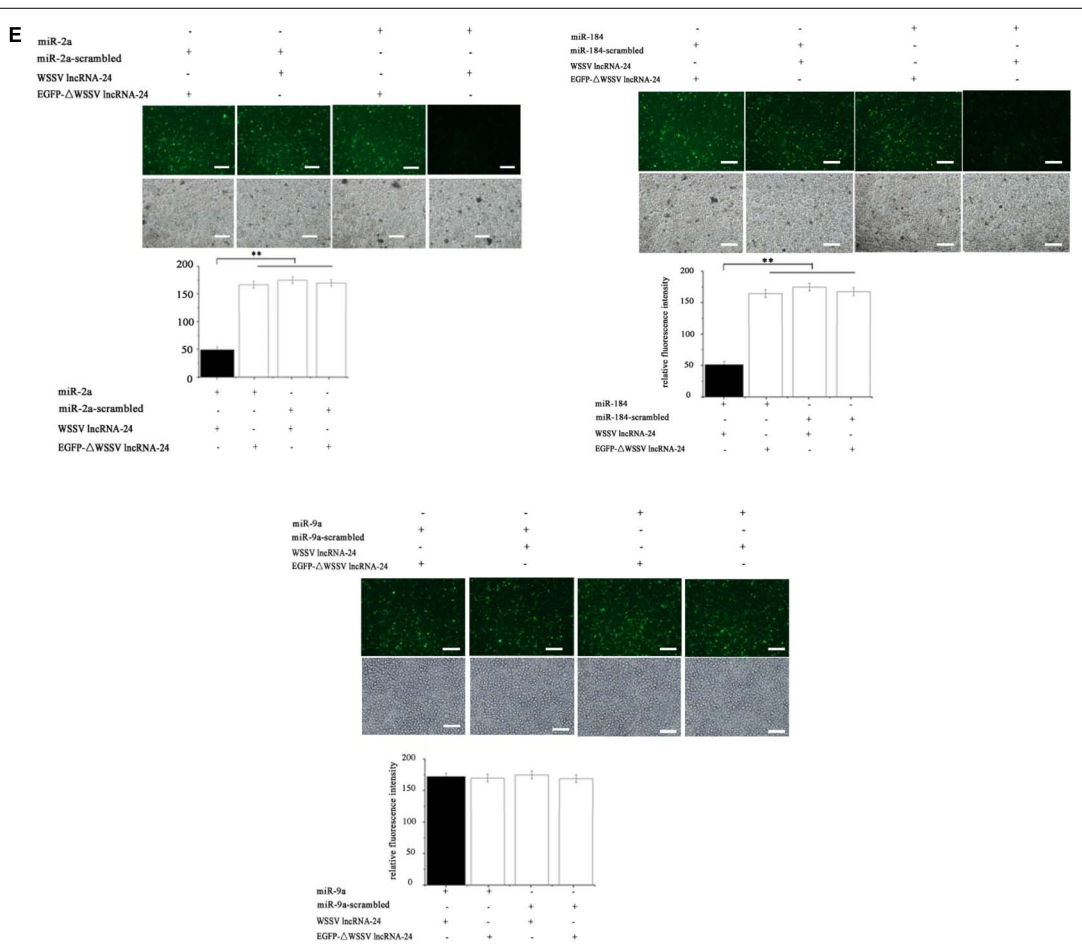

FIGURE 3 | (Continued)

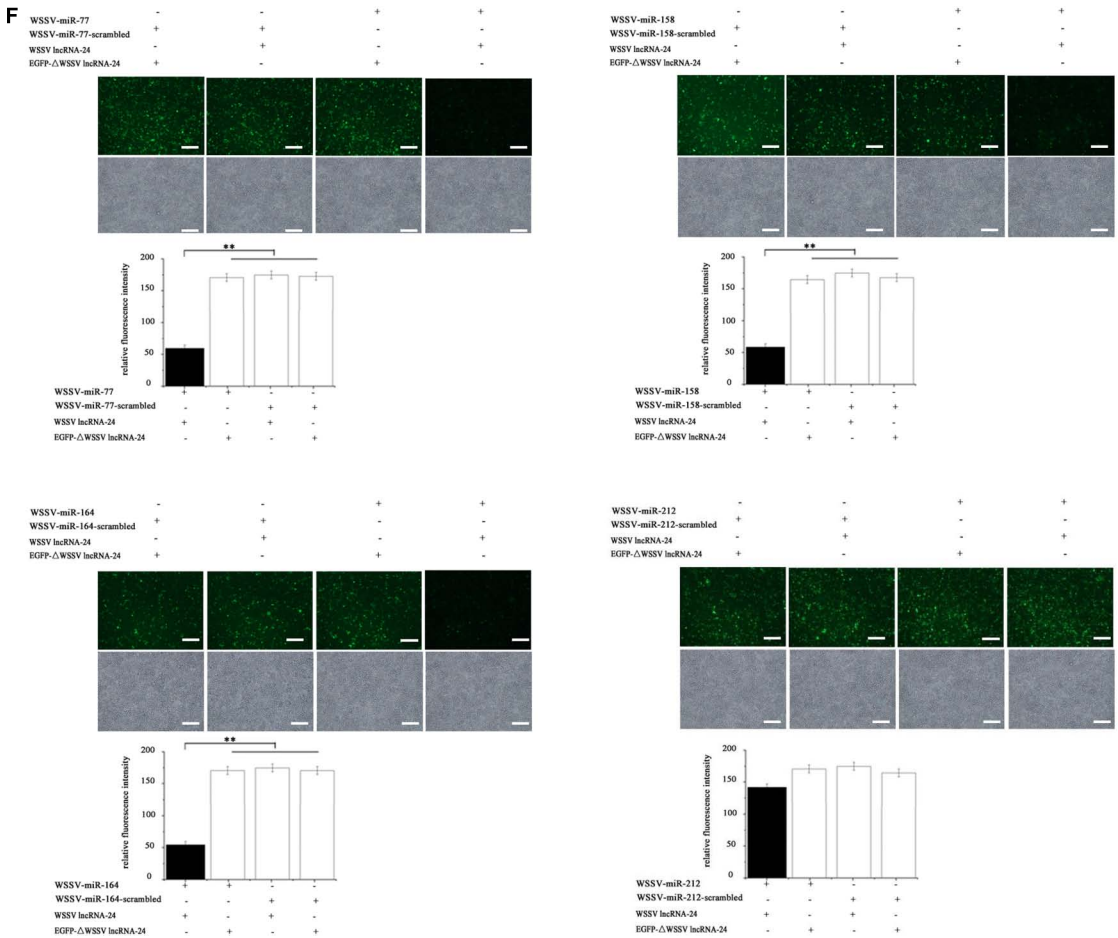

FIGURE 3 | (Continued)

all viruses as well. Interestingly, pleomorphism is common among enveloped viruses, with filamentous morphology common in the filoviridae, pneumoviridae, and paramyxoviridae families (Pierson and Diamond, 2012). More generally, the size, composition, and epitopes displayed on the surface of many viruses influence how they gain entry into a cell and interact with the innate and adaptive immune response (Feng and Gao, 2007; Barba-Spaeth et al., 2016), suggesting that the complementary effects in these properties could influence replicative fitness or viral tropism. The complementary effects of virus population could contribute to viral persistence in a wide variety of viruses. The more complementary the virions of a virus with heterogeneous viral genomes are, the more virulent the virus becomes. Since therapeutic interventions against virus can alter viral phenotypes in genetically independent ways, direct characterization of virus populations in the manner described here may help in evaluating the impact of emerging antiviral therapies (Furuta et al., 2013; Strauch et al., 2017). Overall, understanding the extent to which complementary effects of virus population contributes to viral persistence can help to guide the development of a new class of therapies aimed at reducing natural variability or applying combinatorial pressure that mitigates the survival benefits of phenotypic variability.

MATERIALS AND METHODS

Animal Culture and White Spot Syndrome Virus Infection

Shrimp (*Marsupenaeus japonicus*) about 10 g/shrimp, crayfish (*Procambarus clarkii*) about 20 g/crayfish and mud crab (*Scylla paramamosain*) about 50 g/crab were cultured in tanks containing 80 liters of aerated seawater at room temperature (25°C), respectively. Based on PCR detection using WSSV-specific primers (5′-TATTGTCTC TCCTGACGTAC-3′ and 5′-CACATTCTTCACGAGTCTAC-3′), shrimp, crayfish and crab were WSSV-free prior to experimental infection. The virus-free shrimp, crayfish and crab were infected with WSSV (10^5 virus copies/ml) by injection at 100 μl WSSV/animal, respectively. At different times postinfection, three shrimp, crayfishes or crabs were randomly collected for each treatment. The hemocytes of shrimp, crayfishes or crabs were mixed for later use.

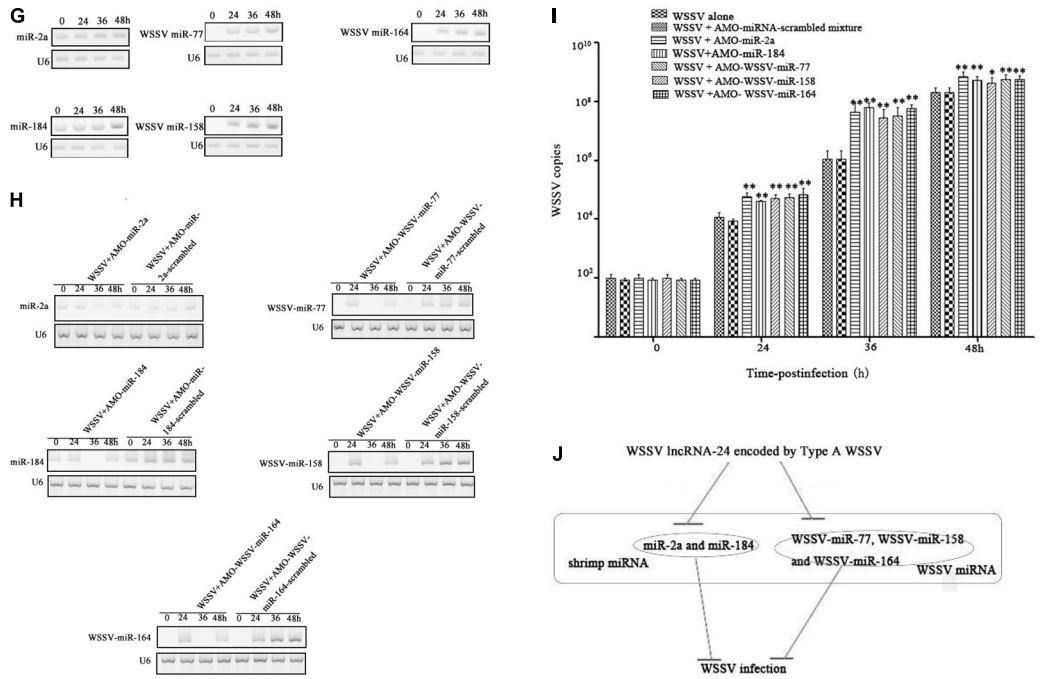

FIGURE 3 | Influence of Type A WSSV in the virus population on virus infection. **(A)** Silencing of WSSV lncRNA-24 encoded by Type A WSSV in WSSV-infected shrimp. Sequence-specific siRNA targeting WSSV lncRNA-24 and WSSV were coinjected into shrimp to knock down WSSV lncRNA-24. WSSV lncRNA-24-siRNA-scrambled was included in the injection as a control. At different time points post infection, the expression level of WSSV lncRNA-24 was examined using quantitative real-time PCR. **(B)** Effects of WSSV lncRNA-24 silencing on virus replication in shrimp. The WSSV copy numbers in shrimp treated with WSSV lncRNA-24-siRNA were quantified by real-time PCR. PBS, WSSV alone and WSSV lncRNA-24-siRNA-scrambled were used as controls. **(C)** Influence of WSSV lncRNA-24 silencing on shrimp mortality. The mortality of shrimp treated with WSSV lncRNA-24-siRNA was examined every day. The treatments are indicated at the top. **(D)** Prediction of miRNAs targeted by WSSV lncRNA-24. The seed sequences of miRNAs are underlined. **(E)** Direct interaction between WSSV lncRNA-24 and shrimp miR-2a, miR-9a or miR-184. Insect High Five cells were cotransfected with miR-2a, miR-9a or miR-184 and the plasmid EGFP-WSSV lncRNA-24 or EGFP-ΔWSSV lncRNA-24. At 36 h after cotransfection, the fluorescence intensity of insect cells was evaluated. Scale bar, 50 μm. **(F)** Interaction between WSSV lncRNA-24 and WSSV miRNAs. Insect High Five cells were cotransfected with a WSSV miRNA (WSSV-miR-158, WSSV-miR-77, WSSV-miR-212, or WSSV-miR-164) and the plasmid EGFP-WSSV lncRNA-24 or EGFP-ΔWSSV lncRNA-24. At 36 h after cotransfection, the fluorescence intensity of insect cells was examined. Scale bar, 50 μm. **(G)** Expression levels of miR-2a, miR-184, WSSV miR-77, WSSV miR-158, and WSSV miR-164 in virus-infected shrimp. Shrimp were challenged with WSSV. At different times post infection, the expression of miR-2a, miR-184, WSSV miR-77, WSSV miR-158, and WSSV miR-164 was detected in the haemocytes of virus-infected shrimp by Northern blot analysis. U6 was used as a control. The probes are indicated on the left. **(H)** Silencing of shrimp or WSSV miRNAs in WSSV-infected shrimp. Shrimp were coinjected with WSSV and AMO-miR-2a, AMO-miR-184, AMO-WSSV-miR-77, AMO-WSSV-miR-158, or AMO-WSSV-miR-164. AMO-miRNA-scrambled was included in the assays as a control. At different times post infection, the miRNA was detected by Northern blot analysis. The probes used are indicated on the left. The numbers show the time points post infection. U6 was used as a control. **(I)** Effects of shrimp or WSSV miRNA silencing on virus infection. WSSV and AMO-miRNA were coinjected into shrimp. A mixture of AMO-miR-2a-scrambled, AMO-miR-184-scrambled, AMO-WSSV-miR-77-scrambled, AMO-WSSV-miR-158- scrambled and AMO-WSSV-miR-164-scrambled was used as a control. At different times after coinjection, the WSSV copies were examined with quantitative real-time PCR. **(J)** Model for the role of Type A WSSV in virus infection. All the assays were biologically repeated for three times. In all panels, the statistical significance between treatments is indicated with asterisks (*$p < 0.05$; **$p < 0.01$).

RNA-Seq and Data Analysis

Total RNAs were extracted from WSSV-infected shrimp hemocytes using Trizol reagent (Invitrogen, CA, United States) following the manufacturer's procedure. The extracted RNAs were subjected to RNA-seq and then analyzed by LC Sciences (Houston, TX, United States). The sequences were mapped to the WSSV genome to find lncRNAs of WSSV. To predict WSSV lncRNAs, two independent computational algorithms CNCI[1] and CPC (coding potential calculator) were used (Kang et al., 2017; Luo et al., 2017).

[1]https://github.com/www-bioinfo-org/CNCI

Detection of wsv195 mRNA, White Spot Syndrome Virus lncRNA-24 and Their Corresponding DNAs by Quantitative Real-Time PCR

Total RNAs were extracted from WSSV-infected shrimp using RNAprep Pure Tissue Kit (Tiangen Biotech, Beijing, China) according to the manufacturer's instructions. The first strand of cDNA was synthesized using PrimeScript ® 1st Strand cDNA Synthesis Kit (Takara, Japan) with Oligo dT as the primer. U6 was used as a control. The expression levels of WSSV lncRNA-24 and wsv195 mRNA were examined using quantitative real-time PCR with specific primers (5′-GGAAGGGTTA AAGAAATCG-3′ and 5′-CTCGTTCCTCTTCATTCA-3′) and sequence-specific probe

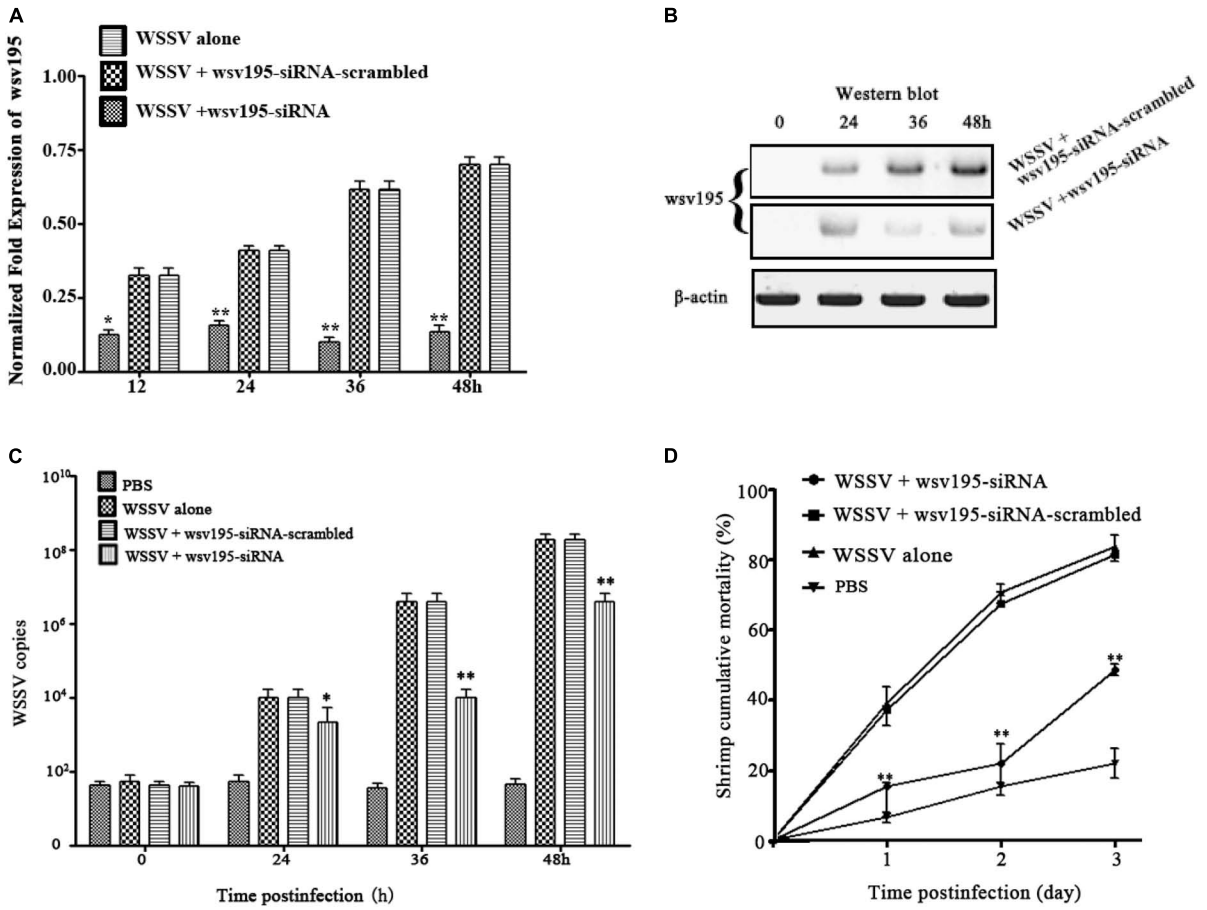

FIGURE 4 | Impact of Type B WSSV in the virus population on virus infection. **(A)** Silencing of wsv195 encoded by Type B WSSV in WSSV-infected shrimp. Wsv195-siRNA and WSSV were coinjected into shrimp. As a control, wsv195-siRNA-scrambled was included in the assay. At different time points post infection, the wsv195 mRNA level was examined using quantitative real-time PCR. The number indicates the time post infection. **(B)** Western blot analysis of wsv195-silenced shrimp. The treatments are indicated on the right. β-Actin was used as a control. **(C)** Effects of wsv195 silencing on virus replication in shrimp. The WSSV copy numbers in shrimp treated with wsv195-siRNA were quantified by real-time PCR. PBS, WSSV alone and wsv195-siRNA-scrambled were used as controls. **(D)** Influence of wsv195 knockdown on WSSV-infected shrimp mortality. All the experiments were biologically repeated for three times. In all panels, the statistical significance between treatments is indicated with asterisks (*$p < 0.05$; **$p < 0.01$).

(WSSV lncRNA-24, 5′-CAGTAAAGACCCTGGCTATACGC-3′; wsv195 mRNA, 5′-CAGTAAAGACCCCTTGGCTATACG-3′). Quantitative real-time PCR was performed using a 2 × SYBR Premix Ex Taq Kit (Takara, Japan) according to the manufacturer's manual. PCR was conducted at 95°C for 3 min, followed by 40 cycles at 95°C for 15 s and 60°C for 30 s.

For examination of WSSV encoding WSSV lncRNA-24 or wsv195 mRNA, the WSSV genome was extracted from virus-infected shrimp using an SQ Tissue DNA Kit (Omega Bio-Tek, United States). The viral genomic DNA was subjected to quantitative real-time PCR as described above.

RNA Interference Assay in Shrimp *in vivo*

To silence gene expression, siRNA specifically targeting a gene was synthesized according to the design rule for siRNA with a commercial kit according to the manufacturer's instructions (TaKaRa, Japan). The siRNAs used were WSSV lncRNA-24 siRNA (5′-CCTGAAGGAGGAGACCTAT-3′) and wsv195 siRNA (5′-G CGGCGACAGAGACTCATT-3′). As controls, the siRNA sequences were scrambled, generating WSSV lncRNA-24-siRNA-scrambled (5′-GGCGGTACGCACGAATTAA -3′) and wsv195-siRNA-scrambled (5′-GCGCAGACGCGACGTATA-3′). RNA Interference (RNAi) assay in shrimp was conducted by injecting siRNA (30 μg/shrimp) into the lateral area of the fourth abdominal segment of shrimp using a 1-ml sterile syringe. The siRNA (15 μg) and WSSV (10^5 copies/ml) were co-injected into virus-free shrimp at 100 μl/shrimp. At 12 h after co-injection, the siRNA (15 μg) was injected into the same shrimp (100 μl/shrimp). WSSV alone (10^5 copies/ml) and phosphate buffered saline (PBS) were included in injections as controls. For each treatment, 20 shrimps were used. At different time after injection, the shrimp were collected for later use. The assays were biologically repeated three times.

Detection of White Spot Syndrome Virus Copies With Quantitative Real-Time PCR

To quantify WSSV copies in shrimp, the WSSV genome was extracted from virus-infected shrimp using an SQ Tissue DNA Kit (Omega Bio-Tek, United States) and then subjected to quantitative real-time PCR using WSSV-specific primers (5′-TTGGTTT CAGCCCGAGATT-3′ and 5′-CCTTGGTCAGCCCCTTGA-3′) and TaqMan probe (5′-FAM-TGCTGCCGTCTCCAA-TAMRA-3′). A linearized plasmid with a 1,400-bp DNA fragment of WSSV genome was used as an internal standard for quantitative real-time PCR. PCR was conducted at 95°C for 1 min, followed by 45 cycles at 95°C for 30 s, 52°C for 30 s, and 72°C for 30 s.

Western Blot Analysis

Proteins were separated by 12% SDS-polyacrylamide gel electrophoresis and then transferred onto a nitrocellulose membrane. After blocking with 5% non-fat milk in TBST (10 mM Tris-HCl, 150 mM NaCl, 20% Tween 20, pH7.5) for 2 h at room temperature, the membrane was incubated with a primary antibody overnight, followed by incubation with horseradish peroxidase-conjugated secondary antibody (Bio-Rad, United States) for 2 h at room temperature. The primary antibodies were prepared in our laboratory. Subsequently the membrane was detected using a Western Lightning Plus-ECL kit (Perkin Elmer, United States).

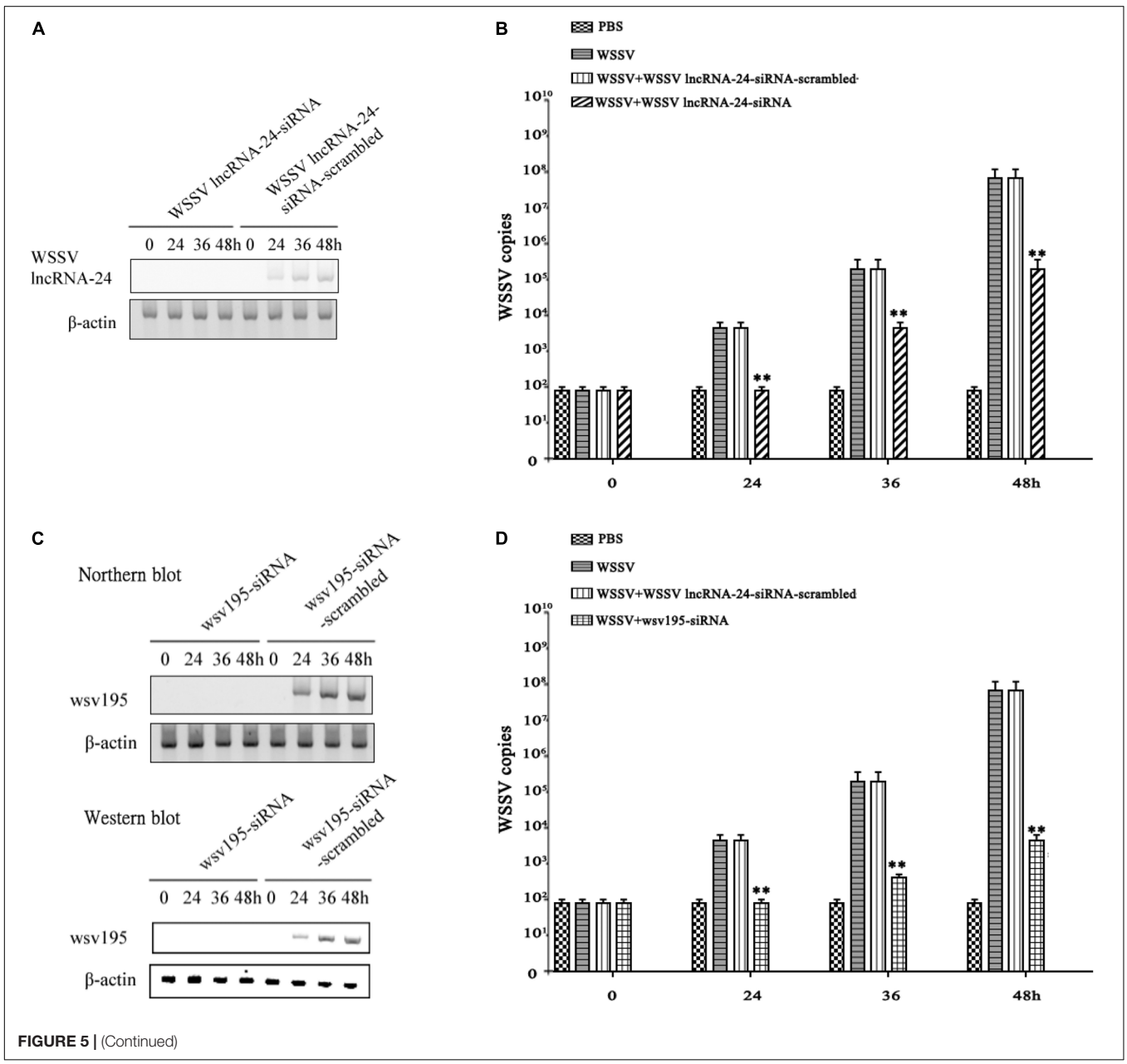

FIGURE 5 | (Continued)

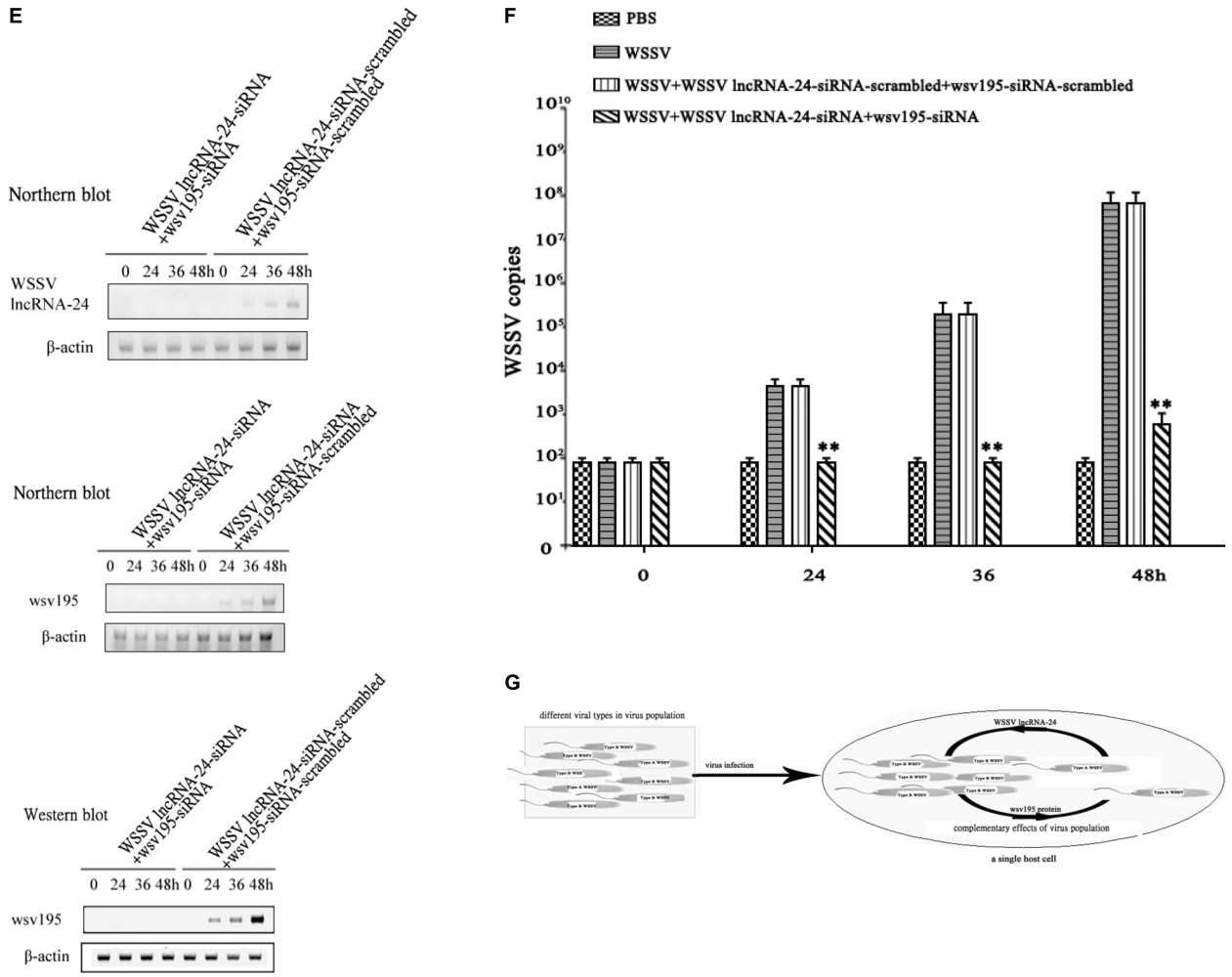

FIGURE 5 | Complementary effects of Type A WSSV and Type B WSSV in the virus population on virus infection. **(A)** Knockdown of WSSV lncRNA-24 encoded by Type A WSSV in shrimp. Shrimp were injected with WSSV lncRNA-24-siRNA or WSSV lncRNA-24-siRNA-scrambled. Twelve hours later, the shrimp were coinjected with siRNA and WSSV and then with siRNA three times at 12-h intervals. At different times after the WSSV injection, the expression levels of WSSV lncRNA-24 in shrimp haemocytes were examined by Northern blot analysis. β-actin was used as a control. **(B)** Influence of Type A WSSV on WSSV content in shrimp. Shrimp were injected with WSSV and WSSV lncRNA-24-siRNA. At different times post infection, the WSSV copy numbers in shrimp haemocytes were determined by quantitative real-time PCR. PBS, WSSV, and siRNA-scrambled were included in the assays as controls. The statistical significance between treatments is indicated with asterisks (**$p < 0.01$). **(C)** Silencing of wsv195 in shrimp. Shrimp were injected with wsv195-siRNA or wsv195-siRNA-scrambled. Twelve hours later, the shrimp were coinjected with siRNA (wsv195-siRNA or wsv195-siRNA-scrambled) and WSSV and then with the siRNA three times at 12-h intervals. At different times after the last injection, the expression level of WSSV lncRNA-24 in shrimp haemocytes was examined by Northern blot analysis (top) and Western blot analysis (bottom). Shrimp β-actin was used as a control. **(D)** Role of Type B WSSV in virus infection. Shrimp were injected with WSSV and WSSV wsv195-siRNA. At different times post infection, the WSSV copies in shrimp hemocytes were determined by quantitative real-time PCR. PBS, WSSV and siRNA-scrambled were used as controls. The statistical significance between treatments is indicated with asterisks (**$p < 0.01$). **(E)** Simultaneous depletion of Type A WSSV and Type B WSSV in WSSV-infected shrimp. Shrimp were injected with WSSV lncRNA-24-siRNA and wsv195-siRNA. Twelve hours later, the shrimp were co-injected with siRNAs (WSSV lncRNA-24-siRNA and wsv195-siRNA) and WSSV and then with the siRNAs three times at 12-h intervals. WSSV lncRNA-24-siRNA-scrambled and wsv195-siRNA-scrambled were included in the injection as controls. At different times after the last injection, the expression levels of WSSV lncRNA and wsv195 in shrimp haemocytes were examined by Northern blot and Western blot. Shrimp β-actin was used as a control. **(F)** Impact of simultaneous loss of Type A WSSV and Type B WSSV on virus infection in shrimp. Shrimp were co-injected with wsv195-siRNA, WSSV lncRNA-24 and WSSV. The WSSV content in shrimp was examined at different time after injection. The statistical significance between treatments is indicated with asterisks (**$p < 0.01$). **(G)** Model for the complementary effects of virus population during virus infection. All the experiments were biologically repeated for three times.

Interactions Between White Spot Syndrome Virus lncRNA-24 and miRNAs

Insect High Five cells (Invitrogen, United States) were cultured at 27°C in Express Five serum-free medium (Invitrogen) containing l-glutamine (Invitrogen). The cells at about 70% confluence were co-transfected with a synthesized WSSV or shrimp miRNA (300 nM) and a plasmid consisting of the EGFP gene and WSSV lncRNA-24. The miRNAs were synthesized with the D6140 *in vitro* transcription T7 kit (TaKaRa, Japan). All transfections were carried out in triplicate with Cellfectin

transfection reagent (Invitrogen) according to the manufacturer's protocol. At 48 h after transfection, the fluorescence of cells was examined with a Flex Station II microplate reader (Molecular Devices, United States) at 490 and 510 nm for excitation and emission, respectively. The fluorescence values were corrected by subtracting the auto fluorescence of cells not expressing EGFP. All the experiments were repeated biologically three times.

Detection of miRNAs by Northern Blotting

Total RNAs were extracted from shrimp hemocytes with mirVana miRNA isolation kit (Ambion, United States). After separation on a denaturing 15% polyacrylamide gel containing 7 M urea, the RNAs were transferred to a Hybond-N+ nylon membrane, followed by ultraviolet cross-linking. The membrane was prehybridized in DIG (digoxigenin) Easy Hyb granule buffer (Roche, Switzerland) for 0.5 h at 42°C and then hybridized with a DIG-labeled miRNA (miR-2a, 5′-TATCACAGCCAGCTTTG ATGAGCG-3′; miR-184, 5′-UGGACGGAGAACUGAUAAGGGC-3′; WSSV-miR- 77, 5′-TTTCTTATAATGATGAAGATGT-3′; WSSV-miR-158, 5′-CTTCTCCTTTT TCTTCTTCTTC-3′; WSSV-miR-158, 5′-CTTCCTTCTTTTTCTTCTCTA-3′; U6, 5′ -GGGCCATGCTAATCTTCTCTGTATCGTT-3′) at 42°C overnight. Subsequently the detection was performed with the DIG High Prime DNA labeling and detection starter kit II (Roche).

Silencing of miRNA in Shrimp

To knock down the expression of miR-2a, miR-184, WSSV-miR-77, WSSV-miR-158 or WSSV-miR-164 in shrimp, a sequence-specific anti-miRNA oligonucleotide (AMO) was injected into WSSV-infected shrimp. AMO-miR-2a (5′-CGCTCATCAAAGCTGGCTGTGATA-3′), AMO-miR-184 (5′-GCCCTTATCA GTTCTCCGTCCA-3′), AMO-WSSV-miR-77 (5′-ACATCTTCATCATTATAAGAA A-3′), AMO-WSSV-miR-158 (5′-GAAGAAGAAGAAAAAGGAGAAG-3′) and AMO-WSSV-miR-164 (5′-TAGAGAAGAA AAAGAAGGAAG-3′) were synthesized (Sangon Biotech, Shanghai, China) with a phosphorothioate backbone and a 2′-O-methyl modification at the 12th nucleotide. AMO (10 nM) and WSSV (10^5 copies/ml) were co-injected into virus-free shrimp at a 100 μl/shrimp. At 12 h after the co-injection, AMO (10 nM) was injected into the same shrimp. As controls, AMO-miR -2a-scrambled (5′-TTGCATGTCTGTCGAG-3′), AMO-miR-184-scrambled (5′-TTG CATGTCTGTCGAG-3′), AMO-WSSV-miR-77-scrambled (5′-TTGCATGTCTGTC GAG-3′), AMO-WSSV-miR-158-scrambled (5′-TTGCATGTCTGTCGAG-3′), AMO-WSSV-miR-164-scrambled (5′-TTGCATGTCTGTCGAG-3′), WSSV alone (10^5 copies/ml) and phosphate buffered saline (PBS) were included in the injections. At different time after injection, the shrimp hemocytes were collected for later use.

Statistical Analysis

To calculate the mean and standard deviation, the numerical data from three independent experiments were analyzed by one-way analysis of variance (ANOVA). The differences between treatments were analyzed by *t*-test.

DATA AVAILABILITY STATEMENT

The data presented in the study are deposited in the NCBI repository, accession number SRR18218566.

AUTHOR CONTRIBUTIONS

XZ and YS conceptualized the study and designed the experiments. YS and YZ performed the experiments. XZ and YS wrote the manuscript with contributions from all authors.

FUNDING

This work was supported by the National Key Research and Development Program of China (2018YFD0900504) and the China Ocean Mineral Resources R&D Association (DY135-B-04).

REFERENCES

Bao, Q., Li, X., Han, G., Zhu, Y., Mao, C., and Yang, M. (2019). Phage-based vaccines. *Adv. Drug Deliv. Rev.* 145, 40–56. doi: 10.1016/j.addr.2018.12.013

Barba-Spaeth, G., Dejnirattisai, W., Rouvinski, A., Vaney, M. C., Medits, I., Sharma, A., et al. (2016). Structural basis of potent Zika-dengue virus antibody cross-neutralization. *Nature* 536, 48–53. doi: 10.1038/nature18938

Belshe, R. B., Smith, M. H., Hall, C. B., Betts, R., and Hay, A. J. (1988). Genetic basis of resistance to rimantadine emerging during treatment of influenza virus infection. *J. Virol.* 62, 1508–1512. doi: 10.1128/JVI.62.5.1508-1512.1988

Casey, E., van Sinderen, D., and Mahony, J. (2018). In vitro characteristics of phages to guide 'real life' phage therapy suitability. *Viruses* 10:163. doi: 10.3390/v10040163

Chen, H. Y., Di Mascio, M., Perelson, A. S., Ho, D. D., and Zhang, L. (2007). Determination of virus burst size in vivo using a single-cycle SIV in rhesus macaques. *Proc. Natl. Acad. Sci. U.S.A.* 104, 19079–19084. doi: 10.1073/pnas.0707449104

Dingens, A. S., Haddox, H. K., Overbaugh, J., and Bloom, J. D. (2017). Comprehensive Mapping of HIV-1 escape from a broadly neutralizing antibody. *Cell Host Microbe* 21, 777–787. doi: 10.1016/j.chom.2017.05.003

Feng, Y., and Gao, G. F. (2007). Towards our understanding of SARS-CoV, an emerging and devastating but quickly conquered virus. *Comp. Immunol. Microbiol. Infect. Dis.* 30, 309–327. doi: 10.1016/j.cimid.2007.05.009

Furuta, Y., Gowen, B. B., Takahashi, K., Shiraki, K., Smee, D. F., and Barnard, D. L. (2013). Favipiravir (T-705), a novel viral RNA polymerase inhibitor. *Antiviral Res.* 100, 446–454. doi: 10.1016/j.antiviral.2013.09.015

Goel, S., Hawi, S., Goel, G., Thakur, V. K., Agrawal, A., Hoskins, C., et al. (2020). Resilient and agile engineering solutions to address societal challenges such as coronavirus pandemic. *Mater. Today Chem.* 17:100300. doi: 10.1016/j.mtchem.2020.100300

Hufsky, F., Ibrahim, B., Modha, S., Clokie, M. R. J., Deinhardt-Emmer, S., Dutilh, B. E., et al. (2019). The third annual meeting of the european virus bioinformatics center. *Viruses* 11:420. doi: 10.3390/v11050420

Imai, M., Watanabe, T., Hatta, M., Das, S. C., Ozawa, M., Shinya, K., et al. (2012). Experimental adaptation of an influenza H5 HA confers respiratory droplet transmission to a reassortant H5 HA/H1N1 virus in ferrets. *Nature* 486, 420–428. doi: 10.1038/nature10831

Jeyanathan, M., Afkhami, S., Smaill, F., Miller, M. S., Lichty, B. D., and Xing, Z. (2020). Immunological considerations for COVID-19 vaccine strategies. *Nat. Rev. Immunol.* 20, 615–632. doi: 10.1038/s41577-020-00434-6

Kang, Y. J., Yang, D. C., Kong, L., Hou, M., Meng, Y. Q., Wei, L., et al. (2017). CPC2: a fast and accurate coding potential calculator based on sequence intrinsic features. *Nucleic Acids Res.* 45, W12–W16. doi: 10.1093/nar/gkx428

Lau, B. T., Pavlichin, D., Hooker, A. C., Almeda, A., Shin, G., Chen, J., et al. (2020). Profiling SARS-CoV-2 mutation fingerprints that range from the viral pangenome to individual infection quasispecies. *medRxiv* [Preprint] medRxiv: 2020.11.02.20224816.

Li, C., Weng, S., and He, J. (2019). WSSV-host interaction: host response and immune evasion. *Fish Shellfish Immunol.* 84, 558–571. doi: 10.1016/j.fsi.2018.10.043

Luo, H., Bu, D., Sun, L., Fang, S., Liu, Z., and Zhao, Y. (2017). Identification and function annotation of long intervening noncoding RNAs. *Brief Bioinform.* 18, 789–797. doi: 10.1093/bib/bbw046

Ma, E. J., Hill, N. J., Zabilansky, J., Yuan, K., and Runstadler, J. A. (2016). Reticulate evolution is favored in influenza niche switching. *Proc. Natl. Acad. Sci. U. S. A.* 113, 5335–5339. doi: 10.1073/pnas.1522921113

Mahmoudabadi, G., and Phillips, R. (2018). A comprehensive and quantitative exploration of thousands of viral genomes. *eLife* 7:e31955. doi: 10.7554/eLife.31955

McNaughton, A. L., Revill, P. A., Littlejohn, M., Matthews, P. C., and Ansari, M. A. (2020). Analysis of genomic-length HBV sequences to determine genotype and subgenotype reference sequences. *J. Gen. Virol.* 101, 271–283. doi: 10.1099/jgv.0.001387

Mostafa, A., Abdelwhab, E. M., Mettenleiter, T. C., and Pleschka, S. (2018). Zoonotic potential of influenza A viruses: a comprehensive overview. *Viruses* 10:497. doi: 10.3390/v10090497

Pierson, T. C., and Diamond, M. S. (2012). Degrees of maturity: the complex structure and biology of flaviviruses. *Curr. Opin. Virol.* 2, 168–175. doi: 10.1016/j.coviro.2012.02.011

Rangayasami, A., Kannan, K., Murugesan, S., Radhika, D., Sadasivuni, K. K., Reddy, K. R., et al. (2021). Influence of nanotechnology to combat against COVID-19 for global health emergency: a review. *Sens. Int.* 2:100079. doi: 10.1016/j.sintl.2020.100079

Sanjuán, R., and Domingo-Calap, P. (2016). Mechanisms of viral mutation. *Cell Mol. Life Sci.* 73, 4433–4448. doi: 10.1007/s00018-016-2299-6

Sanjuán, R. (2012). From molecular genetics to phylodynamics: evolutionary relevance of mutation rates across viruses. *PLoS Pathog.* 8:e1002685. doi: 10.1371/journal.ppat.1002685

Schroeder, K. M. S., Agazio, A., Strauch, P. J., Jones, S. T., Thompson, S. B., Harper, M. S., et al. (2017). Breaching peripheral tolerance promotes the production of HIV-1-neutralizing antibodies. *J. Exp. Med.* 214, 2283–2302. doi: 10.1084/jem.20161190

Seah, I., and Agrawal, R. (2020). Can the coronavirus disease 2019 (COVID-19) affect the eyes? a review of coronaviruses and ocular implications in humans and animals. *Ocul. Immunol. Inflamm.* 28, 391–395. doi: 10.1080/09273948.2020.1738501

Strauch, E. M., Bernard, S. M., La, D., Bohn, A. J., Lee, P. S., Anderson, C. E., et al. (2017). Computational design of trimeric influenza-neutralizing proteins targeting the hemagglutinin receptor binding site. *Nat. Biotechnol.* 35, 667–671. doi: 10.1038/nbt.3907

Stray, S. J., and Air, G. M. (2001). Apoptosis by influenza viruses correlates with efficiency of viral mRNA synthesis. *Virus Res.* 77, 3–17. doi: 10.1016/s0168-1702(01)00260-x

Sun, T. W., Yang, C. L., Kao, T. T., Wang, T. H., Lai, M. W., and Ku, C. (2020). Host range and coding potential of eukaryotic giant viruses. *Viruses* 12:1337. doi: 10.3390/v12111337

Suttle, C. A. (2005). Viruses in the sea. *Nature* 437, 356–361.

Verhagen, J. H., Fouchier, R. A. M., and Lewis, N. (2021). Highly pathogenic avian influenza viruses at the wild-domestic bird interface in Europe: future directions for research and surveillance. *Viruses* 13:212. doi: 10.3390/v13020212

Wigington, C. H., Sonderegger, D., Brussaard, C. P., Buchan, A., Finke, J. F., Fuhrman, J. A., et al. (2016). Re-examination of the relationship between marine virus and microbial cell abundances. *Nat. Microbiol.* 1:15024.

Yamamoto, N., and Bauer, G. (2020). Apparent difference in fatalities between Central Europe and East Asia due to SARS-COV-2 and COVID-19: four hypotheses for possible explanation. *Med. Hypotheses* 144:110160. doi: 10.1016/j.mehy.2020.110160

Conflict of Interest: The authors declare that the research was conducted in the absence of any commercial or financial relationships that could be construed as a potential conflict of interest.

Publisher's Note: All claims expressed in this article are solely those of the authors and do not necessarily represent those of their affiliated organizations, or those of the publisher, the editors and the reviewers. Any product that may be evaluated in this article, or claim that may be made by its manufacturer, is not guaranteed or endorsed by the publisher.

Copyright © 2022 Sun, Zhang and Zhang. This is an open-access article distributed under the terms of the Creative Commons Attribution License (CC BY). The use, distribution or reproduction in other forums is permitted, provided the original author(s) and the copyright owner(s) are credited and that the original publication in this journal is cited, in accordance with accepted academic practice. No use, distribution or reproduction is permitted which does not comply with these terms.

frontiers | Frontiers in Microbiology

ORIGINAL RESEARCH
published: 26 May 2022
doi: 10.3389/fmicb.2022.884044

Strawberry Vein Banding Virus Movement Protein P1 Interacts With Light-Harvesting Complex II Type 1 Like of *Fragaria vesca* to Promote Viral Infection

Shiqiang Xu[1†], Xiangxiang Zhang[1†], Kai Xu[1†], Zhanqi Wang[2], Xueping Zhou[3], Lei Jiang[1,4,5] and Tong Jiang[1,4,5*]*

[1]Department of Plant Pathology, School of Plant Protection, Anhui Agricultural University, Hefei, China, [2]Key Laboratory of Vector Biology and Pathogen Control of Zhejiang Province, College of Life Sciences, Huzhou University, Huzhou, China, [3]State Key Laboratory for Biology of Plant Disease and Insect Pest, Institute of Plant Protection, China Academy of Agricultural Sciences, Beijing, China, [4]Anhui Province Key Laboratory of Crop Integrated Pest Management, School of Plant Protection, Anhui Agricultural University, Hefei, China, [5]Key Laboratory of Biology and Sustainable Management of Plant Diseases and Pests of Anhui Higher Education Institutes, School of Plant Protection, Anhui Agricultural University, Hefei, China

Chlorophyll a/b-binding protein of light-harvesting complex II type 1 like (LHC II-1L) is an essential component of photosynthesis, which mainly maintains the stability of the electron transport chain. However, how the LHC II-1L protein of *Fragaria vesca* (FvLHC II-1L) affects viral infection remains unclear. In this study, we demonstrated that the movement protein P1 of strawberry vein banding virus (SVBV P1) interacted with FvLHC II-1L *in vivo* and *in vitro* by bimolecular fluorescence complementation and pull-down assays. SVBV P1 was co-localized with FvLHC II-1L at the edge of epidermal cells of *Nicotiana benthamiana* leaves, and FvLHC II-1L protein expression was upregulated in SVBV-infected *F. vesca*. We also found that FvLHC II-1L effectively promoted SVBV P1 to compensate for the intercellular movement of movement-deficient potato virus X ($PVX^{\Delta P25}$) and the systemic movement of movement-deficient cucumber mosaic virus ($CMV^{\Delta MP}$). Transient overexpression of FvLHC II-1L and inoculation of an infectious clone of SVBV showed that the course of SVBV infection in *F. vesca* was accelerated. Collectively, the results showed that SVBV P1 protein can interact with FvLHC II-1L protein, which in turn promotes *F. vesca* infection by SVBV.

Keywords: strawberry vein banding virus, intercellular movement, FvLHC II-1L protein, P1 protein, viral infection

OPEN ACCESS

Edited by:
Sean Michael Prager, University of Saskatchewan, Canada

Reviewed by:
Nobumitsu Sasaki, Tokyo University of Agriculture and Technology, Japan
Yongliang Zhang, China Agricultural University, China

***Correspondence:**
Tong Jiang
jiangtong4650@sina.com
Lei Jiang
jianglei062x@ahau.edu.cn

[†]These authors have contributed equally to this work and share first authorship

Specialty section:
This article was submitted to Virology, a section of the journal Frontiers in Microbiology

Received: *25 February 2022*
Accepted: *06 May 2022*
Published: *26 May 2022*

Citation:
Xu S, Zhang X, Xu K, Wang Z, Zhou X, Jiang L and Jiang T (2022) Strawberry Vein Banding Virus Movement Protein P1 Interacts With Light-Harvesting Complex II Type 1 Like of Fragaria vesca to Promote Viral Infection. Front. Microbiol. 13:884044. doi: 10.3389/fmicb.2022.884044

INTRODUCTION

The strawberry vein banding virus (SVBV) is a latent virus that severely harms strawberry plants in major strawberry growing areas worldwide (Ratti et al., 2009; Chen et al., 2016a). In China, SVBV, which is primarily transmitted by aphids or tissue culture seedlings, is mainly distributed in the Sichuan, Hebei, Liaoning, Shandong, and Anhui provinces (Pan et al., 2018; Jiang et al., 2021), where SVBV-infected strawberries display characteristic symptoms, such as weak growth,

uneven leaf color, a decrease in the number of creeping stems, and deformed fruits (Frazier, 1974).

Strawberry vein banding virus is a double-stranded DNA virus belonging to the genus *Caulimovirus* of the *Caulimoviridae* family. It contains seven open reading frames (ORFs), each of which encode a protein (Pattanaik et al., 2004). ORF I encodes a movement protein (MP) called P1 that can promote the intercellular movement of SVBV, which plays an essential role in the process of viral infection (Rui et al., 2021). SVBV shares similar genome structure with cauliflower mosaic virus (CaMV) belonging to the same genus. According to the proteins encoded by each ORF of CaMV, it was inferred that ORF II, III, IV, and V of SVBV may encode proteins associated with aphid infection, a DNA-binding protein, a coat protein (CP), a reverse transcriptase protein (Pan et al., 2018). P6, encoded by ORF VI, is a multifunctional protein that functions as an RNA silencing suppressor and translation transactivator (Li et al., 2018a), and ORF VII encodes an unknown protein (Schoelz et al., 2016). Our previous study showed that SVBV P1 may regulates intracellular and intercellular movement of SVBV during viral infection (Rui et al., 2021).

After invading the host plants, viruses spread through plasmodesmata (PD) to neighboring cells with the help of MPs (Schoelz et al., 2011). MPs can be transported intracellularly and distantly by binding virus particles, binding viral nucleic acids, inducing the formation of PD tubular structures, and changing the size of the PD aperture (Chen et al., 2000; Lucas, 2006; Park et al., 2014). It has been shown that host-encoded proteins interacting with viral MPs can control the pore size of PD and/or change the localization of viral MP on the PD to affect the process of viral infection (Peiro et al., 2014; Wu and Cheng, 2020). For example, the Alfalfa mosaic virus (AMV) MP can interact with *Arabidopsis thaliana* patellin 3 (AtPATL3); furthermore, overexpression of *AtPATL3* makes AMV MP unable to target PD, thereby affecting the intercellular movement of the virus (Peiro et al., 2014). Similarly, the rice membrane-associated protein remorin (REM1), which interacts with the MP NSvc4 encoded by the rice stripe virus (RSV), is involved in viral infection. Silencing of the *NbREM1* gene in *Nicotiana benthamiana* can reduce the deposition of callose, enhance the permeability of PD, and promote viral infection (Fu et al., 2018). Triple gene block protein 1, encoded by barley stripe mosaic virus (BSMV), can hijack the nucleolar protein fibrillarin 2 to form a viral ribonucleoprotein movement complex, thus promoting viral cell-to-cell movement (Li et al., 2018b). Moreover, *Citrus macrophylla* miraculin-like protein 2 is capable of hijacking MP P33 of Citrus tristeza virus to form aggregates in the cytoplasm and inhibit the cell-to-cell movement of the virus (Sun et al., 2021). Thus, host factors may interact with MPs to affect the process of viral infection.

In higher plants, photosystem II (PSII) is a large protein complex located on the thylakoid membrane of chloroplasts. It comprises the PSII core complex and light-harvesting complex II (LHC II), which drive water oxidation and are key components of photosynthesis (Huang et al., 2013). LHC II mainly binds to chlorophyll a/b and has three transmembrane domains, generally in the form of small monomers and macromeres (Neilson and Durnford, 2010). LHC II is responsible for transferring the absorbed light energy to the PSII reaction center and maintaining the stability of the PSII electron transport chain (Allen et al., 1981; Nilsson et al., 1997). LHC II not only participates in plant photosynthesis but also regulates plant growth and development. Silencing of *AtLhcb1* in *Arabidopsis thaliana* hindered the formation of LHC II trimers, affected photosynthesis, and caused plant dwarfing (Pietrzykowska et al., 2014); loss-of-function mutations in *AtTHF1* decreased the rate of LHC II degradation and delayed leaf yellowing (Huang et al., 2013). Our previous study indicated that SVBV P1 can interact with chlorophyll a/b-binding protein of LHC II type 1 like of *Fragaria vesca* (FvLHC II-1L), based on the results of yeast two-hybrid (Y2H) assay (Zhang et al., 2019), but the role of FvLHC II-1L in SVBV infection is still largely unknown.

In this study, we used bimolecular fluorescence complementation (BiFC) and pull-down assays to demonstrate that P1 interacts with FvLHC II-1L *in vivo* and *in vitro*. Quantitative real-time polymerase chain reaction (RT-qPCR) showed that FvLHC II-1L expression was significantly upregulated following SVBV infection. The subcellular localization assay revealed that SVBV P1 and FvLHC II-1L co-localized at the edge of the plant cell and that FvLHC II-1L was able to promote SVBV P1 aggregation. Furthermore, we showed that FvLHC II-1L promoted SVBV P1 to compensate for the movement of movement-deficient potato virus X ($PVX^{\Delta P25}$) and cucumber mosaic virus ($CMV^{\Delta MP}$). Overexpression of FvLHC II-1L enhanced SVBV infection in *F. vesca*.

Abbreviations: *A. tumefaciens*, *Agrobacterium tumefaciens*; AMV, Alfalfa mosaic virus; BiFC, Bimolecular fluorescence complementation; BSMV, Barley stripe mosaic virus; $CMV^{\Delta MP}$, Movement-defective cucumber mosaic virus; CAT1, chloroplast catalase 1; cDNA, Complementary DNA; CP, Coat protein; dpi, Days post inoculation; erGFP, Endoplasmic reticulum-targeted green fluorescent protein; EV, Empty vector; FD1, Ferridoxin 1 protein; *F. vesca*, *Fragaria vesca*; FvLHC II-1L, Chlorophyll a/b-binding protein of light-harvesting complex II type 1 like of *Fragaria vesca*; GFP, Green fluorescent protein; LHC II, Light-harvesting complex II; MP, Movement protein; *N. benthamiana*, *Nicotiana benthamiana*; NdhM, NADH dehydrogenase-like complex M subunit; NTRC, NADPH-dependent thioredoxin reductase C; PD, Plasmodesmata; PepMV, Pepino mosaic virus; PSII, Photosystem II; $PVX^{\Delta P25}$-GFP, Movement-deficient potato virus X green fluorescent protein; RT-qPCR, Quantitative real-time polymerase chain reaction; REM1, Remorin protein; RFP, Red fluorescent protein; ROS, Reactive oxygen species; RSV, Rice stripe virus; SVBV, Strawberry vein banding virus; SVBV P1, Movement protein P1 of strawberry vein banding virus; TMV, Tobacco mosaic virus; TRV, Tobacco rattle virus; YFP, Yellow fluorescent protein; Y2H, Yeast two-hybrid.

MATERIALS AND METHODS

Plant Materials, *Agrobacterium* and Vacuum Infiltration

All plants used in this study were grown in a growth chamber, set at 25°C, under 60% relative humidity and a 16 h light and 8 h dark photoperiod.

Six- to eight-week-old *N. benthamiana* plants were used for *Agrobacterium tumefaciens* infiltration, as described previously (Chen et al., 2016b). Equal volumes of individual *Agrobacterium* cultures (optical density at 600 nm, $OD_{600} = 1.0$) were mixed before co-infiltration.

Strawberry plants were infiltrated as described previously (Tian et al., 2015). The roots of strawberry plant seedlings were rinsed with distilled water, and then, whole plants were submerged in *A. tumefaciens* inoculum containing pTRV1 and pTRV2 or its derivatives ($OD_{600} = 1.0$) and placed in a vacuum at 101 kPa atmospheric pressure for 30 s; this procedure was repeated. The treated plants were washed with distilled water and cultured in pots containing nutrient solution, and after 24 h, they were transplanted into pots containing nutrient soil.

BiFC Assay

The coding sequences of SVBV P1 (GenBank No: X97304.1) and FvLHC II-1L (GenBank No: XM_004303830.2) were cloned into pCV-cYFP and pCV-nYFP, respectively (Li et al., 2018a), to generate cYFP-SVBV P1, nYFP-FvLHC II-1L, nYFP-P1, and cYFP-FvLHC II-1L. The recombinant plasmids were transformed into *A. tumefaciens* (GV3101) and co-infiltrated into *N. benthamiana* leaves. The agro-infiltrated leaves were observed using confocal microscopy (Olympus FV1000, Tokyo, Japan) at approximately 3 days post inoculation (dpi).

Pull-Down Assay

The full-length FvLHC II-1L or cyan fluorescent protein (CFP) respectively was inserted between the *BamH*I/*Sal*I restriction sites within the pCAM1307-3*Flag based expression vector to produce pCAM1307-FvLHC II-1L-3*Flag (FvLHC II-1L-Flag) or pCAM1307-CFP-3*Flag (CFP-Flag). To detect the SVBV P1–FvLHC II-1L interaction, a pull-down assay was conducted using protein extracts of FvLHC II-1L-Flag from infiltrated *N. benthamiana* leaves at 3 dpi. The full-length cDNAs of SVBV P1 were amplified and inserted into the pHMTc. The plasmid pHMTc was kindly supplied by Prof. Xiaorong Tao (Nanjing agricultural University, China). The construct pHMTc-SVBV P1 was transformed into *Escherichia coli* BL21 (DE3) cells. Total protein extracts were incubated with the maltose-binding protein (MBP)-SVBV P1 fusion proteins. The MBP pull-down assay was performed as previously described (Zhu et al., 2017).

Subcellular Localization Assay

For the subcellular localization study, SVBV P1 and FvLHC II-1L were inserted into a modified pCAM2300 containing green fluorescent protein (GFP) or red fluorescent protein (RFP), respectively, and then transformed into *A. tumefaciens* (Feng et al., 2013). The cultures were co-infiltrated with *N. benthamiana*. After 3 days, the infiltrated leaves were imaged using a confocal microscope (Olympus FV1000, Tokyo, Japan). Excitation wavelength was 488 nm for GFP, 514 nm for yellow fluorescent protein (YFP), 561 nm for RFP, and 640 nm for chloroplast.

RNA Extraction and RT-qPCR

Total RNA was extracted from agro-infiltrated leaves using the Omini Plant RNA Plant Kit (CWBIO, Beijing, China). cDNA was synthesized using PrimeScript™ RT reagent kit (TaKaRa, Tokyo, Japan). RT-qPCR was performed as described previously (Li et al., 2019).

Protein Extraction and Western Blotting

Total protein was extracted from agro-infiltrated leaves using RIPA lysis buffer II (Sangon Biotech, Shanghai, China). After electrophoresis, the gel was placed in Coomassie Brilliant Blue stain (CBB, BeyoBlue™ Coomassie Blue Super Fast Staining Solution; Beyotime, Shanghai, China), soaked for 1 h, then decolorized with pure water. Western blotting was performed as previously described (Tian et al., 2014; Li et al., 2018a). Total protein was separated *via* sodium dodecyl sulfate–polyacrylamide gel electrophoresis, transferred to nitrocellulose membranes, then separately incubated using GFP mouse monoclonal antibody, c-Myc mouse monoclonal antibody, DYKDDDDK (Flag) mouse monoclonal antibody, MBP mouse monoclonal antibody (TransGen, Beijing, China), FvLHC II-1L rabbit polyclonal antibody, SVBV P1 rabbit polyclonal antibody, and then incubated using goat anti-rabbit IgG (H + L), HRP Conjugate and goat anti-mouse IgG (H + L), HRP Conjugate (TransGen, Beijing, China) with dilutions at 1:5,000 was used in immunoblot analysis. The detection signal was visualized using the EasySee Western Blot Kit (Transgene Biotech, Beijing, China).

PVX Movement Complementation Experiment

For potato virus X movement complementation experiments, a movement-deficient PVX-GFP construct ($PVX^{\Delta P25}$-GFP) and construct P25, expressing the PVX P25 protein, were kindly supplied by Prof. Fei Yan (Ningbo University, China). The segment of FvLHC II-1L fused Myc-tag in the 5-termius was inserted between the *BamH*I/*Sal*I restriction sites within the pBin438 based expression vector to produce pBin438-Myc-FvLHC II-1L. The full-length SVBV P1 was inserted between the BamHI/SalI restriction sites within the pBin438 based expression vector to produce pBin438-SVBV P1, and the assays were performed as previously described (Yan et al., 2012; Rui et al., 2021). The GFP fluorescence of the infiltrated leaves was observed using a confocal microscope (Olympus FV1000, Tokyo, Japan).

CMV Complementation Assay

The CMV complementation assay was performed as previously described (Shen et al., 2014). The full-length SVBV P1 was inserted between the *Nco*I/*Xba*I restriction sites within the pCB301-CMV $RNA3^{\Delta MP}$ based expression vector to produce pCB301-CMV $RNA3^{\Delta MP}$-SVBV P1. The plasmid pCB301-CMV $RNA3^{\Delta MP}$ was kindly supplied by Prof. Xiaorong Tao (Nanjing agriculture University, China). *A. tumefaciens* containing pCB301-CMV RNA3 or pCB301-CMV $RNA3^{\Delta MP}$-SVBV P1 was mixed with *A. tumefaciens* containing pCB301-CMV RNA1 and RNA2 in a 1:1:1 ratio.

Tobacco Rattle Virus (TRV)-Based Gene Overexpression Assay

The full-length ORF of FvLHC II-1L was inserted behind the CP of the TRV2 vector as previously described (Tian et al., 2014). pTRV1 and pTRV2 or its derivatives were transformed, in order, into *A. tumefaciens* and co-transfected into *F. vesca* using a vacuum-infiltration method, as previously described (Tian et al., 2015).

DNA Extraction and Southern Blot Analysis

Strawberry vein banding virus-infected strawberry leaves were harvested at 35 dpi. Total DNA was extracted from the strawberry leaves using the CTAB method. Southern blotting was performed as previously described (Feng et al., 2016). SVBV DNA accumulation in SVBV-infected plants was detected by digoxigenin-labeled probes from the 5-termius of SVBV *CP* gene using DIG High Prime DNA Labeling and Detection Starter Kit II (Roche, Basel, Switzerland) according to manufacturer instructions.

Genetic Transformation of FvLHC II-1L in *Nicotiana benthamiana*

The full-length FvLHC II-1L was inserted between the *Xba*I/*Hind*III restriction sites within the pCAM1307-Myc based expression vector to produce pCAM1307-Myc-FvLHC II-1L. The plasmid was transformed into *A. tumefaciens* strain LBA4404. The transgenic *N. benthamiana* plants of T0 generation were obtained by leaf disc transformation method. The homozygous FvLHCII-1L transgenic *N. benthamiana* was obtained after screening. RT-qPCR and Western blot analyzes were used to detect the expression of FvLHC II-11L. The primers used for vector construction are listed in **Supplementary Table S1**.

RESULTS

SVBV P1 Interacts With FvLHC II-1L *in vitro* and *in vivo*

To examine how SVBV P1 causes plant disease during viral infection, we screened a *F. vesca* cDNA library using the Y2H assay to identify the host proteins involved. Consequently, FvLHC II-1L was noted to interact with SVBV P1 (Zhang et al., 2019). To further verify the interaction between SVBV P1 and FvLHC II-1L, a pull-down experiment was performed. The results showed that MBP-SVBV P1 specifically pulled down the FvLHC II-1L-Flag protein (**Figure 1A**). SVBV P1 was absent in the cyan fluorescent protein (CFP)-Flag pulldown products, and FvLHC II-1L-Flag was not able to pull down MBP (**Figure 1A**), indicating that SVBV P1 can interact with FvLHC II-1L *in vitro*. Furthermore, a BiFC assay was performed to examine the interaction between SVBV P1 and FvLHC II-1L *in vivo* using *N. benthamiana*. As shown in **Figure 1B**, when cYFP-SVBV P1 and nYFP-FvLHC II-1l were co-expressed in *N. benthamiana* leaf cells, strong YFP fluorescence was observed, similar to the co-infiltration with nYFP-4A and cYFP-P2 (positive control). As expected, no fluorescence could be observed in *N. benthamiana* leaf epidermal cells co-infiltrated with cYFP-SVBV P1 and nYFP or nYFP-FvLHC II-1L and cYFP (negative controls; **Figure 1B**), indicating that SVBV P1 can interact with FvLHC II-1L *in vivo*. Collectively, these results suggest that SVBV P1 interacts with FvLHC II-1L *in vitro* and *in vivo*.

Interaction Between SVBV P1 and FvLHC II-1L Alters Subcellular Localization of SVBV P1

To investigate the subcellular localization of SVBV P1 and FvLHC II-1L, SVBV P1 and FvLHC II-1L were fused to the C-terminus of GFP, respectively, to obtain SVBV P1-GFP and FvLHC II-1L-GFP. The constructs were then transformed into *A. tumefaciens* and infiltrated into *N. benthamiana* leaves, as described previously (Rui et al., 2021). GFP fluorescence was observed in the cytoplasm and cell periphery of SVBV P1-GFP-infiltrated *N. benthamiana* leaves, and GFP fluorescence was observed in chloroplasts of FvLHC II-1L-GFP-infiltrated *N. benthamiana* leaves (**Figure 2A**). To determine whether FvLHC II-1L affects the localization of SVBV P1, we co-expressed SVBV P1-GFP and FvLHC II-1L-RFP in *N. benthamiana* leaves using the agroinfiltration method. The results showed that SVBV P1-GFP and FvLHC II-1L-RFP were co-localized at the edge of *N. benthamiana* epidermal cells, and GFP fluorescence converged at the edge of cells (**Figure 2B**). These results suggest that FvLHC II-1L promotes SVBV P1 aggregation at the periphery of plant cells.

FvLHC II-1L Gene Expression IsUpregulated in SVBV-Infected Fragariavesca

To investigate the response of FvLHC II-1L to SVBV infection, healthy *F. vesca* was inoculated with *A. tumefaciens* containing the infectious clone of SVBV using the vacuum-infiltration method, as described previously (Tian et al., 2015). Compared with the mock control, *F. vesca* inoculated with the infectious clone of SVBV showed vein banding symptoms at 35 dpi (**Figure 3A**). Next, leaves with vein banding symptoms were collected from infected plants and subjected to RT-qPCR analysis. As shown in **Figure 3B**, the expression of *FvLHC II-1L* was significantly upregulated by approximately 3.5-fold following SVBV infection. This result suggests that SVBV can upregulate the transcript levels of *FvLHC II-1L* in *F. vesca*.

FvLHC II-1L Assists SVBV P1 to Complement Movement-Defective PVX

Protein P1 of strawberry vein banding virus has been shown to complement the cell-to-cell movement of movement-defective PVX (Rui et al., 2021). To determine whether FvLHC II-1L affects the function of SVBV P1, we performed a complement assay. *A. tumefaciens* containing pBin438, P25, pBin438-SVBV P1, and pBin438-MYC-FvLHC II-1L were co-infiltrated with movement-defective PVX ($PVX^{\Delta P25}$-GFP) into *N. benthamiana*

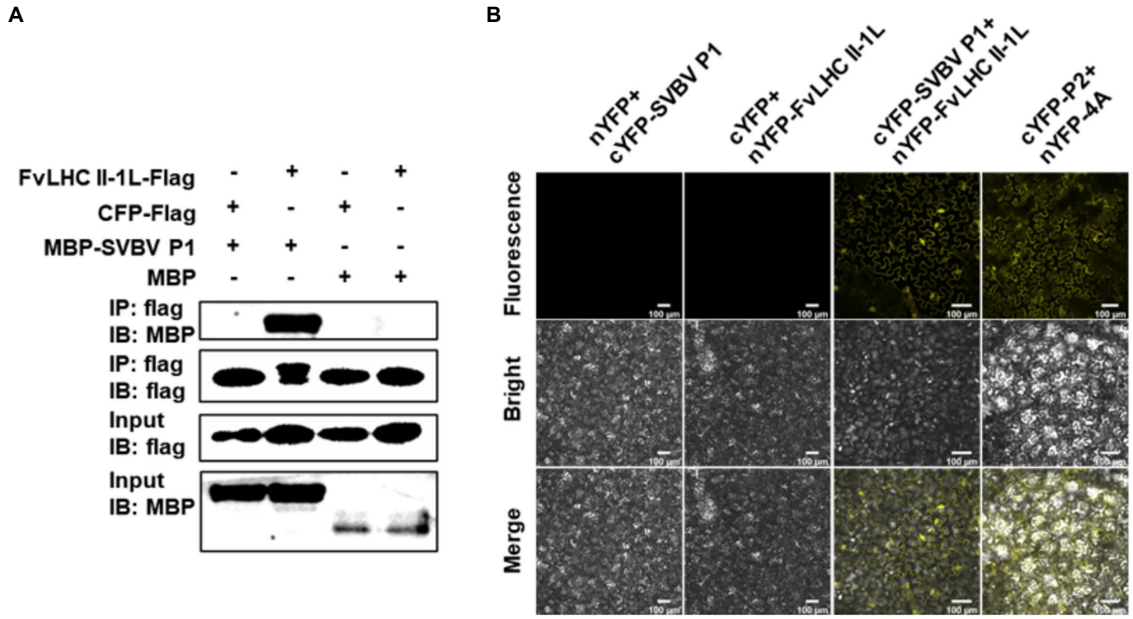

FIGURE 1 | Strawberry vein banding virus (SVBV) P1 interacts with chlorohyll a/b-binding protein of light-harvesting complex II type 1 like of *Fragaria vesca* (FvLHC II-1L) *in vitro* and *in vivo*. **(A)** Interaction between SVBV P1 and FvLHC II-1L was elucidated using an *in vitro* pull-down assay. Maltose-binding protein (MBP)-SVBV P1 or MBP was expressed in, and purified from, *Escherichia coli* BL21(DE3). FvLHC II-1L-Flag or cyan fluorescent protein (CFP)-Flag was expressed in *Nicotiana benthamiana* leaves and harvested at 3 days post inoculation (dpi). Purified MBP-SVBV P1 or MBP was mixed with plant extract of FvLHC II-1L-Flag or CFP-Flag and pulled down with Flag beads. **(B)** Interaction between SVBV P1 and FvLHC II-1L was examined using an *in vivo* bimolecular fluorescence complementation (BiFC) assay. *N. benthamiana* leaves were co-agroinfiltrated with the following combinations of plasmids: cYFP-SVBV P1 and nYFP-FvLHC II-1L, nYFP-4A and cYFP-P2 (positive control), cYFP-SVBV P1 and nYFP, and nYFP-FvLHC II-1L and cYFP (negative controls). Yellow fluorescent protein (YFP) fluorescence was observed *via* confocal microscopy at 3 dpi. Bar scale = 100 μm.

leaves. At 3 dpi, strong GFP fluorescence was observed in infiltrated and adjacent cells of *N. benthamiana* leaves co-expressing pBin438-FvLHC II-1L and pBin438-SVBV P1, which was stronger than that observed in *N. benthamiana* leaves infiltrated with SVBV P1 alone (**Figure 4A**). *N. benthamiana* leaves infiltrated with pBin438 or P25 were used as negative and positive controls, respectively (**Figure 4A**). The accumulation of GFP protein in *N. benthamiana* leaves (**Figure 4A**) was also determined by western blot analysis. As expected, higher GFP protein accumulation was observed in *N. benthamiana* leaves co-expressing FvLHC II-1L and SVBV P1, compared to *N. benthamiana* leaves infiltrated with pBin438, P25, or pBin438-SVBV P1 (**Figure 4B**).

To further understand the role of FvLHC II-1L, with respect to SVBV P1 complementing PVX$^{\Delta P25}$-GFP, transgenic *N. benthamiana* plants overexpressing MYC-tagged FvLHC II-1L (p1307-MYC-FvLHC II-1L) were generated. The mRNA and protein levels of FvLHC II-1L in transgenic plants were quantified *via* RT-qPCR and western blotting, respectively (**Supplementary Figure S1**). Then, *A. tumefaciens* containing pBin438-SVBV P1 and PVX$^{\Delta P25}$-GFP was co-infiltrated into FvLHC II-1L transgenic *N. benthamiana* leaves. As shown in **Figure 4C**, the area of GFP fluorescence in FvLHC II-1L transgenic plant leaves was noticeably larger than that in empty vector transgenic *N. benthamiana* plant leaves. Western blot analysis revealed a greater accumulation of GFP protein in FvLHC II-1L transgenic plant leaves, compared to leaves of the empty vector control plant (**Figure 4D**). Collectively, these results suggest that FvLHC II-1L can assist SVBV P1 in complementing movement-defective PVX.

FvLHC II-1L Assists SVBV P1 to Complement Movement-Defective CMV

To investigate whether SVBV P1 can complement the systemic movement of CMV$^{\Delta MP}$, the recombinant plasmid CMV$^{\Delta MP}$-SVBV P1 was constructed. The construct was then transformed into *A. tumefaciens*, followed by infiltration into *N. benthamiana* seedlings. After 8 days, compared with the CMV plant (positive control), more mild leaf crimping was observed in systemic leaves of *N. benthamiana* seedlings infiltrated with CMV$^{\Delta MP}$-SVBV P1, while the systemic leaves of CMV$^{\Delta MP}$-erGFP-infected *N. benthamiana* seedlings showed no symptoms (**Figure 5A**). As shown in **Figure 5B**, the accumulation of CMV CP was detected in CMV$^{\Delta MP}$-SVBV P1-infected *N. benthamiana* systemic leaves but not in CMV$^{\Delta MP}$-erGFP-infected *N. benthamiana* systemic leaves.

To determine whether FvLHC II-1L promotes SVBV P1 to complement the movement of CMV$^{\Delta MP}$, empty vector and FvLHC II-1L transgenic *N. benthamiana* leaves were infiltrated with CMV$^{\Delta MP}$-SVBV P1. Compared with the empty vector plants, more severe symptoms were observed in the systemic

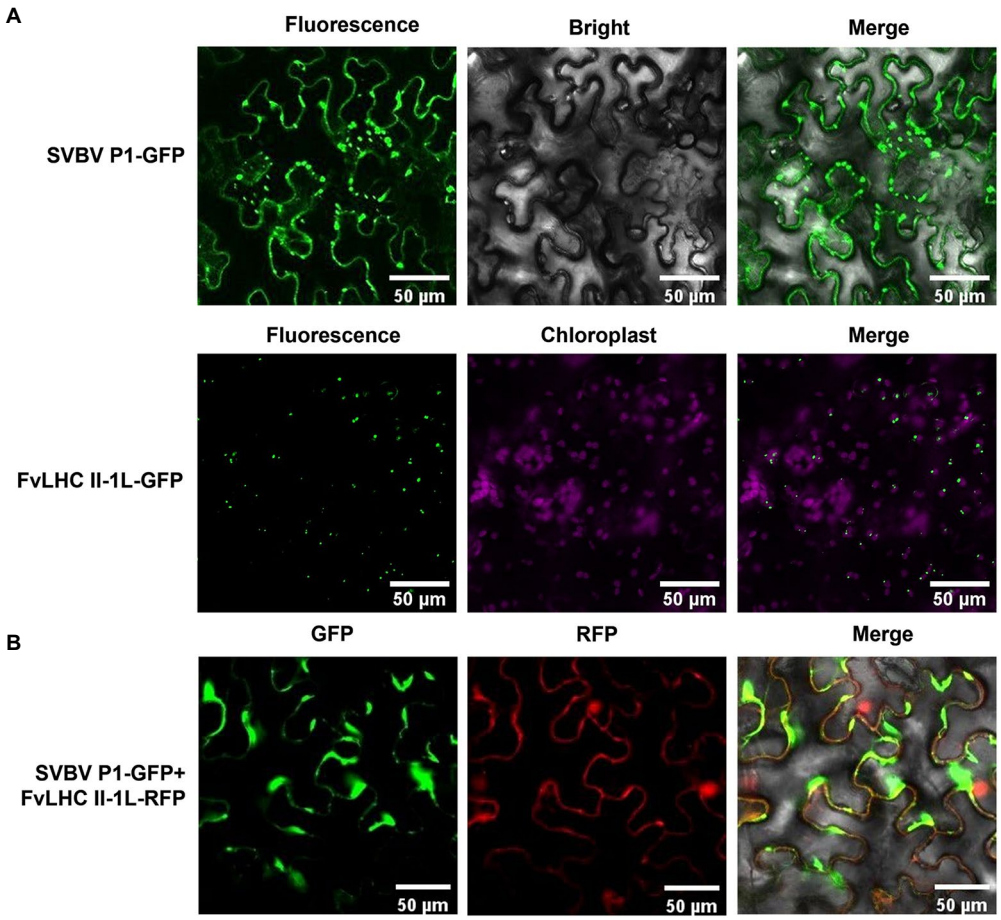

FIGURE 2 | Subcellular localization of SVBV P1 and FvLHC II-1L. **(A)** Subcellular localization of SVBV P1 and FvLHC II-1L in *N. benthamiana* leaves. *N. benthamiana* leaves were infiltrated with the indicated vector combinations. Green fluorescent protein (GFP) was observed at 3 dpi. **(B)** The co-localization of SVBV P1 and FvLHC II-1L in *N. benthamiana* leaves. The fluorescence was observed *via* confocal microscopy at 3 dpi. Bar scale = 50 μm.

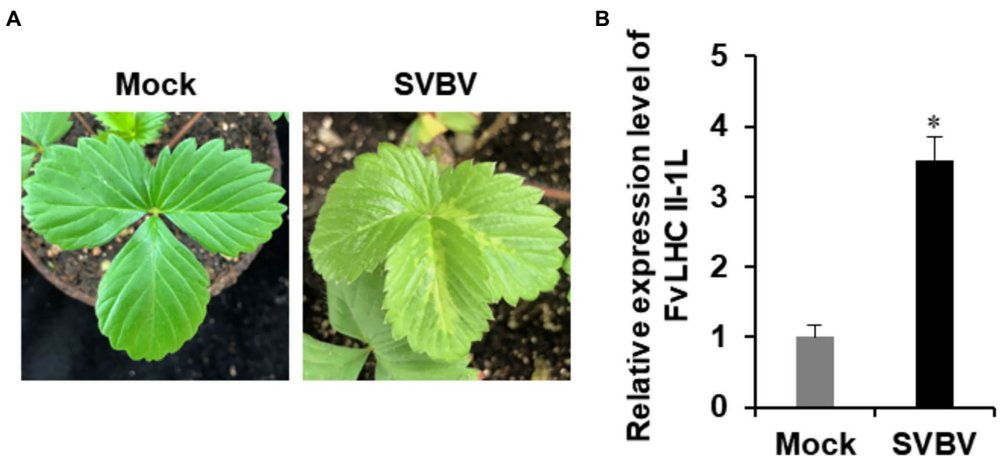

FIGURE 3 | Expression of *FvLHC II-1L* is upregulated by SVBV in infected *F. vesca*. **(A)** Phenotype of mock-inoculated or SVBV-inoculated *F. vesca*. **(B)** The transcript levels of *FvLHC II-1L* in mock-inoculated and SVBV-infected leaves of *F. vesca* were determined using quantitative real-time polymerase chain reaction (RT-qPCR) analysis. Error bars indicate the mean ± standard deviation of three replicates. A two-sample unequal variance directional *t*-test was used to test the significance of the difference (*$p < 0.05$).

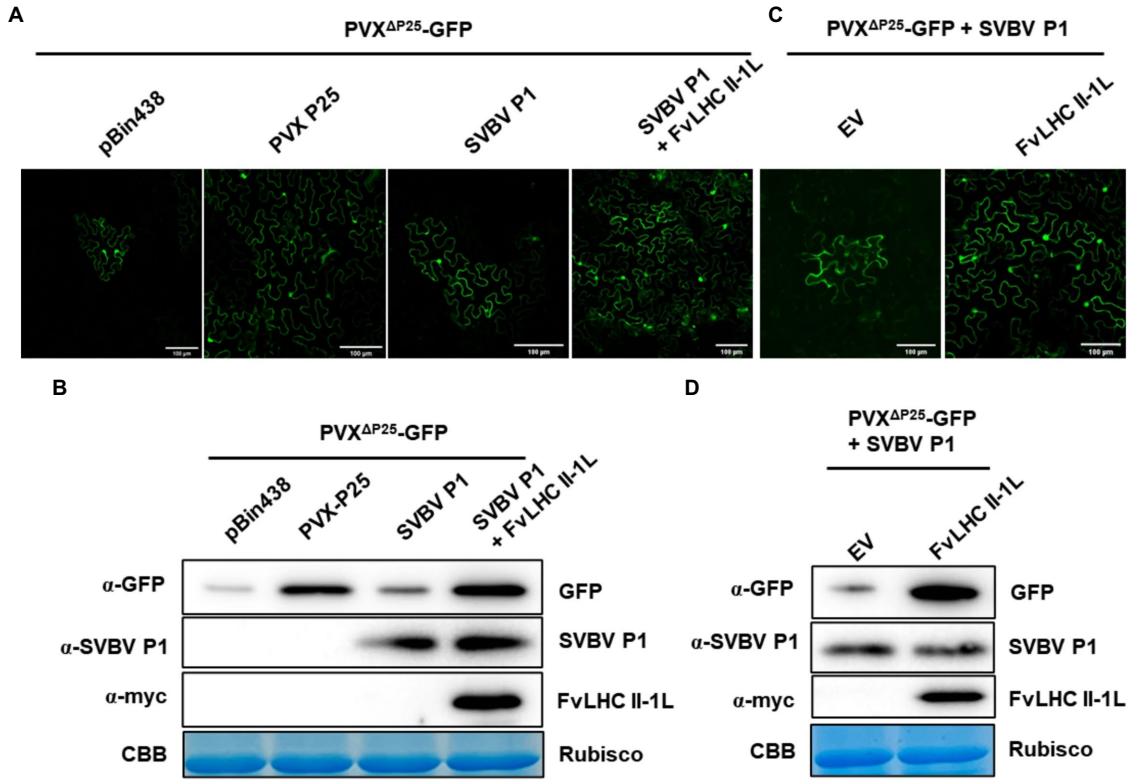

FIGURE 4 | FvLHC II-1L assists SVBV P1 in complementing movement-defective potato virus X (PVX). **(A)** FvLHC II-1L promotes SVBV P1 to complement movement-defective PVX (PVX$^{\Delta P25}$-GFP) in *N. benthamiana*. PVX$^{\Delta P25}$-GFP was co-infiltrated with pBin438 empty vector, P25, SVBV P1, or SVBV P1 and FvLHC II-1L in *N. benthamiana*. GFP fluorescence was observed at 3 dpi. Bar scale = 100 μm. **(B)** Western blot analysis of GFP, SVBV P1, or FvLHC II-1L protein accumulation in infiltrated leaves at 3 dpi. α-GFP, α-SVBV P1, and α-myc antibodies were used to detect the accumulation of GFP, SVBV P1, and FvLHC II-1L, respectively. Coomassie Brilliant Blue-stained RuBisCO was used as the loading control. **(C)** FvLHC II-1L promotes SVBV P1 to complement PVX$^{\Delta P25}$-GFP in FvLHC II-1L transgenic *N. benthamiana*. PVX$^{\Delta P25}$-GFP was co-expressed with SVBV P1 in empty vector (EV) or FvLHC II-1L transgenic *N. benthamiana*. GFP fluorescence was observed at 3 dpi. **(D)** The accumulation of GFP, SVBV P1, and FvLHC II-1L proteins in infiltrated leaves was detected *via* western blotting at 3 dpi.

leaves of CMV$^{\Delta MP}$-SVBV P1-infected FvLHC II-1L transgenic *N. benthamiana* (**Figure 5C**). As expected, CMV CP and SVBV P1 protein accumulation was higher in FvLHC II-1L plants (**Figure 5D**). These results suggest that SVBV P1 was able to complement the systemic movement of CMV$^{\Delta MP}$, and FvLHC II-1L can enhance the complement function of SVBV P1.

Overexpression of FvLHC II-1L Promotes *Fragaria vesca* Infection by SVBV

To further clarify the role of FvLHC II-1L in the infection progression of SVBV in *F. vesca* plants, we used the TRV system to overexpress'in *F. vesca* seedlings before inoculation with SVBV. At 15 dpi, systemic leaves of *F. vesca* seedlings were sampled and subjected to RT-qPCR and western blot analyses. The results showed that the transcript levels of *FvLHC II-1L* and the accumulation of CP-FvLHC II-1L fusion protein in *F. vesca* seedlings infiltrated with pTRV-FvLHC II-1L were higher than those in the seedlings infiltrated with TRV:00 (negative control; **Figure 6A**).

At 15 dpi, TRV:00-infiltrated or TRV:FvLHC II-1L-infiltrated plants were infiltrated with the infectious clone of SVBV. After 35 days, the systemic symptoms of TRV:FvLHC II-1L-infiltrated plants were more severe than those of TRV:00-infiltrated plants (**Figure 6B**). As expected, RT-qPCR, western blotting, and Southern blotting showed that the levels of SVBV CP mRNA transcripts, SVBV CP protein, and DNA accumulation were significantly increased in TRV:FvLHC II-IL plants (**Figures 6C,D**). These results indicated that FvLHC II-1L promoted *F. vesca* infection by SVBV.

DISCUSSION

To infect host plants, plant viruses have to move between cells to achieve local infection, and then move further, over longer distances through the phloem vascular bundles to achieve systematic infection. Both these processes are related to MPs encoded by viruses (Zhou et al., 2019). Not only is SVBV P1 essential for SVBV intercellular movement but it can also complement the movement function of heterologous viruses and promote the intercellular movement of movement-deficient PVX (Rui et al., 2021). In this study, we found that compared with the movement-deficient CMV, the movement-deficient CMV inserted with SVBV P1 systematically moved to the upper leaves *via* long-distance movement,

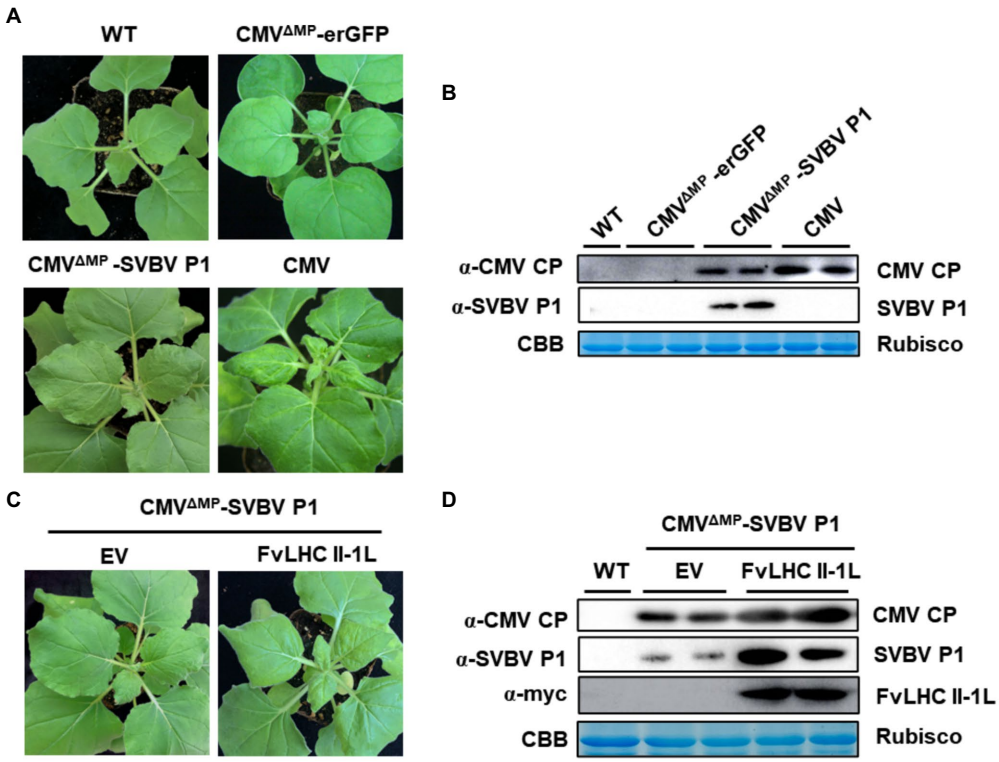

FIGURE 5 | FvLHC II-1L assists SVBV P1 in complementing movement-defective cucumber mosaic virus (CMV). **(A)** Systemic symptoms of wild-type *N. benthamiana* plants agroinfiltrated with CMV, CMV$^{\Delta MP}$-erGFP, or CMV$^{\Delta MP}$-SVBV P1 at 8 dpi. WT indicates non-infiltrated plants that served as the negative control. **(B)** Accumulation of CMV coat protein (CP) and SVBV P1 in systemically infected leaves was detected *via* western blotting. **(C)** Systemic symptoms of empty vector (EV) or FvLHC II-1L transgenic *N. benthamiana* plants agroinfiltrated with CMV$^{\Delta MP}$–SVBV P1 at 8 dpi. **(D)** Accumulation of CMV CP, SVBV P1, and FvLHC II-1L in systemically infected leaves was detected *via* western blotting.

indicating that SVBV P1 complemented the movement-deficient CMV (**Figures 5A,B**). This complement function is not unique to SVBV P1. The MP Nsvc4 encoded by RSV can complement cell-to-cell movement of movement-deficient PVX (Fu et al., 2018). The MP NSm, encoded by tomato spotted wilt virus, can complement cell-to-cell and long-distance movement of movement-deficient tobacco mosaic virus (TMV) and CMV (Li et al., 2009). The MPs encoded by some Rhabdoviruses can complement the intercellular movement of movement-deficient tomato mosaic virus and PVX (Zhou et al., 2019). Thus, the functions of MPs of different viruses are complementary.

During viral infection, many proteins encoded by plant viruses can interact with chloroplast proteins and affect the course of disease development (Bhat et al., 2013; Mathioudakis et al., 2013; Cheng et al., 2021). The replicase protein of TMV interacts with the chloroplast ATPase γ subunit AtpC to block ATP synthesis, decrease photosynthate accumulation, and aggravate viral symptoms (Bhat et al., 2013). The replicase protein of tobacco vein banding mosaic virus interacts with the chloroplast 50S ribosomal protein large submit 1 to promote the accumulation of viral replicase and improve viral replication (Cheng et al., 2021). Pepino mosaic virus (PepMV) MP P26 interacts with tomato chloroplast catalase 1 (CAT1) to improve the activity of CAT1. Silencing of the *CAT1* gene of *N. benthamiana* resulted in a significant decrease in RNA accumulation of PepMV and inhibition of systemic infection by the virus (Mathioudakis et al., 2013). These results suggest that host chloroplast proteins have a close association with plant viral infection. In the present study, the FvLHC II-1L protein, which is another chloroplast protein responsible for maintaining the stability of the electron transport chain of PS II, is an important regulatory factor of photosynthesis and participates in normal plant growth and development. In a previous study, we screened the FvLHC II-1L protein from the cDNA library of *F. vesca* using SVBV P1 as the bait protein (Zhang et al., 2019). Here, FvLHC II-1L was shown to interact with SVBV P1 both *in vitro* and *in vivo* (**Figure 1**). Further experiments showed that the transcription of *FvLHC II-1L* was upregulated during SVBV infection, suggesting that FvLHC II-1L may be involved in viral infection (**Figure 3**). This finding is consistent with those of previous studies showing that chloroplast proteins frequently have important roles in facilitating viral infection (Cheng et al., 2021).

Furthermore, we noted that SVBV P1 and FvLHC II-1L were co-located at the edge of cells, wherein SVBV P1 formed irregular aggregates (**Figure 2**). FvLHC II-1L not only assists

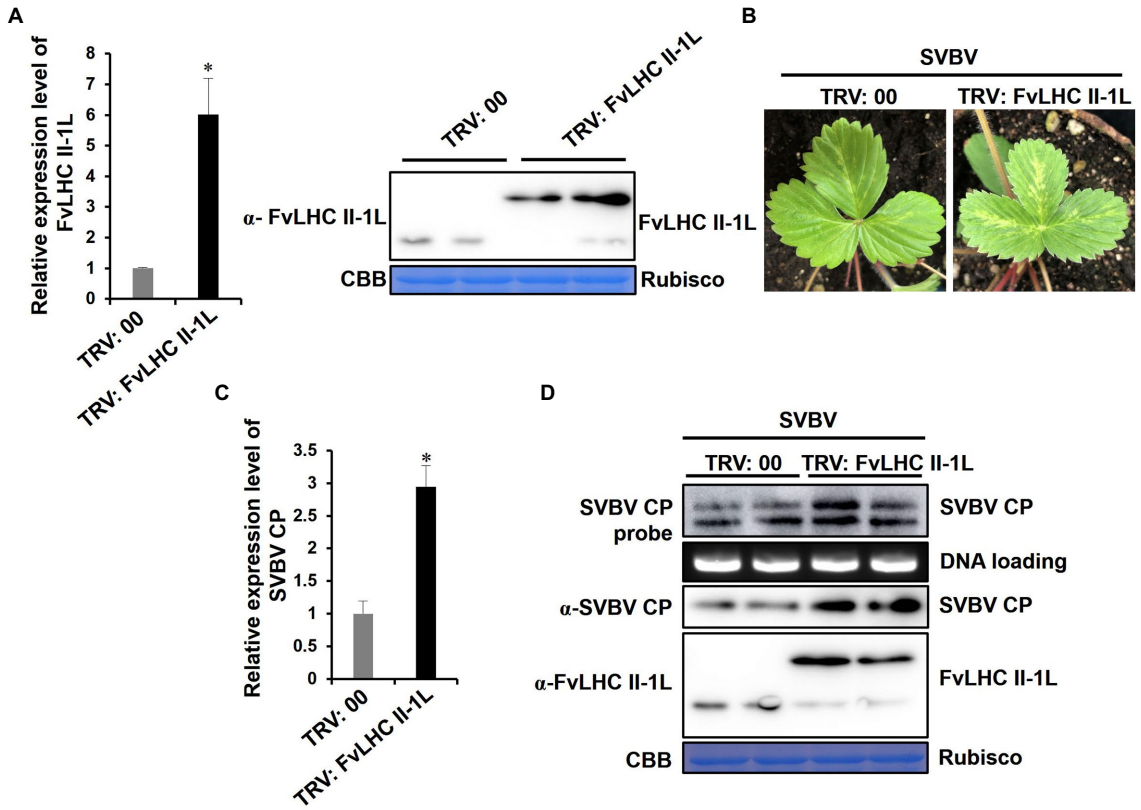

FIGURE 6 | Overexpression of FvLHC II-1L promotes *F. vesca* infection by SVBV. **(A)** The transcript levels of *FvLHC II-1L* and the accumulation of FvLHC II-1L protein in TRV:00-infected or TRV:FvLHC II-1L-infected leaves of *F. vesca* were determined *via* RT-qPCR analysis and Western blot at 15 dpi. TRV:00 indicates plants infiltrated with tobacco rattle virus (TRV) empty vector, serving as the negative control. **(B)** Systemic symptoms of TRV:00 or TRV:FvLHC II-1L pre-infected plants inoculated with SVBV *via* vacuum-infiltration. The phenotype of SVBV infection was monitored and photographed at 35 days post SVBV inoculation. **(C)** The transcript levels of *SVBV CP* in systemically infected leaves of TRV:00 and TRV:FvLHC II-1L pre-infected *F. vesca* were quantified using RT-qPCR analysis. **(D)** Accumulation of SVBV CP and FvLHC II-1L proteins and SVBV CP DNA, in systemically infected leaves, was detected *via* Western and Southern blotting, respectively.

SVBV P1 to accelerate the intercellular movement of the PVX transport-deficient mutant but also promotes SVBV P1 to complement the systemic movement of the CMV transport-deficient mutant (**Figures 4, 5**). It has been reported that the MP P3N-PIPO of turnip mosaic virus (TuMV) interacts with *Arabidopsis thaliana* plasma membrane-associated Ca^{2+} binding protein 1 to expand the diameter of PD and promote viral infection (Vijayapalani et al., 2012). The PVX MP TGB12K interacts with tobacco TIP1 protein, which can act on β-1,3-glucanase and increase the diameter of PD, thereby promoting intercellular transport of PVX (Fridborg et al., 2003). The P25 protein of PVX interacts with the chloroplast ferridoxin 1 (FD1) protein to reduce callose deposition in PD and enhance viral infection (Yang et al., 2020). Rice chloroplast FD1 has previously been demonstrated to be an important component of the photosynthetic electron transport chain that can affect plant growth and development. Therefore, it is reasonable to speculate that FvLHC II-1L functions as a key protein in the photosynthetic electron transport chain of *F. vesca*, which can interact with SVBV P1 and co-locate with it in cell walls, decrease callose deposition, increase the diameter of PD, and promote viral intercellular and systemic movement. Additionally, in the current study, we showed that overexpression of FvLHC II-1L accelerated the course of SVBV infection (**Figure 6**).

Chloroplasts are not only involved in photosynthesis but also have a close association with salicylic acid and other resistance pathways that are activated by the accumulation of reactive oxygen species (ROS; Nomura et al., 2012; Chan et al., 2016; Serrano et al., 2016). The C4 protein encoded by tomato yellow leaf curve virus can move from the cell membrane to the chloroplast during tobacco infection and can bind to the calcium sensor protein of chloroplasts to inhibit resistance signal transduction (Medina-Puche et al., 2020). The γb protein, encoded by BSMV, interacts with chloroplast NADPH-dependent thioredoxin reductase C (NTRC) to inhibit NTRC-mediated antioxidant defense and promote viral infection (Wang et al., 2021). Similarly, the VPg protein of TuMV interacts with the NADH dehydrogenase-like complex M subunit (NdhM) of *N. benthamiana* chloroplasts to prevent export from the nucleus and inhibit the NdhM-mediated defense response in the host (Zhai et al., 2021). FvLHC II-1L is the core protein of the

light-harvesting complex of PS II in *F. vesca*. We speculated that the overexpression of FvLHC II-1L would result in chloroplasts absorbing excess light energy, leading to disruption of the balance between ROS production and cleanup and initiation of ROS-dependent resistance signal pathways. Interaction of SVBV P1 with FvLHC II-1L likely reduces the levels of FvLHC II-1L in chloroplasts, leading to a reduction in the intensity of photosynthesis, and subsequently, the reduction of ROS accumulation, inhibition of immune response, and promotion of viral infection.

DATA AVAILABILITY STATEMENT

The original contributions presented in the study are included in the article/**Supplementary Material**; further inquiries can be directed to the corresponding authors.

AUTHOR CONTRIBUTIONS

XZ, LJ, and TJ conceived and designed the study. SX, XZ, KX, and ZW performed the experiments and data analysis. SX, XZ, and KX wrote the manuscript. All authors contributed to the article and approved the submitted version.

FUNDING

This research was funded by the Grants from the National Natural Science Foundation of China (nos. 32072386 and 31801700), the Anhui Provincial Key Research and Development Plan (no. 202004a06020013), the Zhejiang Basic Public Welfare Research Project of China (no. LGN19C140002), and the Postdoctoral Science Foundation of Anhui Province (no. 2019B360).

ACKNOWLEDGMENTS

We thank Xiaorong Tao (Nanjing Agricultural University, China) for providing the system of movement-defective CMV. We also thank Fei Yan (Ningbo University, China) for providing the wild-type PVX-GFP and the movement-deficient PVX$^{\Delta P25}$.

SUPPLEMENTARY MATERIAL

The Supplementary Material for this article can be found online at: https://www.frontiersin.org/articles/10.3389/fmicb.2022.884044/full#supplementary-material

REFERENCES

Allen, J. F., Bennett, J., Steinback, K. E., and Arntzen, C. J. (1981). Chloroplast protein phosphorylation couples plastoquinone redox state to distribution of excitation energy between photosystems. *Nature* 291, 25–29. doi: 10.1038/291025a0

Bhat, S., Folimonova, S. Y., Cole, A. B., Ballard, K. D., Lei, Z., Watson, B. S., et al. (2013). Influence of host chloroplast proteins on tobacco mosaic virus accumulation and intercellular movement. *Plant Physiol.* 161, 134–147. doi: 10.1104/pp.112.207860

Chan, K. X., Phua, S. Y., Crisp, P., McQuinn, R., and Pogson, B. J. (2016). Learning the languages of the chloroplast: retrograde signaling and beyond. *Annu. Rev. Plant Biol.* 67, 25–53. doi: 10.1146/annurev-arplant-043015-111854

Chen, M. H., Sheng, J., Hind, G., Handa, A. K., and Citovsky, V. (2000). Interaction between the tobacco mosaic virus movement protein and host cell pectin methylesterases is required for viral cell-to-cell movement. *EMBO J.* 19, 913–920. doi: 10.1093/emboj/19.5.913

Chen, J., Zhang, H., Feng, M., Zuo, D., Hu, Y., and Jiang, T. (2016a). Transcriptome analysis of woodland strawberry (*Fragaria vesca*) response to the infection by strawberry vein banding virus (SVBV). *Virol. J.* 13:128. doi: 10.1186/s12985-016-0584-5

Chen, X., Zhu, M., Jiang, L., Zhao, W., Li, J., Wu, J., et al. (2016b). A multilayered regulatory mechanism for the autoinhibition and activation of a plant CC-NB-LRR resistance protein with an extra N-terminal domain. *New Phytol.* 212, 161–175. doi: 10.1111/nph.14013

Cheng, D. J., Xu, X. J., Yan, Z. Y., Tettey, C. K., Fang, L., Yang, G. L., et al. (2021). The chloroplast ribosomal protein large subunit 1 interacts with viral polymerase and promotes virus infection. *Plant Physiol.* 187, 174–186. doi: 10.1093/plphys/kiab249

Feng, Z., Chen, X., Bao, Y., Dong, J., Zhang, Z., and Tao, X. (2013). Nucleocapsid of tomato spotted wilt tospovirus forms mobile particles that traffic on an actin/endoplasmic reticulum network driven by myosin XI-K. *New Phytol.* 200, 1212–1224. doi: 10.1111/nph.12447

Feng, M., Zhang, H., Pan, Y., Hu, Y., Chen, J., Zuo, D., et al. (2016). Complete nucleotide sequence of strawberry vein banding virus Chinese isolate and infectivity of its full-length DNA clone. *Virol. J.* 13:164. doi: 10.1186/s12985-016-0624-1

Frazier, N. W. (1974). Detection of graft-transmissible diseases in strawberry by a modified leaf grafting technique. *Plant Dis. Rep.* 58, 203–207.

Fridborg, I., Grainger, J., Page, A., Coleman, M., Findlay, K., and Angell, S. (2003). TIP, a novel host factor linking callose degradation with the cell-to-cell movement of potato virus X. *Mol. Plant Microbe Interact.* 16, 132–140. doi: 10.1094/MPMI.2003.16.2.132

Fu, S., Xu, Y., Li, C., Li, Y., Wu, J., and Zhou, X. (2018). Rice stripe virus interferes with S-acylation of Remorin and induces its autophagic degradation to facilitate virus infection. *Mol. Plant* 11, 269–287. doi: 10.1016/j.molp.2017.11.011

Huang, W., Chen, Q., Zhu, Y., Hu, F., Zhang, L., Ma, Z., et al. (2013). Arabidopsis thylakoid formation 1 is a critical regulator for dynamics of PSII-LHCII complexes in leaf senescence and excess light. *Mol. Plant* 6, 1673–1691. doi: 10.1093/mp/sst069

Jiang, L., Li, S., Jiang, X., and Jiang, T. (2021). Complete genome sequence of two strawberry vein banding virus isolates from China. *Biocell* 45, 1695–1702. doi: 10.32604/biocell.2021.015250

Li, S., Hu, Y., Jiang, L., Rui, P., Zhao, Q., Feng, J., et al. (2018a). Strawberry vein banding virus P6 protein is a translation trans-activator and its activity can be suppressed by FveIF3g. *Viruses* 10:717. doi: 10.3390/v10120717

Li, W., Lewandowski, D. J., Hilf, M. E., and Adkins, S. (2009). Identification of domains of the tomato spotted wilt virus NSm protein involved in tubule formation, movement and symptomatology. *Virology* 390, 110–121. doi: 10.1016/j.virol.2009.04.027

Li, P., Liu, C., Deng, W. H., Yao, D. M., Pan, L. L., Li, Y. Q., et al. (2019). Plant begomoviruses subvert ubiquitination to suppress plant defenses against insect vectors. *PLoS Pathog.* 15:e1007607. doi: 10.1371/journal.ppat.1007607

Li, Z., Zhang, Y., Jiang, Z., Jin, X., Zhang, K., Wang, X., et al. (2018b). Hijacking of the nucleolar protein fibrillarin by TGB1 is required for cell-to-cell movement of barley stripe mosaic virus. *Mol. Plant Pathol.* 19, 1222–1237. doi: 10.1111/mpp.12612

Lucas, W. J. (2006). Plant viral movement proteins: agents for cell-to-cell trafficking of viral genomes. *Virology* 344, 169–184. doi: 10.1016/j.virol.2005.09.026

Mathioudakis, M. M., Veiga, R. S., Canto, T., Medina, V., Mossialos, D., Makris, A. M., et al. (2013). Pepino mosaic virus triple gene block protein

1 (TGBp1) interacts with and increases tomato catalase 1 activity to enhance virus accumulation. *Mol. Plant Pathol.* 14, 589–601. doi: 10.1111/mpp.12034

Medina-Puche, L., Tan, H., Dogra, V., Wu, M., Rosas-Diaz, T., Wang, L., et al. (2020). A defense pathway linking plasma membrane and chloroplasts and co-opted by pathogens. *Cell* 182, 1109–1124.e25. doi: 10.1016/j.cell.2020.07.020

Neilson, J. A., and Durnford, D. G. (2010). Structural and functional diversification of the light-harvesting complexes in photosynthetic eukaryotes. *Photosynth. Res.* 106, 57–71. doi: 10.1007/s11120-010-9576-2

Nilsson, A., Stys, D., Drakenberg, T., Spangfort, M. D., Forsén, S., and Allen, J. F. (1997). Phosphorylation controls the three-dimensional structure of plant light harvesting complex II. *J. Biol. Chem.* 272, 18350–18357. doi: 10.1074/jbc.272.29.18350

Nomura, H., Komori, T., Uemura, S., Kanda, Y., Shimotani, K., Nakai, K., et al. (2012). Chloroplast-mediated activation of plant immune signalling in Arabidopsis. *Nat. Commun.* 3:926. doi: 10.1038/ncomms1926

Pan, Y., Zhou, X., Li, S., Feng, M., Shi, M., Zuo, D., et al. (2018). Strawberry vein banding virus P6 protein intracellular transport and an important domain identifcation. *J. Integr. Agr.* 17, 2031–2041. doi: 10.1016/S2095-3119(18)61978-1

Park, M. R., Jeong, R. D., and Kim, K. H. (2014). Understanding the intracellular trafficking and intercellular transport of potexviruses in their host plants. *Front. Plant Sci.* 5:60. doi: 10.3389/fpls.2014.00060

Pattanaik, S., Dey, N., Bhattacharyya, S., and Maiti, I. B. (2004). Isolation of full-length transcript promoter from the strawberry vein banding virus (svbv) and expression analysis by protoplasts transient assays and in transgenic plants. *Plant Sci.* 167, 427–438. doi: 10.1016/j.plantsci.2004.04.011

Peiro, A., Izquierdo-Garcia, A. C., Sanchez-Navarro, J. A., Pallas, V., Mulet, J. M., and Aparicio, F. (2014). Patellins 3 and 6, two members of the plant Patellin family, interact with the movement protein of alfalfa mosaic virus and interfere with viral movement. *Mol. Plant Pathol.* 15, 881–891. doi: 10.1111/mpp.12146

Pietrzykowska, M., Suorsa, M., Semchonok, D. A., Tikkanen, M., Boekema, E. J., Aro, E. M., et al. (2014). The light-harvesting chlorophyll a/b binding proteins Lhcb1 and Lhcb2 play complementary roles during state transitions in Arabidopsis. *Plant Cell* 26, 3646–3660. doi: 10.1105/tpc.114.127373

Ratti, C., Pisi, A., Rubies Autonell, C., Babini, A., and Vicchi, V. (2009). First report of strawberry vein banding virus on strawberry in Italy. *Plant Dis.* 93:675. doi: 10.1094/PDIS-93-6-0675A

Rui, P., Wang, Z., Shan, W., Xia, W., Zhou, X., Yang, L., et al. (2021). P1 of strawberry vein banding virus is a multilocalized protein that functions as a movement protein and interacts with the coat protein. *J. Integr. Agr.* 21, 1071–1083. doi: 10.1016/S2095-3119(21)63711-5 [Epub ahead of print].

Schoelz, J. E., Angel, C. A., Nelson, R. S., and Leisner, S. M. (2016). A model for intracellular movement of cauliflower mosaic virus: the concept of the mobile virion factory. *J. Exp. Bot.* 67, 2039–2048. doi: 10.1093/jxb/erv520

Schoelz, J. E., Harries, P. A., and Nelson, R. S. (2011). Intracellular transport of plant viruses: finding the door out of the cell. *Mol. Plant* 4, 813–831. doi: 10.1093/mp/ssr070

Serrano, I., Audran, C., and Rivas, S. (2016). Chloroplasts at work during plant innate immunity. *J. Exp. Bot.* 67, 3845–3854. doi: 10.1093/jxb/erw088

Shen, Y., Zhao, X., Yao, M., Li, C., Miriam, K., Zhang, X., et al. (2014). A versatile complementation assay for cell-to-cell and long distance movements by cucumber mosaic virus based agro-infiltration. *Virus Res.* 190, 25–33. doi: 10.1016/j.virusres.2014.06.013

Sun, Y. D., Zhang, L., and Folimonova, S. Y. (2021). Citrus miraculin-like protein hijacks a viral movement-related p33 protein and induces cellular oxidative stress in defence against citrus tristeza virus. *Plant Biotechnol. J.* 19, 977–991. doi: 10.1111/pbi.13523

Tian, J., Cheng, L., Han, Z., and Yao, Y. (2015). Tobacco rattle virus mediated gene silencing in strawberry plants. *Plant Cell Tiss. Org.* 120, 1131–1138. doi: 10.1007/s11240-014-0669-z

Tian, J., Pei, H., Zhang, S., Chen, J., Chen, W., Yang, R., et al. (2014). TRV-GFP: a modified tobacco rattle virus vector for efficient and visualizable analysis of gene function. *J. Exp. Bot.* 65, 311–322. doi: 10.1093/jxb/ert381

Vijayapalani, P., Maeshima, M., Nagasaki-Takekuchi, N., and Miller, W. A. (2012). Interaction of the trans-frame potyvirus protein P3NPIPO with host protein PCaP1 facilitates potyvirus movement. *PLoS Pathog.* 8:e1002639. doi: 10.1371/journal.ppat.1002639

Wang, X., Jiang, Z., Yue, N., Jin, X., Zhang, X., Li, Z., et al. (2021). Barley stripe mosaic virus γb protein disrupts chloroplast antioxidant defenses to optimize viral replication. *EMBO J.* 40:e107660. doi: 10.15252/embj.2021107660

Wu, X., and Cheng, X. (2020). Intercellular movement of plant RNA viruses: targeting replication complexes to the plasmodesma for both accuracy and efficiency. *Traffic* 21, 725–736. doi: 10.1111/tra.12768

Yan, F., Lu, Y., Lin, L., Zheng, H., and Chen, J. (2012). The ability of PVX p25 to form RL structures in plant cells is necessary for its function in movement, but not for its suppression of RNA silencing. *PLoS One* 7:e43242. doi: 10.1371/journal.pone.0043242

Yang, X., Lu, Y., Wang, F., Chen, Y., Tian, Y., Jiang, L., et al. (2020). Involvement of the chloroplast gene ferredoxin 1 in multiple responses of *Nicotiana benthamiana* to potato virus X infection. *J. Exp. Bot.* 71, 2142–2156. doi: 10.1093/jxb/erz565

Zhai, Y., Yuan, Q., Qiu, S., Li, S., Li, M., Zheng, H., et al. (2021). Turnip mosaic virus impairs perinuclear chloroplast clustering to facilitate viral infection. *Plant Cell Environ.* 44, 3681–3699. doi: 10.1111/pce.14157

Zhang, X. X., Jiang, X. Z., Li, S., Jiang, L., and Jiang, T. (2019). Screening of the host factors of woodland strawberry interacting with P1 of strawberry vein banding virus by yeast two-hybrid system. *Acta Phytopathol. Sin.* 49, 56–63. doi: 10.13926/j.cnki.apps.000362

Zhou, X., Lin, W., Sun, K., Wang, S., Zhou, X., Jackson, A. O., et al. (2019). Specificity of plant Rhabdovirus cell-to-cell movement. *J. Virol.* 93, e00296–e00219. doi: 10.1128/JVI.00296-19

Zhu, M., Jiang, L., Bai, B., Zhao, W., Chen, X., Li, J., et al. (2017). The intracellular immune receptor Sw-5b confers broad-Spectrum resistance to Tospoviruses through recognition of a conserved 21-amino acid viral effector epitope. *Plant Cell* 29, 2214–2232. doi: 10.1105/tpc.17.00180

Conflict of Interest: The authors declare that the research was conducted in the absence of any commercial or financial relationships that could be construed as a potential conflict of interest.

Publisher's Note: All claims expressed in this article are solely those of the authors and do not necessarily represent those of their affiliated organizations, or those of the publisher, the editors and the reviewers. Any product that may be evaluated in this article, or claim that may be made by its manufacturer, is not guaranteed or endorsed by the publisher.

Copyright © 2022 Xu, Zhang, Xu, Wang, Zhou, Jiang and Jiang. This is an open-access article distributed under the terms of the Creative Commons Attribution License (CC BY). The use, distribution or reproduction in other forums is permitted, provided the original author(s) and the copyright owner(s) are credited and that the original publication in this journal is cited, in accordance with accepted academic practice. No use, distribution or reproduction is permitted which does not comply with these terms.

frontiers | Frontiers in Microbiology

ORIGINAL RESEARCH
published: 09 June 2022
doi: 10.3389/fmicb.2022.910712

Coinfection of Two Mycoviruses Confers Hypovirulence and Reduces the Production of Mycotoxin Alternariol in *Alternaria alternata* f. sp. *mali*

*Bo Li†, Yuhan Cao†, Zixuan Ji, Jingyi Zhang, Xianglong Meng, Pengbo Dai, Tongle Hu, Shutong Wang, Keqiang Cao and Yanan Wang**

State Key Laboratory of North China Crop Improvement and Regulation, College of Plant Protection, Hebei Agricultural University, Baoding, China

OPEN ACCESS

Edited by:
Beilei Wu,
Institute of Plant Protection (CAAS), China

Reviewed by:
Jiatao Xie,
Huazhong Agricultural University, China
Liying Sun,
Northwest A&F University, China

***Correspondence:**
Yanan Wang
wyn3215347@163.com

† These authors have contributed equally to this work and share first authorship

Specialty section:
This article was submitted to Microbe and Virus Interactions with Plants, a section of the journal Frontiers in Microbiology

Received: *01 April 2022*
Accepted: *28 April 2022*
Published: *09 June 2022*

Citation:
Li B, Cao Y, Ji Z, Zhang J, Meng X, Dai P, Hu T, Wang S, Cao K and Wang Y (2022) Coinfection of Two Mycoviruses Confers Hypovirulence and Reduces the Production of Mycotoxin Alternariol in Alternaria alternata f. sp. mali. Front. Microbiol. 13:910712. doi: 10.3389/fmicb.2022.910712

Alternaria leaf blotch caused by *Alternaria alternata* apple pathotype (*Alternaria mali*) is an important fungal disease that affects the production of apples worldwide. Mycoviruses harbored in plant pathogenic fungi can confer hypovirulence in their hosts and have attracted widespread attention as potential biocontrol tools. In this study, the coinfection of two mycoviruses, named *A. alternata* chrysovirus 1 strain QY2 (AaCV1-QY2) and *A. alternata* magoulivirus 1 (AaMV1), respectively, were isolated from *A. alternata* f. sp. *mali* strain QY21. Sequence analyses revealed that AaCV1-QY2 virus belonged to the genus *Betachrysovirus* and AaMV1 virus belonged to the genus *Magoulvirus.* These two mycoviruses were found to be associated with hypovirulence in *A. alternata*, among which AaCV1-QY2 might play a relatively leading role. Because the elimination of AaMV1 from the strain QY21 does not affect the hypovirulence trait, which indicates that the virus AaCV1-QY2 can independently induce slow growth and reduce host virulence. Moreover, the presence of viruses decreased the accumulation of the mycotoxin alternariol (AOH) in *A. alternata* strains. Intriguingly, AaCV1-QY2/AaMV1 mycoviruses can be horizontally transmitted to other *A. alternata* strains, and this coinfection can promote the interspecific transmission efficiency of AaCV1-QY2. To our knowledge, this study reports the first description of the member of *Chrysovirus* is related to hypovirulence in *Alternaria* spp. that facilitates the development of biocontrol measures of *A. mali* Roberts.

Keywords: mycovirus, mycotoxin, co-infection, *Alternaria alternata*, apple leaf blotch disease, hypovirulence

INTRODUCTION

Mycoviruses (fungal viruses) are universally found in the main taxonomic groups of fungi, including phytopathogenic species. The majority of mycoviruses have double-stranded RNA (dsRNA) or positive-sense single-stranded RNA (+ssRNA) genomes, and they can or cannot have a capsid (Ghabrial et al., 2015). Due to the lack of external transmission pathways in most cases,

mycoviruses are not typically infectious in the traditional sense (Yu et al., 2013). They are horizontal transmitted between strains mainly through hyphal anastomosis and vertically transmitted *via* spore production (García-Pedrajas et al., 2019). Most viral infections in fungi are commonly latent; however, some of them are capable of altering the phenotypic features and/or pathogenicity of fungal phytopathogenic hosts, that is, to say, conferring hypervirulence or hypovirulence of their hosts (Sun et al., 2020). From an agricultural perspective, innovative biocontrol measures to fungal diseases with the least negative impact on the environment and human health have attracted much more attention. In this context, the use of hypovirulent mycoviruses as control agents to protect plants from fungal diseases has become an up-and-coming biocontrol strategy.

During the last few decades, the most typical examples of the application of hypovirulent mycoviruses are that *Cryphonectria hypovirus* 1 (CHV1) is used to control chestnut blight caused by *Cryphonectria parasitica*, and is effectively commercialized in Europe (Martins et al., 2014). Because CHV1 infection causes phenotypic changes such as the suppression of sexual spore production, decreased pigmentation, and induces transmissible hypovirulence, which provides a foundation for biocontrol of chestnut blight. Except hypovirulence-assocated virus CHV1, which is a +ssRNA virus belonging to the family *Hypoviridae*, to date, several hypovirulence-inducing mycoviruses have been identified in the *Chrysoviridae* [*Botryosphaeria dothidea* Chrysovirus 1 (BdCV1)] (Ding et al., 2017), *Botourmiaviridae* [*Fusarium oxysporum* ourmia-like virus 1 (FoOuLV1)] (Zhao et al., 2020), *Partitiviridae* [*Colletotrichum liriopes* partitivirus 1 (ClPV1)] (Zhu et al., 2021), *Endornaviridae* [*Rhizoctonia solani* endornavirus 1 (RsEV1)] (Das et al., 2014), *Mitoviridae* [*Sclerotinia sclerotiorum* mitovirus 1 (SsMV1)] (Xu et al., 2015), *Reoviridae* [*Rosellinia necatrix* mycoreovirus 3 (RnMYRV-3)] (Yang et al., 2021), and *Genomoviridae* [*S. sclerotiorum* hypovirulence-associated DNA virus 1 (SsHADV-1)] (Yu et al., 2010) families form important phytopathogenic fungi. Moreover, the coinfection of mycoviruses is a very common phenomenon in nature. There are several interactions between co-infected mycoviruses, which variously regulate the phenotype and/or pathogenicity of the hosts according to the combination of virus partners, ranging from synergism to neutrality and antagonism (Thapa and Roossinck, 2019). For example, dual infection with Heterobasidion partitivirus 13 (HetPV13)-an1 and HetPV15-pa1 stably and drastically inhibited host growth, whereas the presence of co-infected viruses HetPV13-an1 and HetPV11-au1 had no or very little impact on their host (Kashif et al., 2019). The recognition that mycoviruses have the ability to induce hypovirulence in their hosts, which elicited great interest in the identification and characterization of viruses from phytopathogenic fungi because of their potential for controlling fungal diseases.

Alternaria species are very successful pathogenic genera that cause a wide range of plant diseases (Thomma, 2003). Approximately 300 species of the genus Alternaria have been identified worldwide, including *Alternaria tenuifolia*, *A. tenuifolia*, and *Alternaria solani*, of which *A. alternata* infects nearly 100 plant species. Some *A. alternata* strains even produce non-host-specific toxins (nHSTs) that induce phytotoxic effects on a broad range of plant species, generally as virulence factors, aggravating the severity of disease symptoms (Meena et al., 2017). *A. alternata* f. sp. *mali* is the forma specialis of *A. alternata* that infects apple (*Malus pumila Mill*), causing severe leaf blotch disease all over the world (Fontaine et al., 2021). Considering that *Alternaria* blotch disease has become a serious threat to apple production in China, it is necessary to explore hypovirulence-associated mycoviruses that may be used as virocontrol agents against *A. alternata* f. sp. *mali*.

To date, many mycoviruses infecting different *A. alternata* strains have been reported; however, few of them have been amply proven to possess hypovirulent effects on their hosts. The first mycovirus in *A. alternata* was discovered in 1988 with dsRNAs associated with virus-like particles in six isolates that produce tentoxin (Shepherd, 1988). To our knowledge, mycoviruses from more than six families have been found to be associated with *A. alternata*. These include multiple dsRNA mycoviruses *A. alternata* partitivirus 1 (AtPV1) (da Silva Xavier et al., 2018), *A. alternata* polymycovirus 1 (AaPmV1) (Ma et al., 2022), *A. alternata* victorivirus 1 (AalVV1) (Jamal et al., 2019), *A. alternata* virus 1 (AAV1) (Wu et al., 2021), *A. alternata* chrysovirus 1 (AaCV1) (Aoki et al., 2009; Okada et al., 2018), and *A. alternata* botybirnavirus 1 (AaBRV1) (Ma et al., 2019), classified as the families *Partitiviridae*, *Polymycoviridae*, *Totiviridae*, *Alternaviridae*, *Chrysoviridae*, and unassigned, respectively. Among them, AaCV1 infection has been shown to impair host growth in phenotype, but has been shown to enhance host virulence in pathogenicity by increasing the production of AK toxins during spore germination (Okada et al., 2018). Moreover, a novel ssRNA mycovirus *A. alternata* magoulivirus 1 (AaMV1), belonging to the family *Hypoviridae*, was identified from an apple orchard in China. And AaHV1 is the first mycovirus reported to slow the growth and attenuate the pathogenicity of *Alternaria* spp. (Li H. et al., 2019). Hypovirulence-associated mycovirus infection might be considered one of the meaningful mechanisms of natural decline of fungal diseases. However, in comparison with plant and animal viruses, the molecular characterization of mycoviruses and the virulence attenuation mechanisms of their host are still poorly understood.

In this study, we screened the dsRNAs in *A. alternata* f. sp. *mali* strain QY-2 isolated from an orchard in North China, which cause apple leaf blotch disease, and two hypovirulence-inducing mycoviruses, designated as *A. alternata* chrysovirus 1 strain QY2 (AaCV1-QY2) and *A. alternata* ourmia-like virus 1 (AaMV1) was identified. Meanwhile, we performed genome characterization to clarify the molecular properties of AaMV1 and AaCV1-QY2, investigate their influence on phenotypic alteration, pathogenicity, transmission efficiency, and nHST production in *A. alternata*. We also preliminarily explored the interplay between these two mycoviruses in the induction of hypovirulence during coinfection in the laboratory. This is the

first description of the coinfection of mycoviruses associated with impaired growth and attenuation of virulence in *A. alternata*.

MATERIALS AND METHODS

Fungal Isolates and Culturing Conditions

Alternaria alternata f. sp. *mali* strain QY-2 was isolated from an *Alternaria* blotch-diseased leaf of *Malus domestica* cv. Tengmu 1 in Hebei province of China in 2018. All collected and derived strains were cultured on potato dextrose agar (PDA) plate at 25°C in the dark. The hypovirulence strain QY21 is a single-conidium isolate progeny of QY-2. Mycelial plugs and asexual spores were preserved in glycerol (15%) at −80°C in the Lab of Plant Disease Epidemiology and IPM of Hebei Agricultural University (AUH), Baoding, Hebei province, China, all of which were verified by Koch's rule and identified by sequencing of the translation elongation factor-1 α (*TEF-1α*) gene.

RNA Extraction and Purification

The 5 mm mycelial plug of the strain QY21 was cultured on PDA medium overlaid with sterile cellophane for 4 days, then fungal mycelia were harvested and ground in liquid nitrogen. Viral dsRNA was extracted from 400 mg of mycelia or virus particles using cellulose (Sigma-Aldrich, St. Louis, MO, United States) column chromatography as previously described (Yang et al., 2021). Separated dsRNA samples digested with RNase-free DNase I and S1 nuclease were analyzed by electrophoresis in an agarose gel (1% wt/vol) at 80 V and visualized by staining with ethidium bromide under 350 nm ultraviolet (UV) illumination. Total RNA was isolated form 200 mg of fresh mycelia or Begonia (*Malus micromalus*) leaf using the TRIzol reagent (Newbio Industry, Wuhan, China) as described by the manufacturer. Total RNA quality was evaluated by agarose gel electrophoresis.

cDNA Cloning and Sequencing

Virome sequencing was performed on the Illumina HiSeq 2000 sequencing platform by SHBIO Biotechnology Corporation (Shanghai, China). Total RNA of the strain QY21 was used as a template for deep sequencing analysis. Preparation of the cDNA library was performed with TruSeq RNA Sample Prep kit v2 (Illumina, San Diego, CA, United States). Raw reads were cleaned by removing adapter sequences, and low quality reads were trimmed with FASTP version 1.5.6 before assembly. All clean reads were assemble *de novo* using MEGAHIT version 1.0 (Li et al., 2016). The assembled contigs were classified based on viral sequence identities by BLASTX searches with the cutoff[1] of $E \leq 1e^{-5}$. To obtain the complete sequence of mycoviruses, rapid RNA ligase-mediated amplification of cDNA ends (RACE) was performed using the SMART TM RACE cDNA Amplification kit (Takara, Dalian, China) according to the manufacturer's protocol.

Sequence and Phylogenetic Analyses

Sequence assembly of each region of genome was performed with the SeqMan software v7.1.0 (DNASTAR, Inc., Madison, WI, United States). The open reading frames (ORFs) and conserved domains of the mycoviruses were predicted from the National Center for Biotechnology Information (NCBI) website, and their homologous amino acid (AA) sequences were searched using BLASTp programs, respectively. Multiple sequence alignment was performed using the CLUSTAL X v2.0 (Larkin et al., 2007). A maximum likelihood (ML) phylogenetic tree was constructed based on AA alignments using MEGA X with 1,000 bootstrap replicates (Kumar et al., 2018). The virus reference sequence used for comparative analyses in this study was obtained from the NCBI database.

Reverse Transcription-Polymerase Chain Reaction Detection

For reverse transcription-polymerase chain reaction (RT-PCR) detection of the different mycoviruses in fungal strains, first-strand cDNA was synthesized using the TransScript One-Step gDNA Removal and cDNA Synthesis SuperMix kit (TransGen Biotech, Shanghai, China) using total RNA as template. Then, the segmental sequences were amplified using Taq DNA polymerase (TaKaRa, Dalian, China) with the specific primers (AaCV1-QY2f and AaCV1-QY2r for ORF1 of AaCV1-QY2; AaMV1f and AaMV1r for ORF6 of AaMV1) to identify the presence of the corresponding mycoviruses. All primers used in this study are listed in **Supplementary Table 1**.

Purification of Virus Particles

Mycoviruses-infected QY21 strain was used for virus particle purification. Approximately 20 g of mycelia cultured on PDB for 7 days were harvested and ground into fine power in liquid nitrogen. The obtained powder was homogenized with 0.1 M phosphate buffer (pH 7.0) containing 0.1% β-mercaptoethanol and shaken at 150 rpm for 30 min at 4°C, and then centrifuged two times at 10,000 × *g* for 15 min to remove cell debris. The resulting supernatant was further ultracentrifuged at 100,000 × *g* for 1 h (Optima LE-80K, Beckman Coulter, Inc., United States) to collect pellets. The precipitates were resuspended in 0.5 ml of PB buffer. Followed by centrifugation at 10,000 × *g* for 1 min, the final supernatants were overlaid and ultracentrifuged at 70,000 × *g* for 3 h in sucrose density gradients (10–60%). Virus particle fractions were further centrifuged at 100,000 × *g* for 3 h, and the resulting pellets were re-suspended in 50 μl of 0.05 M PB buffer. The purified virus particle was visualized with the transmission electron microscope (TEM) Hitachi H-7650 (Tokyo, Japan) after staining with 2% (wt/vol) phosphotungstic acid solution (pH 7.4).

Elimination of the Mycovirus From the Strain QY21

We performed cycloheximide treatment to eliminate the virus from the strain QY21 as previously described with minor modifications (Shah et al., 2020). Briefly, 0.2-mm hyphal tips or a single spore of the strain QY21 was transferred to PDA medium containing two different chemicals 100 μg/ml ribavirin and 100 μg/ml cycloheximide, and cultured at 25°C for 5 days in the dark. After three –to five successive treatments, hyphal tips

[1] http://blast.ncbi.nlm.nih.gov/

were subcultured on PDA at 25°C for 7 days. After successive transfer culture three to five times on cycloheximide-treated PDA medium, the hyphal tips were individually subcultured on cycloheximide-free PDA at 25°C for another 5 days. Finally, the presence of the virus in the regenerated fungal strains was detected by RT-PCR.

Extraction and Quantification of Mycotoxins

After removal of the mycelium cultured on PDA plates, 1 g of agar plugs were cut from the center of 7-day-old fungal colonies and placed in a 5-ml microcentrifuge tube. Extraction solvent [ethyl acetate/dichloromethane/methanol (3: 2: 1, v/v/v)] containing 2% formic acid was added to each tube, and the plugs were extracted by ultrasonic treatment for 60 min. Then the supernatant was transferred to a clean tube after centrifugation at 4,000 × g for 2 min and freeze-drying the samples for 12–24 h to remove all water. Thereafter, the samples were redissolved in 500 μl of methanol-water (50:50 v/v) with 1% formic acid and filtered through a 0.22-μm pore size nylon membrane (RephiLe Bioscience, Philadelphia, PA, United States). Mycotoxins in the extract were then quantitatively analyzed by high-performance liquid chromatography (HPLC) Agilent 1290 system (CA, United States) using an Agilent Eclipse Plus C18 (50 nm × 2.1 mm × 1.8 μm).

The sample injection volume was 2 μl with a flow rate of 0.25 ml/min at 40°C. The mobile phase was composed of phases A (water) and B (methanol), both with 1% formic acid. The elution program was set as follows: 10% B (initial), 10–90% B (0–6 min), 90% B (6–7 min), 90–10% B (7–7.1 min), 10% B (7.1–9 min), and held for further 3 min for re-equilibration (total run time 12 min). The mycotoxin alternariol (AOH) stock standard was diluted with methanol-water (50:50 v/v) solution containing 1% formic acid to six concentrations (2.5, 5, 10, 50, and 100 μg/ml) to construct a calibration curve, so as to determine the concentration of mycotoxin in the samples. The toxigenic potential of the virus-free and virus-infected strains was evaluated by testing the pathogenicity of 10 μl of mycotoxins extracted from the different strains inoculated in Begonia leaves.

Horizontal Transmission Assay

The co-culture experiment was chosen to evaluate the potential horizontal transmission of viruses harbored in *Alternaria* strains. Virus-carrying strains QY21 or QY21-C1 were used as virus donors; the virus-free isogenic strain QY21-C2 or other 99 virus-free allogenetic strains were used as virus recipients, respectively. First, a mycelial plug of the fungal strains QY21 or QY21-C1, respectively, was co-cultured for 14 days on a fresh PDA plate with mycelial plug of each recipient, which was kept close to each other (10–15 mm). Then, the mycelial plugs, which were close to the recipient strain but far away from the strain QY21, are transferred to a new PDA plate and cultured in the dark at 25°C for 7 days. Virus transport in these derivative strains was evaluated based on visual observation of distinctive mycovirus-associated colony morphologies and virus detection by RT-PCR with virus-specific primers.

To determine the transmission trait of the mycovirus of virus-infected strain QY21 to Begonia leaves. Plugs of virus-carrying and virus-free fungal strains were inoculated onto Begonia leaves, respectively. After 7 days of culture, total RNA was extracted from leaves (0, 1, and 2 cm away from the diseased spot or inoculated site). The presence of the virus in leaves was confirmed by RT-PCR detection.

Vertical Transmission Assay

Conidia collected from the cultures of the infected strains QY21 and QY21 were used to prepare the subculture of single spore to analyze mycovirus vertical transmission rates. A total of 100 single-spore cultures were carried out for each virus-carrying strain. The number of single-spore isolates containing the virus AaCV1-QY2 was recorded. The presence of the virus in these isolates was confirmed by RT-PCR detection.

Effects of the Mycovirus on Host Biological Properties

To assess morphology and growth rates, 4-day-old mycelial plugs of the strains QY21, QY21-C1, and QY21-C2 were transferred to a PDA plate and cultured at 25°C for 3–7 days in the dark. The morphology of colonies was photographed, and the morphology of hyphae and spores was observed with a light microscope. And the diameters of each colony were measured using the crisscross method at 7 days to calculate mycelial growth rates, with each strain having five replicates.

The potential effects of mycoviruses on spore production and germination were investigated using the following method. Fresh 5 mm fresh mycelial plugs of each strain were inoculated on PDA medium under near-UV light (12 h light/12 h dark) for 7 days. Spores were collected by flushing the culture with sterile distilled water containing 0.05% (v/v) Tween and residual mycelia were removed by filtration through a glass fiber filter. The spore production of mycelia per square centimeter was measured with a hemocytometer. For the spore germination assay, the concentration of spore suspensions of each strain was adjusted to 1×10^5 spores/ml with sterile distilled water. The prepared spore suspension was dropped onto a concave glass slide and placed on a culture dish containing wet filter paper for 18 h. The germination rate of spores was calculated by counting the number of germinated spores. Spores were considered to have germinated when bud tube length is equal to or greater than the diameter of spores. Approximately 100 spores of *A. alternata* per strain were observed within each replicate, and all experiments were repeated three times.

Effects of the Mycovirus on Host Virulence

For virulence assessment, mycelial plugs or mycotoxin of each strain were inoculated on detached apple fruit and Begonia leaves. Diameters of lesions developed after 7 days of inoculation were photographed and measured. All tests were maintained at 25°C in a humid container. Each of the above tests was conducted three times, and each strain had five replicates.

Statistical Analyses

Statistical analyses were performed using a one-way analysis of variance (ANOVA) followed by *post hoc t*-tests to determine significant differences at a significant level of $p < 0.05$ with SPSS 22.0 software. Unless otherwise stated, all experiments were repeated at least three times independently.

RESULTS

Viruses in Pathogenic *A. alternata* Strain QY-2

The dsRNA was extracted from the virus particles of *A. alternata* strain QY21, and it was treated with DNase I and S1 nuclease before 1% agarose gel. Multiple dsRNAs were detected, especially three distinct dsRNA bands with the size of approximately 0.8, 3.0, and 3.5 kbp, respectively, indicating the presence of viral infection in the strain QY21 (**Figure 1A**). The next-generation sequencing (NGS) result showed the presence of six virus-like contigs derived from the different dsRNA molecules of the isolate QY21. Those contigs were used for homology searches against the NCBI virus AA sequence database using BLASTx. We found that two novel mycoviruses associated with the members of *Betachrysovirus* in the family *Chrysoviridae* and the members of *Magoulvirus* in the family *Botourmiaviridae*, respectively, were harbored in the causal agent of Apple *Alternaria* Blotch. Virus particles with a size of around 30–40 nm in diameter were purified from the mycelium of the QY-2 isolate (**Figure 1B**), and the extraction of dsRNA from the purified virus particles and RT-PCR with primers corresponding to the two identified viruses confirmed the genomic profile previously detected in the initial screening (**Figures 1A,C**).

Molecular Characterization of Mycovirus Associated With the Strain QY21

The full-length cDNA sequences of the dsRNA segments were determined by the combination of RT-PCR with specific primers (**Supplementary Table 1**) and the rapid cDNA ends amplification (RLM-RACE) protocol. As a result, six complete genomic sequences from dsRNA1 to dsRNA6, 3,665, 3,054, 2,824, 2,819, 831, and 2,798 bp in length, respectively, were obtained. Each dsRNA strand encoded a single putative ORF on the positive strand of the genome (**Figure 2A**). The dsRNA1-6 were designated as ORF1, ORF2, ORF3, ORF4, ORF5, and ORF6, respectively. All dsRNA sequences of AaCV1-QY2 and AaMV1 were deposited in GenBank with accession numbers MK672910, MK672913, MK672912, MK672911, MK836314, and MW492539, respectively. The NGS raw data were uploaded to the NCBI database (SRA accession: PRJNA832420).

The putative genomic organization of AaMV1 and AaCV1-QY2 were shown in **Figures 2A,B**. BLASTp search against NCBI databases revealed that ORF1-encoded protein displayed the highest identity to the RNA-dependent RNA polymerase (RdRp) of AaCV1 (accession no: LC350277.1, identity: 93%). The length of ORF1 is 3,351 bp, which has the potential to encode 1,117 AA residues contained a putative RdRp domain, starting at position 205 nt with an AUG codon and terminating with a UAA codon at positions 3,556–3,558 bp (**Figure 2A**). ORF2-encoded protein showed the highest sequence similarity to the putative coat protein of AaCV1 (accession no: LC350278.1, identity: 91%). No known domains were predicted in ORF3, ORF4, or ORF5; however, ORF3-, ORF4-, and ORF5-encoded proteins showed the highest sequence identities with proteins deduced from dsRNA3, dsRNA4, and dsRNA5 of AaCV1, respectively. The 5′-untranslated regions (UTRs) are relatively conserved among the five RNA segments of AaCV1-QY2 (**Figure 2C**). With the exception of segment 4, the 5′-terminal sequences of each of the other segments of AaCV1-QY2 contain a highly conserved motif (5′-GCAAAAAAGxxxxAAAGG-3′), which is a typical motif for viruses in the family Chrysoviridae (cluster II). Meanwhile, the conserved motif 5′-CGGC(A/G)TT-3′ appears in 3′-UTRs of all five segments (**Figure 2C**), and similar sequence structures are found in 3′-termini region of reported chrysoviruses such as AaCV1-N18 and AaCV1-AT1. Thus, this virus containing five ORFs was designated as AaCV1-QY2. Likewise, the genome of another virus contained only one large ORF6 that initiated at position 43 bp and terminated at positions 2,182–2,184 bp, potentially encoding 727 AA residues from an AUG codon to a UAG codon (**Figure 2B**). OFR6-encoded protein showed the most closely related to the RdRp of *Cladosporium cladosporioides* ourmia-like virus 1 (CcOLV1, accession no: MK584838, identity: 90%), so it was temporary named as *A. alternata* ourmia-like virus 1 (AaMV1).

To clarify the evolutionary status of the AaCV1-QY2 or AaMV1, maximum likelihood phylogenetic analyses were performed based on the alignment of RdRp AA sequences of AaCV1-QY2 and AaMV1, respectively, with other related mycoviruses (**Figure 3**). RdRp-based phylogenetic tree showed that AaCV1-QY2 clustered together with AaCV1, suggesting that AaCV1-QY2 is a new strain of the genus *Betachrysovirus* in the family *Chrysoviridae* (**Figure 3**, top). In addition, phylogenetic analysis also indicated a close relationship of AaMV1 to CcOLV1, the member of the genus *Magoulvirus* in the family *Botourmiaviridae* (**Figure 3**, bottom). Combined with the above results, AaMV1 derived from *A. alternata* might belong to a new species of *Magoulvirus*.

Effects of AaCV1-QY2/AaMV1 on the Biological Properties of *A. alternata*

To determine the effect of AaCV1-QY2 and AaMV1 on *A. alternata*, we attempted to cure the virus-infected strain of *A. alternata* by chemical treatment. Two types of virus-cured strains were obtained, namely, complete virus-free strain QY21-C2, and only AaCV1-QY2 virus-infected strain QY21-C1 (**Figure 4B**). In addition, we observed that AaCV1-QY2 was vertically transmitted through conidia with an efficiency of approximately 95% regardless of the presence of AaMV1 in the subculture strains. However, we did not succeed when we attempted to obtain a single AaMV1 virus-infected strain. This means that AaMV1 cannot be solely and stably accumulated in the cured strains after fungal subculture.

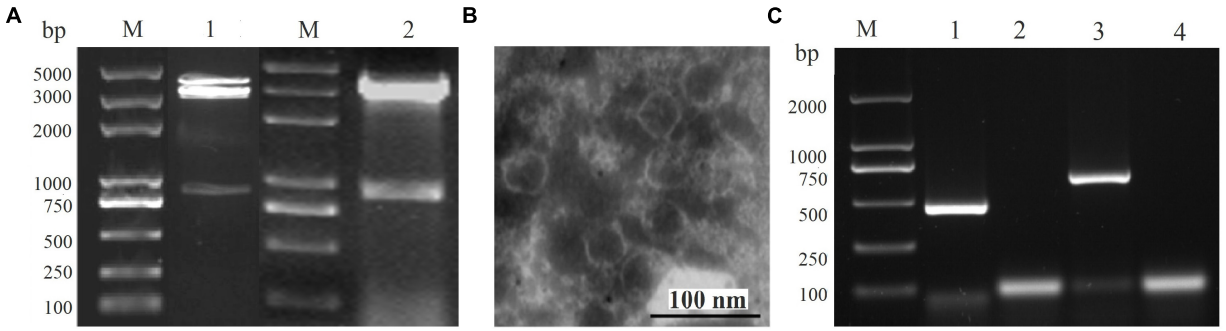

FIGURE 1 | Infection of *Alternaria alternata* chrysovirus 1 strain QY2 (AaCV1-QY2) and *A. alternata* magoulivirus 1 (AaMV1) in *A. alternata* QY21 strain. **(A)** Agarose gel electrophoresis analysis of the double-stranded RNA (dsRNA) extracted from the mycelium (lane 1) and virus particles (line 2), lane M is for markers. **(B)** Electron micrograph of purified particles of mycoviruses extracted from the strain QY21. The scale bar denotes 100 nm. **(C)** AaCV1-QY2 (lane 1) and AaMV1 (lane 3) in the strain QY21 were detected by reverse transcription-polymerase chain reaction (RT-PCR) using specific primers AaCV1-QY2f/r or AaMV1f/r directed to the RNA-dependent RNA polymerase (RdRp) sequence of mycoviruses AaCV1-QY2 and AaMV1, respectively. Lane M is for markers; lanes 2 and 4 represent the negative controls (NCs).

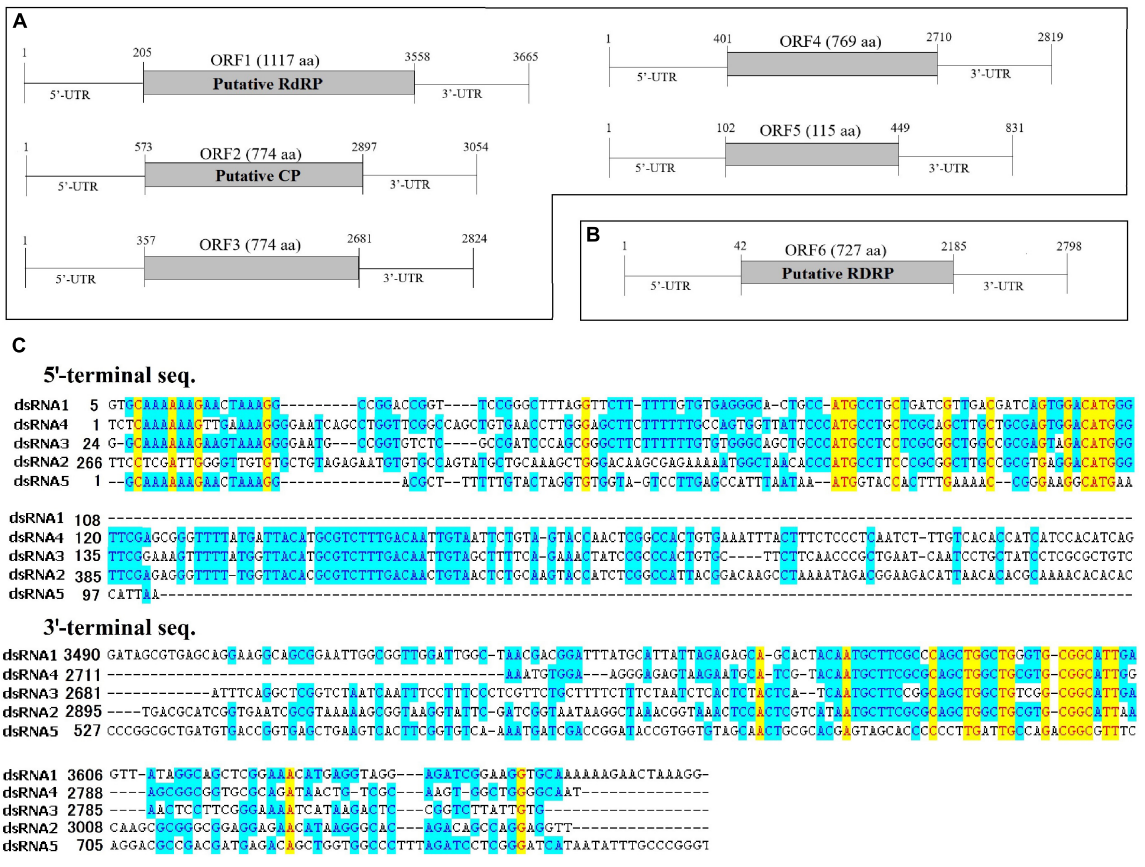

FIGURE 2 | The genome organization and the terminal structure of AaCV1-QY2 and AaMV1. **(A,B)** A schematic diagram of the genome organization of AaCV1-QY2 (A) and AaMV1 **(B)**. The boxes and lines represent the open reading frames (ORFs) and untranslated regions (UTRs), respectively. RdRp represents viral RNA-directed RNA-polymerase domain; CP represents coat protein. **(C)** Multiple sequence alignments of the 5'- and 3'-terminal regions of the coding strands of the five AaCV1-QY2 dsRNA segments.

The biological characteristics of the original strain QY21 and the two virus-cured strains QY21-C1 and QY21-C2 were compared, including colony and spore morphology, mycelial growth, and sporulation ability. The colony morphology of the virus-free strain QY21-C2 exhibited a round and significantly higher mycelium density than that of the virus-infected strains

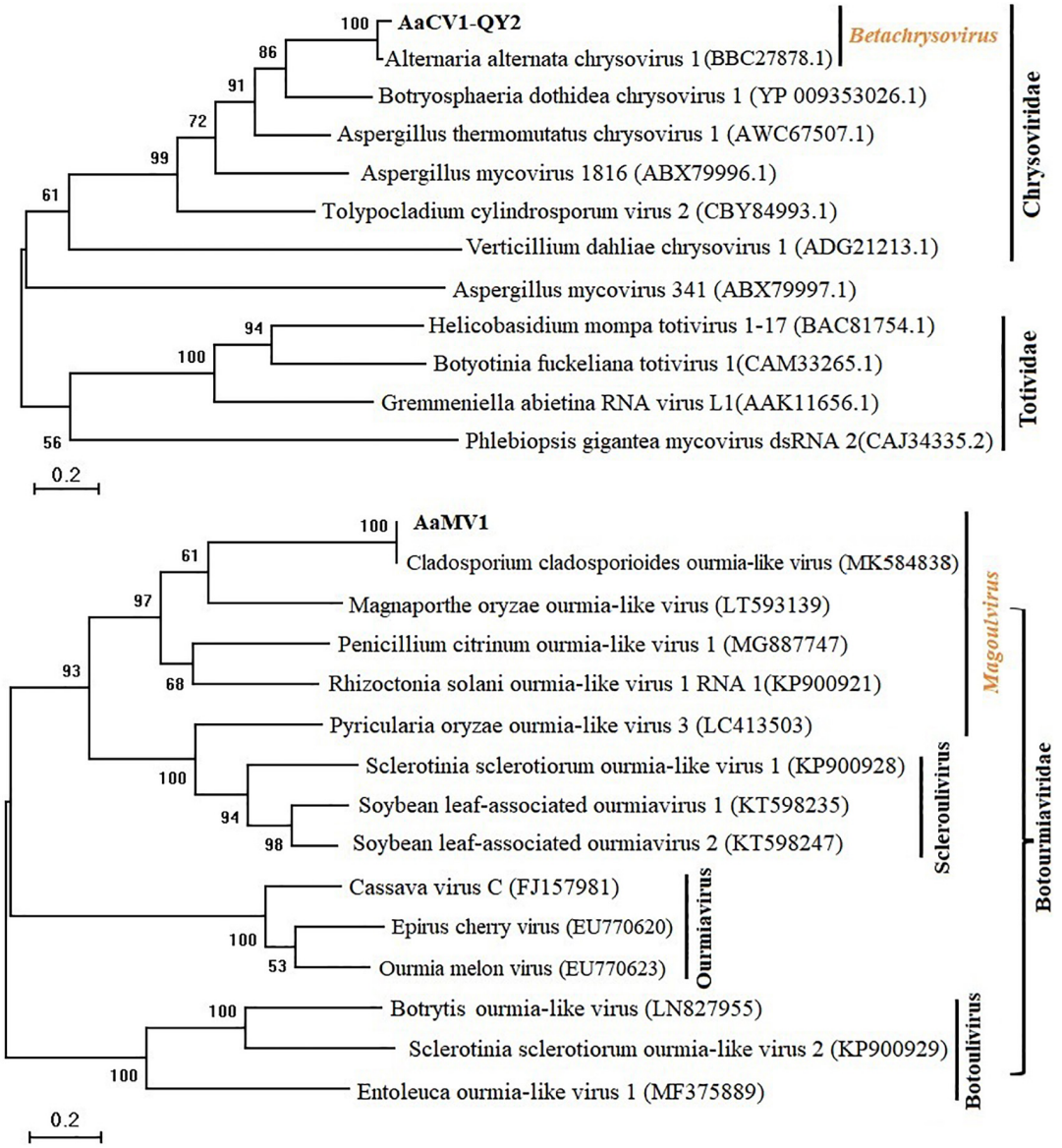

FIGURE 3 | Maximum likelihood (ML) phylogenetic tree based on the RdRps of AaCV1-QY2 (Upper) or AaMV1 (Lower) and other related viruses. The phylogenetic tree was generated using the software MEGA X. The bootstrap values (%) were obtained with 1,000 replicates. The scale bar at the lower left represents a genetic distance of 0.2.

QY21 and QY21-C1, while the colony of the virus-infected strains had less and collapsed aerial mycelium and a larger area in black pigments (**Figure 4A**, left). Also, the mycelia of the strains QY21 and QY21-C1 formed an abnormal configuration, which showed irregular and shorter ramification and poor sporulation compared with the virus-free strain QY21-C2. Especially, the strain QY21-C1 displayed more and distorted ramification with some parts of the mycelia contracted and some parts swelled (**Figure 4A**, right). Moreover, we found that the spore length of AaCV1-QY2- and AaMV1-infected strain QY21 was shorter than that of the other two strains (**Figure 4C**), which explained that the spore production ability of the virus-infected strain QY21 (5.2×10^5 spores/cm^2) was significantly lower than that of the virus-free strain QY21-C2 (1.6×10^6 spores/cm^2) (**Figure 5A**).

In addition to the influence of virus infection on the morphology of fungal host, the mycelial growth and spore germination rate of virus-infected strains was significantly inhibited compared with the virus-free strain (**Figures 5B,C**). The result indicated that the spore germination rate of AaCV1-QY2- and AaMV1-co-infected strain QY21 was the lowest (39.3%), not only lower than that of the virus-free strain QY21-C2 (57.2%), but also statistically lower than that of the AaCV1-QY2-infected strain QY21-C1 (82.7%). These results suggested

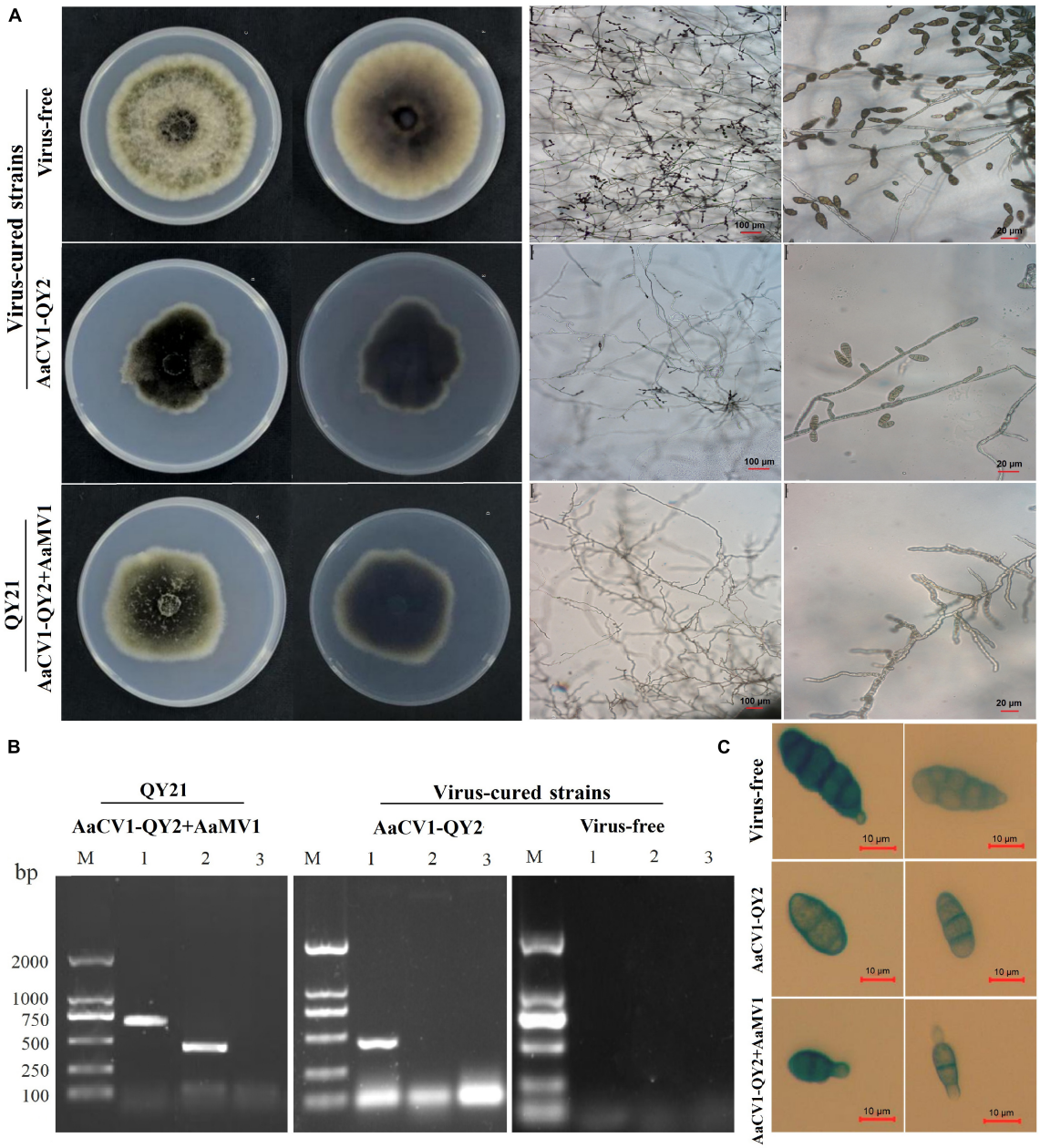

FIGURE 4 | Virus elimination and biological properties of the co-infected and isogenic virus-cured *A. alternata* strains. The strain QY21 is doubly infected with AaCV1-QY2 and AaMV1; the strain QY21-C1 has eliminated the virus AaMV1 and retains the virus AaCV1-QY2; QY21-C2 strain has completely eliminated all viruses and is virus-free. **(A)** Colony and mycelial morphology of QY21 and virus-cured strains [potato dextrose agar (PDA), 4 days, 25°C]. **(B)** The dsRNA of AaCV1-QY2 and AaMV1 in the co-infected and virus-cured strains was detected by RT-PCR amplification. Lane M is for markers; lanes 1 and 2 show the results of PCR performed with AaCV1-QY2 and AaMV1 specific primers, respectively; lane 9 is for NC. **(C)** Spore morphology of strains (PDA, 4 days, 25°C).

that AaMV1/AaCV1-QY2 infection probably reduced host strain virulence by inhibiting mycelial growth and spore production.

Effects of AaCV1-QY2/AaMV1 on the Pathogenicity of *A. alternata*

To verify and evaluate the hypovirulence-inducing effect of the mycoviruses AaMV1/AaCV1-QY2 on the fungal host, virulence assays were performed on detached apple fruits and Begonia leaves. After 7 days of inoculation, the average diameter of diseased spots on Begonia leaves caused by the virus-infected strains QY21 (0.18 cm) and QY21-C1 (0.21 cm) were significantly smaller than that caused by the virus-free strain QY21-C2 (1.51 cm) (**Figure 6A**). Meanwhile, similar results were obtained in pathogenicity evaluation of the viruses on apple fruits. The average diameter of lesion areas in apple fruits inoculated with the

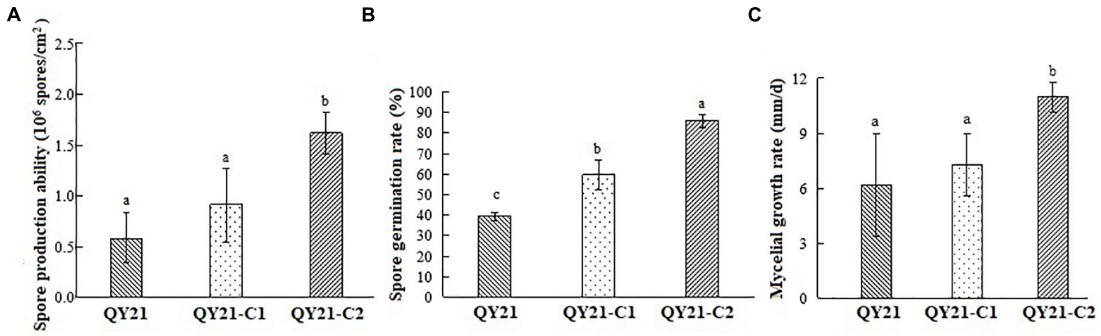

FIGURE 5 | Biological comparison of the co-infected strain QY21 and the isogenic virus-cured strains QY21-C1 and QY21-C2. The strain QY21 is doubly infected with AaCV1-QY2 and AaMV1; the strain QY21-C1 has eliminated the virus AaMV1 and retains the virus AaCV1-QY2; QY21-C2 strain has completely eliminated all viruses and is virus-free. **(A)** The number of spores produced by the strains QY21, QY21-C1, and QY21-C2 (PDA, 7 days, 25°C). **(B)** Spore germination rate (PDA, 25°C). **(C)** Radial mycelial growth rate (PDA, 25°C). Different letters indicate a significant difference at $p < 0.05$ according to the *post hoc t*-tests.

virus-infected strains QY21 (1.78 mm) and QY-2-C1 (2.69 mm) decreased meaningfully compared with fruits inoculated with the virus-free strain QY21-C2 (9.15 mm) (**Figure 6B**). Taken together, these results indicated that AaMV1/AaCV1-QY2 might confer hypovirulence to its fungal host.

In this study, AaMV1/AaCV1-QY2 attenuated the nHST-producing ability of the host strain. According to the HPLC results, the virus-free strains QY21-C2 have the highest AOH toxin production, which is about two times as much as that of the AaCV1-QY2 virus-carrying strain QY21-C1 and approximately 10 times as much as that of the AaMV1 + AaCV1-QY2 virus-carrying strain QY21 (**Figure 6C**). Generally, the mycotoxin AOH production is positively correlated with the potential risks to human health and the pathogenicity of pathogenic fungi *A. alternata*. In this study, the virulence assay of toxins extracted from the three *A. alternata* strains in this study showed that total mycotoxins of the strains QY21-C1 and QY21-C2 had a remarkably stronger pathogenicity in Begonia leaves than in the strain QY21 (**Figure 6D**).

Transmission and Colonization of AaMV1/AaCV1-QY2 in the Fungal Host and Plants

The horizontal transmission ability of the mycovirus among single, double virus-infected, and virus-free strains was determined by co-culture and hyphal anastomosis (**Figure 7A**). The results revealed that the recipient strain QY21-C2 was successfully transfected with AaMV1 and/or AaCV1-QY2 obtained from the donor strains QY21 and QY21-C1, yielding the derived strains (recipients 1 and 2) that showed an obvious virus-infected phenotype in subculture (**Supplementary Figure 2**). The presence of AaMV1/AaCV1-QY2 was confirmed by RT-PCR with specific primers (**Figure 7B**). In addition, the colony morphology of the derived strains was similar to that of the original virus-infected strains QY21 or QY21-C1. The virulence assay showed that the hypovirulence traits were also successfully transmitted, and the symptoms of apple fruit or Begonia leaves inoculated with the derived strains were obviously alleviated relative to those inoculated with the virus-free strain, which appeared in the same way as the strains QY21 or QY21-C1 (**Supplementary Figure 2**). To further examine whether the coinfection condition affects the interspecific virus transmission ability of AaCV1-QY2, AaCV1-QY2, and AaMV1 + AaCV1-QY2-infected strains were co-cultured with the other 99 allogenetic virus-free strains (recipient N) collected from apple orchards. The results of co-culture assays showed that AaCV1-QY2 could effectively spread to the recipient side of heterologous fungi, regardless of the type of virus-infected strains used as donors. Also, the interspecific transmission efficiency of AaCV1-QY2 with double virus-infected strain as the donor is much higher than that with a single AaCV1-QY2 virus-infected strain as the donor (**Figure 7C** and **Supplementary Figure 3**), suggesting that coinfection with AaMV1 interferes with the efficient horizontal transmission of AaCV1-QY2 in *A. alternata*.

On the other hand, although Begonia is the host of *A. alternata* strain QY21, the virus harbored in QY21 cannot be transferred to Begonia leaves. According to our RT-PCR detection results, the viruses AaCV1-QY2/AaMV1 can only be detected in the lesion area, but not at 1 and 2 cm away from the lesion area (**Supplementary Figure 1**). Therefore, it is demonstrated that AaCV1-QY2/AaMV1 cannot colonize in the leaves of Begonia, which also indicates that the mycoviruses in this study are harmless to plants.

DISCUSSION

The identification of more hypovirulence-associated mycoviruses not only contributes to a better knowledge of viral variety and evolution, but also provides more resources with valuable biological potential (Sun et al., 2020). With the development of NGS technology, it is more feasible and convenient to detect and discover novel and meaningful viruses from fungi, plants, insects, and other environmental samples (Barba et al., 2013; Shahid et al., 2021). In this study, we identified two mycoviruses (AaMV1 and AaCV1-QY2) that co-infect an isolate of the plant pathogenic fungus *A. alternata* f. sp. *mali* strain QY21 *via*

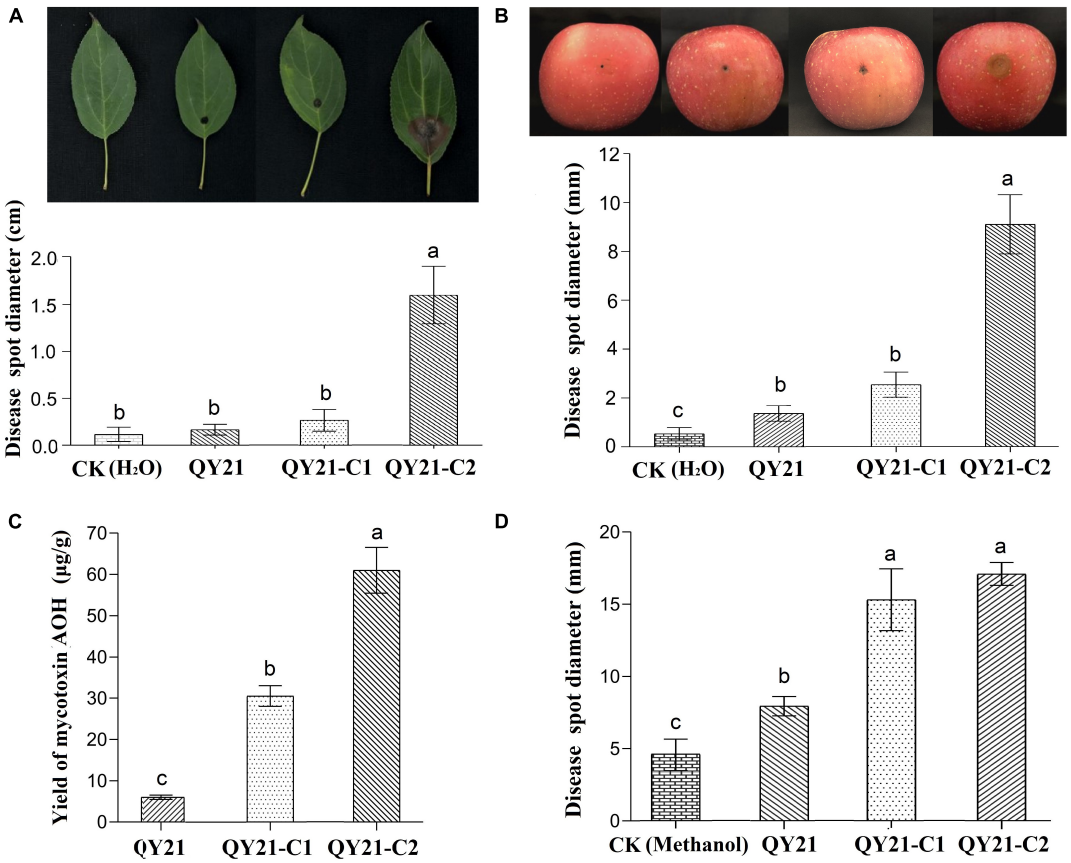

FIGURE 6 | The virulence levels of *A. alternata* virus-infected strain QY21 and the isogenic virus-cured strains QY21-C1 and QY21-C2. **(A)** Disease spot diameter and representative images showing the lesions on *Malus begonia* leaf induced by *A. alternata* strains. **(B)** Disease spot diameter and representative images showing the lesions on apple fruits induced by *A. alternata* strains. The lesions were photographed at 5 days post-inoculation. **(C)** The yield of the mycotoxin alternariol (AOH) of different *A. alternata* strains. **(D)** Lesion lengths on the Begonia leaf induced by the mycotoxin AOH extracted from *A. alternata* strains. Different letters indicate a significant difference at $p < 0.05$ according to the *post hoc t*-tests.

NGS sequencing. Of them, AaCV1-QY2 presents chrysovirus-like properties, with a genome consisting of five dsRNA segments between 1.0 and 3.5 kbp in length, encapsidated by isometric particles of approximately 30 nm in diameter. The virus AaCV1-QY2 clustered together with AaCV1 derived from *A. alternata* Japanese pear pathotype strain N18, the member of the genus *Betachrysovirus* in the family of *Chrysoviridae*. On the other hand, only one type of viral particle was detected in this study, presumably because AaMV1 was temporary assigned as ourmia-like mycovirus, which is one of the simplest viruses. Its genome usually consists of a (+)ssRNA with a size of 2.3–3.6 kb and includes a single ORF encoding RdRp. In addition, ourmia-like mycoviruses frequently lack coat protein and movement protein, hence the genomes are commonly found in the lipid vesicles of cells as an RNA/RdRp nucleoprotein complex rather than as virus particles (Wang et al., 2020). Therefore, the virus particles observed in this study may be formed by the virus AaCV1-QY2 (**Figure 1B**). This is also consistent with previous research findings: dsRNA mycoviruses are generally considered to have obvious virus particles, such as *Chrysoviridae*, *Megabirnaviridae*, *Partitivridae*, *Quadriviridae*, *Reoviridae*, and *Totiviridae*, whereas mycoviruses without obvious virus particles are considered as ssRNA viruses such as *Endornaviridae* and *Narnaviridae* (Ghabrial et al., 2015). To the best of our knowledge, this was the first report of two mycoviruses from different families co-infecting in *A. alternata* f. sp. *mali*.

In this study, we also found these viruses confer hypovirulence in *A. alternata*, the causal fungal pathogen of apple blotch disease. The virus-free *A. alternata* strain CY21-C2 induced the largest lesions on apple fruits and Begonia leaves, while *A. alternata* strains infected with AaCV1-QY2 or AaCV1-QY2 + AaMV1 exhibited significantly smaller lesions (**Figures 6A,B**). It suggests that single AaCV1-QY2 infection or double AaCV1-QY2/AaMV1 infection strongly reduces the virulence of *A. alternata*. Typically, hypovirulence-associated mycovirus infection can cause important physiological changes such as the malformation of morphological characters, the retardation of vegetative growth, and the inhibition of conidia production, thus affecting pathogenic behavior (Sharma et al., 2018; Li P. et al., 2019). Our observations also showed that the presence of the mycovirus AaCV1-QY2 alone or in combination with AaMV1 in *A. alternata* altered the host morphology, which

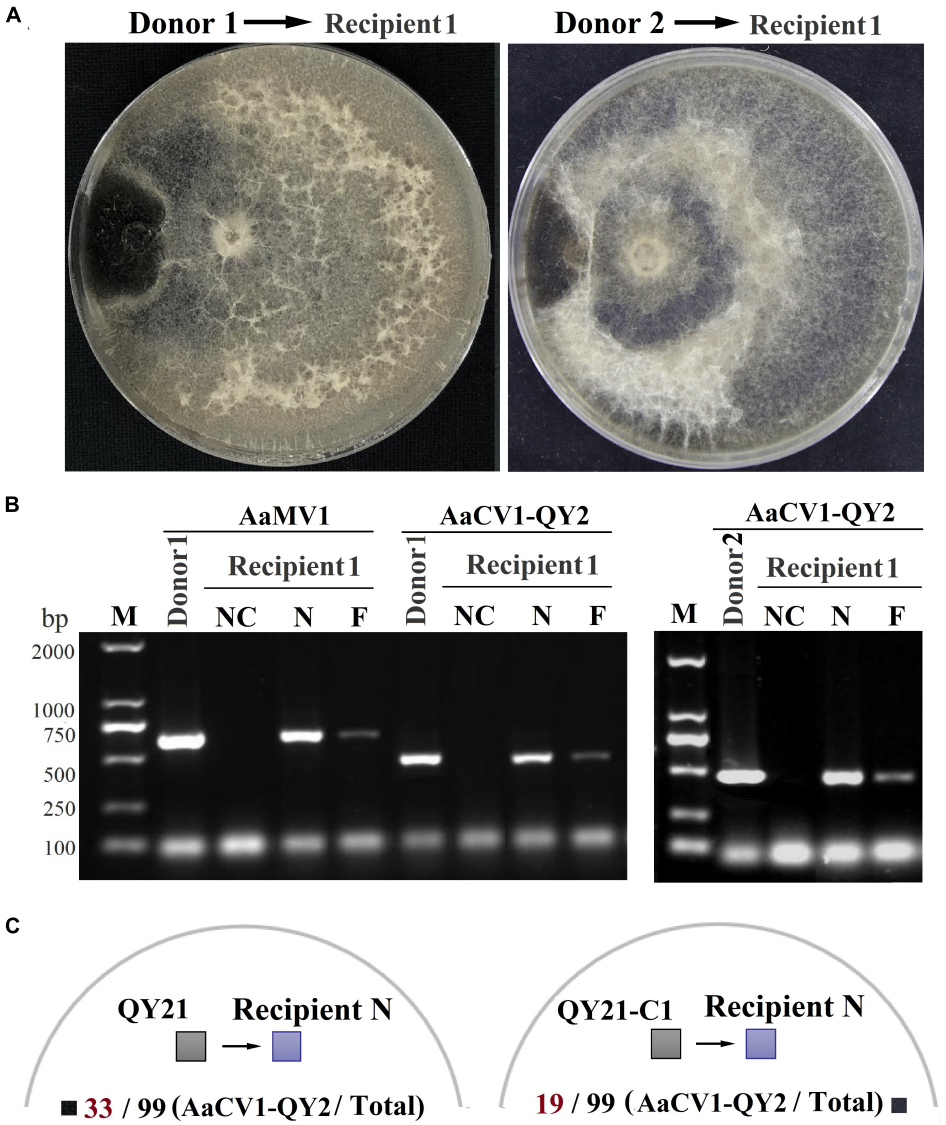

FIGURE 7 | The efficiency of AaCV1-QY2 and AaMV1 horizontal transmission *via* hyphal anastomosis in *A. alternata*. The strain QY21 is doubly infected with AaCV1-QY2 and AaMV1; the strain QY21-C1 has eliminated the virus AaMV1 and retains the virus AaCV1-QY2; QY21-C2 strain has completely eliminated all viruses as virus-free. **(A)** Co-culture on PDA plates of the virus-infected strains QY21 (left) and QY21-C1 (right) as donors and the isogenic virus-free strain QY21-C2 as the recipient, respectively. After 2 weeks of hyphal contact, mycelial plugs were collected from two locations (N: near and F: far distance from the hyphal fusion areas) in the recipient side, transferred onto new PDA plates for dsRNA extraction; NC, negative control. **(B)** The detection of viral dsRNAs of AaCV1-QY2 or AaMV1 in recipient strains co-cultured with the AaCV1-QY2 + AaMV1-infected strain QY21 (left) and the AaCV1-QY2-infected strain QY21-C1 (right). **(C)** A schematic diagram of co-culture on PDA plates of the virus-infected strains QY21 (left) and QY21-C1 (right) as donors and the other 99 allogenetic virus-free strains collected from different orchards as recipients. The numbers below the schematic diagram indicate the number of samples with AaCV1-QY2 detected in the total number of samples.

might be one of the important factors in debilitating fungal host virulence. On the other hand, similar levels of hypovirulence were observed between *A. alternata* strains QY21 with double AaCV1-QY2 + AaMV1 infection and QY21-C1 with single AaCV1-QY2 infection, which supported that AaCV1-QY2 played a dominant role in fungal host hypovirulence caused by the coinfection of mycoviruses. Nevertheless, it is still unknown whether AaMV1 plays a synergistic role or merely serves as an accompanying virus, and related experiments cannot be conducted to demonstrate this in this study because a single AaMV1-infected strain cannot survive in the subculture.

Members of the family *Chrysoviridae* have been identified to infect a wide array of fungal species and are considered to debilitate the virulence of their phytopathogenic fungal hosts (Moriyama et al., 2018; Kotta-Loizou et al., 2020; Casas et al., 2023). For example, the viruses *Colletotrichum fructicola* chrysovirus 1 (CfCV1), *Magnaporthe oryzae* chrysovirus 1-A (MoCV1-A), *F. oxysporum* f. sp. *dianthi* mycovirus 1 (FodV1),

and BdCV1 induce hypovirulence in the their hosts (Moriyama et al., 2018; Wang et al., 2018; Zhai et al., 2018; Torres-Trenas et al., 2019). Also, in this study, AaCV1-QY2 infection reduced the synthesis of AOH toxins in the *A. alternata* host and alleviated the symptoms caused by host fungi on apple fruits and Begonia leaves. However, it has been reported that AaCV1-N18 isolated from *A. alternata* causing a pear black spot endowed the host with enhanced pathogenicity by promoting host-specific AK toxin level (Okada et al., 2018) and AaCV1-AT derived from *Alternaria tenuissima* causing watermelon leaf blight provided enhanced sensitivity of the host fungus to difenoconazole or tebuconazole (Ma et al., 2020). These two viruses share the closest homology with AaCV1-QY2, but their infection behavior had completely different effects on host pathogenicity, except that the growth of their respective hosts was consistently reduced compared with AaCV1-QY2. To our knowledge, this is the first report of hypovirulence caused by *chrysovirus* infection in the pathogenic fungus *Alternaria* species.

Recently, an increasing number of ourmia-like viruses have been identified in different fungi, but most of them have little or no impact on the virulence (Illana et al., 2017; Wang et al., 2020; Zhou et al., 2020). So far, only one ourmia-like mycovirus FoOuLV1, has been reported to induce hypovirulence (Zhao et al., 2020). However, FoOuLV1 is unique among ourmia-like mycoviruses because there are two segments, L-segment and S-segment, which were harbored in the host strain HuN8. And, the S-segment associated with FoOuLV1 was proven to play an important role in its hypovirulence (Zhao et al., 2020). In this study, the results of morphological comparison and virulence assay showed that the extra presence of AaMV1 had no superimposed influence on morphological alterations and the level of hypovirulence compared with AaMV1 elimination strain, but the accumulation of nHST toxin AOH, as a virulence factor, was restored to a certain extent, and it is positively correlated with the aggravation of disease symptoms and human health risks (Meena et al., 2017). We speculate that this contradictory phenomenon is because the presence of AaMV1 not only affected the metabolic pathway of AOH toxin in the host, but could also regulate other physiological metabolic processes related to host virulence, such as the synthesis of other types of nHST and HST toxins that were not detected in this study due to some technical obstacles. Finally, due to the combined effects of various factors, there was no significant difference in reducing host pathogenicity between the host strains with both mycoviruses and single AaCV1-QY2 infection.

Coinfection of mycoviruses is rather common in plant pathogenic fungi. Generally, co-infected mycoviruses are reported to be dependently harbored, there is a close and complex interaction between mycoviruses, which may affect the pathogenicity and transmission efficiency of mycoviruses, especially during transmission through vegetatively incompatible fungi (Kashif et al., 2019; Thapa and Roossinck, 2019). For example, the horizontal transmission efficacy of the mycovirus HetPV15-pa1 to a pre-infected host was elevated from 0 to 50% by the presence of HetPV13-an1. Furthermore, Heterobasidion partitiviruses in recipient strains have extremely varied impacts on the transmission of new viruses, depending on specific virus combinations, they can synergistically enhance the overall transmission rate or antagonistically alter their transmission (Kashif et al., 2019). In this study, the coinfection of both viruses (AaCV1-QY2 and AaMV1) did not alter the virulence of *A. alternata* compared with single AaCV1-QY2 infection, but improved the horizontal transmission rate of AaCV1-QY2 from CY21 strain to the virus-free strains CY21-C2 and to the other *A. alternata* strains via hyphal anastomosis. This change in interspecific transmission ability is associated with the coinfection involving the virus AaMV1, coinfection perhaps inducing the suppression of fungal non-self-recognition and RNA silencing are two most common protective mechanisms against virus infection and transmission. This hypothesis was confirmed by the study that hypovirulence-associated *S. sclerotiorum* mycoreovirus 4 (SsMYR4) suppresses non-self-recognition of the fungal host and facilitate coinfection through the horizontal transmission of mycoviruses between different strains (Wu et al., 2017). However, if there is more accurate information about vegetative compatibility between QY21 or QY21-C1 and the other 99 allogeneic virus-free strains, it would offer further insights into the impact of coinfection on the horizontal transmission of AaCV1-QY2. Taken together, the interaction between co-infected viruses and their hosts is multifaceted, their underlying mechanism remains to be elucidated, which depends on the property of the fungal host, the type of mycoviruses, and the interactions between the co-infected viruses themselves.

In recent studies, more and more hypovirulent mycoviruses have been identified and explored as potential biocontrol agents against fungal diseases. Nonetheless, with the exception of the two mycoviruses CHV1 and SsHADV-1, there are few attempts to use mycoviruses to control diseases in the field. So far, many mycoviruses have been identified from the genus *Alternaria*; but, to our knowledge, only seven mycoviruses have been identified in *A. alternata*. Furthermore, among them, only AaHV1 is considered to authentically induce hypovirulence. In this study, the coinfection of AaCV1-QY2 or AaCV1-QY2 + AaMV1 was not only able to forcibly induce hypovirulence in *A. alternata*, but also exhibited excellent horizontal transmission ability, especially with AaCV1-QY2 + AaMV1 infection. We also determined that these two mycoviruses could not infect Begonia leaves, so they would not pose a safety risk to plant health. These are considered to be important conditions and advantages for the successful application of mycoviruses to the control of fungal plant disease.

CONCLUSION

We have characterized two mycoviruses (AaCV1-QY2 and AaMV1) related to members of the genera *Betachrysovirus* and *Megoulvirus*, respectively, from a phytopathogenic fungus, *A. alternata* f. sp. *mali* strain QY21. AaCV1-QY2 plays a dominant role in causing morphological alterations and hypovirulent phenotype. This is the first report of the phenomenon of hypovirulence conferred in *A. alternata* by the coinfection of two mycoviruses. Furthermore, AaMV1 harbored

in *A. alternata* facilitates the horizontal transmission ability of the mycovirus AaCV1-QY2 and mediate the accumulation of the mycotoxin AHO. Therefore, these mycoviruses can be considered as potential biological control agents to control *Alternaria* blotch disease. However, further studies are needed to determine the role of each mycovirus in viral transmission, pathogenic behavior, physiological changes, and their interactions in influencing the biology and adaptability of *A. alternata* host strains.

DATA AVAILABILITY STATEMENT

The datasets presented in this study can be found in online repositories. The names of the repository/repositories and accession number(s) can be found below: https://www.ncbi.nlm.nih.gov/genbank/, MK672910; https://www.ncbi.nlm.nih.gov/genbank/, MK672913; https://www.ncbi.nlm.nih.gov/genbank/, MK672912; https://www.ncbi.nlm.nih.gov/genbank/, MK672911; https://www.ncbi.nlm.nih.gov/genbank/, MK836314; https://www.ncbi.nlm.nih.gov/genbank/, MW492539; and https://www.ncbi.nlm.nih.gov/, PRJNA832420.

AUTHOR CONTRIBUTIONS

YW and KC designed the study and revised this manuscript. BL analyzed the data and wrote the manuscript. YC, JZ, PD, and ZJ performed the experimental work. XM, TH, and SW helped to revise this manuscript. All authors approved the final manuscript.

FUNDING

This work was supported by the Provincial Key R&D Program of Hebei (21326506D), Natural Science Foundation of Hebei province (C2019204327), China Agriculture Research System of MOF and MARA (CARS-27), and Funding Program of Hebei province for Talents with Overseas Experience (C201839).

SUPPLEMENTARY MATERIAL

The Supplementary Material for this article can be found online at: https://www.frontiersin.org/articles/10.3389/fmicb.2022.910712/full#supplementary-material

REFERENCES

Aoki, N., Moriyama, H., Kodama, M., Arie, T., Teraoka, T., and Fukuhara, T. (2009). A novel mycovirus associated with four double-stranded RNAs affects host fungal growth in *Alternaria alternata*. *Virus Res.* 140, 179–187. doi: 10.1016/j.virusres.2008.12.003

Barba, M., Czosnek, H., and Hadidi, A. (2013). Historical perspective, development and applications of next-generation sequencing in plant virology. *Viruses* 6, 106–136. doi: 10.3390/v6010106

Casas, L. L., Azevedo, J. L., Almeida, L. N., Costa-Neto, P. Q., Bianco, R. A., and Pereira, J. O. (2023). Mycoviruses infecting *Colletotrichum* spp.: a comprehensive review. *Braz. J. Biol.* 83:e248975. doi: 10.1590/1519-6984.248975

da Silva Xavier, A., Oliveira de Barros, A. P., Godinho, M. T., Zerbini, F. M., de Oliveira Souza, F., Bruckner, F. P., et al. (2018). A novel mycovirus associated to *Alternaria alternata* comprises a distinct lineage in *Partitiviridae*. *Virus Res.* 244, 21–26. doi: 10.1016/j.virusres.2017.10.007

Das, S., Falloon, R. E., Stewart, A., and Pitman, A. R. (2014). Molecular characterisation of an endornavirus from *Rhizoctonia solani* AG-3PT infecting potato. *Fungal Biol.* 118, 924–934. doi: 10.1016/j.funbio.2014.08.003

Ding, Z., Zhou, T., and Guo, L. Y. (2017). Characterization of a novel strain of *Botryosphaeria dothidea* chrysovirus 1 from the apple white rot pathogen *Botryosphaeria dothidea*. *Arch. Virol.* 162, 2097–2102. doi: 10.1007/s00705-017-3320-6

Fontaine, K., Fourrier-Jeandel, C., Armitage, A. D., Boutigny, A.-L., Crépet, M., Caffier, V., et al. (2021). Identification and pathogenicity of *Alternaria* species associated with leaf blotch disease and premature defoliation in French apple orchards. *PeerJ* 9:e12496. doi: 10.7717/peerj.12496

García-Pedrajas, M. D., Cañizares, M. C., Sarmiento-Villamil, J. L., Jacquat, A. G., and Dambolena, J. S. (2019). Mycoviruses in biological control: from basic research to field implementation. *Phytopathology* 109, 1828–1839. doi: 10.1094/PHYTO-05-19-0166-RVW

Ghabrial, S. A., Castón, J. R., Jiang, D., Nibert, M. L., and Suzuki, N. (2015). 50-plus years of fungal viruses. *Virology* 479–480, 356–368. doi: 10.1016/j.virol.2015.02.034

Illana, A., Marconi, M., Rodríguez-Romero, J., Xu, P., Dalmay, T., Wilkinson, M. D., et al. (2017). Molecular characterization of a novel ssRNA ourmia-like virus from the rice blast fungus *Magnaporthe oryzae*. *Arch. Virol.* 162, 891–895. doi: 10.1007/s00705-016-3144-9

Jamal, A., Sato, Y., Shahi, S., Shamsi, W., Kondo, H., and Suzuki, N. (2019). Novel Victorivirus from a Pakistani isolate of *Alternaria alternata* lacking a typical translational stop/restart sequence signature. *Viruses* 11:577. doi: 10.3390/v11060577

Kashif, M., Jurvansuu, J., Vainio, E. J., and Hantula, J. (2019). Alphapartitiviruses of *Heterobasidion* wood decay fungi affect each other's transmission and host growth. *Front. Cell. Infect. Microbiol.* 9:64. doi: 10.3389/fcimb.2019.00064

Kotta-Loizou, I., Castón, J. R., Coutts, R. H. A., Hillman, B. I., Jiang, D., Kim, D. H., et al. (2020). ICTV virus taxonomy profile: *Chrysoviridae*. *J. Gen. Virol.* 101, 143–144. doi: 10.1099/jgv.0.001383

Kumar, S., Stecher, G., Li, M., Knyaz, C., and Tamura, K. (2018). MEGA X: molecular evolutionary genetics analysis across computing platforms. *Mol. Biol. Evol.* 35, 1547–1549. doi: 10.1093/molbev/msy096

Larkin, M. A., Blackshields, G., Brown, N. P., Chenna, R., Mcgettigan, P. A., McWilliam, H., et al. (2007). Clustal W and Clustal X version 2.0. *Bioinformatics* 23, 2947–2948. doi: 10.1093/bioinformatics/btm404

Li, D., Luo, R., Liu, C. M., Leung, C. M., Ting, H. F., Sadakane, K., et al. (2016). MEGAHIT v1.0: a fast and scalable metagenome assembler driven by advanced methodologies and community practices. *Methods* 102, 3–11. doi: 10.1016/j.ymeth.2016.02.020

Li, H., Bian, R., Liu, Q., Yang, L., Pang, T., Salaipeth, L., et al. (2019). Identification of a novel hypovirulence-inducing hypovirus from *Alternaria alternata*. *Front. Microbiol.* 10:1076. doi: 10.3389/fmicb.2019.01076

Li, P., Bhattacharjee, P., Wang, S., Zhang, L., Ahmed, I., and Guo, L. (2019). Mycoviruses in *Fusarium* species: an update. *Front. Cell. Infect. Microbiol.* 9:257. doi: 10.3389/fcimb.2019.00257

Ma, G., Liang, Z., Hua, H., Zhou, T., and Wu, X. (2019). Complete genome sequence of a new botybirnavirus isolated from a phytopathogenic *Alternaria alternata* in China. *Arch. Virol.* 164, 1225–1228. doi: 10.1007/s00705-019-04189-x

Ma, G., Wu, C., Li, Y., Mi, Y., Zhou, T., Zhao, C., et al. (2022). Identification and genomic characterization of a novel polymycovirus from *Alternaria alternata* causing watermelon leaf blight. *Arch. Virol.* 167, 223–227. doi: 10.1007/s00705-021-05272-y

Ma, G., Zhang, X., Hua, H., Zhou, T., and Wu, X. (2020). Molecular and biological characterization of a novel strain of *Alternaria alternata* chrysovirus 1 identified from the pathogen *Alternaria tenuissima* causing watermelon leaf blight. *Virus Res.* 280:197904. doi: 10.1016/j.virusres.2020.197904

Martins, L. M., Castro, J. P., and Gouveia, M. E. (2014). Biological control of chestnut blight in Portugal. *Acta Hortic.* 1043, 51–56. doi: 10.17660/ActaHortic.2014.1043.5

Meena, M., Gupta, S. K., Swapnil, P., Zehra, A., Dubey, M. K., and Upadhyay, R. S. (2017). *Alternaria* toxins: potential virulence factors and genes related to pathogenesis. *Front. Microbiol.* 8:1451. doi: 10.3389/fmicb.2017.01451

Moriyama, H., Urayama, S., Higashiura, T., Le, T., and Komatsu, K. (2018). Chrysoviruses in *Magnaporthe oryzae*. *Viruses* 10:697. doi: 10.3390/v10120697

Okada, R., Ichinose, S., Takeshita, K., Urayama, S. I., Fukuhara, T., Komatsu, K., et al. (2018). Molecular characterization of a novel mycovirus in *Alternaria alternata* manifesting two-sided effects: down-regulation of host growth and up-regulation of host plant pathogenicity. *Virology* 519, 23–32. doi: 10.1016/j.virol.2018.03.027

Shah, U. A., Kotta-Loizou, I., Fitt, B. D. L., and Coutts, R. H. A. (2020). Mycovirus-induced hypervirulence of *Leptosphaeria biglobosa* enhances systemic acquired resistance to *Leptosphaeria maculans* in *Brassica napus*. *Mol. Plant Microbe Interact.* 33, 98–107. doi: 10.1094/MPMI-09-19-0254-R

Shahid, M. S., Sattar, M. N., Iqbal, Z., Raza, A., and Al-Sadi, A. M. (2021). Next-generation sequencing and the CRISPR-Cas nexus: a molecular plant virology perspective. *Front. Microbiol.* 11:9376. doi: 10.3389/fmicb.2020.609376

Sharma, M., Guleria, S., Singh, K., Chauhan, A., and Kulshrestha, S. (2018). Mycovirus associated hypovirulence, a potential method for biological control of *Fusarium* species. *Virusdisease* 29, 134–140. doi: 10.1007/s13337-018-0438-4

Shepherd, H. S. (1988). Viruslike particles in tentoxin-producing strains of *Alternaria alternata*. *J. Virol.* 62, 3888–3891. doi: 10.1128/jvi.62.10.3888-3891.1988

Sun, L., Suzuki, N., Jiang, D., Turina, M., and Xie, J. (2020). Editorial: frontiers in fungal virus research. *Front. Cell. Infect. Microbiol.* 9:456. doi: 10.3389/fcimb.2019.00456

Thapa, V., and Roossinck, M. J. (2019). Determinants of coinfection in the *Mycoviruses*. *Front. Cell. Infect. Microbiol.* 9:169. doi: 10.3389/fcimb.2019.00169

Thomma, B. P. H. J. (2003). *Alternaria* spp.: from general saprophyte to specific parasite. *Mol. Plant Pathol.* 4, 225–236. doi: 10.1046/j.1364-3703.2003.00173.x

Torres-Trenas, A., Prieto, P., Cañizares, M. C., García-Pedrajas, M. D., and Pérez-Artés, E. (2019). Mycovirus *Fusarium oxysporum* f. sp. dianthi virus 1 decreases the colonizing efficiency of its fungal host. *Front. Cell. Infect. Microbiol.* 9:51. doi: 10.3389/fcimb.2019.00051

Wang, L., Wang, L., Luo, H., Hu, W., Yang, Y., Hong, N., et al. (2018). *De novo* transcriptomic assembly and mRNA expression patterns of *Botryosphaeria dothidea* infection with mycoviruses chrysovirus 1 (BdCV1) and partitivirus 1 (BdPV1). *Virol. J.* 15:126. doi: 10.1186/s12985-018-1033-4

Wang, Q., Mu, F., Xie, J., Cheng, J., Fu, Y., and Jiang, D. (2020). A single ssRNA segment encoding RdRp is sufficient for replication, infection, and transmission of ourmia-like virus in Fungi. *Front. Microbiol.* 11:379. doi: 10.3389/fmicb.2020.00379

Wu, C. F., Aoki, N., Takeshita, N., Fukuhara, T., Chiura, H. X., Arie, T., et al. (2021). Unique terminal regions and specific deletions of the segmented double-stranded RNA genome of *Alternaria alternata* virus 1, in the proposed family alternaviridae. *Front. Microbiol.* 12:773062. doi: 10.3389/fmicb.2021.773062

Wu, S., Cheng, J., Fu, Y., Chen, T., Jiang, D., Ghabrial, S. A., et al. (2017). Virus-mediated suppression of host non-self recognition facilitates horizontal transmission of heterologous viruses. *PLoS Pathog.* 13, 1–25. doi: 10.1371/journal.ppat.1006234

Xu, Z., Wu, S., Liu, L., Cheng, J., Fu, Y., Jiang, D., et al. (2015). A mitovirus related to plant mitochondrial gene confers hypovirulence on the phytopathogenic fungus *Sclerotinia sclerotiorum*. *Virus Res.* 197, 127–136. doi: 10.1016/j.virusres.2014.12.023

Yang, S., Dai, R., Salaipeth, L., Huang, L., Liu, J., Andika, I. B., et al. (2021). Infection of two heterologous mycoviruses reduces the virulence of *Valsa mali*, a fungal agent of Apple *Valsa* canker disease. *Front. Microbiol.* 12:659210. doi: 10.3389/fmicb.2021.659210

Yu, X., Li, B., Fu, Y., Jiang, D., Ghabrial, S. A., Li, G., et al. (2010). A geminivirus-related DNA mycovirus that confers hypovirulence to a plant pathogenic fungus. *Proc. Natl. Acad. Sci. U.S.A.* 107, 8387–8392. doi: 10.1073/pnas.0913535107

Yu, X., Li, B., Fu, Y., Xie, J., Cheng, J., Ghabrial, S. A., et al. (2013). Extracellular transmission of a DNA mycovirus and its use as a natural fungicide. *Proc. Natl. Acad. Sci. U.S.A.* 110, 1452–1457. doi: 10.1073/pnas.1213755110

Zhai, L., Zhang, M., Hong, N., Xiao, F., Fu, M., Xiang, J., et al. (2018). Identification and characterization of a novel hepta-segmented dsRNA virus from the phytopathogenic fungus *Colletotrichum fructicola*. *Front. Microbiol.* 9:754. doi: 10.3389/fmicb.2018.00754

Zhao, Y., Zhang, Y., Wan, X., She, Y., Li, M., Xi, H., et al. (2020). A novel ourmia-like mycovirus confers hypovirulence-associated traits on *Fusarium oxysporum*. *Front. Microbiol.* 11:569869. doi: 10.3389/fmicb.2020.569869

Zhou, J., Wang, Y., Liang, X., Xie, C., Liu, W., Miao, W., et al. (2020). Molecular characterization of a novel ourmia-like virus infecting *Phoma matteucciicola*. *Viruses* 12:231. doi: 10.3390/v12020231

Zhu, J. Z., Guo, J., Hu, Z., Zhang, X. T., Li, X. G., and Zhong, J. (2021). A novel *Partitivirus* that confer hypovirulence to the plant pathogenic fungus *Colletotrichum liriopes*. *Front. Microbiol.* 12:653809. doi: 10.3389/fmicb.2021.653809

Conflict of Interest: The authors declare that the research was conducted in the absence of any commercial or financial relationships that could be construed as a potential conflict of interest.

Publisher's Note: All claims expressed in this article are solely those of the authors and do not necessarily represent those of their affiliated organizations, or those of the publisher, the editors and the reviewers. Any product that may be evaluated in this article, or claim that may be made by its manufacturer, is not guaranteed or endorsed by the publisher.

Copyright © 2022 Li, Cao, Ji, Zhang, Meng, Dai, Hu, Wang, Cao and Wang. This is an open-access article distributed under the terms of the Creative Commons Attribution License (CC BY). The use, distribution or reproduction in other forums is permitted, provided the original author(s) and the copyright owner(s) are credited and that the original publication in this journal is cited, in accordance with accepted academic practice. No use, distribution or reproduction is permitted which does not comply with these terms.

frontiers | Frontiers in Microbiology

TYPE Review
PUBLISHED 26 July 2022
DOI 10.3389/fmicb.2022.935735

Check for updates

OPEN ACCESS

EDITED BY
Beilei Wu,
Institute of Plant Protection (CAAS), China

REVIEWED BY
Guanwei Wu,
Ningbo University, China
Xuefeng Yuan,
Shandong Agricultural University, China

*CORRESPONDENCE
Kun Zhang
zk@yzu.edu.cn;
zhangkun880324@cau.edu.cn

SPECIALTY SECTION
This article was submitted to Microbe and Virus Interactions with Plants, a section of the journal Frontiers in Microbiology

RECEIVED 04 May 2022
ACCEPTED 28 June 2022
PUBLISHED 26 July 2022

CITATION
Zhuang X, Guo X, Gu T, Xu X, Qin L, Xu K, He Z and Zhang K (2022) Phosphorylation of plant virus proteins: Analysis methods and biological functions. *Front. Microbiol.* 13:935735. doi: 10.3389/fmicb.2022.935735

COPYRIGHT
© 2022 Zhuang, Guo, Gu, Xu, Qin, Xu, He and Zhang. This is an open-access article distributed under the terms of the Creative Commons Attribution License (CC BY). The use, distribution or reproduction in other forums is permitted, provided the original author(s) and the copyright owner(s) are credited and that the original publication in this journal is cited, in accordance with accepted academic practice. No use, distribution or reproduction is permitted which does not comply with these terms.

Phosphorylation of plant virus proteins: Analysis methods and biological functions

Xinjian Zhuang[1], Xiao Guo[1], Tianxiao Gu[1], Xiaowei Xu[1], Lang Qin[1], Kai Xu[2], Zhen He[1] and Kun Zhang[1,2]*

[1]Department of Plant Protection, College of Horticulture and Plant Protection, Yangzhou University, Yangzhou, China, [2]Jiangsu Key Laboratory for Microbes and Functional Genomics, Jiangsu Engineering and Technology Research Center for Microbiology, College of Life Sciences, Nanjing Normal University, Nanjing, China

Phosphorylation is one of the most extensively investigated post-translational modifications that orchestrate a variety of cellular signal transduction processes. The phosphorylation of virus-encoded proteins plays an important regulatory role in the infection cycle of such viruses in plants. In recent years, molecular mechanisms underlying the phosphorylation of plant viral proteins have been widely studied. Based on recent publications, our study summarizes the phosphorylation analyses of plant viral proteins and categorizes their effects on biological functions according to the viral life cycle. This review provides a theoretical basis for elucidating the molecular mechanisms of viral infection. Furthermore, it deepens our understanding of the biological functions of phosphorylation in the interactions between plants and viruses.

KEYWORDS

phosphorylation, replication, intracellular movement, long-distance movement, infection cycle

Introduction

Rapid responses to internal and external cues are vital for complex life on the earth. Whether to maintain optimal conditions for growth or to avoid biotic/abiotic stresses, these responses must occur on a timescale that affords the organisms an obvious survival advantage. Cells have evolved sophisticated regulatory systems that can

Abbreviations: AbMV, abutilon mosaic virus; BaMV, bamboo mosaic virus; BBSV, beet black scorch virus; BSMV, barley mosaic stripe virus; CaLCuV, cabbage leaf curl virus; CMV, cucumber mosaic virus; CNV, cucumber necrosis virus; CWMV, Chinese wheat mosaic virus; CP, coat protein; MP, movement protein; Nu, nucleolus; PD, plasmodesmata; PLRV, potato leaf roll virus; PMTV, potato mop-top virus; PPV, plum pox virus; PSLV, poa semilatent virus; PTM, post-translational modifications; PVA, potato virus A; PVX, potato virus X; TLCYnV, Yunnan tomato leaf curl virus; TGMV, tomato golden mosaic virus; CaLCuV, cabbage leaf curl virus; TYLCV, tomato yellow leaf curl virus; RdRp, RNA-dependent RNA polymerase; Ren, replication enhancer; Rep, replicase; RNPs, ribonucleoprotein; TMV, tobacco mosaic virus; TYMV, turnip yellow mosaic virus; VSR, virus-encoded RNA silencing suppressors; REn, replication enhancer.

sense, transmit, sort, store, and interpret information that could enact a coordinated and timely response to the changes in environments. Post-translational modification (PTM) is an elegant transducer of the signals for adaptations of living organisms by the reversible and rapid nature, relatively small expenses, and profoundly function modulation of the target protein. Examples of PTM include phosphorylation (Ramazi and Zahiri, 2021), glycosylation (Vigerust and Shepherd, 2007), ubiquitination (Shen et al., 2016), acetylation (Diallo et al., 2019), lipidization (Chiang et al., 2013), small ubiquitin-like modifier (SUMOylation) (Cheng et al., 2017), and lysine succinylation (Zhang et al., 2011), butyrylation (Chen et al., 2007), or crotonylation (Wan et al., 2019). Phosphorylation is the most intensively investigated PTM and is involved in almost every cellular process (Cohen, 2002; Duan and Walther, 2015). Numerous metabolic enzymes, such as pyruvate dehydrogenase and glycogen synthase, occur in the phosphorylation PTM (Fischer and Krebs, 1955). The mechanisms by which phosphorylation controls protein functions include modulation of protein–protein interactions and changes in protein conformation. Phosphorylation often functions as a docking site for intra- or inter-molecular protein interactions via protein conformation changes, and directly modulates enzymatic activity, regulates subcellular localization, targets turnover, and affects signaling transduction by other PTMs (**Figure 1**). Overall, the phosphorylation by kinases and de-phosphorylation by phosphatases serve as low-cost and high-efficiency molecular regulators that can alter the behavior of the targets directly or indirectly.

There are four types of phosphorylations, the first being *O*-phosphorylation, which mainly occurs at the hydroxyl residues of serine (Ser), threonine (Thr), tyrosine (Tyr), and hydroxyproline (Emmer et al., 2013). The second is *N*-phosphorylation, which occurs on histidine and lysine amino residues (Ni et al., 2009). The third is *S*-phosphorylation, which occurs in the sulfhydryl group of cysteine (Buchowiecka, 2014). The last type is *Acyl*-phosphorylation, which is mainly observed in the acyl groups of aspartic acid and glutamate (Cheng et al., 1996). *O*-phosphorylation is the most common type of phosphorylation in eukaryotes (Panni, 2019). Heibeck et al. (2009) showed that the relative abundance ratio of three phosphorylated amino acids (AA) (pSer : pThr : pTyr) in a single cell is 1800 : 200 : 1, indicating that Ser phosphorylation is the most common modification (Heibeck et al., 2009). In eukaryotes, *O*-phosphorylation is catalyzed by protein kinases, which function by adding the γ-phosphate group of ATP or GTP to the hydroxyl side chain of Ser, Thr, Tyr, and hydroxyproline (Krupa et al., 2004). Different protein kinases can recognize and modify different sites of the target protein. Phosphorylated proteins can also be dephosphorylated by phosphatases, which reduce the phosphate group from the side chain of the target protein (Millar et al., 2019). These dynamic and reversible PTM changes are energy-consuming processes that require coordination between the protein kinase and phosphatase to regulate the folding style and conformation of the target protein (Jakubiec and Jupin, 2007). The reversible processes of phosphorylation and dephosphorylation act as an "ON-OFF SWITCH"-like modulator of their functions, such as regulating enzymatic activity, protein stability, protein virulence, subcellular localization of target proteins, signaling transduction and recognition, and interaction with other proteins (Friso and van Wijk, 2015).

In plant virology, studies on the phosphorylation modification of viral proteins have recently progressed. The regulatory function of phosphorylation is involved in most steps of the plant viral life cycle, including protein translation (Martínez-Turiño et al., 2018), replication of viral genomic materials (Gao et al., 2020), intercellular movement (Nemes et al., 2017), cell-to-cell movement (Hung et al., 2014), virion assembly (Nemes et al., 2019), and long-distance movement (Zhao et al., 2015). Although several viral proteins have been extensively studied, the molecular mechanisms of their action in viral infection have not been elucidated. A lack of unified, standard, and high-efficiency phosphorylation detection methods and detailed phosphorylation site identification still remains. In addition, the biological functions of phosphorylated viral proteins are distinct and independent for each plant virus studied. In this review, the functional phosphorylation analyses that were not within the scope of the plant virus life cycle and, accordingly, the relevant studies have not been included.

A clear understanding of the phosphorylation status of plant viral proteins in different environments would be helpful to further analyze the biological functions of phosphorylation. Hence, summarizing the methods for identifying the phosphorylation of plant viral proteins and the biological functions of phosphorylated plant viral proteins is urgently needed to gain a deeper understanding of the multiple functions of viral proteins during infection. This study aims to provide a reference for further study of the molecular mechanisms of plant viral protein phosphorylation and underlines the significance of the PTM in virus infection cycles.

Common assays for identification of phosphorylated plant viral proteins

The online services, such as Kinasephos[1] and Netphos 3.1[2], can accurately predict the phosphorylation sites of plant virus proteins and the corresponding kinases involved (Zhang et al., 2018). Furthermore, various methods, including liquid chromatography-mass spectrometry (LC-MS/MS)

1 http://kinasephos2.mbc.nctu.edu.tw

2 http://www.cbs.dtu.dk/services/NetPhos/

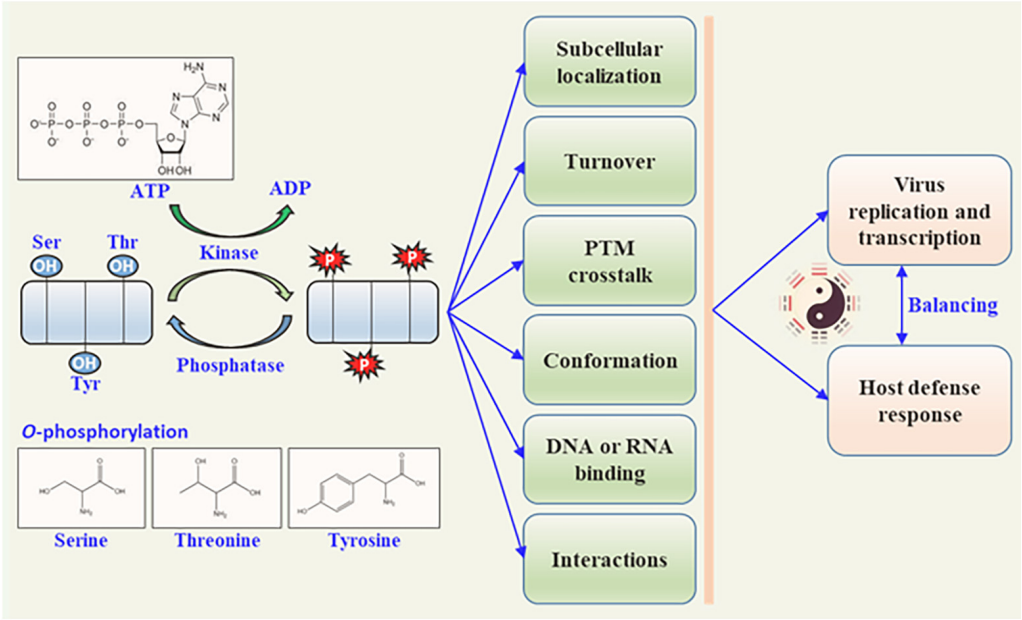

FIGURE 1
Biological function of plant viral protein phosphorylation. Protein kinases phosphorylate plant viral proteins to regulate the viral protein activity by phosphorylation and dephosphorylation (catalyzed by phosphatases). The functions of viral proteins are altered in different ways, including subcellular location, pathogenicity, intrinsic biological activity, DNA or RNA binding activity, self-interaction, and interaction with other proteins. These functional changes in plant viral proteins further affect viral replication or transcription, and the host defense responses.

(Gao et al., 2020) and radioisotope labeling ([γ-^{32}P]ATP) experiments *in vivo* and *in vitro*, have been widely used for the identification of viral protein phosphorylation (Hu et al., 2015). Selective protein kinase inhibitor screening (Zhang et al., 2018), commercial pSer/pThr/pTyr phosphorylation-specific antibodies (Li et al., 2022), and commercial Phos-tag^{TM} gel-based immunoblotting have been widely used for the identification of the phosphorylation of viral proteins. Here, we summarize the recently published phosphorylation identification assays for plant viral proteins, which include identification of the phosphorylation of target proteins and the detailed phosphorylation sites on target proteins, in order to provide a basis and reference for further studies.

Liquid chromatography-mass spectrometry-based identification of phosphorylated plant viral proteins

The continuous and rapid development of mass spectrometry and computer-based bioinformatics have improved the feasibility of research on viral protein PTMs and the interactions between plant viruses and hosts. Trypsinized protein samples are ionized and analyzed via mass spectrometry using the time-of-flight under an electric or magnetic field (Domon and Aebersold, 2006). The detector reports the relative intensity and mass-to-charge ratio of each peptide or signal. Based on the extra 79.966 KDa difference between the phosphorylated and unphosphorylated peptides under the condition of one potential phosphorylation site, AA sequences of the target peptide, and other fragmented ion signals from secondary mass spectrometry, phosphorylation can be easily identified with the bioinformatics software available nowadays (Zhang G. et al., 2014).

Various strategies have emerged for enriching phosphorylated peptides or proteins to improve the sensitivity and validity of phosphorylation assays. These approaches increase the abundance of phosphorylated peptides or proteins in LC-MS/MS assays. These enrichment methods include pSer/pThr/pTyr phosphorylation-specific antibody-based affinity capture (Stoevesandt and Taussig, 2013), chemical derivatization of phosphorylated AAs (Deng et al., 2007), metal ion-based affinity capture (Blacken et al., 2008), ion-exchange chromatography (Jungbauer and Hahn, 2009), and classical immunoprecipitation technology using phosphorylation-specific antibodies (Kurosaki et al., 2019). The enriched proteins are hydrolyzed to form peptides via trypsin digestion *in vitro*, and LC-MS/MS analyses are performed to detect the phosphorylated sites. Various phosphorylation sites can be identified using conventional LC-MS/MS analysis combined with the appropriate software. However, it is not sufficient to show that the target protein is phosphorylated, and additional phosphorylation analyses are necessary to further confirm the results.

Radioisotope (^{32}P) labeling of plant viral proteins *in vitro*

Under kinase catalysis, the radioisotope ^{32}P-labeled ATP that acts as an energy source (γ-position phosphate group) is transferred to the substrate protein by kinase (Lamberti et al., 2011). In the study by Lamberti et al. (2011), the corresponding proteins were separated via sodium dodecyl sulfate polyacrylamide gel electrophoresis (SDS-PAGE) after *in vitro* catalytic reactions were completed. The gel was dried using a Model 583 Gel Dryer (Bio-Rad, Hercules, CA, United States), and the phosphorylated proteins were detected using X-autoradiography or a phosphorous storage screen (BAS-IP TR 2040 E Tritium Screen, GE Healthcare, Chicago, IL, United States). This method is the most direct protein phosphorylation detection assay *in vitro*. It has the advantages of high sensitivity and accuracy and has been widely applied in the identification of plant viral protein phosphorylation. Using this method, the phosphorylation of a single protein was proven *in vitro*, and the detailed AA sequences of the substrate protein and catalytic kinase were validated. However, this is a hazardous procedure for operators, especially for first-time and inexperienced researchers.

The specific steps for *in vitro* phosphorylation experiment are as follows. A 20 μL phosphorylation reaction system is prepared with 20 mmol.L^{-1} Tris-HCl buffer (pH = 7.5), 0.1 μg kinase/total protein extractions, 1.0 μg substrate (purified protein), 25 μmol.L^{-1} ATP, 1 μCi [γ-^{32}P]-ATP (China Isotope & Radiation Corporation, Beijing, China), 5 mmol.L^{-1} $MgCl_2$ (or $MnCl_2$, $CaCl_2$, etc.), and ultrapure water. After incubation at 30°C for 30 min, 5 μL of 2 × SDS loading buffer [100 mM Tris–HCl, pH = 6.8, 4% SDS (v/v), 20% glycerol (v/v), 0.2% bromophenol blue (v/v), and 5% β-mercaptoethanol (v/v)] are added. The reaction is terminated by denaturation at 95°C for 5 min. All proteins in the reaction system are then separated via 12.5% SDS-PAGE for 2 h at 80 V. The gel is placed on a filter paper (8 cm × 10 cm), and dried in a gel dryer for 40 min. The dried gel is exposed to X-rays and detected using a phosphorous storage screen or film (Kodak X-OMAT BT, Nanjing, China) (Hu et al., 2015). Specific antibodies or phosphorylated antibodies can also be used to detect the target substrate proteins via western blotting.

Phos-tag^{TM} sodium dodecyl sulfate polyacrylamide gel electrophoresis for identification of phosphorylated plant viral protein

Phos-tag^{TM} reagent can specifically bind to the phosphate group on the phosphorylated protein after binding with Mn^{2+} or Zn^{2+} to form a relatively stable compound (Kinoshita-Kikuta et al., 2014). When Mn^{2+} or Zn^{2+} and Phos-tag^{TM} are added to a conventional SDS-polyacrylamide gel, the phosphorylated protein binds to the Phos-tag^{TM}. It forms a larger complex than the unphosphorylated protein, leading to a significant reduction in the electrophoretic migration rate of the phosphorylated protein in the gel under electrophoretic conditions (Kinoshita et al., 2006). Therefore, the Phos-tag^{TM} reagent can specifically separate the phosphorylated proteins from non-phosphorylated proteins. Specific or phosphorylated antibodies are usually combined with a Phos-tag^{TM} for western blotting.

This simple method can be used to detect all types of phosphorylation *in vivo* and *in vitro*. The Phos-tag^{TM} reagent in SDS-polyacrylamide gel is generally twice the concentration used in most experiments, often at a concentration of 20–100 μM (Nagy et al., 2018). The optimal concentration of the Phos-tag^{TM} reagent used for phosphorylation assays should be determined based on the actual characteristics of the specific protein in the experiment. Combined with the western blotting and LC-MS/MS, the Phos-tag^{TM} reagent could be used for protein purification in some situations. However, it often has low accuracy in protein phosphorylation assays used for the preliminary determination of protein phosphorylation. Further identification of protein phosphorylation usually requires additional evidence, such as western blotting or LC-MS/MS.

Western blotting for identification of phosphorylated plant viral proteins

The target protein or system containing the target protein is electrophoresed via SDS-PAGE at 80 V for 2 h and then transferred onto a piece of nitrocellulose membranes (Bio-Rad, United States). Specific antibodies with high affinity for the target protein or phosphorylated Ser/Thr/Tyr are used to detect the target protein (Mei et al., 2018a). Secondary antibodies are cross-linked with the horseradish peroxidase or alkaline phosphate. Based on the specific binding activity of the antibody to the corresponding antigen, only the phosphorylated target protein can be detected, as evidenced by the strong bands or signals at specific positions on the membrane (Li et al., 2022).

The western blot assay is relatively easy to perform and has no equipment or location restrictions. Antigen–antibody recognition of the phosphorylation site is specific and has high resolution in western blotting. It is often used for the validation of LC-MS/MS results in phosphorylation assays. However, this method is semi-quantitative, it is difficult to identify new or multiple phosphorylation sites in a single protein because of

the problems in preparing the corresponding specific phosphorylation antibody.

Common kinases that phosphorylate plant viral proteins

Phosphorylation/dephosphorylation is involved in multiple biological processes that regulate plant growth, development, and aging, such as plant biotic/abiotic stresses, hormone signal transduction, ion transportation, and material metabolism (Yin et al., 2018). Different kinases often mediate different types of phosphorylation in the target protein. An increasing number of studies indicate that phosphorylation plays an important role in regulating viral genome replication, viral intracellular/intercellular movement, viral gene transcription, virus infectivity to the host plant, defense and counter-defense of plant innate immunity, and virion assembly.

Understanding the recognition mechanisms and biological functions of kinases and their substrates is essential. The surrounding phosphorylated AAs (Tyr/Ser/Thr) can be specifically recognized by the modular phosphoprotein-binding domains of kinases, called p-motifs. van Wijk et al. (2014) have explored the certain kind of kinases that phosphoprotein of the p-motifs (van Wijk et al., 2014). Several algorithms, such as PTMphinder, Motif-x, and Motif-All, have been developed to predict the relatively conserved motifs in phosphopeptides, based on the concept of p-motifs. The obvious phosphorylation motifs were categorized into two major types: pS type and pT types. The pS type was clustered into seven clades, including glutamate-rich, glycine-rich, DS with acidic residues downstream or basic residues upstream, SP motif, pS with acid residues, and serine-rich pS motif. The pT types were also divided into seven clades, namely, aspartate-rich, glutamate-rich, proline-rich (2 X), arginine-rich (2 X), and lysine-rich pT (van Wijk et al., 2014). The acidic S-type motifs included S-[DE], S-E, S-X-[DE], and S-X-X-[DE], and the common basic S-type motifs comprised [RK]-X-X-S, R-S, and [RK]-X-S. T-P is the most common motif in the pT motif. Arginine was often present in the basic T-type motif ([RK]-X-X-T), while aspartate or glutamate was included in the acidic T-type motifs (X-T-X-[ED]). Annotation from the PhosPhAt 4.0 database and the known-target relationships were obtained for the p-motifs identified by Li et al. (2022) in common substrates of different kinase families. This analysis revealed that one-third of the identified p-motifs in the substrate of MAPK were T/S-P (Pitzschke, 2015; Rayapuram et al., 2018). CDKs are tightly associated substrates that contained the S-E, S-[DE], and S-X-[DE] motifs (Xi et al., 2021). The basic S-motif was over-represented in the substrates of SnRK1, SnRK2, SnRK3, and LRR-RK. In the T-motifs group, T-P was found in substrates of multiple kinase families, such as CKII, CDK, CDPK, SnRK1, and SnRK3 (Xi et al., 2021). The existing database and the corresponding relationship between substrates and kinases contribute to the prediction of target kinases that are capable of phosphorylating proteins containing the specific p-motifs.

Rapid and directed identification of hundreds of p-motifs via advanced mass-spectrometry and faster bioinformatics techniques has become feasible (Amanchy et al., 2007). Several phosphorylation prediction databases based on these accumulated datasets have based customized retrieval (Gao et al., 2009; Cheng et al., 2014; Schulze et al., 2015; Millar et al., 2019), thereby allowing the prediction of a possible optimal kinases type. In this study, we summarized the identification methods used in published studies. According to the operations, these methods are divided into three types. The first method involves comparative LC-MS/MS and the kinase-interaction assay, which can identify the corresponding kinase that can phosphorylate and directly interact with the target substrate (**Figure 2A**; Gil et al., 2019). The second method is high-throughput phosphoproteomics analyses, which can be applied where the corresponding kinase can phosphorylate but not interact with the target substrate (**Figure 2B**; Poss et al., 2016). The third method is the use of *in vitro* methods for validation of phosphorylation (**Figure 2C**; Lipton et al., 2015). Generally, the phosphorylation reaction *in vitro* (**Figure 2C**) is often combined with the top two analysis methods (**Figures 2A,B**) to further validate the substrate and the corresponding kinase. An *in vitro* phosphorylation reaction system or a cell lysis reaction should contain a phosphatase inhibitor.

Previous investigations have shown that a variety of plant kinases can phosphorylate the proteins encoded by plant viruses, including the casein kinase family (CKs) (Martínez-Turiño et al., 2018), glycogen synthase kinase-3 (GSK-3) (Mei et al., 2018a), sucrose non-fermenting-1-related protein kinase (SnRK) (Shen et al., 2018), protein kinase A (PKA) (Makarov et al., 2012), and protein kinase C (PKC) (Samuilova et al., 2013). We have summarized these publications and listed the common motifs of phosphorylated substrates of these different protein kinases in **Table 1**. This summary will provide information to help identify common kinases in phosphorylation assays. In particular, by combining the *in vitro* and *in vivo* phosphorylation reaction experiments, the corresponding kinase or target phosphorylation site can be quickly confirmed.

Casein kinase family

Protein kinase 1 (CK1) is a highly conserved serine/threonine kinase in eukaryotes. Its N-terminal catalytic domain is relatively conserved and functions in the recognition of substrate proteins (Gross and Anderson, 1998). The

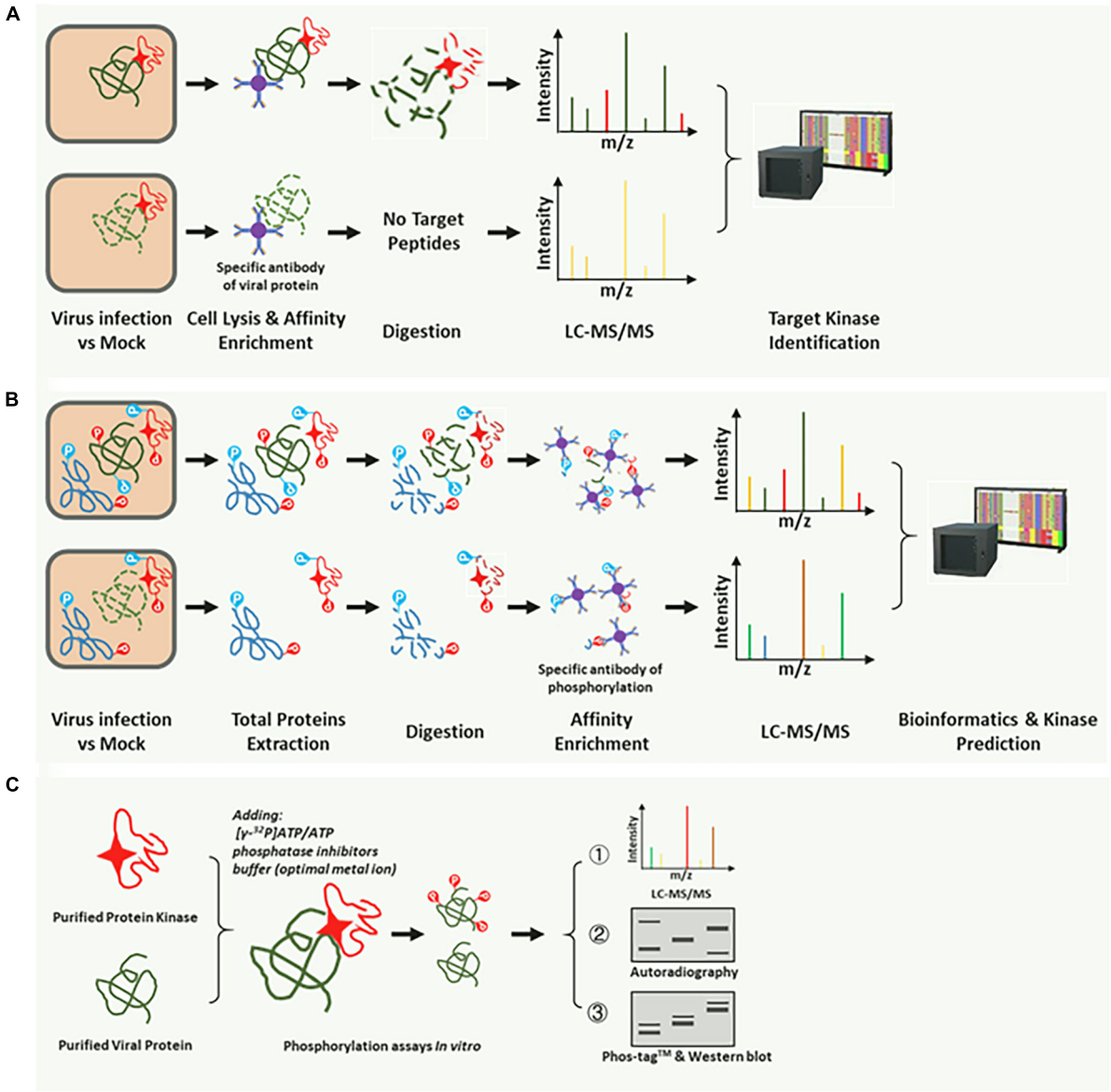

FIGURE 2
Common methods for identification of the corresponding kinase of the target substrate. **(A)** The target substrate interacts with and is phosphorylated by a specific kinase. A substrate-specific antibody was used for co-immunoprecipitation (Co-IP) of the corresponding kinase. The kinase could be identified by the LC-MS, and BLASTP was performed on the NCBI or the species-specific database. **(B)** High-throughput phosphoproteomic analysis based on the LC-MS/MS. The p-motifs could be determined using phosphor-peptides and interrogation of the corresponding database. Then, the kinase type could be identified using the already phosphorylation mode in the database. Using the third method (C), a specific kinase can be confirmed. **(C)** *In vitro* phosphorylation reaction system for further validation of the target kinase. Radioisotope (^{32}P)-labeled ATP, Phos-tag^{TM} SDS-PAGE, and pS/pT-specific antibodies were used in the reaction, and specific kinases were easily identified.

C-terminal domain of CK1 has low conservation in different species and is responsible for the binding specificity of different substrate proteins (Graves et al., 1993; Graves and Roach, 1995; Cegielska et al., 1998). CK1 has been widely studied in both yeasts and animals (Knippschild et al., 2005). To date, seven CK1 types have been identified in mammals that are involved in the regulation of vesicle transport, growth, development, morphological changes, DNA repair, and cytokinesis. CK1 participates in signal transduction and hormone metabolism in rice (Liu et al., 2003; Dai and Xue, 2010). In *Arabidopsis*, CK1 regulates blue-light signaling and ethylene biosynthesis through phosphorylation (Tan and Xue, 2014). Additionally, the *Arabidopsis* genome encodes at least 14 CK1-like (CKL) protein kinases located in the cytoplasm, nucleus, endoplasmic

TABLE 1 Consensus phosphorylation sites catalyzed by common plant kinases.

Protein kinase	Full name	Consensus of the phosphorylation site	References
AMPK	Adenosine 5'-monophosphate (AMP)-activated protein kinase	B-(X, R/K/H)-X-X-S /T-X-X-X-B	Pinna and Ruzzene, 1996
CDK	Cyclin-dependent kinase	S/T-P-X-K/R	Pinna and Ruzzene, 1996
CKI	Casein kinase-1	pS-X-X-S/T	Flotow et al., 1990
CK2	Casein kinase-2	S/T-D/E-X-E/D	Meggio and Pinna, 2003
GSK3	Glycogen synthase kinase-3	S/T XXX pS/pT	Fiol et al., 1990
PKA	Protein kinase A	R-R-X-S/T-Φ	Songyang et al., 1994
PKB	Protein kinase B	R-X-R-X-X-S/T	Obata et al., 2000
PKC	Protein kinase C	X-R-X-X-S/T-X-R-X	Pinna and Ruzzene, 1996
PKD	Protein kinase D	L/I-X-R-X-X-S/T	Hutti et al., 2004

pS/pT, phosphorylated Ser/Thr; X, any residue except those which may play a negative role; Φ, hydrophobic residue; B stands for any hydrophobic amino acid.

reticulum, and vesicular granular structure and participates in the regulation of multiple biological processes (Lee, 2009).

Protein kinase 2 (CK2) phosphorylates various plant viral proteins and plays an important role in the regulation of viral infection and host defense. CK2 is a highly conserved serine/threonine-specific kinase with multiple physiological functions in eukaryotes (Mulekar and Huq, 2014). The CK2 holoenzyme comprises two α-catalytic subunits and two β-regulatory subunits that constitute heterotetramers *in vivo* (Litchfield, 2003). In plants, the core CK2α catalytic subunits can play an independent role in the phosphorylation of target proteins (Filhol et al., 2004). Most CK2 proteins belong to a multigene family in plants. CK2 homologous genes have been cloned from various plants, including *Nicotiana attenuata*, wheat, corn, rice, and barley (Mulekar and Huq, 2014). CK2 is involved in the regulation of plant growth, development, biotic/abiotic stresses, light signals, and circadian rhythms (Huq, 2006; Moreno-Romero et al., 2008; Nagel and Kay, 2012; Mulekar and Huq, 2014). CK2-mediated phosphorylation of substrate proteins usually leads to changes in protein quaternary structure and conformation, which results in changes in DNA binding, RNA-binding, dimerization, stability, protein–protein interactions, and subcellular localization (Mulekar and Huq, 2014).

Glycogen synthesis kinase-3

Glycogen synthesis kinase-3 (GSK3) is a serine/threonine phosphokinase that participates in all biological processes (Kim and Kimmel, 2000). In mammals, GSK3 regulates cell metabolism, signal transduction, embryonic development, and neuronal differentiation (Doble and Woodgett, 2003; Kim and Kimmel, 2006; Hur and Zhou, 2010; Wu and Pan, 2010). Most protein substrates of GSK3 contain a common phosphorylation motif (Ser/Thr-x-x-Ser/Thr) (Fiol et al., 1990; Pinna and Ruzzene, 1996; **Table 1**). Various GSK3-like kinases are also present in plants. Compared with animal GSK3, plant *GSK* genes are more diverse (Yoo et al., 2006). Phosphorylation of the C-terminal serine/threonine residue of GSK3 is catalyzed by another kinase, which promotes its catalytic activity in animals (Thomas et al., 1999). In plants, the GSK3-like kinases tend to interact directly with the substrate proteins and phosphorylate them. GSK3-like kinases play different roles in cell growth, root and stomatal cell development, flowering, and fruiting (Youn and Kim, 2015).

Protein kinase A and protein kinase C

Protein kinase A (PKA) is an enzyme family whose catalytic activity depends on the levels of cyclic adenylate (cAMP) (Gold, 2019). It is a serine/threonine phosphokinase that is involved in the regulation of multiple biological processes, including cell proliferation and glycogen, and lipid metabolism (Endicott et al., 2012). PKA is a tetramer comprising two regulatory and catalytic subunits (Zelada et al., 2002). In eukaryotic cells, cAMP activates PKA, which in turn phosphorylates the target substrate proteins. The activated PKA catalytic subunit can phosphorylate the serine or threonine residues of target proteins in cells, leading to changes in the activity, which further affects the expression of related genes (Yang, 2018). Although PKA has not been identified in plants thus far, plant virologists have found that the PKA-like kinases, which phosphorylate plant viral proteins and regulate their functions in the viral life cycle, are common in plants.

Protein kinase C is also a serine/threonine phosphokinase, composed of an N-terminal regulatory region (approximately 20—40 kDa) and a C-terminal catalytic region (approximately 45 kDa) (Newton, 1995). It regulates the functions of the target protein *in vivo* by phosphorylating the hydroxyl groups and adding a phosphate group to the serine/threonine side chains (Lim et al., 2015). PKC can be divided into three subtypes according to its structural motifs and activation conditions (Keenan et al., 1997). It plays an important role in apoptosis and immune gene expression in mammals (Newton, 2018).

Functions of phosphorylated plant viral protein

An increasing number of recent studies have revealed that plant viral proteins, including coat protein (CP), movement protein (MP), RNA-dependent RNA polymerase (RdRp), and viral suppressors of RNA silencing (VSRs), undergo phosphorylation during viral infection. The phosphorylation state of viral proteins is important for the stable infection of the virus in the host plant. *In vivo*, phosphorylation can regulate the interaction between large and small subunits of replicase, viral genomic RNA or DNA catalytic synthesis activity of replicase, stability of the viral replication complex (VRC), the interaction between viral proteins and host factors, and the binding of viral protein to RNA/DNA. This study summarizes the research on the biological functions of phosphorylated plant viral proteins (**Figures 3**, **4**) from the perspective of the life cycle of plant viruses in plant viruses. Our research provides a reference for further plant viral protein phosphoproteomics research and provides a theoretical basis for plant viral disease prevention and control.

Effects of phosphorylation on viral replication and transcription

Cucumber necrosis virus (CNV) belongs to the genus *Tombusvirus* (Alam et al., 2021). The p33 protein of CNV ($p33^{CNV}$) can be phosphorylated by membrane-related kinases and PKC. The phosphorylation sites of $p33^{CNV}$ are Thr-205, Ser-210, and Thr-211. The replicase cofactor function of $p33^{CNV}$ is completely lost in plant protoplasts and yeast when p33 is mutated to a phosphorylation mimic (T/S to D). Contrastingly, when p33 was mutated to the state of dephosphorylation (T/S to A), replication can occur in plant protoplasts and yeast could occur, but the viral infection efficiency is lower than that of the wild-type virus. These results indicate that in the process of viral infection, the alanine mutants of $p33^{CNV}$ in the viral genome affected the synthesis of subgenomic RNA and reduced the proportions of positive- and negative-strand RNA, ultimately affecting viral replication (**Figure 3**, Replication). Phosphorylated $p33^{CNV}$ attenuates the RNA-binding ability and RdRp activity in plants (Stork et al., 2005).

Turnip yellow mosaic virus (TYMV) is a member of *Tymovirus* (Ni et al., 2017). The ORF1 of TYMV ($ORF1^{TYMV}$) encodes an RdRp with a mass of 206 kDa, which functions in viral RNA replication. *In vivo*, $ORF1^{TYMV}$ produces 140 kDa (p140) and 66 kDa (p66) replicase subunits via self-cleavage. The 66 kDa replicase subunits can be phosphorylated in plants, three main phosphorylation sites, thr-64, Ser-80, and Ser-326, have been identified via mass spectrometry. Dephosphorylation or phosphorylation-mimic mutants at the three phosphorylation sites of the 66 kDa replicase subunit have different effects on viral infectivity. The double phosphorylation-mimic mutant $p66^{T64D/S80D}$ and the single mutants $p66^{S326A}$, $p66^{S326D}$, and $p66^{S326T}$ have remarkable effects on viral infectivity, thereby significantly reducing the viral genomic RNA and CP protein accumulation levels. Phosphorylation of p66 does not affect its interaction with p140. In the viral infection cycle, the p66 phosphorylation is inhibited by the interactions between p140 and p66 subunits. These interactions mark the initiation of the viral replication complex assembly at the host cell membrane. Ser-326 site of p66 is the key to viral RNA synthesis regulation, and the phosphorylation/dephosphorylation of $p66^{S326}$ affects the binding and depolymerization of viral genomic RNA and the replication complex. These results indicate that the phosphorylation of p66 is a molecular switch that regulates the speed of viral replication speed in a self-optimized manner and balances the interaction between the virus and the host plant. The speed of adaptive viral genomic RNA replication could guarantee the long-term coexistence of the virus in the host plant in terms of evolution (Jakubiec et al., 2006; Jakubiec and Jupin, 2007; **Figure 3**, Replication).

Barley stripe mosaic virus (BSMV) γb protein is a typical VSR and viral symptom determinant (Bragg et al., 2004). The γb^{BSMV} can be phosphorylated by PKA-like protein kinase in *N. benthamiana in vitro* and *in vivo*. Ser-96 is the main phosphorylation site of γb in plants. The γb^{S96A} mutant has reduced local and systemic VSR activities due to the compromised 21-bp dsRNA binding activity and causes necrosis of infected leaves. Overexpression of other VSRs *in trans* or *cis* cannot rescue the necrosis induced by the BSMV γb^{S96A} mutant. These results demonstrated that suppression of cell death via γb phosphorylation at Ser-96 is functionally distinct from the RNA silencing suppressor activity. In addition, the serine/threonine/tyrosine kinase (NbSYT46) phosphorylates and interacts with γb. The antiviral role of NbSTY46 involves kinase activity, accordingly, the $NbSTY46^{T436A}$ mutant lacking kinase activity not only loses the ability to phosphorylate or interact with γb but also fails to sustain virus systemic infection in plants. Self-phosphorylated NbSYT46 directly interacts with and phosphorylates the γb protein, which negatively regulates the viral replication and inhibits viral infection (Zhang et al., 2018, 2021; **Figure 3**, Replication).

Barley yellow striate mosaic virus (BYSMV) is a member of the genus *Cytorhabdovirus*, which elicits chlorotic striate and mosaic symptoms in the leaves of cereal plant species (Cao et al., 2018). BYSMV genome is a long, negative, single-stranded RNA (Yan et al., 2015). In BYSMV infection cycle, the phosphoprotein (P) in barley has two forms, with different migration rates corresponding to 42 kDa (p42) and 44 kDa (p44). Mass-spectrometry identified five C-terminal serine-rich

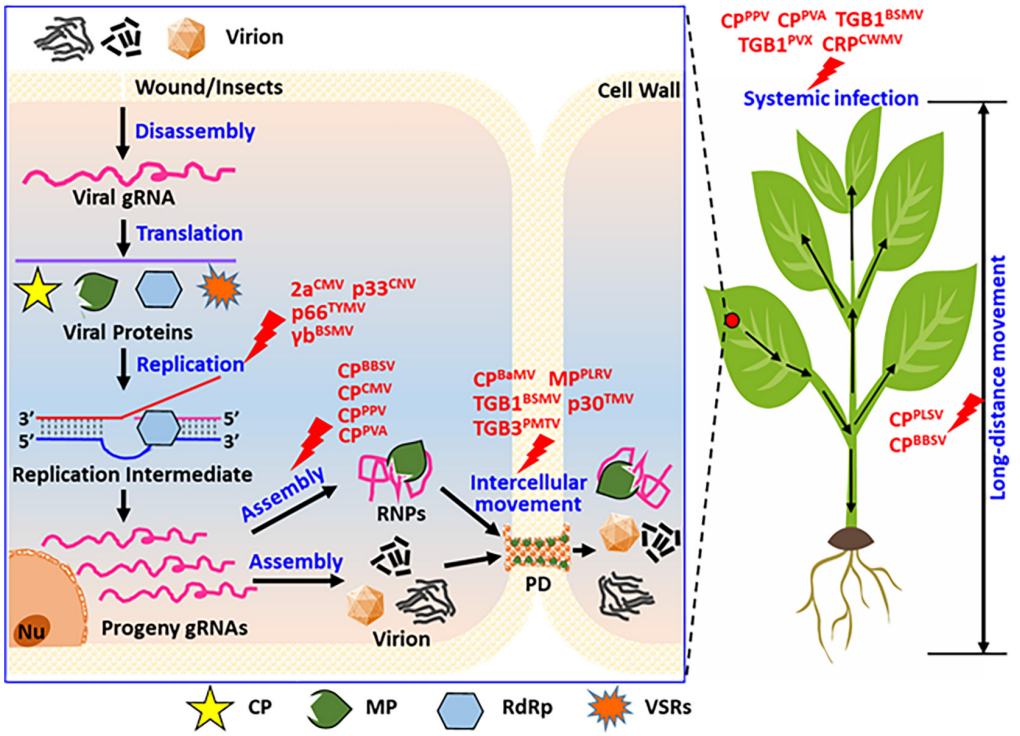

FIGURE 3
Summary of the functions of phosphorylated proteins encoded by positive single-strand RNA viruses during their life cycle. In view of the entire cell and whole plants, viral protein phosphorylation affects the replication, virion assembly, intracellular movement, long-distance movement, and systemic infection of the plants. As displayed, phosphorylation modification affected virus replication, for instance, the replicase of CMV (2a), CNV (p33), TYMV (p66), and the suppressor of BSMV (γb), these proteins not all are replicase, also contains virus-encoded RNA silencing suppressor. Phosphorylation modification of CP affected virion assemblies, such as the coat protein of BBSV, CMV, PPV, and PVA. Phosphorylation modification of viral proteins affected virus intercellular movement, such as movement protein of PLRV (MP), BSMV (TGB1), TMV (p30), PMTV (TGB3), also contains the coat protein of BaMV (CP). Phosphorylation modification of viral proteins affected virus long-distance movement, such as coat protein of PLSV (CP^{PLSV}) and BBSV (CP^{BBSV}). Phosphorylation modification of viral proteins affected virus systemic infection of host plant, such as coat protein of PPV (CP^{PPV}), PVA (CP^{PVA}), and movement protein of BSMV ($TGB1^{BSMV}$), PVX ($TGB1^{PVX}$), and the cysteine-rich protein of CWMV (CRP^{CWMV}). These viruses display rod-shaped, filamentous, and spherical particles under electron-microscopy.

regions (SR) of the phosphoprotein (^{189}SASRPSSIAS^{198}) that were phosphorylated. The viral dephosphorylation mutant (BYSMV-P^{S5A}) enhanced viral replication, whereas the transcription was facilitated by the phosphorylation-mimic mutant (BYSMV-P^{S5D}). *In vivo*, the two forms of P proteins (P^{S5A} and P^{S5D}) were preferentially associated with the nucleocapsid protein-RNA template and large polymerase protein, providing optimal replication and transcription of BYSMV, respectively. Biochemical assays demonstrated that plant and insect CK1 proteins can phosphorylate the SR motif of the P protein. Superphosphorylation of SR induces conformational changes in proteins. Moreover, the overexpression of CK1 or a dominant-negative mutant impairs the phosphorylation/dephosphorylation balance between p42 and p44, thereby compromising viral infection in barley. These observations indicate that BYSMV recruits the conserved CK1 kinases to finely regulate the replication-transcription phase during the viral life cycle and achieve optimal cross-kingdom infection of plants and insect vectors (Gao et al., 2020).

Ding et al. (2022) demonstrated that the barley (*Hordeum vulgare*) MAPK-MPK3 (HvMPK3) and the planthopper ERK (LsERK) proteins can interact with the viral structural protein nucleoprotein and directly phosphorylate this N protein at Ser-290. Overexpression of HvMPK3 could inhibit BYSMV infection, and barley plants treated with the MAPK pathway inhibitor U0126 are more susceptible to BYSMV. The dsRNA was synthesized and microinjected into the planthopper to knock down the *LsERK*, then the virus infection was promoted. A phosphomimetic mutant of the nucleoprotein Ser-290 (S290D) completely abolished virus infection because of the impaired self-interaction of BYSMV N and the formation of unstable N–RNA complexes. These results demonstrated that the conserved MAPK and ERK directly phosphorylate the viral nucleoprotein to trigger immunity against cross-kingdom

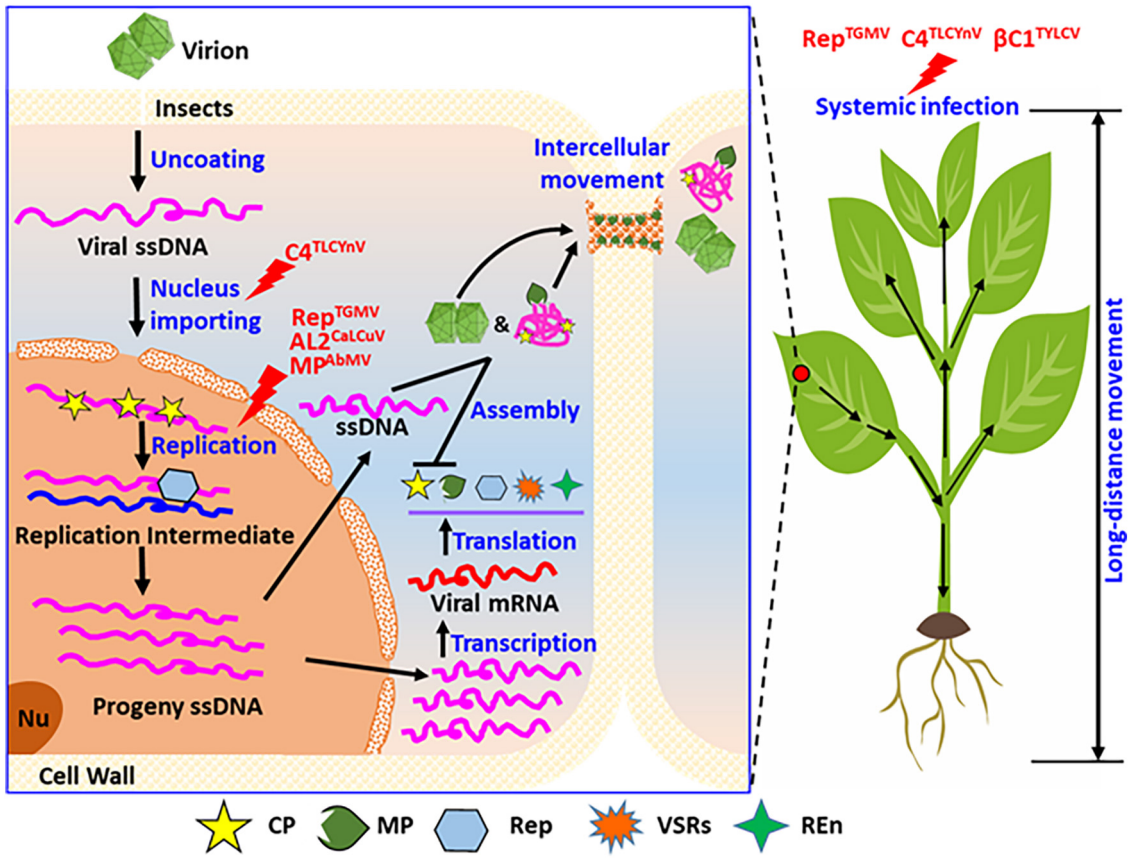

FIGURE 4
Summary of the phosphorylation functions of proteins encoded by geminiviruses during their life cycle. Considering the entire cell and whole plants, phosphorylation modification of the viral proteins regulates the different infection steps in the life cycle of geminiviruses in host plants, including the nuclear import, genomic DNA replication, and systemic infection. As shown, phosphorylation modification of C4 ($C4^{TLCYnV}$) affected virus nucleocytoplasmic shuttling. Phosphorylation modification also affects the virus replication, for instance, replicase of TGMV (Rep^{TGMV}), AL2 of CaLCuV ($AL2^{CaLCuV}$), and MP of AbMV (MP^{AbmV}). Phosphorylation modification also affects virus systemic infection of host plant, such as replicase of TGMV (Rep^{TGMV}), C4 of TLCYnV ($C4^{TLCYnV}$), and βC1 of TYLCV ($βC1^{TYLCV}$). REn, replication enhancer; PD, plasmodesmata; Nu, nucleolus.

immunity to BYSMV in host plants and its insect vectors (Ding et al., 2022).

Effect of phosphorylation on the packaging of viral particles

Beet black scorch virus (BBSV) belongs to the genus *Necrovirus* in the family *Tombusviridae* (Xu et al., 2016). CP^{BBSV} can be phosphorylated at Thr-41 by the cAMP-dependent protein kinase (PKA)-like kinases *in vivo* and *in vitro*. The non-phosphorylated state of CP^{T41} does not affect the initial viral RNA replication stage, however, viral genomic RNA accumulation is affected as the infection progresses. CP^{BBSV} phosphorylation is inferred to be involved in the later stages of genomic RNA replication, effectively interfering with the host defense system. RNase-sensitivity assays revealed that the $BBSV^{T41A}$ and $BBSV^{T41E}$ mutant viruses are easily degraded by endogenous ribonucleases in *Nicotiana benthamiana*. Electron microscopy revealed that the $BBSV^{T41A}$ and $BBSV^{T41E}$ mutants are abnormal compared to the wild-type BBSV particle (**Figure 3**, Virion Assembly). These findings indicated that the CP^{T41} mutant could not package viral RNAs into intact viral particles to protect against genomic RNA degradation. The phosphorylation state of CP^{T41} can regulate the virus particles in plants, thereby finely regulating BBSV infection in plants (Zhao et al., 2015).

Effect of phosphorylation on viral movement

Bamboo mosaic virus (BaMV) is a member of the genus *Potexvirus* and possesses a positive single-stranded RNA genome (Chen et al., 2017). The CP is phosphorylated by CK2 in *N. benthamiana* (NbCK2). Studies revealed that the main

phosphorylation site is Ser-241 and both CP^{BaMV} and NbCK2α subunits are colocalized on the plasmodesmata (PD). These results suggest that phosphorylation of CP^{BaMV} may be involved in the viral cell-to-cell movement. Although *in vitro* binding assays showed that the RNA-binding ability of CPS^{241A} mutant was not impaired, the cell-to-cell movement ability of mutant BaMV-CPS^{241A} was reduced. If the Ser-241 site is mutated to D (phosphorylation mimics, CP^{S241D}), its RNA-binding ability is significantly weakened, and the cell-to-cell movement ability of the corresponding mutant virus is blocked. Further deletion of the AA from 240 to 242 in CP^{BaMV} enhances the RNA-binding ability of CP, but the cell-to-cell movement ability of the corresponding mutant virus is affected. These results indicate that the NbCK2 regulates the RNA-binding ability of CP^{BaMV} by phosphorylating the AA 241 (Hung et al., 2014). The p20 protein, encoded by BaMV satellite RNA (satBaMV), can also be phosphorylated in plants. *In vitro* experiments showed that p20 can be phosphorylated via a total intracellular protein extraction and the Ser-11 is the phosphorylation site. The $p20^{S11D}$ mutant almost completely loses its ability to bind to wild-type p20 and mutant $p20^{S11A}$ *in vitro* (Vijayapalani et al., 2012; **Figure 3**, Intercellular Movement).

Potato mop-top virus (PMTV), belongs to the genus of *Pomovirus* and the family *Virgaviridae* (Cowan et al., 2018). Genomic RNA3 of PMTV encodes TGB3, which is one of the three movement proteins. $TGB3^{PMTV}$ participates in viral intracellular movement in plants. Studies have found that the Tyr-87, Tyr-88, Tyr-89, and Tyr-120 are phosphorylated in TGB3. *In vitro* phosphorylation experiments have shown that the phosphorylation signal of TGB3 is absent when the tyrosine (Y) is mutated to alanine (A). These results demonstrated that the Tyr (87—89, 120) is the actual phosphorylation site of TGB3.

In addition, the phosphorylation/dephosphorylation state of TGB3 affects the intensity of its interaction with TGB2. Mutation of the tyrosine to alanine at positions 87–89 of $TGB3^{PMTV}$ enhances the interaction intensity between TGB3 and TGB2 in yeast. However, the intercellular movement ability of the corresponding viral mutant (PMTV-$TGB3^{T87-89A}$) is weakened in *N. benthamiana*. Although the $TGB3^{Y120A}$ mutant does not affect the interaction with TGB2 protein, it cannot infect *N. benthamiana*. This demonstrates that tyrosine phosphorylation modification exists in plant viral proteins and is also a method of regulating plant virus movement and infectivity (**Figure 3**, Intercellular Movement; Samuilova et al., 2013).

Barley stripe mosaic virus (BSMV) is a representative species of *hordeivirus* (Wang et al., 2021). The triple gene blocks 1 (TGB1) protein is one of the three movement proteins encoded by BSMV. *In vitro* phosphorylation experiments showed that $TGB1^{BSMV}$ can be phosphorylated by CK2 kinase in the *N. benthamiana* and barley. Further research revealed that the Thr-401 is the main phosphorylation site, and Thr-395 is the anchor site of CK2 *in vivo*. Mutations in Thr-395 and Thr-401 mimic the dephosphorylation status (T395A, T395E, T401A, and T401E). The mutant viruses can systematically infect barley and wheat, however, the infection efficiency and viral accumulation levels decreased dramatically. In *N. benthamiana*, only the mutant virus BSMV-$TGB1^{T395A}$ can establish a systemic infection. Together, these results demonstrate that the phosphorylation/dephosphorylation status of TGB1 at Thr-395 and Thr-401 affects the viral systemic movement ability differently in monocot and dicot hosts. This may be a consequence of the architecture of host-specific vasculature. Furthermore, the phosphorylation of TGB1 promotes viral infection by enhancing the interaction intensity with TGB3 proteins, which is apt to form the viral ribonucleoprotein complex (BSMV intracellular movement complex). However, the phosphorylation modification of TGB1 is not sufficient to substantially alter the TGB localization patterns visualized via laser confocal microscopy (**Figure 3**, Intercellular Movement; Hu et al., 2015).

Effects of phosphorylation on viral infectivity and pathogenicity

Chinese wheat mosaic virus (CWMV), a member of the genus *Furovirus* and family of *Virgaviridae*, is an RNA virus with two positive-sense single-stranded genomic RNAs (Yang et al., 2020). Ser-162 and Ser-165 of the CWMV cysteine-rich protein (CRP^{CWMV}) are the two phosphorylation sites catalyzed by wheat SAPK7 protein *in vivo* and *in vitro*. Mutational analyses have shown that the double-site phosphorylation-mimic mutant virus (CWMV-$CRP^{S162/165D}$) enhances viral infectivity in plants because of the suppressed cell death activity and hydrogen peroxide production by the $CRP^{S162/165D}$ protein. Furthermore, the CWMV-$CRP^{S162/165D}$ interacts with the RNA-binding protein UBP1-associated protein 2C (TaUBA2C) in wheat, whereas the phosphorylation-deficient mutant virus (CWMV-$CRP^{S162/165A}$) does not. Silencing of TaUBA2C promotes viral infection in wheat plants, while the overexpression of TaUBA2C inhibits viral infection. TaUBA2C recruits the pre-mRNAs of TaNPR1, TaPR1, and TaRBOHD to induce plant cell death and hydrogen peroxide production, ultimately inhibiting viral infection. This effect can be suppressed by phosphorylated $CRP^{S162/165D}$ through direct binding of TaUBA2C, resulting in changes in the chromatin-bound status and the attenuation of the RNA- or DNA-binding activity of TaUBA2C in plants (**Figure 3**, Systemic Infection; Li et al., 2022).

Tomato yellow leaf curl virus (TYLCV) is a member of *Geminivirus* with a single genomic component that is composed of a single-stranded circular DNA (DNA-A) and satellite DNA (DNA-B) (Prasad et al., 2020). The βC1 protein is encoded by satellite DNA-B, which functions as a VSR and a symptom determinant (Hu et al., 2019). $βC1^{TYLCV}$ interacts with a variety of host factors that

interfere with multiple antiviral immune pathways in plants. An *in vitro* yeast two-hybrid assay (Y2H) and *in vivo* bimolecular fluorescence complementation (BiFC) revealed that $\beta C1^{TYLCV}$ interacts with tomato SNFI-related kinase (SnRK1). Phosphorylation experiments showed that $\beta C1^{TYLCV}$ is phosphorylated by SnRK1 kinase, and Ser-33, Thr-78, Tyr-5, and Tyr-110 are the main phosphorylation sites. The symptoms of phosphorylation-deficient mutant viruses (TYLCV-$\beta C1^{S33A}$, -$\beta C1^{T78A}$, -$\beta C1^{S33A}$, and -$\beta C1^{T78A}$) are aggravated, and the viral genomic DNA accumulation levels are significantly higher than those of the wild-type virus. The phosphorylation-mimic mutant viruses (TYLCV-$\beta C1^{S33D}$, -$\beta C1^{T78D}$, and -$\beta C1^{S33D/T78D}$) delay infection, and the viral DNA accumulation levels are completely opposed to those in the phosphorylation-deficient mutant viruses. These results indicate that SnRK1 interacts with and phosphorylates $\beta C1^{TYLCV}$ protein to weaken viral infectivity in tomatoes. Compared with those of the double mutant virus TYLCV-βC1-2D infection, the symptoms of TYLCV-βC1-2D/2E (S33D/T78D/Y5E/Y110E) infection are further attenuated, whereas the VSR activity of βC1-2D/2E is significantly weakened. Furthermore, phosphorylation of the βC1 protein by SnRK1 greatly affects its interaction with *N. benthamiana* ASYMMETRIC LEAVES 1, and regulates the induction of symptoms (**Figure 4**, Systemic Infection; Shen et al., 2011; Zhong et al., 2017).

Yunnan tomato leaf curl virus (TLCYnV) is a member of the *Geminivirus* family with a single-component genomic DNA (Mei et al., 2020). The C4 protein of TLCYnV ($C4^{TLCYnV}$) is a symptom determinant in plants (Mei et al., 2018b). *In vivo* and *in vitro* phosphorylation experiments demonstrated that $C4^{TLCYnV}$ is phosphorylated by the host NbSKη, and the Thr-51 is the corresponding phosphorylation site. Phosphorylation of $C4^{TLCYnV}$ plays a key role in plant viral pathogenicity. The pathogenicity and viral genomic DNA accumulation levels of the dephosphorylation mutant (TLCYnV-$C4^{T51A}$) are significantly reduced. Furthermore, subcellular localization revealed that the $C4^{T51A}$ mutant confines the NbSKη protein to the cell membrane, and myristoylation of the C4 N-terminal Gly-2 position directly results in the cell membrane localization. The pathogenicity and viral genomic DNA accumulation levels of the mutant TLCYnV-$C4^{G2A}$ virus are significantly reduced, respectively. During TLCYnV-$C4^{G2A}$ virus infection, NbSKη cannot localize to the cell membrane. Chemical inhibition of *N*-myristoyltransferases or exportin-α enhances the nuclear retention of $C4^{TLCYnV}$, and mutations in the putative phosphorylation (T51A) or myristoylation sites (G2A) of $C4^{TLCYnV}$ result in increased nuclear localization and reduced severity of the C4-induced developmental abnormalities. These results suggest that the nucleocytoplasmic shuttling of $C4^{TLCYnV}$ via protein modifications, including NbSKη-mediated protein phosphorylation, protein myristoylation, and the interaction with exportin-α, is critical for viral pathogenicity in plants (**Figure 4**, Systemic Infection; Mei et al., 2018a).

Table 2 shows several plant virus-encoded proteins that can be phosphorylated. Single viral protein phosphorylation often changes the biological characteristics of the protein itself and can affect the viral infection cycle in plants. The host CK2 is not only involved in plant growth and development but also regulates the function of a variety of viral proteins through phosphorylation. The virus often achieves maximum replication during co-evolution through an interaction balance between host defense and survival. Phosphorylation modifications often act as a molecular switch that guarantees optimal viral replication and prolonged viral existence in virus-specific hosts.

Conclusion and perspectives

As one of the most extensive PTMs, phosphorylation has now reached the stage where it is significant in almost every physiological event and plays important roles in regulating multiple biological activities, including cell signal transduction, protein–protein interactions, PTM-crosstalk, self-stability, and subcellular localization (**Figure 1**). Investigations of protein phosphorylation modification are important for revealing the molecular mechanisms underlying interactions between plant defense and viral counterdefense. Here, we summarized the current phosphorylation detection methods for plant viral proteins. Using the combination of *in vivo* and *in vitro* phosphorylation experiments, it is easy to determine the detailed phosphorylation sites of viral protein and host kinases. Various studies have revealed that viral proteins often act as molecular switches that display functions according to the two statuses, phosphorylation and dephosphorylation, promoting or preventing infection in a particular host. The different statuses of viral proteins are catalyzed by host kinases, including CK1, CK2, GSK3, PKA, and PKC. **Table 2** summarizes the common phosphorylation motifs for the substrates of different kinases and provides a reference for identifying the phosphorylation sites of target viral proteins and their corresponding host kinases. CK2 can phosphorylate the CP and MP of different plant viruses, and the function of CK2 has been widely studied in relation to plant–virus interactions. These findings suggest that CK2 plays an essential role in the regulation of the viral infection cycle. However, it is unclear how the same kinase phosphorylates MP and CP, and how they coordinate with each other to benefit virus infection. Our study reviewed the methods for identifying phosphorylation and the biological functions of phosphorylated viral proteins reported to date. After phosphorylation in plant cells, the subcellular localization, pathogenicity, self-interactions, and interactions with other viral proteins are altered, which finally regulates virus replication and transcription during the infection process (**Figure 1**). The summaries provide a reference and direction for further research into how viral protein phosphorylation balances the continuous viral infection and the host's moderate response

TABLE 2 Phosphorylation modifications of plant virus proteins.

Regulatory functions	Virus taxonomy	Viral protein	Phosphorylation kinase	Phosphorylation site	References
Assembly of virus particles	ss(+)RNA	CP^{BBSV}	PKA	Thr-41	Zhao et al., 2015
		CP^{CMV}	Cellular kinases	Ser-148	Nemes et al., 2019
		CP^{PVA}	CK2	Thr-242	Ivanov et al., 2001; Ivanov et al., 2003
		CP^{PPV}	CK2	Ser-25, Ser-81, Ser-101, Ser-118	Martínez-Turiño et al., 2018
Cell-to-cell movement	ss(+)RNA	CP^{BaMV}	CK2	Ser-241	Hung et al., 2014
		$TGB1^{BSMV}$	CK2	Thr-401, Thr-395	Hu et al., 2015
		$MP17^{PLRV}$	PKC-like kinase	Ser-71, Ser-79, Ser-137, Ser-140	Link et al., 2011
		$TGB3^{PMTV}$	Cellular kinases	Tyr-87,Tyr-88,Tyr-89, Tyr-120	Samuilova et al., 2013
		$P30^{TMV}$	CK2, PAPK1	Ser-258, Thr-261, Ser-264	Trutnyeva et al., 2005; Waigmann et al., 2000
Long-distance movement	ss(+)RNA	CP^{BBSV}	PKA	Thr-41	Zhao et al., 2015
		$TGB1^{PSLV}$	CK1, PKA, PKC	Unknown	Makarov et al., 2012
Interaction with other proteins	ss(+)RNA	CP^{BBSV}	Unknown	Tyr-194	Gao et al., 2022
		$TGB3^{PMTV}$	Cellular kinases	Tyr-87, Tyr-88, Tyr-89, Tyr-120	Samuilova et al., 2013
		$2a^{CMV}$	Cellular kinases	Unknown	Kim et al., 2002
	ssDNA	$C4^{TLCYnV}$	NbSKη	Thr-51	Mei et al., 2018a
		$\beta C1^{TYLCV}$	SnRK1	Ser-33, Thr-78, Tyr-5, Tyr-110	Zhong et al., 2017; Shen et al., 2011
Self-interaction	ss(+)RNA	$TGB1^{PSLV}$	CK1, PKA, PKC	Unknown	Makarov et al., 2012
		$P20^{satBaMV}$	Cellular kinases	Ser-11	Vijayapalani et al., 2012
	ss(-)RNA	NP^{BYSMV}	HvMP3, LsERK	Ser-290	Ding et al., 2022
Subcellular localization	ss(+)RNA	MP^{ToMV}	CK2, NtRIO	Ser-37, Ser-238,	Matsushita et al., 2003; Kawakami et al., 1999; Yoshioka et al., 2004
		$2b^{CMV}$	CK2	Ser-40, Ser-42	Nemes et al., 2017
	ssDNA	$C4^{TLCYnV}$	NbSKη	Thr-51	Mei et al., 2018a
Viral infectivity and pathogenicity	ss(+)RNA	CP^{BBSV}	Unknown	Tyr-194	Gao et al., 2022
	dsDNA	$CP44^{CaMV}$	CK2	Ser-66, Ser-68, Ser-72	Champagne et al., 2007; Chapdelaine et al., 2002
	ssDNA	$MP(\beta C1)^{AbMV}$	CK2	Thr-221, Ser-223, Ser-250	Kleinow et al., 2008; Kleinow et al., 2009
	ss(+)RNA	$TGB1^{BSMV}$	CK2	Thr-401, Thr-395	Hu et al., 2015
		$TGB3^{PMTV}$	Cellular kinases	Tyr-87, Tyr-88, Tyr-89, Tyr-120	Samuilova et al., 2013
		$TGBp1^{PVX}$	CK2-like kinase	Ser-165	Módena et al., 2008
		γb^{BSMV}	PKA, NbSTY46	Ser-96	Zhang et al., 2018; Zhang et al., 2021
		CRP^{CWMV}	TaSAPK7	Ser-162, Ser-165,	Li et al., 2022
	ssDNA	$\beta C1^{TYLCV}$	SnRK1	Ser-33, Thr-78, Tyr-5, Tyr-110	Zhong et al., 2017; Shen et al., 2011
		$C4^{TLCYnV}$	NbSKη	Thr-51	Mei et al., 2018a
		Rep^{TGMV}	SnRK1	Ser-97	Shen et al., 2018
Virus replication and transcription	ss(+)RNA	CP^{PVX}	CK1, CK2	Unknown	Atabekov et al., 2001
		$2a^{CMV}$	Cellular kinases	Unknown	Kim et al., 2002
		$P33^{CNV}$	Cellular kinases	Thr-205, Ser-210, Thr-211	Stork et al., 2005
		66 kDa $RDRP^{TYMV}$	Cellular kinases	Thr-64, Ser-80, Ser-326	Jakubiec and Jupin, 2007; Jakubiec et al., 2006
		γb^{BSMV}	PKA, NbSTY46	Ser-96	Zhang et al., 2018; Zhang et al., 2021
	ss(−)RNA	P^{BYSMV}	CK1	Ser-189, Ser-191, Ser-194, Ser-195, Ser-198	Gao et al., 2020
		NP^{BYSMV}	HvMP3, LsERK	Ser-290	Ding et al., 2022
	ssDNA	$AL2^{CaLCuV}$	SnRK1	Ser-109	Shen et al., 2014

and the defense or counter-defense role of plant kinases in the interactions between the plant virus and host.

In addition to phosphorylation, the side chain hydroxyl group on the serine and threonine residues of the target protein often undergo *O*-GlcNAcylation in eukaryote. The *O*-GlcNAcylation modification is catalyzed and removed by the *N*-acetylglucosamine transferase (OGT) and the O-linked *N*-acetylglucosamine hydrolase (OGA), respectively (Yang and Qian, 2017). The *O*-GlcNAcylation modification can regulate various basic cellular processes, such as transcription (Golks et al., 2007), epigenetic modification (Hanover et al., 2012; Dehennaut et al., 2014; Lewis and Hanover, 2014; Singh et al., 2015), intracellular signaling transduction (Vosseller et al., 2002; Zhang K. et al., 2014; Xu et al., 2019), and virus infection (Chen et al., 2005; Kim et al., 2011; Pérez et al., 2013; Song et al., 2019; Hu et al., 2021). The same serine and threonine target sites determine the interactions between *O*-GlcNAcylation and phosphorylation *in vivo*. Many studies have shown that in various proteins, *O*-GlcNAcylation often occurs with reciprocal or sequential phosphorylation of the same or neighboring residues (Hart et al., 2007, 2011). *O*-GlcNAcylation can temporally regulate the insulin signaling pathways in humans (Zhang K. et al., 2014). ATK is a type of serine/threonine kinases that are involved in cell survival and metabolism (Vosseller et al., 2002). The *O*-GlcNAcylation and phosphorylation sites of AKT were mapped to the same positions (Thr-308 and Ser-473) (Shi et al., 2015). These observations demonstrate that *O*-GlcNAcylation of AKT kinases directly suppresses its phosphorylation, which shows a "Yin-Yang" model with antagonistic effects on specific AAs of particular proteins (Butkinaree et al., 2010). In winter wheat verbalizations, the possible correlation between the modified sites and the computationally predicted structures of the 31 proteins containing both the *O*-GlcNAcylation and phosphorylation modifications were explored, and their result showed that they could be divided into two major patterns: competitive (Yin-Yang model) and coexisting (coordinately regulated) (Xu et al., 2019). In plant virology studies, CP^{PPV} was found to be modified via *O*-GlcNAcylation during virus infection, which promoted the stability of the CP protein and affected the virus movement and replication (Chen et al., 2005; Kim et al., 2011; Pérez et al., 2013). Seven AA sites of the CP^{PPV}, including the Thr-19, Thr-21, Thr-24, Thr-26, Thr-41, Thr-53, and Ser-65, show *O*-GlcNAcylation modifications during PPV infection (Pérez et al., 2013), whereas Ser-25, Ser-81, Ser-101, and Ser-118 were phosphorylated (Martínez-Turiño et al., 2018). The correlation between the Ser-25 phosphorylation and *O*-GlcNAcylation of Thr-19, Thr-21, Thr-24, and Thr-26 in the CP^{PPV} needs further investigation. Exploration of the coexisting or competitive patterns of these two major modifications on neighboring residues (AA 19-26) of CP^{PPV} has profound significance for a deeper understanding of the plant virus life cycle.

More than 20 viral proteins are phosphorylated during viral infection cycle (**Figures 3**, **4**). Do other plant viral proteins also undergo phosphorylation modification with different regulatory effects on viral infection? A variety of kinases in plants have been identified in plants, with less than 10 types found to be directly involved in the phosphorylation. Nevertheless, the types and functions of kinases involved in the phosphorylation of viral proteins require further exploration. This study revealed that only the CK2 and PKA can phosphorylate various plant viral proteins. Are other viral proteins phosphorylated by these two kinases? Can different viral proteins encoded by the same virus be phosphorylated by the same host kinase? We identified numerous phosphorylation sites of plant viral proteins via mass spectrometry, especially in target proteins that can be phosphorylated via total protein extractions *in vitro*. The finding is not representative of the *in vivo* conditions because the total protein obtained from plant contained many kinases, and phosphorylation can occur between the kinase and substrate that would not normally be in contact *in vivo*. Different protein kinases can phosphorylate multiple sites of the same and different viral proteins encoded by the same virus, and these modifications have different regulatory roles in plant–virus interactions.

In plant virology, the core question is how to coordinate plant resistance with yield and quality. The phosphorylation studies discussed here are promising. Massive progress in the identification of the major substrates of each protein kinase and phosphatase has been achieved in recent years using the modern MS-based proteomics. However, major gaps in our knowledge still exist regarding the identities of the key substances and protein kinases, and how their phosphorylation contributes to changes in cell physiology in response to particular stimuli. A certain genome size determines a finite number of kinases and phosphatase in plants, and there are multiple potential phosphorylation sites within a single protein, which implies that the kinase and phosphatase isoforms may have overlapping specificities. These kinases are involved in the phosphorylation of several hundreds of substrates *in vivo*. In addition, the substrate of the target kinase is often cell-specific. Explaining the distinctive effects of various stimuli on different tissues requires further consideration. Hence, powerful methods, coupled with further exploitation of important methodological and technical advances, are needed to identify the substance protein and the corresponding target kinase. Of greater importance is research to control the outbreaks and devastation caused by plant viruses, develop tissue and phosphor-specific antibodies, certain cell-type-specific permeant inhibitors of protein kinase, and design new therapies via taking advantage of the distinct cell types not expressing a particular protein kinase or phosphatase.

In future plant–virus protein phosphorylation studies, the phosphorylation sites on viral proteins can be identified in detail by mass spectrometry combined with the *in vitro* phosphorylation experiments. The corresponding kinases can

also be identified in the follow-up research using reverse genetics techniques. Furthermore, it would be beneficial to explore the impact of certain types of kinase and viral mechanism, including viral replication, viral transcription, and the host's defense response. However, several proteins encoded by one certain plant virus can be phosphorylated by several types of kinases. The elucidation of specific kinases and their substrates and determination of the corresponding relationship are essential aspects that should be considered in future studies of biological function. If the common pathways involved in the broad-spectrum antiviral immunity conferred by kinases can be identified, we could cultivate new antiviral crop germplasm through transgenic or CRISPR-Cas9-mediated gene editing methods. Moreover, small-molecule activators or inhibitors could be designed according to the advanced structures of target kinases, which could be used as novel pesticides for spraying crop leaves in the field for virus control.

Author contributions

KZ and XZ contributed substantially to the conception and design of this review article and co-wrote the manuscript. KZ and ZH reviewed the manuscript before submission for its intellectual content. All authors gave final approval of the published version.

Funding

This work was supported by the National Natural Science Foundation of China (31801699 and 81903764), the Excellent Youth Fund of Jiangsu Natural Science Foundation (SBK2022030096), the Project of Science and Technology Development Plan for Traditional Chinese Medicine of Jiangsu Province (YB201993), and the Guangdong Provincial Key Laboratory for Plant Protection (Zhizhong2021-07).

Conflict of interest

The authors declare that the research was conducted in the absence of any commercial or financial relationships that could be construed as a potential conflict of interest.

Publisher's note

All claims expressed in this article are solely those of the authors and do not necessarily represent those of their affiliated organizations, or those of the publisher, the editors and the reviewers. Any product that may be evaluated in this article, or claim that may be made by its manufacturer, is not guaranteed or endorsed by the publisher.

References

Alam, S. B., Reade, R., Maghodia, A. B., Ghoshal, B., Theilmann, J., and Rochon, D. (2021). Targeting of cucumber necrosis virus coat protein to the chloroplast stroma attenuates host defense response. *Virology* 554, 106–119. doi: 10.1016/j.virol.2020.10.012

Amanchy, R., Periaswamy, B., Mathivanan, S., Reddy, R., Tattikota, S. G., and Pandey, A. (2007). A curated compendium of phosphorylation motifs. *Nat. Biotechnol.* 25, 285–286. doi: 10.1038/nbt0307-285

Atabekov, J. G., Rodionova, N. P., Karpova, O. V., Kozlovsky, S. V., Novikov, V. K., and Arkhipenko, M. V. (2001). Translational activation of encapsidated potato virus X RNA by coat protein phosphorylation. *Virology* 286, 466–474. doi: 10.1006/viro.2001.1013

Blacken, G. R., Sadílek, M., and Turecek, F. (2008). Gallium metal affinity capture tandem mass spectrometry for the selective detection of phosphopeptides in complex mixtures. *J. Mass Spectrom. JMS* 43, 1072–1080. doi: 10.1002/jms.1387

Bragg, J. N., Lawrence, D. M., and Jackson, A. O. (2004). The N-terminal 85 amino acids of the barley stripe mosaic virus gammab pathogenesis protein contain three zinc-binding motifs. *J. Virol.* 78, 7379–7391. doi: 10.1128/JVI.78.14.7379-7391.2004

Buchowiecka, A. K. (2014). Puzzling over protein cysteine phosphorylation–assessment of proteomic tools for S-phosphorylation profiling. *The Analyst* 139, 4118–4123. doi: 10.1039/c4an00724g

Butkinaree, C., Park, K., and Hart, G. W. (2010). O-linked beta-N-acetylglucosamine (O-GlcNAc): Extensive crosstalk with phosphorylation to regulate signaling and transcription in response to nutrients and stress. *Biochim. Biophys. Acta* 1800, 96–106. doi: 10.1016/j.bbagen.2009.07.018

Cao, Q., Xu, W.-Y., Gao, Q., Jiang, Z.-H., Liu, S.-Y., Fang, X.-D., et al. (2018). Transmission characteristics of barley yellow striate mosaic virus in its planthopper vector Laodelphax striatellus. *Front. Microbiol.* 9:1419. doi: 10.3389/fmicb.2018.01419

Cegielska, A., Gietzen, K. F., Rivers, A., and Virshup, D. M. (1998). Autoinhibition of casein kinase I epsilon (CKI epsilon) is relieved by protein phosphatases and limited proteolysis. *J. Biol. Chem.* 273, 1357–1364. doi: 10.1074/jbc.273.3.1357

Champagne, J., Laliberté-Gagné, M.-E., and Leclerc, D. (2007). Phosphorylation of the termini of cauliflower mosaic virus precapsid protein is important for productive infection. *Mol. Plant-Microbe Interact. MPMI* 20, 648–658. doi: 10.1094/MPMI-20-6-0648

Chapdelaine, Y., Kirk, D., Karsies, A., Hohn, T., and Leclerc, D. (2002). Mutation of capsid protein phosphorylation sites abolishes cauliflower mosaic virus infectivity. *J. Virol.* 76, 11748–11752. doi: 10.1128/jvi.76.22.11748-11752.2002

Chen, D., Juárez, S., Hartweck, L., Alamillo, J. M., Simón-Mateo, C., Pérez, J. J., et al. (2005). Identification of secret agent as the O-GlcNAc transferase that participates in Plum pox virus infection. *J. Virol.* 79, 9381–9387. doi: 10.1128/JVI.79.15.9381-9387.2005

Chen, I.-H., Huang, Y.-W., and Tsai, C.-H. (2017). The functional roles of the cis-acting elements in bamboo mosaic virus RNA genome. *Front. Microbiol.* 8:645. doi: 10.3389/fmicb.2017.00645

Chen, Y., Sprung, R., Tang, Y., Ball, H., Sangras, B., Kim, S. C., et al. (2007). Lysine propionylation and butyrylation are novel post-translational modifications in histones. *Mol. Cell. Proteomics MCP* 6, 812–819. doi: 10.1074/mcp.M700021-MCP200

Cheng, C. M., Tu, J., Yang, C. C., and Kuo, T. T. (1996). Rifampicin: an inhibitor of Xp12-specific protein phosphorylation in Xanthomonas oryzae pv. oryzae. *FEMS Microbiol. Lett.* 143, 141–149. doi: 10.1111/j.1574-6968.1996.tb08473.x

Cheng, H., Deng, W., Wang, Y., Ren, J., Liu, Z., and Xue, Y. (2014). dbPPT: a comprehensive database of protein phosphorylation in plants. *Database J. Biol. Databases Curation* 2014, bau121. doi: 10.1093/database/bau121

Cheng, X., Xiong, R., Li, Y., Li, F., Zhou, X., and Wang, A. (2017). Sumoylation of turnip mosaic virus rna polymerase promotes viral infection by counteracting the host NPR1-mediated immune response. *Plant Cell* 29, 508–525. doi: 10.1105/tpc.16.00774

Chiang, C.-Y., Pan, C.-H., Hsieh, C.-H., Tsai, J.-P., Chen, M.-Y., Liu, H.-H., et al. (2013). Lipidated dengue-2 envelope protein domain III independently stimulates long-lasting neutralizing antibodies and reduces the risk of antibody-dependent enhancement. *PLoS Negl. Trop. Dis.* 7:e2432. doi: 10.1371/journal.pntd.0002432

Cohen, P. (2002). The origins of protein phosphorylation. *Nat. Cell Biol.* 4, E127–E130. doi: 10.1038/ncb0502-e127

Cowan, G. H., Roberts, A. G., Jones, S., Kumar, P., Kalyandurg, P. B., Gil, J. F., et al. (2018). Potato mop-top virus co-opts the stress sensor HIPP26 for long-distance movement. *Plant Physiol.* 176, 2052–2070. doi: 10.1104/pp.17.01698

Dai, C., and Xue, H.-W. (2010). Rice early flowering1, a CKI, phosphorylates DELLA protein SLR1 to negatively regulate gibberellin signalling. *EMBO J.* 29, 1916–1927. doi: 10.1038/emboj.2010.75

Dehennaut, V., Leprince, D., and Lefebvre, T. (2014). O-GlcNAcylation, an epigenetic mark. focus on the histone code, TET family proteins, and polycomb group proteins. *Front. Endocrinol.* 5:155. doi: 10.3389/fendo.2014.00155

Deng, Y.-H., Li, R.-J., Zhang, H.-S., Du, X.-L., and Wang, H. (2007). Liquid chromatographic analysis of phosphoamino acids at femtomole level using chemical derivatization with N-hydroxysuccinimidyl fluorescein-O-acetate. *Anal. Chim. Acta* 601, 118–124. doi: 10.1016/j.aca.2007.08.023

Diallo, I., Seve, M., Cunin, V., Minassian, F., Poisson, J.-F., Michelland, S., et al. (2019). Current trends in protein acetylation analysis. *Expert Rev. Proteomics* 16, 139–159. doi: 10.1080/14789450.2019.1559061

Ding, Z.-H., Gao, Q., Tong, X., Xu, W.-Y., Ma, L., Zhang, Z.-J., et al. (2022). MAPKs trigger antiviral immunity by directly phosphorylating a rhabdovirus nucleoprotein in plants and insect vectors. *Plant Cell* koac143. doi: 10.1093/plcell/koac143

Doble, B. W., and Woodgett, J. R. (2003). GSK-3: tricks of the trade for a multi-tasking kinase. *J. Cell Sci.* 116, 1175–1186. doi: 10.1242/jcs.00384

Domon, B., and Aebersold, R. (2006). Mass spectrometry and protein analysis. *Science* 312, 212–217. doi: 10.1126/science.1124619

Duan, G., and Walther, D. (2015). The roles of post-translational modifications in the context of protein interaction networks. *PLoS Comput. Biol.* 11:e1004049. doi: 10.1371/journal.pcbi.1004049

Emmer, J., Vavrinská, A., Sychrovský, V., Benda, L., Kříž, Z., Koča, J., et al. (2013). Influence of the O-phosphorylation of serine, threonine and tyrosine in proteins on the amidic 15N chemical shielding anisotropy tensors. *J. Biomol. NMR* 55, 59–70. doi: 10.1007/s10858-012-9686-6

Endicott, J. A., Noble, M. E. M., and Johnson, L. N. (2012). The structural basis for control of eukaryotic protein kinases. *Annu. Rev. Biochem.* 81, 587–613. doi: 10.1146/annurev-biochem-052410-090317

Filhol, O., Martiel, J.-L., and Cochet, C. (2004). Protein kinase CK2: a new view of an old molecular complex. *EMBO Rep.* 5, 351–355. doi: 10.1038/sj.embor.7400115

Fiol, C. J., Wang, A., Roeske, R. W., and Roach, P. J. (1990). Ordered multisite protein phosphorylation. Analysis of glycogen synthase kinase 3 action using model peptide substrates. *J. Biol. Chem.* 265, 6061–6065.

Fischer, E. H., and Krebs, E. G. (1955). Conversion of phosphorylase b to phosphorylase a in muscle extracts. *J. Biol. Chem.* 216, 121–132.

Flotow, H., Graves, P. R., Wang, A. Q., Fiol, C. J., Roeske, R. W., and Roach, P. J. (1990). Phosphate groups as substrate determinants for casein kinase I action. *J. Biol. Chem.* 265, 14264–14269.

Friso, G., and van Wijk, K. J. (2015). Posttranslational Protein Modifications in Plant Metabolism. *Plant Physiol.* 169, 1469–1487. doi: 10.1104/pp.15.01378

Gao, J., Agrawal, G. K., Thelen, J. J., and Xu, D. (2009). P3DB: a plant protein phosphorylation database. *Nucleic Acids Res.* 37, D960–D962. doi: 10.1093/nar/gkn733

Gao, Q., Yan, T., Zhang, Z.-J., Liu, S.-Y., Fang, X.-D., Gao, D.-M., et al. (2020). Casein Kinase 1 regulates cytorhabdovirus replication and transcription by phosphorylating a phosphoprotein serine-rich motif. *Plant Cell* 32, 2878–2897. doi: 10.1105/tpc.20.00369

Gao, Z., Zhang, D., Wang, X., Zhang, X., Wen, Z., Zhang, Q., et al. (2022). Coat proteins of necroviruses target 14-3-3a to subvert MAPKKKα-mediated antiviral immunity in plants. *Nat. Commun.* 13, 716. doi: 10.1038/s41467-022-28395-5

Gil, M., Lima, A., Rivera, B., Rossello, J., Urdániz, E., Cascioferro, A., et al. (2019). New substrates and interactors of the mycobacterial Serine/Threonine protein kinase PknG identified by a tailored interactomic approach. *J. Proteomics* 192, 321–333. doi: 10.1016/j.jprot.2018.09.013

Gold, M. G. (2019). Swimming regulations for protein kinase A catalytic subunit. *Biochem. Soc. Trans.* 47, 1355–1366. doi: 10.1042/BST20190230

Golks, A., Tran, T.-T. T., Goetschy, J. F., and Guerini, D. (2007). Requirement for O-linked N-acetylglucosaminyltransferase in lymphocytes activation. *EMBO J.* 26, 4368–4379. doi: 10.1038/sj.emboj.7601845

Graves, P. R., and Roach, P. J. (1995). Role of COOH-terminal phosphorylation in the regulation of casein kinase I delta. *J. Biol. Chem.* 270, 21689–21694. doi: 10.1074/jbc.270.37.21689

Graves, P. R., Haas, D. W., Hagedorn, C. H., DePaoli-Roach, A. A., and Roach, P. J. (1993). Molecular cloning, expression, and characterization of a 49-kilodalton casein kinase I isoform from rat testis. *J. Biol. Chem.* 268, 6394–6401.

Gross, S. D., and Anderson, R. A. (1998). Casein kinase I: spatial organization and positioning of a multifunctional protein kinase family. *Cell. Signal.* 10, 699–711. doi: 10.1016/s0898-6568(98)00042-4

Hanover, J. A., Krause, M. W., and Love, D. C. (2012). Bittersweet memories: linking metabolism to epigenetics through O-GlcNAcylation. *Nat. Rev. Mol. Cell Biol.* 13, 312–321. doi: 10.1038/nrm3334

Hart, G. W., Housley, M. P., and Slawson, C. (2007). Cycling of O-linked beta-N-acetylglucosamine on nucleocytoplasmic proteins. *Nature* 446, 1017–1022. doi: 10.1038/nature05815

Hart, G. W., Slawson, C., Ramirez-Correa, G., and Lagerlof, O. (2011). Cross talk between O-GlcNAcylation and phosphorylation: roles in signaling, transcription, and chronic disease. *Annu. Rev. Biochem.* 80, 825–858. doi: 10.1146/annurev-biochem-060608-102511

Heibeck, T. H., Ding, S.-J., Opresko, L. K., Zhao, R., Schepmoes, A. A., Yang, F., et al. (2009). An extensive survey of tyrosine phosphorylation revealing new sites in human mammary epithelial cells. *J. Proteome Res.* 8, 3852–3861. doi: 10.1021/pr900044c

Hu, J., Gao, Q., Yang, Y., Xia, J., Zhang, W., Chen, Y., et al. (2021). Hexosamine biosynthetic pathway promotes the antiviral activity of SAMHD1 by enhancing O-GlcNAc transferase-mediated protein O-GlcNAcylation. *Theranostics* 11, 805–823. doi: 10.7150/thno.50230

Hu, T., Huang, C., He, Y., Castillo-González, C., Gui, X., Wang, Y., et al. (2019). βC1 protein encoded in geminivirus satellite concertedly targets MKK2 and MPK4 to counter host defense. *PLoS Pathog.* 15:e1007728. doi: 10.1371/journal.ppat.1007728

Hu, Y., Li, Z., Yuan, C., Jin, X., Yan, L., Zhao, X., et al. (2015). Phosphorylation of TGB1 by protein kinase CK2 promotes barley stripe mosaic virus movement in monocots and dicots. *J. Exp. Bot.* 66, 4733–4747. doi: 10.1093/jxb/erv237

Hung, C.-J., Huang, Y.-W., Liou, M.-R., Lee, Y.-C., Lin, N.-S., Meng, M., et al. (2014). Phosphorylation of coat protein by protein kinase CK2 regulates cell-to-cell movement of bamboo mosaic virus through modulating RNA binding. *Mol. Plant-Microbe Interact. MPMI* 27, 1211–1225. doi: 10.1094/MPMI-04-14-0112-R

Huq, E. (2006). Degradation of negative regulators: a common theme in hormone and light signaling networks? *Trends Plant Sci.* 11, 4–7. doi: 10.1016/j.tplants.2005.11.005

Hur, E.-M., and Zhou, F.-Q. (2010). GSK3 signalling in neural development. *Nat. Rev. Neurosci.* 11, 539–551. doi: 10.1038/nrn2870

Hutti, J. E., Jarrell, E. T., Chang, J. D., Abbott, D. W., Storz, P., Toker, A., et al. (2004). A rapid method for determining protein kinase phosphorylation specificity. *Nat. Methods* 1, 27–29. doi: 10.1038/nmeth708

Ivanov, K. I., Puustinen, P., Gabrenaite, R., Vihinen, H., Rönnstrand, L., Valmu, L., et al. (2003). Phosphorylation of the potyvirus capsid protein by protein kinase CK2 and its relevance for virus infection. *Plant Cell* 15, 2124–2139. doi: 10.1105/tpc.012567

Ivanov, K. I., Puustinen, P., Merits, A., Saarma, M., and Mäkinen, K. (2001). Phosphorylation down-regulates the RNA binding function of the coat protein of potato virus A. *J. Biol. Chem.* 276, 13530–13540. doi: 10.1074/jbc.M009551200

Jakubiec, A., and Jupin, I. (2007). Regulation of positive-strand RNA virus replication: the emerging role of phosphorylation. *Virus Res.* 129, 73–79. doi: 10.1016/j.virusres.2007.07.012

Jakubiec, A., Tournier, V., Drugeon, G., Pflieger, S., Camborde, L., Vinh, J., et al. (2006). Phosphorylation of viral RNA-dependent RNA polymerase and its role in replication of a plus-strand RNA virus. *J. Biol. Chem.* 281, 21236–21249. doi: 10.1074/jbc.M600052200

Jungbauer, A., and Hahn, R. (2009). Ion-exchange chromatography. *Methods Enzymol.* 463, 349–371. doi: 10.1016/S0076-6879(09)63022-6

Kawakami, S., Padgett, H. S., Hosokawa, D., Okada, Y., Beachy, R. N., and Watanabe, Y. (1999). Phosphorylation and/or presence of serine 37 in the movement protein of tomato mosaic tobamovirus is essential for intracellular localization and stability in vivo. *J. Virol.* 73, 6831–6840. doi: 10.1128/JVI.73.8.6831-6840.1999

Keenan, C., Long, A., and Kelleher, D. (1997). Protein kinase C and T cell function. *Biochim. Biophys. Acta* 1358, 113–126. doi: 10.1016/s0167-4889(97)00080-3

Kim, L., and Kimmel, A. R. (2000). GSK3, a master switch regulating cell-fate specification and tumorigenesis. *Curr. Opin. Genet. Dev.* 10, 508–514. doi: 10.1016/s0959-437x(00)00120-9

Kim, L., and Kimmel, A. R. (2006). GSK3 at the edge: regulation of developmental specification and cell polarization. *Curr. Drug Targets* 7, 1411–1419. doi: 10.2174/1389450110607011411

Kim, S. H., Palukaitis, P., and Park, Y. I. (2002). Phosphorylation of cucumber mosaic virus RNA polymerase 2a protein inhibits formation of replicase complex. *EMBO J.* 21, 2292–2300. doi: 10.1093/emboj/21.9.2292

Kim, Y.-C., Udeshi, N. D., Balsbaugh, J. L., Shabanowitz, J., Hunt, D. F., and Olszewski, N. E. (2011). O-GlcNAcylation of the plum pox virus capsid protein catalyzed by SECRET AGENT: characterization of O-GlcNAc sites by electron transfer dissociation mass spectrometry. *Amino Acids* 40, 869–876. doi: 10.1007/s00726-010-0706-0

Kinoshita, E., Kinoshita-Kikuta, E., Takiyama, K., and Koike, T. (2006). Phosphate-binding tag, a new tool to visualize phosphorylated proteins. *Mol. Cell. Proteomics MCP* 5, 749–757. doi: 10.1074/mcp.T500024-MCP200

Kinoshita-Kikuta, E., Kinoshita, E., Matsuda, A., and Koike, T. (2014). Tips on improving the efficiency of electrotransfer of target proteins from Phos-tag SDS-PAGE gel. *Proteomics* 14, 2437–2442. doi: 10.1002/pmic.201400380

Kleinow, T., Holeiter, G., Nischang, M., Stein, M., Karayavuz, M., Wege, C., et al. (2008). Post-translational modifications of abutilon mosaic virus movement protein (BC1) in fission yeast. *Virus Res.* 131, 86–94. doi: 10.1016/j.virusres.2007.08.011

Kleinow, T., Nischang, M., Beck, A., Kratzer, U., Tanwir, F., Preiss, W., et al. (2009). Three C-terminal phosphorylation sites in the abutilon mosaic virus movement protein affect symptom development and viral DNA accumulation. *Virology* 390, 89–101. doi: 10.1016/j.virol.2009.04.018

Knippschild, U., Gocht, A., Wolff, S., Huber, N., Löhler, J., and Stöter, M. (2005). The casein kinase 1 family: participation in multiple cellular processes in eukaryotes. *Cell. Signal.* 17, 675–689. doi: 10.1016/j.cellsig.2004.12.011

Krupa, A., Preethi, G., and Srinivasan, N. (2004). Structural modes of stabilization of permissive phosphorylation sites in protein kinases: distinct strategies in Ser/Thr and Tyr kinases. *J. Mol. Biol.* 339, 1025–1039. doi: 10.1016/j.jmb.2004.04.043

Kurosaki, T., Myers, J. R., and Maquat, L. E. (2019). Defining nonsense-mediated mRNA decay intermediates in human cells. *Methods San Diego Calif* 155, 68–76. doi: 10.1016/j.ymeth.2018.12.005

Lamberti, G., Gügel, I. L., Meurer, J., Soll, J., and Schwenkert, S. (2011). The cytosolic kinases STY8, STY17, and STY46 are involved in chloroplast differentiation in Arabidopsis. *Plant Physiol.* 157, 70–85. doi: 10.1104/pp.111.182774

Lee, J.-Y. (2009). Versatile casein kinase 1: multiple locations and functions. *Plant Signal. Behav.* 4, 652–654. doi: 10.1104/pp.108.129346

Lewis, B. A., and Hanover, J. A. (2014). O-GlcNAc and the epigenetic regulation of gene expression. *J. Biol. Chem.* 289, 34440–34448. doi: 10.1074/jbc.R114.595439

Li, J., Feng, H., Liu, S., Liu, P., Chen, X., Yang, J., et al. (2022). Phosphorylated viral protein evades plant immunity through interfering the function of RNA-binding protein. *PLoS Pathog.* 18:e1010412. doi: 10.1371/journal.ppat.1010412

Lim, P. S., Sutton, C. R., and Rao, S. (2015). Protein kinase C in the immune system: from signalling to chromatin regulation. *Immunology* 146, 508–522. doi: 10.1111/imm.12510

Link, K., Vogel, F., and Sonnewald, U. (2011). *PD trafficking of potato leaf roll virus movement protein in Arabidopsis depends on site-specific protein phosphorylation. Front. Plant Sci. 2.* Available online at: https://www.frontiersin.org/article/10.3389/fpls.2011.00018 (Accessed April 3, 2022).

Lipton, J. O., Yuan, E. D., Boyle, L. M., Ebrahimi-Fakhari, D., Kwiatkowski, E., Nathan, A., et al. (2015). The circadian protein bmal1 regulates translation in response to S6K1-mediated phosphorylation. *Cell* 161, 1138–1151. doi: 10.1016/j.cell.2015.04.002

Litchfield, D. W. (2003). Protein kinase CK2: structure, regulation and role in cellular decisions of life and death. *Biochem. J.* 369, 1–15. doi: 10.1042/BJ20021469

Liu, W., Xu, Z.-H., Luo, D., and Xue, H.-W. (2003). Roles of OsCKI1, a rice casein kinase I, in root development and plant hormone sensitivity. *Plant J. Cell Mol. Biol.* 36, 189–202. doi: 10.1046/j.1365-313x.2003.01866.x

Makarov, V. V., Iconnikova, A. Y., Guseinov, M. A., Vishnichenko, V. K., and Kalinina, N. O. (2012). In vitro phosphorylation of the N-terminal half of hordeivirus movement protein. *Biochem. Biokhimiia* 77, 1072–1081. doi: 10.1134/S0006297912090155

Martínez-Turiño, S., Pérez, J. D. J., Hervás, M., Navajas, R., Ciordia, S., Udeshi, N. D., et al. (2018). Phosphorylation coexists with O-GlcNAcylation in a plant virus protein and influences viral infection. *Mol. Plant Pathol.* 19, 1427–1443. doi: 10.1111/mpp.12626

Matsushita, Y., Ohshima, M., Yoshioka, K., Nishiguchi, M., and Nyunoya, H. (2003). The catalytic subunit of protein kinase CK2 phosphorylates in vitro the movement protein of tomato mosaic virus. *J. Gen. Virol.* 84, 497–505. doi: 10.1099/vir.0.18839-0

Meggio, F., and Pinna, L. A. (2003). One-thousand-and-one substrates of protein kinase CK2? *FASEB J. Off. Publ. Fed. Am. Soc. Exp. Biol.* 17, 349–368. doi: 10.1096/fj.02-0473rev

Mei, Y., Wang, Y., Hu, T., Yang, X., Lozano-Duran, R., Sunter, G., et al. (2018a). Nucleocytoplasmic shuttling of geminivirus C4 Protein mediated by phosphorylation and myristoylation is critical for viral pathogenicity. *Mol. Plant* 11, 1466–1481. doi: 10.1016/j.molp.2018.10.004

Mei, Y., Yang, X., Huang, C., Zhang, X., and Zhou, X. (2018b). Tomato leaf curl Yunnan virus-encoded C4 induces cell division through enhancing stability of Cyclin D 1.1 via impairing NbSKη -mediated phosphorylation in Nicotiana benthamiana. *PLoS Pathog.* 14:e1006789. doi: 10.1371/journal.ppat.1006789

Mei, Y., Wang, Y., Li, F., and Zhou, X. (2020). The C4 protein encoded by tomato leaf curl Yunnan virus reverses transcriptional gene silencing by interacting with NbDRM2 and impairing its DNA-binding ability. *PLoS Pathog.* 16:e1008829. doi: 10.1371/journal.ppat.1008829

Millar, A. H., Heazlewood, J. L., Giglione, C., Holdsworth, M. J., Bachmair, A., and Schulze, W. X. (2019). The scope, functions, and dynamics of posttranslational protein modifications. *Annu. Rev. Plant Biol.* 70, 119–151. doi: 10.1146/annurev-arplant-050718-100211

Módena, N. A., Zelada, A. M., Conte, F., and Mentaberry, A. (2008). Phosphorylation of the TGBp1 movement protein of potato virus X by a Nicotiana tabacum CK2-like activity. *Virus Res.* 137, 16–23. doi: 10.1016/j.virusres.2008.04.007

Moreno-Romero, J., Espunya, M. C., Platara, M., Ariño, J., and Martínez, M. C. (2008). A role for protein kinase CK2 in plant development: evidence obtained using a dominant-negative mutant. *Plant J. Cell Mol. Biol.* 55, 118–130. doi: 10.1111/j.1365-313X.2008.03494.x

Mulekar, J. J., and Huq, E. (2014). Expanding roles of protein kinase CK2 in regulating plant growth and development. *J. Exp. Bot.* 65, 2883–2893. doi: 10.1093/jxb/ert401

Nagel, D. H., and Kay, S. A. (2012). Complexity in the wiring and regulation of plant circadian networks. *Curr. Biol. CB* 22, R648–R657. doi: 10.1016/j.cub.2012.07.025

Nagy, Z., Comer, S., and Smolenski, A. (2018). Analysis of Protein Phosphorylation Using Phos-Tag Gels. *Curr. Protoc. Protein Sci.* 93, e64. doi: 10.1002/cpps.64

Nemes, K., Gellért, Á, Almási, A., Vági, P., Sáray, R., Kádár, K., et al. (2017). Phosphorylation regulates the subcellular localization of cucumber mosaic virus 2b protein. *Sci. Rep.* 7, 13444. doi: 10.1038/s41598-017-13870-7

Nemes, K., Gellért, Á, Bóka, K., Vági, P., and Salánki, K. (2019). Symptom recovery is affected by cucumber mosaic virus coat protein phosphorylation. *Virology* 536, 68–77. doi: 10.1016/j.virol.2019.08.003

Newton, A. C. (1995). Protein kinase C: structure, function, and regulation. *J. Biol. Chem.* 270, 28495–28498. doi: 10.1074/jbc.270.48.28495

Newton, A. C. (2018). Protein kinase C: perfectly balanced. *Crit. Rev. Biochem. Mol. Biol.* 53, 208–230. doi: 10.1080/10409238.2018.1442408

Ni, F., Sun, S., Huang, C., and Zhao, Y. (2009). N-phosphorylation of amino acids by trimetaphosphate in aqueous solution—learning from prebiotic synthesis. *Green Chem.* 11, 569–573. doi: 10.1039/B817013D

Ni, F., Wu, L., Wang, Q., Hong, J., Qi, Y., and Zhou, X. (2017). Turnip yellow mosaic virus P69 interacts with and suppresses glk transcription factors to cause pale-green symptoms in Arabidopsis. *Mol. Plant* 10, 764–766. doi: 10.1016/j.molp.2016.12.003

Obata, T., Yaffe, M. B., Leparc, G. G., Piro, E. T., Maegawa, H., Kashiwagi, A., et al. (2000). Peptide and protein library screening defines optimal substrate motifs for AKT/PKB. *J. Biol. Chem.* 275, 36108–36115. doi: 10.1074/jbc.M005497200

Panni, S. (2019). Phospho-peptide binding domains in S. cerevisiae model organism. *Biochimie* 163, 117–127. doi: 10.1016/j.biochi.2019.06.005

Pérez, J., de, J., Udeshi, N. D., Shabanowitz, J., Ciordia, S., Juárez, S., et al. (2013). O-GlcNAc modification of the coat protein of the potyvirus Plum pox virus enhances viral infection. *Virology* 442, 122–131. doi: 10.1016/j.virol.2013.03.029

Pinna, L. A., and Ruzzene, M. (1996). How do protein kinases recognize their substrates? *Biochim. Biophys. Acta* 1314, 191–225. doi: 10.1016/s0167-4889(96)00083-3

Pitzschke, A. (2015). Modes of MAPK substrate recognition and control. *Trends Plant Sci.* 20, 49–55. doi: 10.1016/j.tplants.2014.09.006

Poss, Z. C., Ebmeier, C. C., Odell, A. T., Tangpeerachaikul, A., Lee, T., Pelish, H. E., et al. (2016). Identification of mediator kinase substrates in human cells using cortistatin A and quantitative phosphoproteomics. *Cell Rep.* 15, 436–450. doi: 10.1016/j.celrep.2016.03.030

Prasad, A., Sharma, N., Hari-Gowthem, G., Muthamilarasan, M., and Prasad, M. (2020). Tomato yellow leaf curl virus: impact, challenges, and management. *Trends Plant Sci.* 25, 897–911. doi: 10.1016/j.tplants.2020.03.015

Ramazi, S., and Zahiri, J. (2021). Post-translational modifications in proteins: resources, tools and prediction methods. *Database J. Biol. Databases Curation* 2021, baab012. doi: 10.1093/database/baab012

Rayapuram, N., Bigeard, J., Alhoraibi, H., Bonhomme, L., Hesse, A.-M., Vinh, J., et al. (2018). Quantitative phosphoproteomic analysis reveals shared and specific targets of Arabidopsis mitogen-activated protein kinases (MAPKs) MPK3, MPK4, and MPK6. *Mol. Cell. Proteomics MCP* 17, 61–80. doi: 10.1074/mcp.RA117.000135

Samuilova, O., Santala, J., and Valkonen, J. P. T. (2013). Tyrosine phosphorylation of the triple gene block protein 3 regulates cell-to-cell movement and protein interactions of Potato mop-top virus. *J. Virol.* 87, 4313–4321. doi: 10.1128/JVI.03388-12

Schulze, W. X., Yao, Q., and Xu, D. (2015). Databases for plant phosphoproteomics. *Methods Mol. Biol. Clifton NJ* 1306, 207–216. doi: 10.1007/978-1-4939-2648-0_16

Shen, Q., Hu, T., Bao, M., Cao, L., Zhang, H., Song, F., et al. (2016). Tobacco RING E3 ligase NtRFP1 mediates ubiquitination and proteasomal degradation of a geminivirus-encoded βC1. *Mol. Plant* 9, 911–925. doi: 10.1016/j.molp.2016.03.008

Shen, Q., Liu, Z., Song, F., Xie, Q., Hanley-Bowdoin, L., and Zhou, X. (2011). Tomato SlSnRK1 protein interacts with and phosphorylates βC1, a pathogenesis protein encoded by a geminivirus β-satellite. *Plant Physiol.* 157, 1394–1406. doi: 10.1104/pp.111.184648

Shen, W., Bobay, B. G., Greeley, L. A., Reyes, M. I., Rajabu, C. A., Blackburn, R. K., et al. (2018). Sucrose nonfermenting 1-related protein kinase 1 phosphorylates a geminivirus rep protein to impair viral replication and infection. *Plant Physiol.* 178, 372–389. doi: 10.1104/pp.18.00268

Shen, W., Dallas, M. B., Goshe, M. B., and Hanley-Bowdoin, L. (2014). SnRK1 phosphorylation of AL2 delays cabbage leaf curl virus infection in Arabidopsis. *J. Virol.* 88, 10598–10612. doi: 10.1128/JVI.00761-14

Shi, J., Gu, J., Dai, C., Gu, J., Jin, X., Sun, J., et al. (2015). O-GlcNAcylation regulates ischemia-induced neuronal apoptosis through AKT signaling. *Sci. Rep.* 5, 14500. doi: 10.1038/srep14500

Singh, J. P., Zhang, K., Wu, J., and Yang, X. (2015). O-GlcNAc signaling in cancer metabolism and epigenetics. *Cancer Lett.* 356, 244–250. doi: 10.1016/j.canlet.2014.04.014

Song, N., Qi, Q., Cao, R., Qin, B., Wang, B., Wang, Y., et al. (2019). MAVS O-GlcNAcylation Is essential for host antiviral immunity against Lethal RNA Viruses. *Cell Rep.* 28, 2386.e–2396.e. ***2386-2396.e5, doi: 10.1016/j.celrep.2019.07.085

Songyang, Z., Blechner, S., Hoagland, N., Hoekstra, M. F., Piwnica-Worms, H., and Cantley, L. C. (1994). Use of an oriented peptide library to determine the optimal substrates of protein kinases. *Curr. Biol. CB* 4, 973–982. doi: 10.1016/s0960-9822(00)00221-9

Stoevesandt, O., and Taussig, M. J. (2013). Phospho-specific antibodies by design. *Nat. Biotechnol.* 31, 889–891. doi: 10.1038/nbt.2712

Stork, J., Panaviene, Z., and Nagy, P. D. (2005). Inhibition of in vitro RNA binding and replicase activity by phosphorylation of the p33 replication protein of cucumber necrosis tombusvirus. *Virology* 343, 79–92. doi: 10.1016/j.virol.2005.08.005

Tan, S.-T., and Xue, H.-W. (2014). Casein kinase 1 regulates ethylene synthesis by phosphorylating and promoting the turnover of ACS5. *Cell Rep.* 9, 1692–1702. doi: 10.1016/j.celrep.2014.10.047

Thomas, G. M., Frame, S., Goedert, M., Nathke, I., Polakis, P., and Cohen, P. (1999). A GSK3-binding peptide from FRAT1 selectively inhibits the GSK3-catalysed phosphorylation of Axin and β-catenin. *FEBS Lett.* 458, 247–251. doi: 10.1016/S0014-5793(99)01161-8

Trutnyeva, K., Bachmaier, R., and Waigmann, E. (2005). Mimicking carboxyterminal phosphorylation differentially effects subcellular distribution and cell-to-cell movement of Tobacco mosaic virus movement protein. *Virology* 332, 563–577. doi: 10.1016/j.virol.2004.11.040

van Wijk, K. J., Friso, G., Walther, D., and Schulze, W. X. (2014). Meta-Analysis of Arabidopsis thaliana phospho-proteomics data reveals compartmentalization of phosphorylation motifs. *Plant Cell* 26, 2367–2389. doi: 10.1105/tpc.114.125815

Vigerust, D. J., and Shepherd, V. L. (2007). Virus glycosylation: role in virulence and immune interactions. *Trends Microbiol.* 15, 211–218. doi: 10.1016/j.tim.2007.03.003

Vijayapalani, P., Chen, J. C.-F., Liou, M.-R., Chen, H.-C., Hsu, Y.-H., and Lin, N.-S. (2012). Phosphorylation of bamboo mosaic virus satellite RNA (satBaMV)-encoded protein P20 downregulates the formation of satBaMV-p20 ribonucleoprotein complex. *Nucleic Acids Res.* 40, 638–649. doi: 10.1093/nar/gkr705

Vosseller, K., Wells, L., Lane, M. D., and Hart, G. W. (2002). Elevated nucleocytoplasmic glycosylation by O-GlcNAc results in insulin resistance associated with defects in Akt activation in 3T3-L1 adipocytes. *Proc. Natl. Acad. Sci. U. S. A.* 99, 5313–5318. doi: 10.1073/pnas.072072399

Waigmann, E., Chen, M. H., Bachmaier, R., Ghoshroy, S., and Citovsky, V. (2000). Regulation of plasmodesmal transport by phosphorylation of tobacco mosaic virus cell-to-cell movement protein. *EMBO J.* 19, 4875–4884. doi: 10.1093/emboj/19.18.4875

Wan, J., Liu, H., Chu, J., and Zhang, H. (2019). Functions and mechanisms of lysine crotonylation. *J. Cell. Mol. Med.* 23, 7163–7169. doi: 10.1111/jcmm.14650

Wang, X., Jiang, Z., Yue, N., Jin, X., Zhang, X., Li, Z., et al. (2021). Barley stripe mosaic virus γb protein disrupts chloroplast antioxidant defenses to optimize viral replication. *EMBO J.* 40, e107660. doi: 10.15252/embj.2021107660

Wu, D., and Pan, W. (2010). GSK3: a multifaceted kinase in Wnt signaling. *Trends Biochem. Sci.* 35, 161–168. doi: 10.1016/j.tibs.2009.10.002

Xi, L., Zhang, Z., Herold, S., Kassem, S., Wu, X. N., and Schulze, W. X. (2021). Phosphorylation site motifs in plant protein kinases and their substrates. *Methods Mol. Biol. Clifton NJ* 2358, 1–16. doi: 10.1007/978-1-0716-1625-3_1

Xu, J., Liu, D., Zhang, Y., Wang, Y., Han, C., Li, D., et al. (2016). Improved pathogenicity of a beet black scorch virus variant by low temperature and co-infection with its satellite RNA. *Front. Microbiol.* 7:1771. doi: 10.3389/fmicb.2016.01771

Xu, S., Xiao, J., Yin, F., Guo, X., Xing, L., Xu, Y., et al. (2019). The protein modifications of o-glcnacylation and phosphorylation mediate vernalization response for flowering in winter wheat. *Plant Physiol.* 180, 1436–1449. doi: 10.1104/pp.19.00081

Yan, T., Zhu, J.-R., Di, D., Gao, Q., Zhang, Y., Zhang, A., et al. (2015). Characterization of the complete genome of barley yellow striate mosaic virus reveals a nested gene encoding a small hydrophobic protein. *Virology* 478, 112–122. doi: 10.1016/j.virol.2014.12.042

Yang, J., Zhang, T., Li, J., Wu, N., Wu, G., Yang, J., et al. (2020). Chinese wheat mosaic virus-derived vsiRNA-20 can regulate virus infection in wheat through inhibition of vacuolar- (H+)-PPase induced cell death. *New Phytol.* 226, 205–220. doi: 10.1111/nph.16358

Yang, L. (2018). Neuronal cAMP/PKA signaling and energy homeostasis. *Adv. Exp. Med. Biol.* 1090, 31–48. doi: 10.1007/978-981-13-1286-1_3

Yang, X., and Qian, K. (2017). Protein O-GlcNAcylation: emerging mechanisms and functions. *Nat. Rev. Mol. Cell Biol.* 18, 452–465. doi: 10.1038/nrm.2017.22

Yin, X., Wang, X., and Komatsu, S. (2018). Phosphoproteomics: Protein phosphorylation in regulation of seed germination and plant growth. *Curr. Protein Pept. Sci.* 19, 401–412. doi: 10.2174/1389203718666170209151048

Yoo, M.-J., Albert, V. A., Soltis, P. S., and Soltis, D. E. (2006). Phylogenetic diversification of glycogen synthase kinase 3/SHAGGY-like kinase genes in plants. *BMC Plant Biol.* 6:3. doi: 10.1186/1471-2229-6-3

Yoshioka, K., Matsushita, Y., Kasahara, M., Konagaya, K., and Nyunoya, H. (2004). Interaction of tomato mosaic virus movement protein with tobacco RIO kinase. *Mol. Cells* 17, 223–229.

Youn, J.-H., and Kim, T.-W. (2015). Functional insights of plant GSK3-like kinases: multi-taskers in diverse cellular signal transduction pathways. *Mol. Plant* 8, 552–565. doi: 10.1016/j.molp.2014.12.006

Zelada, A., Castilla, R., Passeron, S., Giasson, L., and Cantore, M. L. (2002). Interactions between regulatory and catalytic subunits of the Candida albicans cAMP-dependent protein kinase are modulated by autophosphorylation of the regulatory subunit. *Biochim. Biophys. Acta* 1542, 73–81. doi: 10.1016/s0167-4889(01)00168-9

Zhang, G., Annan, R. S., Carr, S. A., and Neubert, T. A. (2014). Overview of peptide and protein analysis by mass spectrometry. *Curr. Protoc. Mol. Biol.* 108, 10.21.1–10.21.30. doi: 10.1002/0471142727.mb1021s108

Zhang, K., Yin, R., and Yang, X. (2014). O-GlcNAc: A bittersweet switch in liver. *Front. Endocrinol.* 5:221. doi: 10.3389/fendo.2014.00221

Zhang, X., Dong, K., Xu, K., Zhang, K., Jin, X., Yang, M., et al. (2018). Barley stripe mosaic virus infection requires PKA-mediated phosphorylation of γb for suppression of both RNA silencing and the host cell death response. *New Phytol.* 218, 1570–1585. doi: 10.1111/nph.15065

Zhang, X., Wang, X., Xu, K., Jiang, Z., Dong, K., Xie, X., et al. (2021). The serine/threonine/tyrosine kinase STY46 defends against hordeivirus infection by phosphorylating γb protein. *Plant Physiol.* 186, 715–730. doi: 10.1093/plphys/kiab056

Zhang, Z., Tan, M., Xie, Z., Dai, L., Chen, Y., and Zhao, Y. (2011). Identification of lysine succinylation as a new post-translational modification. *Nat. Chem. Biol.* 7, 58–63. doi: 10.1038/nchembio.495

Zhao, X., Wang, X., Dong, K., Zhang, Y., Hu, Y., Zhang, X., et al. (2015). Phosphorylation of beet black scorch virus coat protein by PKA is required for assembly and stability of virus particles. *Sci. Rep.* 5, 11585. doi: 10.1038/srep11585

Zhong, X., Wang, Z. Q., Xiao, R., Cao, L., Wang, Y., Xie, Y., et al. (2017). Mimic phosphorylation of a βC1 protein encoded by TYLCCNB impairs its functions as a viral suppressor of rna silencing and a symptom determinant. *J. Virol.* 91, e300–e317. e00300-17 doi: 10.1128/JVI.00300-17

frontiers | Frontiers in Microbiology

TYPE Original Research
PUBLISHED 25 August 2022
DOI 10.3389/fmicb.2022.930329

Check for updates

OPEN ACCESS

EDITED BY
Humberto J. Debat,
Instituto Nacional de Tecnología Agropecuaria, Argentina

REVIEWED BY
Massimiliano Morelli,
National Research Council, Italy
Yanan Wang,
Agricultural University of Hebei, China

*CORRESPONDENCE
Islam Hamim
hamimppath@bau.edu.bd
John S. Hu
johnhu@hawaii.edu

SPECIALTY SECTION
This article was submitted to Virology, a section of the journal Frontiers in Microbiology

RECEIVED 27 April 2022
ACCEPTED 04 August 2022
PUBLISHED 25 August 2022

CITATION
Hamim I, Suzuki JY, Borth WB, Melzer MJ, Wall MM and Hu JS (2022) Preserving plant samples from remote locations for detection of RNA and DNA viruses. *Front. Microbiol.* 13:930329. doi: 10.3389/fmicb.2022.930329

COPYRIGHT
© 2022 Hamim, Suzuki, Borth, Melzer, Wall and Hu. This is an open-access article distributed under the terms of the Creative Commons Attribution License (CC BY). The use, distribution or reproduction in other forums is permitted, provided the original author(s) and the copyright owner(s) are credited and that the original publication in this journal is cited, in accordance with accepted academic practice. No use, distribution or reproduction is permitted which does not comply with these terms.

Preserving plant samples from remote locations for detection of RNA and DNA viruses

Islam Hamim[1]*, Jon Y. Suzuki[2], Wayne B. Borth[3], Michael J. Melzer[3], Marisa M. Wall[2] and John S. Hu[3]*

[1]Department of Plant Pathology, Bangladesh Agricultural University, Mymensingh, Bangladesh, [2]USDA-ARS, Daniel K. Inouye U.S. Pacific Basin Agricultural Research Center, Hilo, HI, United States, [3]Department of Plant and Environmental Protection Sciences, University of Hawaii at Manoa, Honolulu, HI, United States

Viral diseases in plants have a significant impact on agricultural productivity. Effective detection is needed to facilitate accurate diagnosis and characterization of virus infections essential for crop protection and disease management. For sensitive polymerase chain reaction (PCR)-based methods, it is important to preserve the integrity of nucleic acids in plant tissue samples. This is especially critical when samples are collected from isolated areas, regions distant from a laboratory, or in developing countries that lack appropriate facilities or equipment for diagnostic analyses. RNA*later*® provides effective, reliable sample storage by stabilizing both RNA and DNA in plant tissue samples. Our work indicated that total RNA or DNA extracted from virus-infected leaf samples preserved in RNA*later*® was suitable for reverse transcription polymerase chain reaction (RT-PCR), PCR, Sanger sequencing, high-throughput sequencing (HTS), and enzyme-linked immunosorbent assay (ELISA)-based diagnostic analyses. We demonstrated the effectiveness of this technology using leaf tissue samples from plants with virus symptoms grown in farmers' fields in Bangladesh. The results revealed that RNA*later*® technology was effective for detection and characterization of viruses from samples collected from remote areas and stored for extended periods. Adoption of this technology by developing countries with limited laboratory facilities could greatly increase their capacity to detect and diagnose viral infections in crop plants using modern analytical techniques.

KEYWORDS

sample preservation, remote sampling, plant virus, detection, characterization

Introduction

Studies have shown that leaf tissue samples of virus-infected plants can degrade rapidly during transit or storage and require immediate appropriate sampling and preservation (Wang et al., 2018a). This is needed to obtain DNA and RNA of sufficient quality and quantity, the most important step for subsequent reliable molecular detection and characterization of plant viruses (Huang et al., 2017; Mäki et al., 2017; Patel et al., 2017). Sample preservation for

virus detection usually involves freezing plant tissues with dry ice or liquid nitrogen and then either storing the frozen samples in an ultracold freezer or shipping them on dry ice (Prendini et al., 2002). The cost of shipping with dry ice from remote areas is high and can make sample preservation an obstacle in developing countries. RNA and DNA can be quickly degraded by endogenous nucleases and by oxidative processes. Degraded DNA is of limited use because large DNA fragments may be required for downstream molecular analyses (Sirakov, 2016). RNA can also be degraded by cellular and environmental endogenous ribonucleases if transit or storage conditions are not ideal, or are of long duration (Fleige and Pfaffl, 2006; Relova et al., 2018).

RNA*later*® is a highly effective fixative for preserving biological materials (Bennike et al., 2016; Kruse et al., 2017). It is a commercially available reagent that acts as a nucleic-acid-preserving buffer, containing high concentrations of quaternary ammonium sulfates and cesium sulfates that inhibit degradation of RNA or DNA by RNases and DNases. RNA*later*® can preserve RNA and DNA in plant tissue at room temperature for several weeks and is recommended for PCR and genome sequencing analyses (Yockteng et al., 2013). To date, detection and characterization of plant viruses from leaf tissue stored in RNA*later*® has not been detailed. We assessed the efficacy of collecting papaya (*Carica papaya*), banana (*Musa paradisiaca*), and taro (*Colocasia esculenta*) leaves with virus-like symptoms in RNA*later*® to protect their RNA and DNA. We then analyzed the tissues using enzyme-linked immunosorbent assay (ELISA), polymerase chain reaction (PCR), complementary DNA (cDNA) synthesis, reverse transcription (RT)-PCR, single-tube nested PCR (STNP), and high-throughput sequencing (HTS). We identified complete and partial genomes of viruses and subviral agents using this approach. These findings could be useful in surveillance programs during virus outbreaks in agricultural systems of developing countries.

Materials and methods

Effect of extended storage times in RNA*later*® on nucleic acid quality, quantity and virus detection and characterization by PCR and ELISA

Papaya leaf samples with typical virus-like symptoms such as mosaic, ringspots, and leaf distortions as well as asymptomatic leaf samples, were collected from the island of Oahu, Hawaii. The samples were cut into small pieces and 500 mg added to 2 ml of RNA*later*® solution (Qiagen, Germany). After 7, 15, or 30 days at room temperature, immersed leaf tissues were kept at 4°C for 3 days before being transferred to 20°C for 1 week and then stored at-80°C for 1 month.

Leaf samples selected for plant virus detection were cleaned and dried with a paper towel, and then ground into powder with liquid nitrogen in a sterile mortar and pestle. Total RNAs were extracted from 100 mg of the sample with the RNeasy® Plant Mini Kit (Qiagen Inc., Germany). The RNAs were eluted in 80 µl of RNase-free water and stored at-80°C for later use. Yield and quality of the total RNAs were assayed using 1% agarose gel electrophoresis and spectrophotometry.

Papaya total RNA samples were tested for viruses by RT-PCR assays using universal potyvirus-specific nuclear inclusion body (NIb) primers (Zheng et al., 2010), papaya ringspot virus (PRSV)-specific coat protein (CP) primers (Bateson et al. 1994) and PRSV-specific STNP assay (Hamim et al., 2018), resulting in amplicons of 350 bp, 905 bp and 128 bp, respectively. The reaction mixture consisted of 2 µl RNA, 1 µl random hexamer primers (50 µg/ml) and 6.5 µl RNase-free H_2O. The reaction was incubated for 10 min at 72°C and quickly chilled on ice. A cocktail of 5 µl dNTP mixture (2.5 mmol/l each), 4 µl 5 × MMLV reaction buffer, 1 µl MMLV reverse transcriptase (200 U/µl) and 0.5 µl RNase inhibitor (40 U/µl) was then added (Promega, United States). The RT reaction was incubated at 25°C for 10 min, and then 42°C for 50 min. Reactions were chilled on ice and stored at-20°C prior to potyvirus NIb (Zheng et al., 2010) or PRSV-CP (Bateson et al. 1994) RT-PCR assay and PRSV-specific STNP (Hamim et al., 2018). Specific primer pairs reported by Noa-Carrazana et al. (2007; Table 1) were used to amplify overlapping DNA fragments corresponding to a full-length PRSV genome of a Hawaii isolate from papaya leaf samples.

PRSV-specific ELISA was performed according to the manufacturer's (Agdia, United States) instructions, and absorbance at 405 nm measured with a Bio-Rad Model 680 microplate reader (BioRad, United States). Absorbance ratios of values obtained from samples derived from symptomatic and asymptomatic tissues were calculated from mean values of absorbance for each extract dilution to set a positive/negative threshold (Sreenivasulu and Gopal 2010).

Remote collection of papaya, banana, and taro leaf samples in Bangladesh

Leaf samples of papaya, banana, and taro with and without virus-like symptoms were collected in Bangladesh during a field survey from December 2016 to January 2017 and immediately stored in RNA*later*® solution. The samples were then shipped at room temperature to the University of Hawaii at Mānoa's plant virology laboratory under USDA PPQ 526 permits P526P-16-03156 and P526P-16-03662. The delivery service and quarantine procedures took 1 week to complete. Upon arrival, all samples were stored at 4°C for 3 days, followed by −20°C for 1 week, and − 80°C until total RNA extractions were conducted.

Efficacy of RNA*later*® for determining whole-genome sequences of PRSV isolates by HTS from papaya leaf samples collected in Bangladesh

PRSV-specific STNP (Hamim et al., 2018), and ELISA (Agdia Inc., United States) analyses were carried out on 11 papaya leaf

TABLE 1 Primer pairs used in this study for detection and genome characterization of plant viruses from leaf samples stored in RNA*later*®.

Primer name	Sequence	Virus isolate	Target genome	Amplified product (nt)	Reference
12-FP	AAATAAAACATCTCAACACAACATAATCAAAAG	PRSV HA	1–1,780	1,780	Noa-Carrazana et al., 2007
50-RP	GCCGTAGAAAAGCCCTATTAAAACC				
27-FP	GAAGAAGCATGGACAATACAGATTGGGG	PRSV HA	708–2,303	1,595	Noa-Carrazana et al., 2007
28-RP	GGGTTGAAGTGAGCTTTCCCAGAACGCT				
49-FP	AGAGTAATTGACGAAGTTGGTGAGGA	PRSV HA	1917–3,567	1,650	Noa-Carrazana et al., 2007
51-RP	GCGTAGGTTTTTTCCACAGC				
52-FP	GCAGTTGACGGATGAAGGTCTACTCA	PRSV HA	3,482–4,631	1,149	Noa-Carrazana et al., 2007
53-RP	GAGGTCTGGTGGGCTCTATT				
54-FP	GTCTTTAGATGACATTCGGGATTTCTAT	PRSV HA	4,279–6,305	2,026	Noa-Carrazana et al., 2007
118-RP	GTGAAACCGCATACAATCGCATCCT				
26-FP	CATTTTAAAGCCATGACAAGTTGCACTGG	PRSV HA	5,972–7,542	1,570	Noa-Carrazana et al., 2007
55-RP	GCTCCAGTGTTTGCTCCAAGTTAAAT				
56-FP	GATTGATGATTTAACTTGGA	PRSV HA	7,508–9,389	1881	Noa-Carrazana et al., 2007
59-RP	GACACATCATTTCCGTCACT				
3-FP	GACCATGGTCCTAGAATGAAGCTGTGGATG	PRSV HA	9,249–10,320	1,071	Noa-Carrazana et al., 2007
11-RP	TTTTTTTTCTCTCATTCTAAGAGGCTC				
S11F	CTCAACACAACATAATTCAAAGCAATCTACA	PRSV BD-1	1–1,254	1,254	Hamim et al. 2019a
S11R	TCGAAGTTGCCTGCTTGATACCA				
S12F	GAAATTTCTGTCCCACTCTTGGTGATTA	PRSV BD-1	714–1,869	1,155	Hamim et al. 2019a
S12R	TACACGTTATCTTGTGACAAGG				
S13F	CACGGGTCGAGTGGTCTAATTTACA	PRSV BD-1	1,551–2,946	1,395	Hamim et al. 2019a
S13R	TCTTTTGTTTGTGGTCAACGAGAATCCTT				
S14F	AAC AGA TGG AGC ATA TTG A	PRSV BD-1	2,494–4,363	1,869	Hamim et al. 2019a
S14 R	TCA ATT GGT CCG CGA TTA AT				
S15F	AGA GGC TGT TGA AAA AAC CTA C	PRSV BD-1	3,521–5,987	2,466	Hamim et al. 2019a
S15R	GCGA ATT CAA ACC AGT ACA ACT GGT CAT TG				
S16F	CATTAAGGATGTTCC AGA GAG GTT GTA	PRSV BD-1	5,750–7,636	1866	Hamim et al. 2019a
S16R	CGA CTC CCA CTC TGC TCT ATA ACA T				
S17F	GATTTCGGGAGTCACTGGATCTCA ACT A	PRSV BD-1	7,317–9,561	2,244	Hamim et al. 2019a
S17R	ACT GTG ATT GAG TGG CAC GAG TGT				
S18F	ACG AGT CAA AAA GCT TAG GAG ATT ACC AA	PRSV BD-1	9,172–10,300	1,128	Hamim et al. 2019a
S18R	CTC TCA TTC TAA GAG GCT CAG ATA G				
S21F	CAT AAA CGA TGC CGA CTC AAC AC	PRSV BD-2	1–904	904	Hamim et al. 2019a
S21R	CCA ACT TCC AGT GCC AGA T				
S22F	ACACCATCTGAGATTGATTCAATCG	PRSV BD-2	517–2,051	1,534	Hamim et al. 2019a
S22R	AAAACTCTGTTCAGTTGATCAAGCA				
S23F	AAGCCGAAGTTTGGTGATAAAATAG	PRSV BD-2	1,606–3,194	1,588	Hamim et al. 2019a
S23R	TTTCTGAGCAAATCTCGAAGTTCGT				
S24F	AAGACTCCAACCAAGAATCACAT	PRSV BD-2	2,656–4,334	1,678	Hamim et al. 2019a
S24 R	TTGTCCTCATAGAAGTCCTGAATGTC				
S25F	CAGAGAGATTTTGATCGGTTAGAA	PRSV BD-2	3,985–5,965	1,980	Hamim et al. 2019a
S25R	TTTCACTCTCAATCAGTTTGTCG				
S26F	TGCACTGTACGGCAAGCAC	PRSV BD-2	5,524–7,400	1,876	Hamim et al. 2019a
S26R	AGTGGACTACCACAATCACCATCAT				
S27F	GGATAAAGTTTGCATGATAGGTG	PRSV BD-2	7,257–9,422	2,165	Hamim et al. 2019a
S27R	TTAACATCTCTATCTCTCTCTCCA				
S28F	GGCTCCTTATGTCTCTGAAGTT	PRSV BD-2	9,069–10,325	1,256	Hamim et al. 2019a
S28R	CTCTCATTCTAAGAGGCTCAAATATCA				

(Continued)

TABLE 1 Continued

Primer name	Sequence	Virus isolate	Target genome	Amplified product (nt)	Reference
MKBEGAF4	ATATCTGCAGGGNAARATHTGGATGGA	Begomovirus	646–1,945	1,300	Hamim et al., 2019b
MKBEGAR5	TGGACTGCAGACNGGNAARACNATGTGGGC				
PA	TAATATTACCKGWKGVCCSC	ToLCBV	2,754–1,417	1,424	Hamim et al., 2019b
ToLCBV39R2	CAAGCCGAGAATGGCGTGTATATG				
ToLCBV DNA2F	AGCTGCAGTGATGAGTTCC	ToLCBV	1,440–528	1,849	Hamim et al., 2019b
PB	TGGACYTTRCAWGGBCCTTCACA				
ToLCBVDNA A1F	ACCGGATGGCCGCGATTT	ToLCBV	1–1,417	1,417	Hamim et al., 2019b
ToLCBV39R2	CAAGCCGAGAATGGCGTGTATATG				
ToLCBV DNA2F	AGCTGCAGTGATGAGTTCC	ToLCBV	1,460–2,760	1,321	Hamim et al., 2019b
ToLCBV39R1	AATATTAGTGCGGATGGCCGCTTT				
Beta 01	GGTACCACTACGCTACGCAGCAGCC	Betasatellite	1,303–1,327	1,367	Hamim et al., 2019b
Beta 02	GGTACCTACCCTCCCAGGGGTACAC		1,309–1,284		
ToLCBbetaPaF	ACCGTGGGCGAGCGGGGTTTTTGGC	ToLCB	1–1,367	1,367	Hamim et al., 2019b
ToLCBbetaPaR	AATATTAGAACGTGGGCGAGCTAAG				
J1F	CTATGTACTGGGCAAGATTTGGATG	ToLCJoV	647–1,779	1,132	Hamim et al., 2020
J1R	CAAAGGGACTGGCAATCAAATACG				
J2F	CTAATATTACCGGATGGCCGCGAT	ToLCJoV	2,763–1,441	1,322	Hamim et al., 2020
J2R	CAGGCCGAGAATGGCGTGTTTATC				
J3F	AGCTGCAGTGATGGGTTCC	ToLCJoV	1,442–529	913	Hamim et al., 2020
J3R	TGGACCTTACATGGGCCTTCACA				
J4F	ACCGGATGGCCGCGATTT	ToLCJoV	1–1,441	1,441	Hamim et al., 2020
J4R	CAGGCCGAGAATGGCGTGTTTATC				
J5F	AGCTGCAGTGATGGGTTCC	ToLCJoV	1,422–2,762	1,340	Hamim et al., 2020
J5R	AATATTAGTGCGGATGGCCGCTTT				
B1F	GGTACCACTACGCTACGCAGCAGCC	ToLCJoB	1,301–1,325	1,365	Hamim et al., 2020
B1R	GGTACCTACCCTCCCAGGGGTACAC		1,306–1,282		
B2F	ACCGTGGGCGAGCGGGGTCTTTGGC	ToLCJoB	1–1,365	1,365	Hamim et al., 2020
B2R	AATATTAGAACGTGGGCGAGCTAGG				
B3F	GATTTGTTTATCTGACTGAAACTCC	ToLCJoB	1,197–799	967	Hamim et al., 2020
B3R	GTG ACCTTCTCTCTCCTAAAAACT				
ND1F	CTATGTGCTGGGGAAGATATGGATGGA	ToLCNDV DNA-A	621–1,922	1,301	Hamim et al., 2020
ND1R	GGATAGTAGGACAGGCAAAACAATGTG				
ND2F	TAATATTACCGAATGGCCGC	ToLCNDV DNA-A	2,741–1,415	1,326	Hamim et al., 2020
ND2R	CGAGCAGAGAGTGGCGTATATACC				
ND3F	ATCCGCAGTGATGTATTCC	ToLCNDV DNA-A	1,416–501		Hamim et al., 2020
ND3R	CACCTTGCAAGGGCCTTCACA				
ND4F	ACCGAATGGCCGCGCAAAT	ToLCNDV DNA-A	1–1,415	1,415	Hamim et al., 2020
ND4R	CGAGCAGAGAGTGGCGTATATACC				
ND5F	ATCCGCAGTGATGTATTCC	ToLCNDV DNA-A	1,416–2,740	1,325	Hamim et al., 2020
ND5R	AATATTATACGAATGGCCGCTTT				
ND6F	ACCCGTAACGATCTTGAACTTTGTCC	ToLCNDV DNA-A	1,544–1,569		Hamim et al., 2020
ND6R	GGTACCATATTTGGCAATAGGTCCGAA		1,520–1,546		
ND7F	CAATATACGCGTAAGGAAATATGTG	ToLCNDV DNA-A	623–1,517	894	Hamim et al., 2020
ND7R	AATCATGGGCTAGCAGATCG				
ND8F	ACCGAAAGGCCGCGAAAAT	ToLCNDV DNA-B	1–1,458	1,458	Hamim et al., 2020
ND8R	AAC CTG AGC GGA CTG GAC GAT T				
ND9F	AATATTATACGAAAGGCCGCTT	ToLCNDV DNA-B	1,437–2,688	1,251	Hamim et al., 2020
ND9R	AATCGTCCAGTCCGCTCAGGTT				

(Continued)

TABLE 1 Continued

Primer name	Sequence	Virus isolate	Target genome	Amplified product (nt)	Reference
ND10F	TGCAATCTCTTCCCTTGTGATA	ToLCNDV DNA-B	1,375–767		Hamim et al., 2020
ND10 R	TTAGCTTGATGTACGAACGAA				

samples collected from Bangladesh and preserved in RNA*later*® to confirm the presence of PRSV. RNA*later*® was removed from the plant tissue as described above. Total RNAs were extracted from leaf samples using the RNeasy® Plant Mini Kit, and cDNAs synthesized according to the method described previously. For HTS analyses, PRSV-positive leaf samples were divided into two separate composite samples, pap-1 and pap-2, at Foundation Plant Services, Davis, California. Composite samples, prepared by combining 10-µl aliquots of total RNA from each subsample, were subjected to ribosomal RNA (rRNA) depletion and cDNA library synthesis using the Ribo-Zero® Plant Kit (Illumina, Inc., United States) and TruSeq® Stranded Total RNA (Illumina, Inc., United States), respectively (Hamim, 2019; Hamim et al., 2019a). Sequencing was performed using the Illumina® NextSeq 500 platform, and the raw HTS reads analyzed at Foundation Plant Services (Al Rwahnih et al., 2018). Employing the CLC Bio Genomic Workstation (v8.5.1; Qiagen, Hilden, Germany), Illumina reads were adapter-trimmed and then *de novo* assembled into contigs of at least 200 bp in length. The list of contigs was created by comparing contig sequences to the viral genome section of NCBI RefSeq[1] using tBLASTx software (v. 2.4.0). Candidates included contigs that matched viral genomes and had a total E-value of 10^{-4} or below. To provide the annotation finally required for viral agent identification, the narrowed list of viral hits was then evaluated against the complete nonredundant GenBank databases using BLASTx to match sequences against protein (nr) and BLASTn to compare sequences against nucleotides (nt).

Full-length sequences of PRSV genomes BD-1 and BD-2 obtained by HTS from composite samples pap-1 and pap-2, respectively, were verified by direct sequencing of PCR-amplified overlapping DNA fragments using virus-specific primers designed from the HTS-derived sequences (Table 1). PCR amplifications were performed on cDNA synthesized from total RNA as described above and amplified using the following conditions: 4 min at 94°C; 35 cycles of 1 min at 94°C, 1 min at 50 to 65°C depending on the primers, and 2 min at 72°C; with a final elongation at 72°C for 7 min (Hamim, 2019; Hamim et al., 2019a). The PCR products were resolved on 1% agarose gel in 1X TAE buffer. Gels were stained with ethidium bromide and visualized in a UVP transilluminator. PCR products of the predicted size were purified, cloned into the PGEM-T Easy® cloning vector (Promega, United States), and sequenced at the University of Hawaii's Advanced Genomic and Sequencing Services and at Genewiz, in California.

Efficacy of RNA*later*® for detection of isolates of PRSV and Begomoviruses from papaya leaf samples collected from different remote regions in Bangladesh

The presence of specific PRSV isolates was detected by RT-PCR assays from RNA*later*®-preserved papaya leaf samples with virus-like symptoms: mosaic, ring spots, leaf curl and leaf distortion collected from eight geographical districts in Bangladesh (Table 3). Total RNAs were extracted from the samples using the RNeasy® Plant Mini Kit, and cDNAs synthesized as reported (Hamim, 2019; Hamim et al., 2019a).

Total DNAs were extracted from 100 mg of the papaya leaf samples from Bangladesh stored in RNA*later*® with the DNeasy® Mini extraction kit (Qiagen Inc., Germany). The DNAs were eluted in 50 µl of DNase-free water and stored at-20°C for later use. Yield and quality of the total RNAs were assayed using spectrophotometry (Thermo Fisher Scientific, Waltham, MA, United States). DNA extracted from papaya leaf samples was used to test for the presence of begomoviruses using PCR with begomovirus-specific primer pairs (Table 1), accompanied by Sanger sequencing (Hamim et al., 2020). From these analyses, full-length genome sequences of specific begomoviruses as well as the cognate betasatellites or associated components and defective betasatellites were obtained by direct sequencing of PCR-amplified overlapping DNA fragments using virus-specific primers (Table 1). In addition, RNA*later*®-stored papaya leaf samples were used to examine the geographic distribution of various begomoviruses by PCR using virus-specific primers.

Efficacy of RNA*later*® for detection of viruses in taro and banana leaf samples collected from Bangladesh

Total RNA was extracted from taro leaf samples in RNA*later*® using the RNeasy Plant Mini Kit and synthesis of cDNA was performed using M-MLV reverse transcription (Promega, United States; Wang et al., 2017). A universal potyvirus-specific ELISA (Agdia Inc., USA) and a universal potyvirus-specific RT-PCR (Zheng et al., 2010) were used to test two samples with

1 https://www.ncbi.nlm.nih.gov/genome/viruses/

feathery mottling and distorted leaves, and one asymptomatic sample. RT-PCR with dasheen mosaic virus (DsMV) CI-specific primers and a DsMV-specific triple-antibody sandwich ELISA (Agdia Inc., United States; Wang et al., 2017) were used to confirm DsMV in taro leaf samples.

We used the CTAB method to isolate total DNA from 100 mg banana leaf samples with banana bunchy top virus (BBTV) symptoms kept in RNA*later*® using CTAB method and were tested by PCR using BBTV-Rep gene-specific primers and CP-specific primers BBTV-HAF1 and BBTV-HAR1 (Hamim et al., 2017). Six samples were also tested for BBTV using a BBTV-specific antibody in a triple-antibody sandwich-ELISA (Agdia, Elkhart, Inc.).

Results

Effect of extended storage times in RNA*later*® on detection and characterization of RNA viruses

Average RNA yields obtained from virus-infected papaya leaves collected on Oahu, Hawaii, and stored for 7, 15, and 30 days in RNA*later*® were 315.17 ± 62.23 ng/μl, 355.1 ± 86.5 ng/μl and 211.03 ± 61.03 ng/μl, respectively, compared to 670.17 ± 216.18 ng/μl total RNA from fresh samples. A 260/280 ratio greater than 2.0 was obtained for RNAs isolated from both RNA*later*®-stored and fresh papaya leaf samples. Gel electrophoresis analysis of total RNA in agarose gels confirmed the presence of bands corresponding to the 28S and 18S ribosomal RNA (rRNA) for all storage times and for fresh samples, providing a qualitative assessment of the rRNA integrity in RNA*later*®-stored samples (Figure 1). The absence of smearing in the agarose gel indicated the total RNAs were intact and not degraded. Leaves stored in RNA*later*® tested positive in potyvirus-specific RT-PCR with potyvirus NIb primers NIb2F and NIb3R (Figure 2A). Samples with virus-like symptoms stored in RNA*later*® solution for different lengths of time, and fresh samples, were also positive in STNP reactions specific for PRSV, and RT-PCR reactions using primers specific for PRSV CP (Figures 2B,C, respectively) as were the ELISA assays. In addition, we successfully amplified eight overlapping DNA fragments (F1 to F8) correspond to 3′ to 5′ of the full-length PRSV genome of a Hawaiian PRSV isolate (HA) sequentially from a virus-infected papaya leaf sample that had been collected from Oahu, Hawaii and stored for 1 month in RNAlater®. These DNA fragments were amplified using previously reported primers (Figure 3; Table 1; Noa-Carrazana et al., 2007). Sizes of these amplified products varied from 1,071 to 2,026 bp.

Papaya leaf samples with virus-like symptoms collected from Bangladesh were used to study the efficacy of RNA*later*® in combination with HTS technology for detecting viruses. The 11 samples stored in RNA*later*®, and tested with PRSV-specific STNP and ELISA were positive for PRSV. These samples were divided into two separate composite samples and full-length genomes of the two PRSV isolates, BD-1 and BD-2 identified by HTS (Table 2). The complete genome sequences of BD-1(MH444652) and BD-2 (MH397222) were verified by Sanger sequencing of

TABLE 2 Illumina® NextSeq 500 RNA sequencing of whole papaya ringspot virus (PRSV) genomes from symptomatic papaya leaf samples collected in Bangladesh and stored in RNA*later*®.

PRSV Isolate	BD1	BD2
Total RNA composite	pap-1	pap-2
Total reads	80,648,570	61,307,471
Non-virus contigs	906	1,043
Plant virus contigs	134	79
PRSV-specific contigs	127	74
PRSV contig sequence lengths	200–10,282 nt	200–3,484 nt
Identical matches with reported isolates	52–100%	64–100%
Total genome length	10,300 nt	10,325 nt
GenBank accession no.	MH444652.1	MH397222.1

PRSV: Papaya ringspot virus.

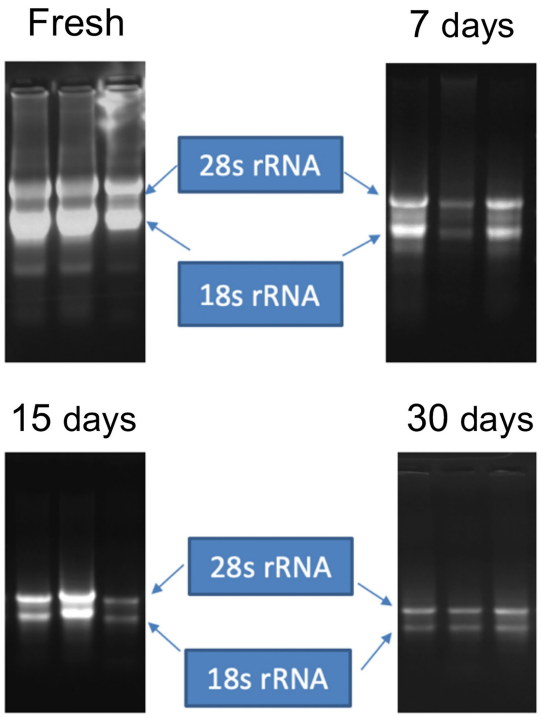

FIGURE 1
Gel electrophoresis of total RNA extracted from fresh leaves or leaves harvested and stored in RNA*later*® for 7, 15 or 30days. Bands corresponding to intact ribosomal RNA (rRNA) species are shown.

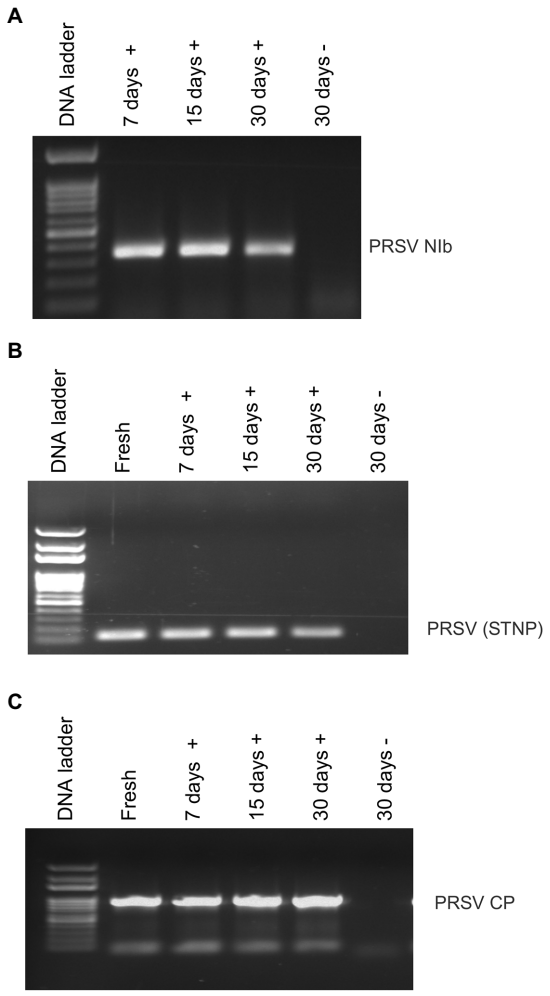

FIGURE 2
Analysis of RT-PCR products from reactions using **(A)** potyvirus-specific nuclear inclusion body (NIb) primers, **(B)** PRSV coat protein (CP) primers or **(C)** PRSV-specific single-tube nested PCR (STNP) and total RNA from symptomatic (+) or asymptomatic (–) fresh papaya leaves or leaves stored in RNA*later*® for various periods.

overlapping DNA fragments obtained by RT-PCR using virus-specific primers and total RNA extracts from papaya leaf samples GAZ-52 and CD-129, respectively, which were stored in RNA*later*® (Figure 3).

The effectiveness of RNA*later*® technology in routine RT-PCR assays for RNA viruses was also tested. Of the 118 papaya samples tested from eight different districts of Bangladesh, 22 were positive for PRSV BD-1, 81 were positive for PRSV BD-2, and both BD-1 and BD-2 were found in 13 of the samples (Table 3).

We investigated the efficacy of RNA*later*® technology for detecting dasheen mosaic virus (DsMV) in RNA*later*®-stored, symptomatic taro leaf samples. The two symptomatic samples tested positive for potyvirus with RT-PCR and ELISA, while an asymptomatic taro leaf sample tested negative (Figure 4). Sanger sequencing of the resulting PCR amplicons confirmed the

TABLE 3 Distribution and prevalence of PRSV isolates BD-1 and BD-2 based on RT-PCR analysis of papaya leaf samples obtained from different districts in Bangladesh and stored in RNA*later*®.

Collection districts	Sample no.	PRSV BD-1 positive	PRSV BD-2 positive	PRSV BD-1 and BD-2 positive
Pabna	17	1	17	1
Rajshahi	5	0	3	0
Chapai Nawabganj	4	0	3	0
Chandpur	33	11	24	8
Munshiganj	9	2	5	1
Gazipur	22	8	15	3
Tangail	13	0	6	0
Mymensingh	15	0	8	0
Total	118	22	81	13

PRSV: Papaya ringspot virus.

presence of DsMV (accession MH036416; Wang et al., 2018b). DsMV CI-specific primers were used with RT-PCR to check for the presence of virus in total RNA extracts from 13 RNA*later*®-stored taro leaf samples (Figure 5; Wang et al., 2017). Eight of the samples produced target virus-specific bands. DsMV-specific triple-antibody sandwich-ELISA also confirmed that these eight samples were positive for DsMV.

Effect of extended storage times in RNA*later*® on detection and characterization of DNA viruses

DNA extracted from RNA*later*®-stored papaya leaf samples was used to test for begomoviruses. A PCR test using a begomovirus-specific primer pair produced the predicted PCR product corresponding to the begomovirus DNA-A component in 43 of 51 samples examined. Of the 43 PCR products, Sanger sequencing identified 29 sequences corresponding to tomato leaf curl Bangladesh virus (ToLCBV; Table 4). The remainder were identified as being deriving from tomato leaf curl Joydebpur virus (ToLCJoV) and tomato leaf curl New Delhi virus (ToLCNDV; Table 4). We amplified and sequenced the full-length 2,760-bp genome of ToLCBV from RNA*later*®-stored Gaz17-Pap samples obtained from Gazipur, Bangladesh. A ToLCBV cognate betasatellite of 1,367 bp was also amplified from the DNA of the same Gaz17-Pap leaf sample (Table 5). Small defective betasatellites DefS39, DefS40, and Defs43 were also amplified from RNAlater®-stored, ToLCBV-positive samples Gaz19-Pap, Gaz-20-Pap, and Gaz21-Pap, respectively (Table 5). The complete 2,762-nucleotide sequence of ToLCJoV (MT127782) was amplified from RNA*later*®-stored papaya leaf sample J^{-1} (Table 5). Additionally, the betasatellite ToLCJoB (MT161673), 1,365 bp in length and associated with ToLCJoV, was obtained from the J1-Pap isolate (Table 5). The full-length DNA-A and DNA-B

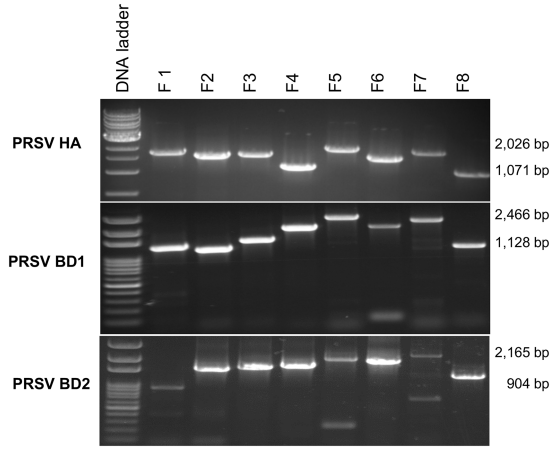

FIGURE 3
Analysis of overlapping RT-PCR DNA fragments (F1 to F8) covering full-length PRSV genomes using published PRSV primer sequences for Hawaii isolate (HA) or using primers designed based on HTS analysis for PRSV Bangladesh isolates BD1 and BD2 and total RNA from symptomatic papaya leaf samples stored in RNA*later*® for one-month. Size ranges of PCR fragments are shown at right.

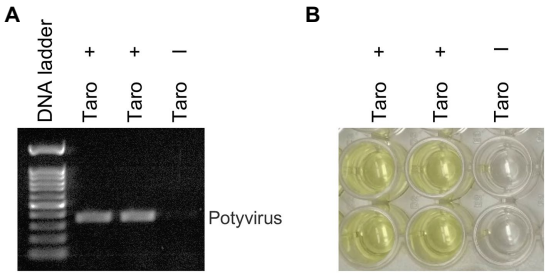

FIGURE 4
Analysis of taro leaf samples stored in RNA*later*® for presence of potyvirus: **(A)** RT-PCR of total RNA from symptomatic (+) and asymptomatic (–) taro leaf samples, respectively using universal potyvirus primers; **(B)** potyvirus-specific ELISA of plant extracts from the same sample sources.

components of ToLCNDV were amplified and sequenced from the RNA*later*®-stored sample ND-71 (Table 5). These results indicated that DNA isolated from papaya tissues stored in RNA*later*® solutions was able to support amplification of full-length plant DNA virus genomes.

Having demonstrated the efficacy of RNA*later*® as a robust tool for sampling and follow-up partial and full-length genome amplifications of begomoviruses, we performed specific PCR assays of 51 papaya leaf samples stored in RNA*later*® for the begomoviruses ToLCBV, ToLCJoV, and ToLCNDV (Table 4). Three asymptomatic samples and three samples with PRSV-like symptoms tested negative for begomoviruses. PRSV-specific STNP and ELISA tests were also PRSV-negative in the asymptomatic samples, but positive for samples with PRSV-like symptoms. When the 45 samples with leaf curl symptoms typical

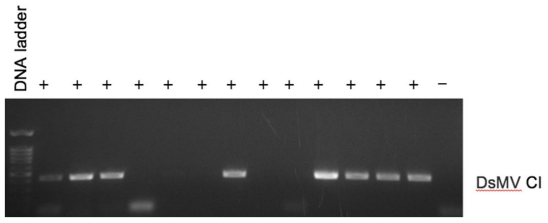

FIGURE 5
RT-PCR analysis of total RNA for detection of DsMV from symptomatic (+) taro leaf samples stored in RNA*later*® or asymptomatic controls (–) using DsMV CI gene-specific primers.

of begomovirus infection were tested, however, ToLCJoV, ToLCBV, and ToLCNDV were detected, respectively, in 10, 29, and 4 of the samples (Table 4).

DNA from six banana samples with symptoms of BBTV tested positive by PCR using BBTV-Rep-gene-specific primers, and CP-specific primers BBTV-HAF1 and BBTV-HAR1 (Hamim et al., 2017; Figure 6). Six PCR-positive samples also tested positive for BBTV by triple-antibody sandwich-ELISA using BBTV-specific antibodies.

Discussion

Our research showed that RNA*later*® technology can be used to transport and store leaf samples with virus-like symptoms from remote locations for extended periods before analysis for viral pathogens. Virus-infected papaya leaf tissue from the island of Oahu, Hawaii was preserved in RNA*later*® solutions for 7 to 30 days at room temperature until RNA extraction, followed by a three-day storage at 4°C, one-week storage at-20°C, and one-month storage at-80°C. Kamitani et al. (2016) used RNA*later*® to prevent RNA degradation of *Arabidopsis halleri* leaf samples. Their samples were maintained in RNA*later* at 4°C for 1 day and then moved to-20°C for 1.5 months before RNA extraction (Kamitani et al., 2016; Honjo et al., 2020).

In our study, RNA yields obtained from RNA*later*®-stored virus-infected papaya leaves were reduced in quantity and quality after different storage times compared to fresh samples. From zero to 30 days, total RNA recovered from samples preserved in RNA*later*® decreased gradually. Although the quantity of total RNA from RNAlater®-stored samples was reduced compared to fresh samples, the quality was sufficient for detection of plant viruses and amplification of their genomic sequences. Storage in RNA*later*® is considered one of the best methods for preserving RNA for subsequent virus diagnosis (Rawiwan et al., 2021). According to Kohl et al. (2017), PCR and sequencing results from RNA*later*®-stored samples were equivalent to those from snap-frozen samples. Because of the additional equipment and costly transportation required, snap-freezing is often challenging in field situations. We have demonstrated that storage in RNA*later*® solutions can overcome some of these limitations.

TABLE 4 Distribution and prevalence of begomoviruses based on PCR analysis of papaya leaf samples obtained from various locations in Bangladesh and stored in RNA*later*®.

Collection districts	Sample no.	Begomovirus positive	ToLCBV Positive	ToLCJoV positive	ToLCNDV Positive
Pabna	11	7	3	3	1
ChapaiNwabgonj	4	4	1	0	3
Rajshahi	4	4	4	0	0
Gazipur	10	9	8	1	0
Tangail	4	4	3	1	0
Chandpur	10	10	5	5	0
Mymensingh	5	5	5	0	0
Total	51	43	29	10	4

ToLCBV: Tomato leaf curl Bangladesh virus.

ToLCJoV: Tomato leaf curl Joydebpur virus.

ToLCNDV: Tomato leaf curl New Delhi virus.

TABLE 5 GenBank *accessions of* Sanger sequence-derived nucleotide (nt) sequences representing begomovirus genome sequences from symptomatic papaya leaf samples collected in Bangladesh and stored in RNA*later*®.

Sample	ToLCBV	ToLCJoV	ToLCNDV
Gazipur17-Pap	MH380003.1: 2,760 nt (98% nt identity to ToLCBV: KM383761)		
Gazipur17-Pap	Beta satellite MH397223.1:1,367 nt (92% nt identity to ToLCB: JN638434)		
Gazipur 19-Pap	Defective beta satellite (DefS)39 MH473589.1:564 nt (99% nt identical to corresponding regions of ToLCBV:MH380003)		
Gazipur 20-Pap	Defective beta satellite (DefS)40 MH507170.1:731 nt (94% nt identical to corresponding regions of ToLCBV:MH380003)		
Gazipur 21-Pap	Defective beta satellite (DefS)43 MH507169.1:738 nt (100% nt identical to corresponding regions of ToLCBV:MH380003)		
J1-Pap		MT127782.1:2,763 nt (95% nt identical to ToLCJV: KM383750)	
J1-Pap		Beta satellite MT161673.1: 1365 nt (95% nt identical to ToLCJoB: AJ966244.1)	
ND-71-Pap			DNA-A, MT161674.1: 2,688 nt (98% nt identical to ToLCNDV_DNA-A: KM383742) DNA-B, MT161675.1: 2,688 nt (93% nt identical to ToLCNDV_DNA-B: MG406983)

ToLCBV-Tomato leaf curl Bangladesh virus.

ToLCJoV-Tomato leaf curl Joydebpur virus.

ToLCNDV-Tomato leaf curl New Delhi virus.

The full-length genomes of two PRSV isolates, BD-1 and BD-2, were identified by HTS in our study from composite RNAs pap-1 and pap-2, respectively. This indicates the effectiveness of storage in RNA*later*® prior to whole-genome characterizations of plant RNA viruses. In Kenya, the presence of Moroccan watermelon mosaic virus (MWMV) and three different species of Carlaviruses in papaya tissues stored in RNA*later*® was also determined using Illumina MiSeq® next-generation sequencing (NGS) and validated using RT-PCR and Sanger sequencing (Mumo et al., 2020). Kamitani et al. (2016)

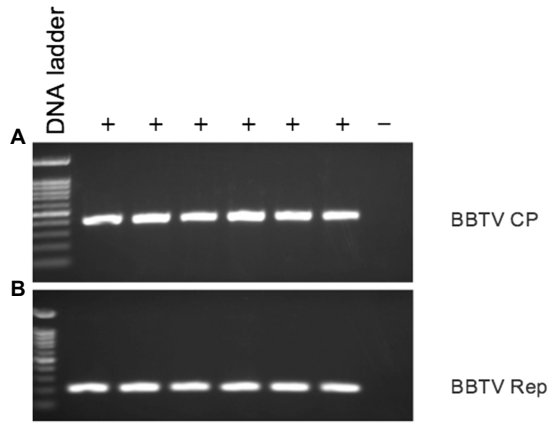

FIGURE 6
PCR analysis of symptomatic (+) and asymptomatic (–) banana leaf samples stored in RNA*later*® for presence of BBTV using BBTV **(A)** CP gene-specific, and **(B)** Rep gene-specific primers.

used RNA-Seq to detect known viruses and identify novel viruses in RNA*later*®-preserved leaf samples of *Arabidopsis halleri* subsp. *gemmifera*. They identified infections by turnip mosaic virus, cucumber mosaic virus, and Brassica yellows virus. We demonstrated the use of RNA*later*® technology for the routine diagnosis of plant RNA viruses and effectively detected distinct PRSV isolates BD-1 and BD-2 from papaya and DsMV from taro.

RNA*later*®-preserved plant material is suitable for the extraction of high-quality DNA and subsequent downstream analyses (LeFrois et al., 2016). In our studies, DNA extracted from papaya leaf samples stored in RNA*later*® was used to detect and obtain complete or partial genomes of specific begomovirus species and their associated components by PCR and Sanger sequencing. In addition, we successfully detected BBTV from banana samples collected in Bangladesh and stored in RNA*later*®, confirming the results of Steward and Culley (2010) that showed RNA*later*® could preserve the genomes of DNA viruses.

The successful immunodetection of plant viruses from material stored in RNA*later*® supports the results of Reiser et al. (2011), who demonstrated that preserving samples in this reagent did not interfere with ELISA protein analysis of tissue extracts. In some cases, RNA*later*® maintained the infectivity of enveloped and nonenveloped viruses for an extended time (Uhlenhaut and Kracht, 2005).

We demonstrated that plant viruses from leaf samples collected from a distant location and stored in RNA*later*® for various lengths of time could still be detected by PCR, RT-PCR, STNP, Sanger sequencing, HTS and ELISA. The product allows fast and easy sampling of plant material in the field. The effective retrieval of RNA and DNA viral sequences from RNA*later*®-stored samples was demonstrated by different molecular techniques in this manuscript. The preservation of plant tissues at room temperature alleviates concerns about nucleic acid damage during storage. Importantly, all downstream analytical procedures were unaffected; no new protocol development was needed with RNA*later*®.

Results obtained from studies of leaf samples from three different plant species stabilized in RNA*later*®, whether collected in Oahu, Hawaii, or brought to Hawaii from farmer's fields in Bangladesh, were acceptable and reproducible among plants. In all cases, these samples yielded total RNA or DNA of a quality and quantity sufficient for plant virus detection using several methods. RNA*later*® was used to preserve the papaya leaf tissues collected for this investigation from several districts of Bangladesh. Then, using specific RT-PCR or PCR tests, we were able to effectively identify, examine the distribution and variability of certain PRSV isolates and begomoviruses in the Bangladeshi papaya samples. Therefore, managing viral diseases in papaya orchards in Bangladesh can benefit from the identification and study of the distribution of viruses and specific virus isolates in RNA*later*®-preserved samples collected from Bangladesh. This technology provides a simple, sensitive, and specific tool for the diagnosis and molecular characterization of plant viral pathogens isolated from plant tissues. We conclude that this technology supports the advanced diagnostic methods used to identify viral pathogens infecting crop plants by allowing samples to be collected from remote areas and stored for extended periods.

Data availability statement

The datasets presented in this study can be found in online repositories. The names of the repository/repositories and accession number(s) can be found in the article/supplementary material.

Author contributions

IH and JH: conceptualization. IH, JH, and WB: methodology. IH: formal analysis, writing—original draft preparation, visualization, and investigation. IH, JH, WB, and MM: data curation. IH, JS, MM, MQ, and JH: writing—review and editing. JH and WB: supervision. All authors contributed to the article and approved the submitted version.

Funding

This research was funded by the United States Agency for International Development as part of the Feed the Future initiative under the CGIAR Fund (award number BFS-G-1100002) and the predecessor fund of the Food Security and Crisis Mitigation II grant (award number EEM-G-0004-00013). The research was also funded by the USDA National Institute of Food and Agriculture,

Hatch HAW09025-H (1001478), and the USDA-Agricultural Research Service (58–5320–4-012).

Conflict of interest

The authors declare this research was conducted without any commercial or financial relationships that could be construed as a potential conflict of interest.

Publisher's note

All claims expressed in this article are solely those of the authors and do not necessarily represent those of their affiliated organizations, or those of the publisher, the editors and the reviewers. Any product that may be evaluated in this article, or claim that may be made by its manufacturer, is not guaranteed or endorsed by the publisher.

References

Al Rwahnih, M., Rowhani, A., Westrick, N., Stevens, K., Diaz-Lara, A., Trouillas, F., et al. (2018). Discovery of viruses and virus-like pathogens in pistachio using high-throughput sequencing. *Plant Dis.* 102, 1419–1425. doi: 10.1094/PDIS-12-17-1988-RE

Bateson, M. F., Henderson, J., Chaleeprom, W., Gibbs, A. J., and Dale, J. L. (1994). Papaya ringspot potyvirus: isolate variability and the origin of PRSV type P (Australia). *J. General Virol.* 75, 3547–3553.

Bennike, T. B., Kastaniegaard, K., Padurariu, S., Gaihede, M., Birkelund, S., Andersen, V., et al. (2016). Comparing the proteome of snap frozen, RNA*later*® preserved, and formalin-fixed paraffin-embedded human tissue samples. *EuPA Open Proteom.* 10, 9–18. doi: 10.1016/j.euprot.2015.10.001

Fleige, S., and Pfaffl, M. W. (2006). RNA integrity and the effect on the real-time qRT-PCR performance. *Mol. Asp. Med.* 27, 126–139. doi: 10.1016/j.mam.2005.12.003

Hamim, I. (2019). Molecular Analyses of Papaya Viruses in Bangladesh: Detection, Characterization, and Distribution (Doctoral dissertation, University of Hawai'i at Manoa), 103, 2920, 2924. doi: 10.1094/PDIS-12-18-2186-RE

Hamim, I., Al Rwahnih, M., Borth, W. B., Suzuki, J. Y., Melzer, M. J., Wall, M. M., et al. (2019a). Papaya ringspot virus isolates from papaya in Bangladesh: detection, characterization, and distribution. *Plant Dis.* 103, 2920–2924. doi: 10.1094/PDIS-12-18-2186-RE

Hamim, I., Borth, W., Melzer, M. J., and Hu, J. (2018). Ultra-sensitive detection of papaya ringspot virus using single-tube nested PCR. *Acta Virol.* 62, 379–385. doi: 10.4149/av_2018_405

Hamim, I., Borth, W. B., Melzer, M. J., Suzuki, J. Y., Wall, M. M., and Hu, J. S. (2019b). Occurrence of tomato leaf curl Bangladesh virus and associated subviral DNA molecules in papaya in Bangladesh: molecular detection and characterization. *Arch. Virol.* 164, 1661–1665. doi: 10.1007/s00705-019-04235-8

Hamim, I., Borth, W. B., Suzuki, J. Y., Melzer, M. J., Wall, M. M., and Hu, J. S. (2020). Molecular characterization of tomato leaf curl Joydebpur virus and tomato leaf curl New Delhi virus associated with severe leaf curl symptoms of papaya in Bangladesh. *Eur. J. Plant Pathol.* 158, 457–472. doi: 10.1007/s10658-020-02086-7

Hamim, I., Green, J. C., Borth, W. B., Melzer, M. J. W., and Hu, J. (2017). First report of Banana bunchy top virus in Heliconia spp. on Hawaii. *Plant Dis.* 101:2153. doi: 10.1094/PDIS-02-17-0205-PDN

Honjo, M. N., Emura, N., Kawagoe, T., Sugisaka, J., Kamitani, M., Nagano, A. J., et al. (2020). Seasonality of interactions between a plant virus and its host during persistent infection in a natural environment. *ISME J.* 14, 506–518. doi: 10.1038/s41396-019-0519-4

Huang, L. H., Lin, P. H., Tsai, K. W., Wang, L. J., Huang, Y. H., Kuo, H. C., et al. (2017). The effects of storage temperature and duration of blood samples on DNA and RNA qualities. *PLoS One* 12:e0184692. doi: 10.1371/journal.pone.0184692

Kamitani, M., Nagano, A. J., Honjo, M. N., and Kudoh, H. (2016). RNA-Seq reveals virus–virus and virus–plant interactions in nature. *FEMS Microbiol. Ecol.* 92:176. doi: 10.1093/femsec/fiw176

Kohl, C., Wegener, M., Nitsche, A., and Kurth, A. (2017). Use of RNAlater® preservation for virome sequencing in outbreak settings. *Front. Microbiol.* 8, 1888. doi: 10.3389/fmicb.2017.01888

Kruse, C. P., Basu, P., Luesse, D. R., and Wyatt, S. E. (2017). Transcriptome and proteome responses in RNAlater® preserved tissue of Arabidopsis thaliana. *PLoS One* 12:e0175943. doi: 10.1371/journal.pone.0175943

LeFrois, C. E., Zhou, M., Amador, D. M., Sng, N., Paul, A. L., and Ferl, R. J. (2016). Enabling the spaceflight methylome: DNA isolated from plant tssues preserved in RNAlater® is suitable for bisulfite PCR assay of genome methylation. *Grav. Space Res.* 4, 28–37. doi: 10.2478/gsr-2016-0010

Mäki, A., Salmi, P., Mikkonen, A., Kremp, A., and Tiirola, M. (2017). Sample preservation, DNA or RNA extraction and data analysis for high-throughput phytoplankton community sequencing. *Front. Microbiol.* 8, 1848. doi: 10.3389/fmicb.2017.01848

Mumo, N. N., Mamati, G. E., Ateka, E. M., Rimberia, F. K., Asudi, G. O., Boykin, L. M., et al. (2020). Metagenomic analysis of plant viruses associated with papaya ringspot disease in *Carica papaya* L. in Kenya. *Front. Microbiol.* 11, 205. doi: 10.3389/fmicb.2020.00205

Noa-Carrazana, J. C., González-de-León, D., and Silva-Rosales, L. (2007). Molecular characterization of a severe isolate of papaya ringspot virus in Mexico and its relationship with other isolates. *Virus Genes* 35, 109–117. doi: 10.1007/s11262-006-0039-y

Patel, P. G., Selvarajah, S., Guérard, K. P., Bartlett, J. M., Lapointe, J., Berman, D. M., et al. (2017). Reliability and performance of commercial RNA and DNA extraction kits for FFPE tissue cores. *PLoS One* 12:e0179732. doi: 10.1371/journal.pone.0179732

Prendini, L., Hanner, R., and DeSalle, R. (2002). 11 obtaining, storing and archiving. *Tech. Molecular System. Evol.* 200:176. doi: 10.1007/978-3-0348-8125-8_11

Rawiwan, P., Khemthong, M., Tattiyapong, P., Huchzermeyer, D., and Surachetpong, W. (2021). Effects of sample preservation and storage times on the detection of tilapia lake virus (TiLV) RNA in tilapia tissues. *Aquaculture* 533:736240. doi: 10.1016/j.aquaculture.2020.736240

Reiser, V., Smith, R. C., Xue, J., Kurtz, M. M., Liu, R., LeGrand, C., et al. (2011). High-throughput simultaneous analysis of RNA, protein, and lipid biomarkers in heterogeneous tissue samples. *Clin. Chem.* 57, 1545–1555. doi: 10.1373/clinchem.2010.157743

Relova, D., Rios, L., Acevedo, A. M., Coronado, L., Perera, C. L., and Pérez, L. J. (2018). Impact of RNA degradation on viral diagnosis: an understated but essential step for the successful establishment of a diagnosis network. *Veterinary Sci.* 5:19.

Sreenivasulu, M., and Gopal, D. V. R. (2010). Development of recombinant coat protein antibody based IC-RT-PCR and comparison of its sensitivity with other immunoassays for the detection of papaya ringspot virus isolates from India. *Plant Pathol. J.* 26, 25–31. doi: 10.5423/PPJ.2010.26.1.025

Sirakov, I. N. (2016). Nucleic acid isolation and downstream applications. *Nucleic Acids-From Basic Aspects to Laboratory Tools*, 1–26. doi: 10.5772/61833

Steward, G. F., and Culley, A. I. (2010). Extraction and purification of nucleic acids from viruses. *Manual. Aqua. Viral Ecol.* 16, 154–165. doi: 10.4319/mave.2010.978-0-9845591-0-7.154

Uhlenhaut, C., and Kracht, M. (2005). Viral infectivity is maintained by an RNA protection buffer. *J. Virol. Methods* 128, 189–191. doi: 10.1016/j.jviromet.2005.05.002

Wang, D., Hamim, I., Borth, W. B., Melzer, M. J., Sun, G. F., and Hu, J. S. (2018b). First report of dasheen mosaic virus infecting taro (*Colocasia esculenta*) in Bangladesh. *Plant Dis.* 102:2668. doi: 10.1094/PDIS-03-18-0442-PDN

Wang, Y., Wu, B., Borth, W. B., Hamim, I., Green, J. C., Melzer, M. J., et al. (2017). Molecular characterization and distribution of two strains of dasheen mosaic virus on Taro in Hawaii. *Plant Dis.* 101, 1980–1989. doi: 10.1094/PDIS-04-17-0516-RE

Wang, M. R., Yang, W., Zhao, L., Li, J. W., Liu, K., Yu, J. W., et al. (2018a). Cryopreservation of virus: a novel biotechnology for long-term preservation of virus in shoot tips. *Plant Methods* 14, 1–10. doi: 10.1186/s13007-018-0312-9

Yockteng, R., Almeida, A. M., Yee, S., Andre, T., Hill, C., and Specht, C. D. (2013). A method for extracting high-quality RNA from diverse plants for next-generation sequencing and gene expression analyses. *Appl. Plant Sci.* 1:1300070. doi: 10.3732/apps.1300070

Zheng, L., Rodoni, B. C., Gibbs, M. J., and Gibbs, A. J. (2010). A novel pair of universal primers for the detection of potyviruses. *Plant Pathol.* 59, 211–220. doi: 10.1111/j.1365-3059.2009.02201.x

frontiers | Frontiers in Microbiology

TYPE Original Research
PUBLISHED 02 November 2022
DOI 10.3389/fmicb.2022.1030042

Check for updates

OPEN ACCESS

EDITED BY
Sean Michael Prager,
University of Saskatchewan,
Canada

REVIEWED BY
Susheel Kumar,
National Botanical Research Institute (CSIR), India
Islam Hamim,
Bangladesh Agricultural University, Bangladesh

*CORRESPONDENCE
Bikash Mandal
leafcurl@rediffmail.com;
bmandal@iari.res.in
Alok Kumar
alok.igib@gmail.com;
alok.kumar@haramaya.edu.et

SPECIALTY SECTION
This article was submitted to Virology, a section of the journal Frontiers in Microbiology

RECEIVED 28 August 2022
ACCEPTED 11 October 2022
PUBLISHED 02 November 2022

CITATION
Kumar A, Solanki V, Katiyar A and Mandal B (2022) Host biology and genomic properties of Plumeria mosaic virus, a tobamovirus discovered in a temple tree in India co-infecting with frangipani mosaic virus.
Front. Microbiol. 13:1030042.
doi: 10.3389/fmicb.2022.1030042

COPYRIGHT
© 2022 Kumar, Solanki, Katiyar and Mandal. This is an open-access article distributed under the terms of the Creative Commons Attribution License (CC BY). The use, distribution or reproduction in other forums is permitted, provided the original author(s) and the copyright owner(s) are credited and that the original publication in this journal is cited, in accordance with accepted academic practice. No use, distribution or reproduction is permitted which does not comply with these terms.

Host biology and genomic properties of Plumeria mosaic virus, a tobamovirus discovered in a temple tree in India co-infecting with frangipani mosaic virus

Alok Kumar[1,2]*, Vikas Solanki[1], Akshay Katiyar[1] and Bikash Mandal[1]*

[1]Advanced Centre for Plant Virology, Division of Plant Pathology, Indian Agricultural Research Institute, New Delhi, India, [2]School of Plant Sciences, College of Agriculture and Environmental Sciences, Haramaya University, Dire Dawa, Ethiopia

Temple tree (*Plumeria rubra* f. *acutifolia*), an important fragrant-flower tree extensively used in the urban landscaping is known to be infected with a tobamovirus, frangipani mosaic virus (FrMV). In this study, we describe another tobamovirus, Plumeria mosaic virus (PluMV) infecting temple tree in India. PluMV was isolated from an old temple tree co-infected with FrMV. The presence of another tobamovirus was initially realized based on the distinct symptoms on *Gomphrena globosa* (globe amaranth), a non-host of FrMV. PluMV was highly transmissible through simple rub-inoculation. In host-range study, brinjal (*Solanum melongena*), chilli (*Capsicum annuum*), datura (*Datura stramonium*), globe amaranth and tobacco (*Nicotiana benthamiana, N. glutinosa, N. tabacum* cv. Xanthi) could differentiate PluMV from FrMV. The complete genome sequence of PluMV was determined (6,688 nucleotides [nt], GenBank KJ395757), which showed the genome structure typical of tobamovirus encoding four proteins: small replicase (3,549nt/130kDa), large replicase (5,061nt/188kDa), movement protein (770nt/29kDa) and coat protein (527nt/19kDa). The 5′ and 3′ UTR of PluMV contained 91 and 284nt, respectively. The PluMV genome was 45 nts longer than that of FrMV and shared only 71.4–71.6% sequence identity with FrMV and <50% sequence identity with the rest of the other members of the genus *Tobamovirus*. PluMV shared a close but a divergent evolutionary relationship with FrMV. Based on the species demarcation guidelines of ICTV (<90% genome sequence identity), PluMV was considered as a new tobamovirus species. As PluMV was serologically related with FrMV, differential diagnostic assays such as simplex and duplex RT-PCR were developed, which revealed that PluMV naturally existed in both the species of temple tree, *P. rubra* f. *acutifolia* and *P. rubra* f. *obtusa* in India either alone or in mixed infection with FrMV.

KEYWORDS

Plumeria mosaic virus, tobamovirus, RT-PCR, frangipani mosaic virus, temple tree, differential host, complete genome

Introduction

The members of the genus *Tobamovirus* (family *Virgaviridae*) have rod-shaped virions of about 300 × 18 nm size and ssRNA genome of ~6.3 – 6.6 kb. Tobacco mosaic virus is the first member discovered under the genus *Tobamovirus*. Subsequently, as many as 37 confirmed and 2 tentative tobamovirus species have been reported infecting several plant species (https://ictv.global/taxonomy/). Tobamoviruses are highly stable and contagious that spread through direct contact with the infected plant materials and/or contaminated soil/water, but not by any insect-vector with specific biological specificity (Adams et al., 2009). The genome of tobamoviruses consists of four open reading frames (ORFs) that encode four proteins. The ORF1 and ORF2 encode smaller (124–132 kDa) and larger (181–189 kDa) replicase proteins (Rep), which are expressed directly from the genomic RNA and help in viral replication (Lewandowski and Dawson, 2000). The ORF3 and ORF4 encode movement protein (MP) and coat protein (CP), which are translated from the sub-genomic RNAs (Ikea et al., 1993), and are responsible for cellular movement and virion formation, respectively (Ikea et al., 1993). Tobamoviruses are classified into three subgroups considering the difference in infected plant species and genome architecture. The subgroup-I includes the members those infect solanaceous crops and the MP and CP genes in the genome is not arranged in overlapping manner. The subgroup-II includes the members those infect legumes, cucurbits, and some other crops, and their MP and CP genes are arranged with slightly overlapping manner in the genome. The subgroup III includes the members that infect brassicas, asterids and some other plant species, and their MP and CP genes are overlapping in a greater extent compared to those in the subgroup II (Pagan et al., 2010; Wylie et al., 2013).

The temple tree or frangipani (*Plumeria* sp., family Apocynaceae) is a deciduous ornamental plant, widely grown for its beautiful foliage and fragrant flowers, and extensively used in urban landscaping. It also has medicinal property, and is used for treating skin inflammation, indigestion, high blood pressure, hemophilia, cough, dysentery, and fever (Bihani et al., 2021). The temple tree, native to Mexico, Central America, Colombia, and Venezuela is commonly grown in the tropical and subtropical regions of the World including India. The temple tree was known to be infected by a tobamovirus, frangipani mosaic virus (FrMV) in Australia (Francki et al., 1971) and India (Varma and Gibbs, 1978) initially based on their host-reactions and virions morphology, and subsequently, the virus was identified as a distinct tobamovirus species based on the genome sequence information generated for the isolate from China (Deng et al., 2000; Lim et al., 2010) and India (Kumar et al., 2015).

While studying the occurrence of FrMV in temple trees at the campus of Indian Agricultural Research Institute (IARI), New Delhi, an old temple tree (*P. rubra* f. *acutifolia*) (>35 years) was observed to exhibit varieties of symptoms such as mosaic, bronzing, vein banding, necrotic spots, and ring-spots on leaves. The RT-PCR test showed the presence of FrMV in this tree. The inoculum prepared from this tree when was used to inoculate different plant species, *Gomphrena globosa* developed bright red local lesion symptoms that was strikingly different from FrMV as *G. globosa* was found to be a non-host of FrMV in our previous study (Kumar et al., 2015). This prompted us to investigate the virus isolate obtained through *G. globosa*, which led to the discovery of a novel tobamovirus, Plumeria mosaic virus from a temple tree, mixed infected with FrMV. The preliminary report of PluMV was presented in an International Conference of Indian Virological Society (Kumar et al., 2013). In this paper, we systematically describe the isolation of the new virus culture, host biology, complete genome sequence and evolutionary relationships of PluMV with FrMV and other members of the genus *Tobamovirus*. Further, simplex and duplex RT-PCR based diagnostic assays were developed for differentiating PluMV from FrMV, which were successfully utilized for demonstrating the natural existence of PluMV in temple trees independently or as a mixed infection with FrMV.

Materials and methods

Virus source and host biology study

The symptomatic leaf sample from an old temple tree (*P. rubra* f. *acutifolia*) at IARI campus was collected during 2010 and analyzed by leaf dip electron microscopy (EM), RT-PCR, and sap-transmission. EM was conducted using a small disc of leaf following the methods described by Hilchborn and Hills (1965). The grid was stained with uranyl acetate (2%), washed with distilled water, air dried, and analysed in a transmission electron microscope (Model JEOL 100 CX-II). RT-PCR was conducted using primers specific to CP genes of FrMV (Kumar et al., 2015). Sap-inoculation was conducted using the leaf extract prepared by grinding the leaf sample in 0.1 M phosphate buffer, pH 7.2 at the ration of 1:5. The test plants were pre-dusted with Carborundum powder (320 grit) and inoculated with the extracted sap. The plants were allowed to grow at 30–35°C in the greenhouse and were observed for symptom expression.

The virus isolate obtained from a single local lesion on *G. globosa* was designated as, PluMV-Plu-Ind-1 and maintained on *N. benthamiana*. The FrMV-Ind-1 culture was established from a single local lesion on *C. annuum* and was maintained on *N. benthamiana* in a separate greenhouse. To compare the host reactions of PluMV-Plu-Ind-1 and FrMV-Ind-1, the virus isolates were used separately for the sap-inoculation to the different plant species (Figure 1; Table 1) at 3–5 leaf stage and maintained in the two separate greenhouses. The symptom expression was recorded and the association of the virus was confirmed by direct antigen coated enzyme-linked immunosorbent assay (DAC-ELISA) using antiserum developed from purified virus preparations of FrMV, and RT-PCR using CP-gene specific primers to FrMV, developed in our previous study (Kumar et al., 2015). All the plant samples were tested again by RT-PCR at the later stage, using the primers specific to each virus, developed in this study (Table 2).

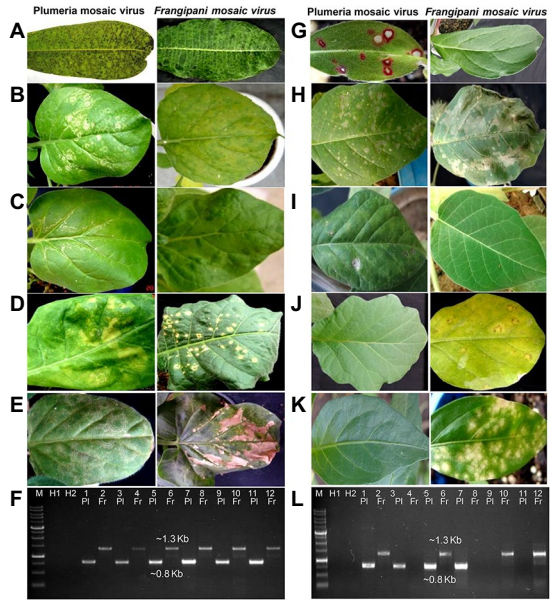

FIGURE 1
Comparison of symptoms of plumeria mosaic virus (PluMV-Plu-Ind-1) and frangipani mosaic virus (FrMV-Ind-1) on various hosts following sap inoculation. **(A)** *Plumeria rubra* f. *acutifolia*, **(B)** *Nicotiana benthamiana* local leaf, **(C)** *N. benthamiana* systemic leaf, **(D)** *N. tabacum* cv. Xanthi, **(E)** *N. glutinosa*, **(G)** *Gomphrena globosa*, **(H)** *Datura stramonium* local leaf, **(H,I)** *Datura stramonium* systemic leaf, **(J)** *Solanum melongena*, **(K)** *Capsicum annuum*. (F & L) Confirmation of transmission of the virus to these hosts by RT-PCR. **(F)** Lane 3–4: *P. acutifolia*; Lane 5–6: local *N. benthamiana*; Lane 7–8: systemic *N. benthamiana*; Lane 9–10: *N. tabacum*; Lane 11–12: *N. glutinosa*. **(L)** Lane 3–4: *G. globosa*; Lane 5–6: local *D. stramonium*; Lane 7–8: Systemic *D. stramonium*; Lane 9–10: *S. melongena*; Lane 11–12: *C. annuum*. Pl: PluMV; Fr: FrMV. M: Marker; H1 and H2: Healthy control; Lane 1: PluMV +ve control (Cloned DNA); Lane 2: FrMV +ve control (Cloned DNA).

RT-PCR and cloning of genome fragment

The RNA was extracted from the symptomatic leaves of *G. globosa* showing red chlorotic lesions using RNeasy Plant Mini Kit (Qiagen. Inc. Chatsworth, CA). The viral genome was amplified by RT-PCR in six different overlapping fragments that covered entire viral genome (Table 2; Figure 2). Further, both the terminal fragments containing 5′- and 3′-UTR were amplified using 5′-Full RACE core set kit (Takara, Shiga, Japan) and FirstChoice RLM-RACE kit (Thermo Fischer Scientific, USA), respectively (Table 2; Figure 2). Initially, the primers were prepared based on the genome sequences of FrMV-P (HM026454), FrMV-Ind-1 (JN555602), and other tobamoviruses. Subsequently, primers were designed based on the genome sequences generated in this study.

For preparing cDNA, the reaction mixture contained 5x First-Strand buffer (4.0 µl), 10 mM dNTP mix (1.0 µl), 20 mM DTT (1.0 µl), 10.0 µM reverse primer (2.0 µl), 100 Units/µl SMARTScribe™ reverse transcriptase enzyme (Clontech, USA) (1.0 µl), and RNA template (400–500 ng, 10 µl). The final volume was adjusted to 20.0 µl with nuclease free water. The reaction mixture was allowed for 90 min at 42°C followed by inactivated at 70°C for 15 min in the Biometra *T* Personal thermal cycler.

The cDNA (2.0 µl) was used for PCR with 10x Ex Taq buffer (5.0 µl), 2.5 mM dNTPs (4.0 µl), 10 µM of each primer (2.0 µl), and 1.25 U of Ex-Taq DNA polymerase (Takara, Shiga, Japan). The final reaction mixture was adjusted to a volume of 50 µl with the nuclease-free water. The amplification conditions were: 40 cycles, each having denaturation at 98°C for 10 s, annealing at 58–62°C (Table 2) for 45 s, and extension at 72°C for 1.0 min/kb. The final extension was allowed at 72°C for 10 min. The amplified products were resolved in agarose gel, purified using gel purification kit (Macherey-Nagel, Germany), and cloned in pT&A vector (Real

TABLE 1 Comparison of local and systemic symptoms of plumeria mosaic virus isolate, PluMV-Plu-Ind-1 and frangipani mosaic virus isolate, FrMV-Ind-1 on different plant species.

Hosts	PluMV-Plu-Ind-1 symptoms		FrMV-Ind-1 symptoms	
	Local	Systemic	Local	Systemic
Plumeria rubra f. *acutifolia*	NS	Brown mosaic	NS	Greenish mosaic, chocolate spots and necrotic ring with central spots
Plumeria rubra f. *obtusa*	NS	Yellow mosaic with brown necrotic spots	NS	Greenish mosaic with necrotic spots
Nicotiana benthamiana	Whitish ring-spot	Whitish wavy lines, mosaic mottling and blistering	Chlorotic spots	Mosaic, mottling and blistering
N. tabacum cv. Xanthi	Whitish ring-spots and mottling	NS	Necrotic white lesions	NS
N. glutinosa	Concentric whitish ring	NS	Large necrotic lesions	NS
Gomphrena globosa	Red spots	NS	NS	NS
Datura stramonium	Chlorotic spots	Chlorosis with mottling	Large blighted patches	NS
Solanum melongena	NS	NS	Chlorotic spots	NS
Capsicum annuum	NS	NS	Chlorotic lesions	NS

NS: No symptoms.

TABLE 2 List of the primers used for the amplification of the complete genome of plumeria mosaic virus (PluMV) from *Plumeria rubra* F. *acutifolia*, and for the detection of PluMV and frangipani mosaic virus (FrMV).

Primer[a] name	Primer sequence (5′ to 3′)	Primer location (nt)	Annealing temperature (°C)	Amplicon length (~Kb)	Remarks
For the amplification of complete genome of PluMV					
BM116R	tgacaagtcgacttgtcatatttagaaacatcaagctc	4,348–4,373	58	1.3	Part of rep
BM115F$_d$[b]	gtawktttwmawywwttwmyaaywacaacaa	1–31			
BM204R	caatgacttggtcaaagtcctca	3,231–3,253	58	3.1	5′ UTR and part of rep gene
BM239F	ggatcc ccaaagggtaatatttaccaacaatt	1–26	58	1.9	5′ UTR and part of rep gene
BM222R	tcgcagccaatgcactctccc	1967–1987			
BM348F	gctagcaaaacatggcttttgac	2,455–2,477	58	3.0	part of replicase and movement
BM240R	gtcgac ctaaatatcttcattatctccacttt	5,793–5,818			protein genes
BM649F	aattacttcccaagtcgatgactag	5,121–5,145	58	1.3	part of movement protein and
BM140R	gcgtaa gtcgac ttacgcggtagtagtacccg	6,382–6,404			coat protein genes
BM205F	gatgcttcggggttggtatggg	6,321–6,342	58	0.4	part of coat protein and 3′ UTR
BM119R	agcccagtcgactgggccgctaccgggggtta	6,668–6,686			
Primers used for 5′ RACE (5′-Full RACE core set)					
BM667R	(p)-aacaaaaagtatcaaccaaag	1,075	42	1.1	cDNA synthesis
BM520F	ggcaggcttacatcgtttttcga	579–601	62	1.0	Outer RACE
BM530R	actctggcaatatctctaatgtcc	478–500			
BM244F	aagatggtagttacgccgtcg	704–724	62	0.8	Inner RACE
BM452R	ttgcaacaatgaacatacgagcgt	444–467			
Primers used for 3′ RACE					
BM210(Adaptor)	gcgagcacagaattaatacgactcactatagggttttttttttttvn	6,688	42	Full length	cDNA synthesis
BM649F	aattacttcccaagtcgatgactag	5,121–5,145	58	1.6	Outer RACE
Outer RACE primer	gcgagcacagaattaatacgact	Outer part of adaptor			
BM205F	gatgcttcggggttggtatggg	6,289–6,310	58	0.4	Inner RACE
Inner RACE primer	cgcggatccgaattaatacgactcactatagg	Inner part of adaptor			
Primers used for the specific detection of plumeria mosaic virus and frangipani mosaic virus					
BM348F	gctacg aaaacatggcttttgac	2,455–2,477	58	0.8 Kb	PluMV
BM204R	caatgacttggtcaaagtcctca	3,231–3,253			
BM520F	ggcaggcttacatcgtttttcga	579–601	58	1.2 Kb	
BM521R	aaacaagcgcctacgttaacctt	1744–1766			
BM200R	aattcctgttttgaacttagattcg	4,282–4,306	58	2.0 Kb	FrMV
BM523F[c]	gacggcaaccttgaacaatttgc	2,333–2,355			
BM607R	attgtagttgcatcaaaattattaagta	3,637–3,664	58	1.3 Kb	

[a]Position of the primers on the viral genome are shown in Figure 1,
[b]BM115$_d$F is a common degenerate primer with BM116R and BM204R.
[c]BM523F is common primer with BM200R and BM607R,
F: Forward, R: Reverse, underline: Restriction site.

Biotech Corporation, Banqiao, Taiwan) using the manufactures' protocol.

Genome sequence analysis

All the cloned fragments of the viral genome were sequenced from both the ends using the commercial facility at Chromous biotech (Bengaluru, India). The vector sequences from all the clones were removed, and assembled to obtain the complete genome sequence of the virus isolate, PluMV-Plu-Ind-1. The ORF finder software available at NCBI site (http://www.ncbi.nlm.nih.gov/gorf/gorf.html) was used to determine the coding sequences. The sequence was compared using basic local alignment search tool (http://www.ncbi.nlm.nih.gov /blast) and BioEdit software (Hall, 1999). The phylogenetic and molecular evolutionary analyses were conducted based on the amino acid sequences of each ORF of PluMV-Plu-Ind-1, and the corresponding sequence of other tobamovirus isolates using the maximum likelihood method in the MEGA version 11 (Tamura et al., 2021) with 1,000 bootstrap values.

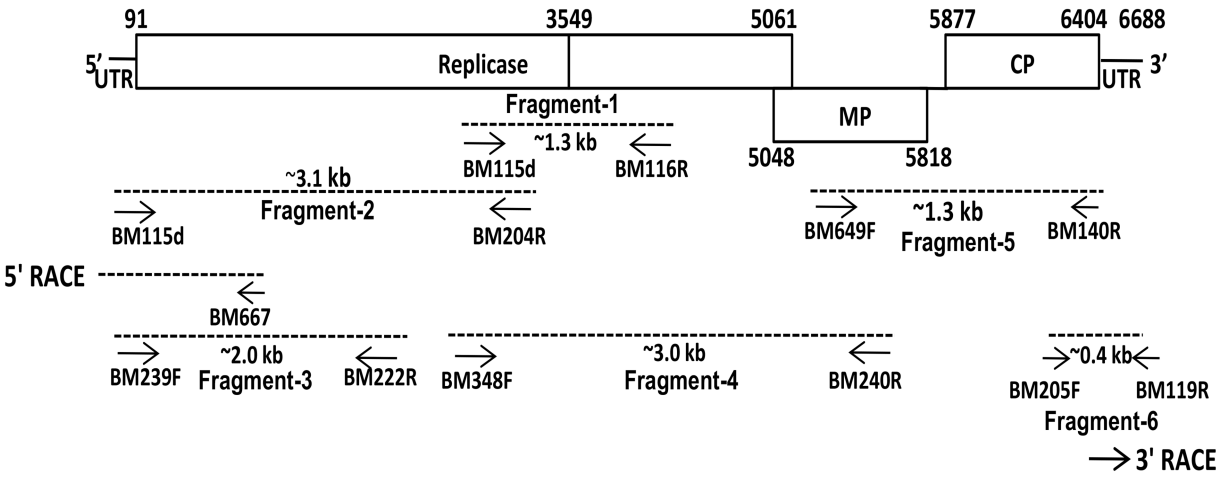

FIGURE 2
Schematic presentation of the strategy used for the amplification of complete genome of plumeria mosaic virus (pluMV-Plu-Ind-1 isolate) infecting *Plumeria rubra* f. *acutifolia*. Small arrows indicate the positions of various primers on the genome. The genome segments, which were used for sequencing, are indicated as dotted lines.

Simplex and duplex RT-PCR

Two pairs of primers, specific to each virus, were designed from the Rep gene sequence of PluMV-Plu-Ind-1 and FrMV-Ind-1, for developing the RT-PCR based diagnostic technique specific to each of these viruses (Table 2). The conditions for the RT-PCR using these primers were optimized using the respective cloned DNA fragments (Figure 2). The duplex PCR conditions were optimised for the primer pairs, BM348F/BM204R and BM523F/BM607R using the mixture of the respective cloned DNA of each virus. Both the simplex and duplex RT-PCR were validated using leaf samples from inoculated plants. Further, duplex RT-PCR was performed using leaf samples collected from fields to confirm the existence of PluMV in other temple trees.

Results

Isolation of PluMV

The EM analysis of leaf sample from an old temple tree plant that exhibited mosaic, vein banding, bronzing, ring-spot and necrotic spot symptoms revealed the presence of numerous rod-shaped virions (300 × 18 nm) similar to tobamovirus. The sap-transmission from the leaf sample of the above temple tree resulted in development of local lesion symptoms in *G. globosa, C. annuum,* and *S. melongena*. The subsequent transmission of the virus from the local lesion hosts, *C. annuum,* and *S. melongena* to *N. benthamiana* resulted in the development of similar type of mosaic, mottling, and blistering symptoms. However, transmission from the local lesion tissues of *G. globosa* resulted in different symptoms such as whitish ring-spots on the inoculated leaves, and mosaic, mottling, and whitish wavy lines on systemic leaves of *N. benthamiana* (Figure 1). Further, the virus isolate from *G. globosa* showed weak amplification in the RT-PCR with the CP gene specific primers to FrMV compared to the virus isolates from *C. annuum* and *S. melongena*. Due to the difference in symptomatology and amplification of CP gene, the virus isolate obtained from *G. globosa* was designated as PluMV-Plu-Ind-1. The virus transmission and RT-PCR results indicated that there was a mixed-infection of viruses/strains in the temple tree.

Comparison of host-reactions of PluMV-Plu-Ind-1 with FrMV-Ind-1

The comparison of host-reactions following mechanical sap inoculation to the various plant species with PluMV-Plu-Ind-1 and FrMV-Ind-1 is presented in Figure 1; Table 1. PluMV-Plu-Ind-1 caused brown mosaic symptoms on *P. rubra* f. *acutifolia* and yellow mosaic with brown necrotic spots on *P. obtusa*, whereas, FrMV-Ind-1 caused greenish mosaic, chocolate spots, and necrotic rings on *P. rubra* f. *acutifolia* and greenish mosaic with necrotic spots on *P. rubra* f. *obtusa* (Figure 1A). Inoculation of PluMV-Plu-Ind-1 to *N. benthamiana* resulted in expression of whitish ring-spot as local symptoms and whitish wavy lines, mosaic mottling, and blistering as systemic symptoms. Whereas, *N. benthamiana* inoculated with FrMV-Ind-1 exhibited chlorotic spots as local symptoms and mosaic, mottling, and blistering as systemic symptoms (Figures 1B,C). *N. tabacum* cv. Xanthi inoculated with PluMV-Plu-Ind-1 developed whitish ring-spots and mottling as local symptoms and FrMV-Ind-1 inoculation developed necrotic white lesions as local symptoms (Figure 1D) whereas, none of the virus isolates induced any systemic symptoms in *N. tabacum* cv. Xanthi. Similarly, *N. glutinosa* developed only

local symptoms with concentric whitish ring pattern when inoculated with PluMV-Plu-Ind-1, whereas, FrMV-Ind-1 induced large necrotic local lesions on *N. glutinosa* (Figure 1E). Bright red colour spots developed on all the inoculated leaves of *G. globosa,* whereas, systemic leaves were symptomless when inoculated with PluMV-Plu-Ind-1. FrMV-Ind-1 did not induce any symptoms on local as well as systemic leaves of *G. globosa* (Figure 1G). *D. stramonium* inoculated with PluMV-Plu-Ind-1 exhibited chlorotic spots on the inoculated leaves and chlorosis with mottling on the systemic leaves. However, FrMV-Ind-1 induced large blighted patches on the inoculated leaves of *D. stramonium* and no systemic symptoms (Figures 1H,I). *S. melongena* and *C. annuum* did not exhibit any symptoms when inoculated with PluMV-Plu-Ind-1, but developed chlorotic spots and chlorotic lesions, respectively upon FrMV-Ind-1 inoculation (Figures 1J,K). All the above host species showing symptoms were positive when examined by EM, ELISA and RT-PCR (Figures 1F,L), whereas, asymptomatic plants were tested negative in all the assays.

Clones and sequence of full-length genome

The full-length genome sequence was generated cloning six overlapping fragments over the entire genome (Figure 2). In the initial attempt to amplify the genomic fragments, primers specific to cucumber green mottle mosaic virus and FrMV were used that did not amplify any fragment from the total RNA isolated either from *N. benthamiana* or *G. globosa* leaves infected with PluMV-Plu-Ind-1. Further attempt using a primer pair, BM115F (a degenerate primer for tobamovirus designed in this study from 5′ UTR region) and BM116R (FrMV specific primer) resulted in amplification of multiple bands. Sequencing of a clone containing ~1.3 kb fragment (fragment-1) from the PCR product contained part of small and large Rep gene, which showed significant differences from FrMV. Therefore, the sequence of fragment-1 was used to design a specific reverse primer (BM204R). The fragment-2 covering the 5′ region of the genome was then generated by degenerate BM115F and PluMV-Plu-Ind-1 specific BM204R. The terminal sequence was confirmed by 5′ RACE using 5′ Full RACE core set kit (Takara, Shiga, Japan), and a pair of specific primers (BM239F and BM222R) were designed based on the sequence of fragment-2 (Table 2). The fragment-2 sequence was further confirmed by generating fragment-3 using PluMV-Plu-Ind-1 specific primers, BM239F and BM222R. The fragment-4 that overlapped with fragment-1 and partly with fragment-2 was generated using PluMV-Plu-Ind-1 specific forward primer, BM348F and FrMV-Ind-1 specific reverse primer, BM240R. To generate the 3′ genome sequence, attempts were made to amplify the 3′ end genome fragment using PluMV-Plu-Ind-1 specific forward primer, BM649F designed from the sequence of fragment-4, and FrMV-Ind-1 specific reverse primers, BM119R and BM140R, unfortunately, no amplification was obtained using these primer combinations. Further attempt was made using a semi-nested PCR; where the first round of PCR was performed with BM649F and BM119R primers followed by the second round of PCR with BM649F and BM140R primers resulted in amplification of the fragment-5 containing MP and CP regions. To obtain 3′ untranslated region (UTR) sequence, the fragment-6 was generated by PluMV-Plu-Ind-1 specific BM205F primer and BM119R from FrMV-Ind-1. Further, the 3′ terminal sequence was confirmed by 3′ RACE using FirstChoice RLM RACE kit (Thermo Fischer Scientific, USA).

Genome organization and sequence comparison of PluMV-Plu-Ind-1

The complete genome of PluMV-Plu-Ind-1 was 6,688 nts long with four ORFs (GenBank KJ395757, 2015). The sequence 1–90 nt contained 5′ UTR. The ORF1 spanned between 91 to 3,549 nt with the start codon AUG and termination codon UAG, encoding the small Rep protein of 130 kDa. The ORF2 that spanned between 91 to 5,061 nt with a readthrough leaky termination amber codon (UAG) at 3,549 nt encoded 188 kDa large replicase protein. The ORF3 (5,048–5,818 nt) that overlapped with 14 nt of the 3′ end of ORF2 encoded a 29 kDa MP. The ORF4 located 60 nt apart from the MP (5,877–6,404 nt) and encoded a 19 kDa CP. The 3′ UTR was located from 6,405 nt to the end of the genome (Figure 3).

The comparison of the sequence of PluMV-Plu-Ind-1 with the another isolate found in the database reported later from Taiwan (DR_TW; KX881422, 2018) revealed that both the isolates were almost similar to each other sharing 98% sequence identity at the genome level and 97.9–100% identity at nt and amino acids (aa) levels of non-coding and individual gene, except in 5′ UTR, which was found to be 5 nt longer than DR_TW, and shared only 91.1% nt sequence identity (Table 3). The comparison of the sequences of PluMV-Plu-Ind-1 with that of 34 other tobamovirus species showed that PluMV-Plu-Ind-1 shared 71.4–71.6% nt sequence identity with FrMV isolates and < 50% sequence identity with the rest of the other tobamovirus species (Table 3). The detailed comparison of the sequences of PluMV-Plu-Ind-1 with FrMV isolates revealed that the 3′ genomic regions (MP and CP) including the 3′ UTR of PluMV-Plu-Ind-1 shared higher sequence conservancy (>85%) with FrMV isolates compared to the 5′ genomic region including both coding (<76% with large and small Rep) and non-coding regions (48.3–49.4% with the 5′ UTR; Table 3). Interestingly, the 5′ coding region containing Rep of other tobamovirus species shared relatively higher sequence identity (34%) with PluMV-Plu-Ind-1 compared to the 3′ coding region containing MP and CP (18.8%; Table 3).

Comparison of genome organization of PluMV with that of FrMV

The comparison of PluMV sequence with that of FrMV-Ind-1 (JN555602) and FrMV-P (HM026454) revealed that the complete

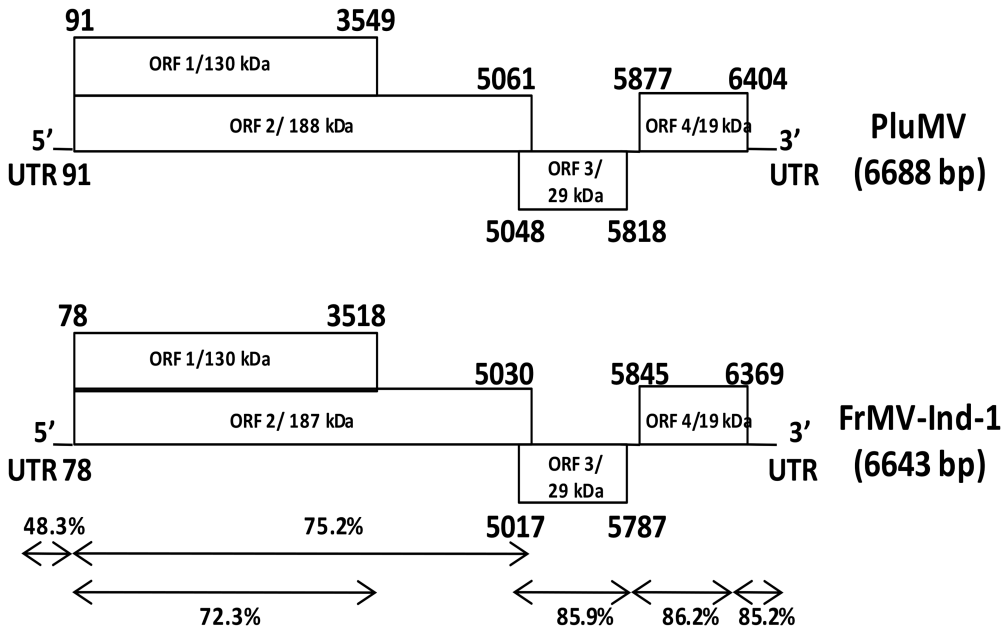

FIGURE 3
Comparison of the genome structure of plumeria mosaic virus (pluMV-Plu-Ind-1) and Indian isolate of frangipani mosaic virus (FrMV-Ind-1). The percent identities between the coding and non-coding regions of the two viruses are indicated with arrows.

genome of PluMV was 45 nt longer than both the isolates of FrMV. The 5′ and 3′ UTRs of PluMV was 13 nt and 10 nt longer, respectively than that of FrMV. The 5′ UTR was relatively more diverse (48.3–49.4% sequence identity) than the 3′ UTR (85.2–85.5% sequence identity; Table 3; Figure 3). The proximal 3′ nts of PluMV contained GTCCCC, which is different from both the FrMV and most of the tobamovirus isolates (data not shown). The MP and CP of PluMV shared closer amino acid (aa) sequence identity (84.7–86.3%) compared to both the Rep (72.2–75.3%) with that of FrMV. Both the Rep proteins of PluMV were 9 aa longer than FrMV isolates and shared 72.2–72.3% and 75.2–75.3% aa sequence identity, respectively. MP of PluMV was of identical in length sharing 84.7–86.3% aa sequence identity, whereas, CP of PluMV was one aa longer and shared 85.7–86.2% identity with FrMV isolates (Table 3). The arrangement of MP and CP genes in genome for both the viruses was very similar. The MP of both the virus overlapped with the terminal 13 nt of large Rep. But, the length of the intergenic region between MP and CP was only one nt longer for PluMV (Figure 3). The comparison of aa sequence of 130 kDa and 188 kDa Rep proteins showed that the aa sequence was highly conserved (only 19 substitutions) within the PluMV isolates from India and Taiwan (PluMV-Plu-Ind-1 and DR_TW), but highly diverse between PluMV and FrMV. The major dissimilarities in Rep protein was found in three stretches, i.e., from 153–164, 646–669, and 674–697 aa positions in the form of substitutions as well as deletions (Figure 4). Apart from these, region corresponds to 182–190, 335–352, and 546–563 positions have also weak aa identity (Figure 4). Irrespective of these many of dissimilarities in 130 kDa/188 kDa proteins of PluMV and FrMV, it was well orchestrated with all three conserved domains; methyltransferase, helicase, and polymerase. The methyltransferase domain (235–1,419 nt) of PluMV, responsible for capping of genomic and sub-genomic RNAs was 12 nt longer than FrMV whereas, the helicase domain (2,692–3,453 nt) responsible for unwinding of nucleic acid, recombination, and transcription (Alonso et al., 1991), and polymerase domain (3,700–5,025 nt) responsible for the elongation of pre-existing chains (Quadt and Jaspars, 1989) were of similar in length. The two conserved sequence motifs (invariant His in the first motif and Asp-X-X-Arg signature site in the second motif) of methyltransferase as described by Rozanov et al. (1990) were well conserved in both the viruses (Figure 4). Among the six conserved sequence motifs for the helicase domain of tobamovirus (Goldbach and Wellink, 1988), motif I and II were well conserved for both the viruses whereas, some conservative and non-conservative substitutions were seen in motif III to VI of PluMV in comparison to FrMV (Figure 4). The nucleotide sequences (ATAGCAATTACAG) at the position of termination of 130 kDa protein are strictly conserved in all the tobamoviruses (Strauss et al., 1988), but in case of both PluMV and FrMV, the last three nt sequences were not conserved, and were replaced by ATG, whereas in PluMV-DR_TW, it was replaced by GCG (data not shown). The four conserved sequence motifs (A - D) of polymerase (Poch et al., 1989) were also conserved for both the viruses except a single substitution of Val to Ile at position 1,423 in motif-A and Tyr to Phe at position 1,545 in motif-D in FrMV isolates (Figure 4). In tobamovirus Rep protein, the consensus sequences (GXXXXGKT and DEAD box

TABLE 3 Percent nucleotide/amino acid sequence identity of plumeria mosaic virus isolate, PluMV-Plu-Ind-1 from India with the isolate from Taiwan (PluMV-DR_TW), and with the other tobamoviruses.

Virus	Accession no.	Complete genome	5′ UTR	3′ UTR	Large Rep		Small Rep		MP		CP	
					nt	aa	nt	aa	nt	aa	nt	aa
PluMV-DR_TW	KX881422	98.0	91.1	99.2	97.9	98.7	97.7	98.6	98.3	98.8	99	100
FrMV-Ind-1	JN555602	71.4	48.3	85.2	68.8	75.2	67.1	72.3	79.5	85.9	78.7	86.2
FrMV-P	HM026454	71.6	49.4	85.5	69.1	75.3	67.3	72.2	79.5	86.3	78.5	85.7
Fr-Adel	AF165884	–	–	85.5	–	–	–	–	79.1	84.7	79.5	86.2
BrMMV	AM398436	45.4	27.1	31.0	48.6	41.1	44.2	36.1	36.7	23.9	44.6	37.1
BPMoV	DQ355023	45.2	30.4	29.2	48.2	41.6	44.4	37.0	37.3	23.7	43.6	38.9
CFMMV	AF321057	48.7	33.6	30.9	48.7	41.6	47.2	37.4	46	29.4	44.0	33.1
CGMMV	D12505	48.0	23.9	28.5	48.5	42.7	47.3	38.4	45.3	32.5	47.2	36.5
ClYMV	JN566124	44.4	30.4	34.6	48.0	42.7	44.6	39.0	33.1	21.4	44.4	36.5
CMMoV	EU043335	43.9	19.5	31.5	45.9	38.5	42.9	34.0	32.6	23.4	39.0	29.9
CuMoV	AB261167	48.8	27.1	28.3	49.0	43.4	47.8	38.9	45.1	32.4	47.8	38.8
HLFPV	FJ196834	47.2	19.5	23.5	51.1	44.1	46.9	39.9	38.3	24.5	47.8	40.0
HLSV	AF395898	46.0	23.9	26.6	49.7	44.3	47.0	41.5	38.7	24.0	46.1	39.4
KGMMV	AJ295948	48.1	32.6	24.3	48.0	42.2	46.3	38.0	44.5	29.4	43.6	34.2
MarMV	DQ356949	40.8	14.1	27.4	45.9	41.6	44.6	39.4	33.4	19.0	45.5	37.1
NTLV	AY137775	-	-	-	-	-	-	-	38.3	25.2	45.0	37.2
ObPV	D13438	43.5	27.4	41.5	47.4	41.4	42.9	36.0	38.3	23.7	40.1	37.8
ORSV	X82130	42.8	22.8	26.9	47.0	39.1	43.0	34.7	35.1	20.4	41.8	37.2
PaMMV	AB089381	44.4	29.6	33.2	47.7	41.6	43.4	36.5	37.6	25.6	43.7	37.8
PFMV	HQ389540	40.7	16.3	29.2	48.6	42.7	43.8	39.4	32.7	20.3	46.7	34.8
PMMoV	M81413	45.6	27.4	28.9	48.3	41.9	44.1	36.9	39.3	26.2	44.0	40.6
RaCNaV	JF729471	44.3	43.3	27.6	46.6	40.4	42.8	35.7	31.0	18.8	41.1	27.4
RehMV	AB628188	46.3	33.6	31.0	49.0	42.5	44.7	37.1	35.9	22.7	47.8	41.2
RMV	HQ667979	45.4	25.0	31.7	49.0	42.3	44.4	38.0	38.6	22.8	42.3	37.8
SFBV	AM040955	44.9	26.0	26.4	48.8	42.2	44.1	37.1	36.5	23.3	37.4	32.2
SHMV	MW057697	45.4	28.2	39.1	48.6	42.1	45.3	38.1	33.9	23.7	47.6	40.1
TBRFV	KT383474	45.5	34.7	32.0	48.3	42.0	44.0	36.7	36.6	22.7	47.0	41.8
TMGMV	M34077	46.1	33.6	31.3	49.5	41.4	45.0	37.4	39.8	25.7	45.1	39.5
TMV	AJ011933	45.6	32.6	31.3	48.5	42.3	43.9	37.0	35.8	21.6	45.7	41.2
ToMV	X02144	45.9	31.5	31.3	48.9	42.5	44.5	37.5	36.7	23.0	44.4	40.1
ToMMV	KF477193	45.9	33.6	29.2	49.0	42.3	44.1	37.4	39.2	22.3	45.9	40.1
TSAMV	KU659022	45.2	28.5	27.8	48.2	41.2	44.2	36.5	39.7	27.1	44.0	38.4
TVCV	U03387	45.5	25.0	30.6	49.1	42.3	44.5	37.4	38.6	21.7	43.6	38.9
WMoV	KJ207375	45.1	26.0	30.3	48.8	42.3	44.2	37.2	38.4	23.9	43.8	37.2
YoMV	AB261175	45.3	26.0	29.8	49.0	42.5	44.8	38.0	39.6	23.4	42.3	38.4
YTMMV	KF495564	45.5	31.8	25.0	49.1	41.9	44.5	36.2	37.0	24.6	41.9	34.8
ZGMMV	AJ295949	48.5	29.3	24.6	48.4	42.1	46.6	37.8	45.7	29.4	46.5	36.0

FrMV, Frangipani mosaic virus; BrMMV, Brugmansia mild mottle virus; BPMoV, Bell pepper mottle virus; CFMMV; Cucumber fruit mottle mosaic virus; CGMMV, Cucumber green mottle mosaic virus; ClYMV, Clitoria yellow mottle virus; CMMoV, Cactus mild mottle virus; CuMoV, Cucumber mottle virus; HLFPV, Hibiscus latent fort pierce virus; HLSV, Hibiscus latent Singapur virus; KGMMV, Kyuri green mottle mosaic virus; MarMV, Maracuja mosaic virus; NTLV, Nigerian tobacco latent virus; ObPV, Obuda pepper virus; ORSV, Odontoglossum ringspot virus; PaMMV, Paprika mild mottle virus; PFMV, Passion fruit mosaic virus; PMMoV, Pepper mild mottle virus; RaCNaV, Rattail cactus necrosis-associated virus; RehMV, Rehmannia mosaic virus; RMV, Ribgrass mosaic virus; SFBV, Streptocarpus flower break virus; SHMV, Sunn-hemp mosaic virus; TBRFB, Tomato brown rugose fruit virus; TMGMV, Tobacco mild green mosaic virus; TMV, Tobacco mosaic virus; ToMV, Tomato mosaic virus; ToMMV, Tomato mottle mosaic virus; TSAMV, Tropical soda apple mosaic virus; TVCV, Turnip vein clearing virus; WMoV, Wasabi mottle virus; YoMV, Youcai mosaic virus; YTMMV, Yellow tailflower mild mottle virus; ZGMMV, Zucchini green mottle mosaic virus; –, not available; UTR, Untranslated region; Rep, Replicase; MP, Movement protein; CP, Coat protein

in the helicase domain, and GDD and SGXXXTXXXNT in polymerase domain) were also conserved, except the last amino acid Thr in GXXXXGKT has been substituted by Ser in both the viruses (Figure 4).

Phylogenetic relationships

Phylogenetic analyses based on the amino acid sequences of each protein showed that PluMV was closely related to

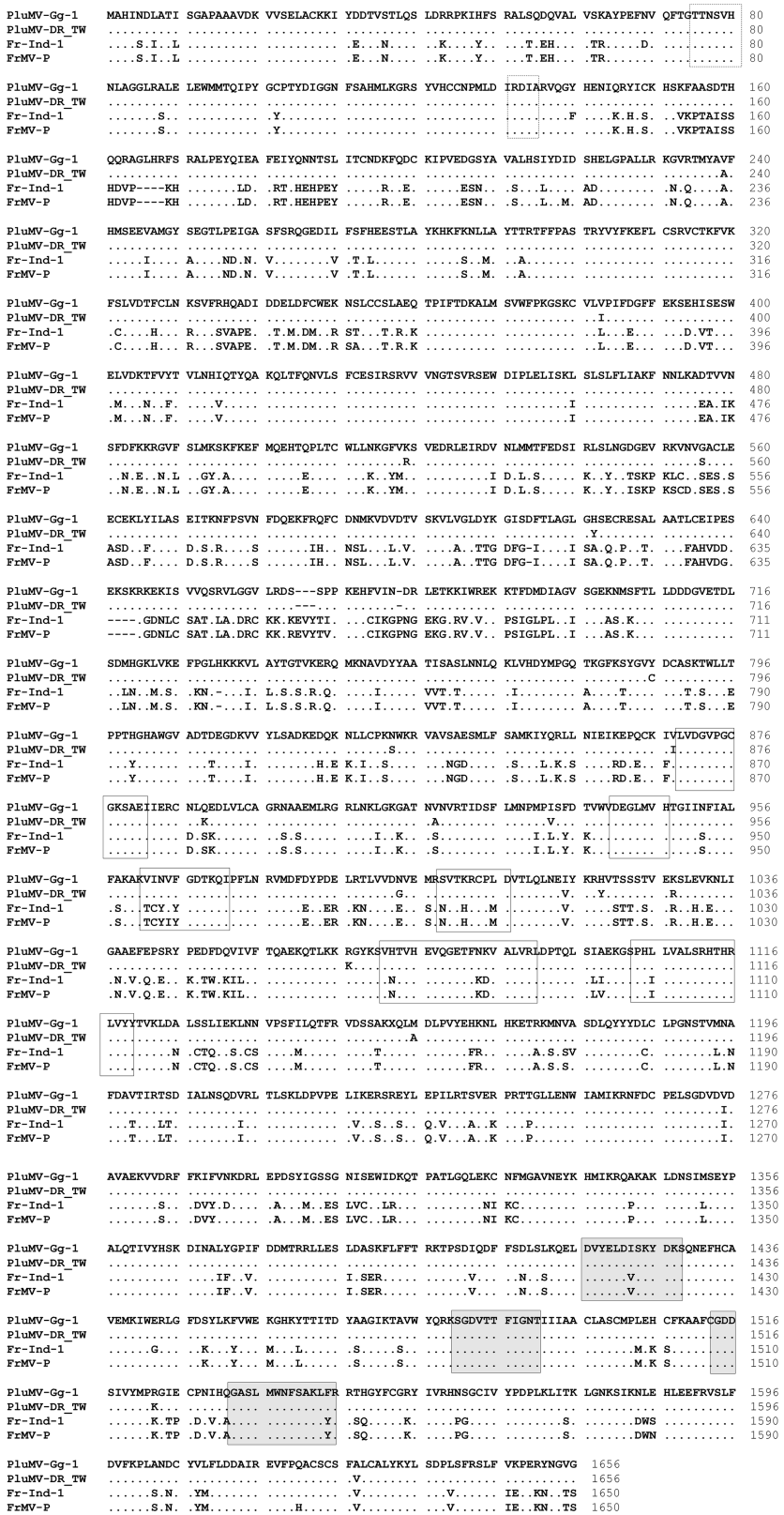

FIGURE 4
Comparison of the amino acid sequence of the large replicase protein of two isolates of plumeria mosaic virus (PluMV-Plu-Ind-1 and PluMV-DR_TW) with that of the isolates of closely related frangipani mosaic virus (FrMV-Ind-1 and FrMV-P). Boxes with dotted line showing conserved motifs of methyltransferase domain, boxes with continuous line showing motifs for helicase domain, and shaded boxes showing motifs for polymerase domain. Dot indicates identical amino acid, dash indicates gap.

10.3389/fmicb.2022.1030042

FrMV, however PluMV formed a separate branch away from FrMV isolates (Figure 5). The phylogenetic analysis of both the Rep proteins revealed that PluMV together with FrMV was closely related with clitoria yellow mottle virus and sunn-hemp mosaic virus (Figures 5A,B), and to the lesser extent to malvaceae-, passifloraceae- and cucurbitaceae-infecting tobamoviruses. Phylogenetic analysis of MP indicated that both the PluMV and FrMV isolates were somewhat related with cucurbitaceae-, brassicaceae- and solanaceae-infecting tobamoviruses (Figure 5C), whereas, the CP of PluMV and FrMV were more related with solanaceae- and brassicaceae-infecting tobamoviruses (Figure 5D).

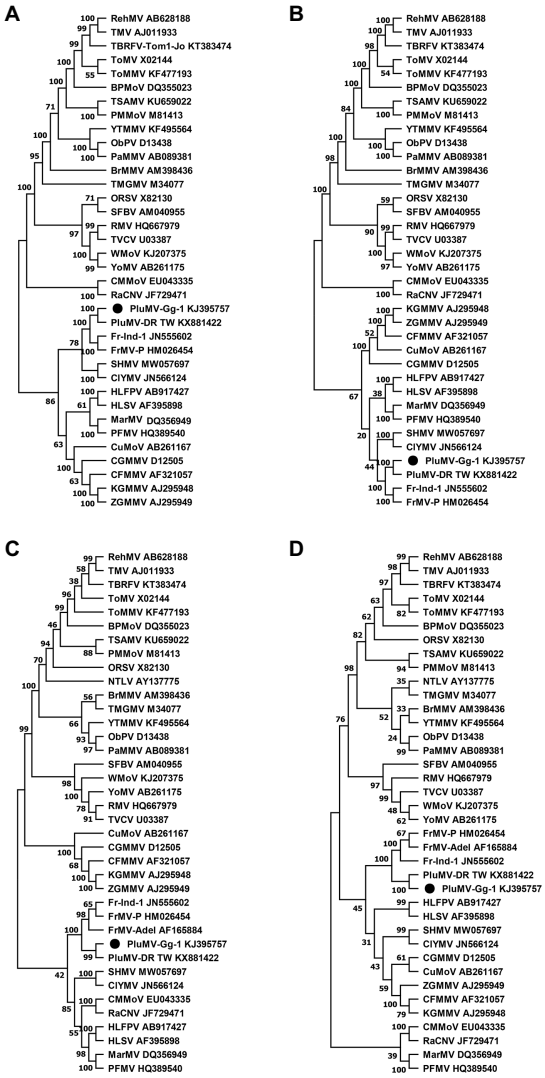

FIGURE 5
Phylogenetic tree of plumeria mosaic virus isolate, PluMV-Plu-Ind-1 and members of the genus *Tobamovirus* based on the 188kDa large replicase protein **(A)**, the 130kDa small replicase protein **(B)**, the 30kDa movement protein **(C)**, and the 18kDa coat protein **(D)**. The tree was constructed based on maximum likelihood method using MEGA version 11 with 1,000 bootstraps value. Full name of the viruses is indicated in Table 3.

Detection of PluMV and FrMV in naturally infected temple tree plants

The antiserum developed using purified virus preparation of FrMV-Ind-1 (Kumar et al., 2015) was used for primary detection of both the viruses in ELISA (data not shown). Further, two pairs of specific primers BM348F/BM204R and BM520F/BM521R were optimized for the specific detection of PluMV, which resulted in amplification of ~0.8 kb from fragment-4 and ~ 1.2 kb from fragment-3 of PluMV cloned DNA (Figure 2), respectively in RT-PCR, whereas, no amplification was found with the FrMV-Ind-1 cloned DNA. Similarly, BM523F/BM200R and BM523F/BM607R have been optimized for the specific detection of FrMV-Ind-1, which resulted in amplification of ~2.0 kb and ~ 1.3 kb bands in the RT-PCR, respectively only with the FrMV-Ind-1 cloned DNA and not with the PluMV cloned DNA (Figure 6A). The primer pairs BM348F/BM204R and BM523F/BM607R were then used to detect the virus in the inoculated plants, where all the symptomatic plants inoculated with PluMV-Plu-Ind-1 and FrMV-Ind-1 gave a specific amplification of ~0.8 kb and ~ 1.3 kb amplifications, respectively in RT-PCR (Figure 1L), whereas, non-symptomatic plants did not give any amplification. Further, a duplex PCR system has been established for the simultaneous detection of PluMV and FrMV using the mixture of both the primer sets (BM348F/BM204R and BM523F/BM607R) and cloned DNA of PluMV-Plu-Ind-1 and FrMV-Ind-1 (Figure 6B). The simplex and duplex PCR systems were successfully utilized to confirm the presence of both the viruses in the original temple tree from where the virus was originally isolated. A specific amplification of ~0.8 kb band for PluMV-Plu-Ind-1 and ~ 1.3 kb band for FrMV-Ind-1 was obtained in simplex RT-PCR performed with the RNA extracted from the symptomatic leaf collected from the original temple tree and two bands of the desired size were obtained in the duplex RT-PCR with the same RNA indicating mixed infection of both the viruses (Figure 6C).

The RT-PCR testing of leaf samples of temple trees from the different locations at IARI campus revealed that FrMV was common in *P. rubra* f. *acutifolia* as 4 out of 7 leaf samples of acutifolia trees were positive for FrMV infection; whereas, PluMV was found common in *P. rubra* f. *obtusa* as 5 out of 8 leaf samples of obtusa trees were positive for PluMV infection. However, both the *Plumeria* species were found susceptible for both the viruses, as single and mixed infections were detected in both the plant species using duplex RT-PCR (Figure 6D).

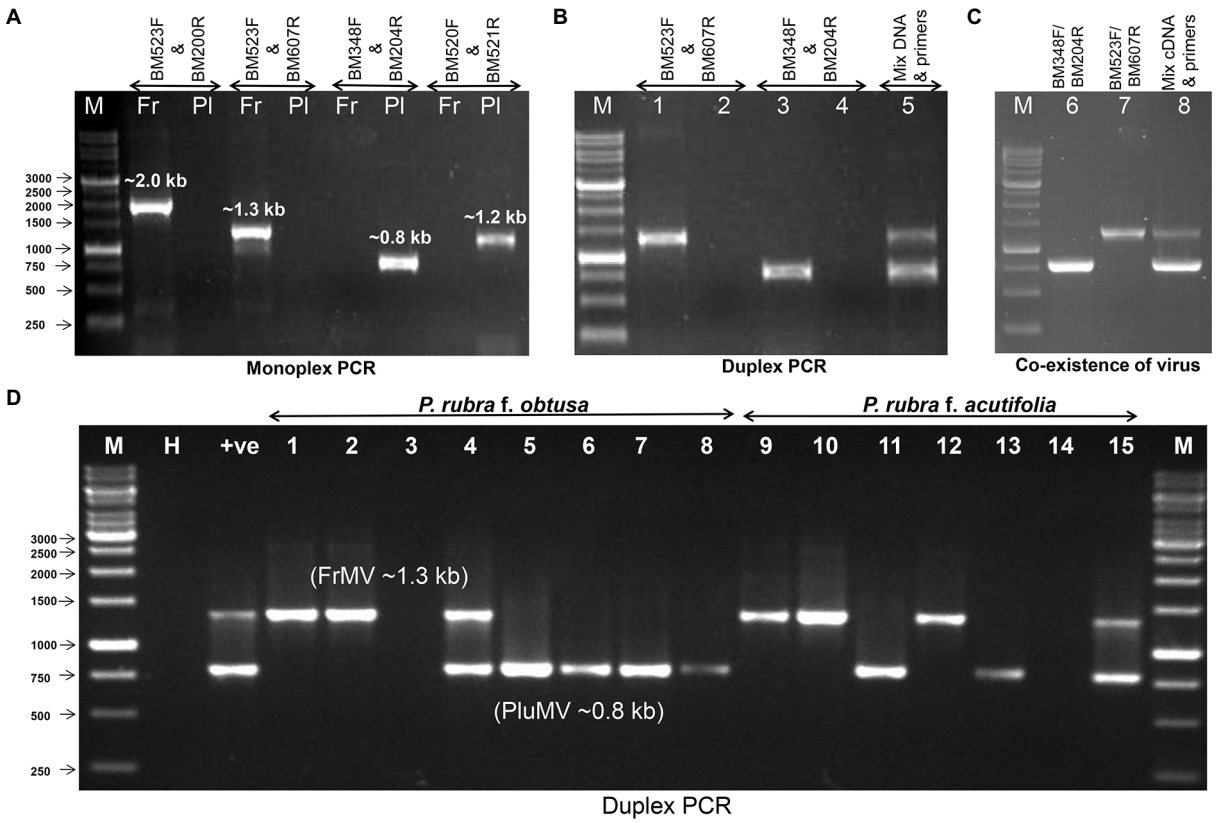

FIGURE 6
Detection of frangipani mosaic virus (FrMV-Ind-1) and plumeria mosaic virus (PluMV-Plu-Ind-1) by RT-PCR. **(A)** Optimization of specificity of the primers using the cloned DNA of FrMV-Ind-1 and PluMV-Plu-Ind-1. **(B)** Duplex PCR using the cloned DNA of FrMV-Ind-1 and PluMV-Plu-Ind-1 with the specific primers BM523F/BM607R and BM348F/BM204R, respectively. M: Marker, Lane 1: FrMV clone tested by FrMV specific primers, Lane 2: FrMV clone tested by PluMV specific primers, Lane 3: PluMV clone tested by PluMV specific primers, Lane 4: PluMV clone tested with FrMV specific primers, Lane 5: Duplex PCR (mixture of both the clone tested with mixture of primers). **(C)** Confirmation of co-infection of both the virus (FrMV and PluMV) in original frangipani tree (*Plumeria rubra* f. *acutifolia*) from where both the viruses were isolated. M: Marker, Lane 1: RT-PCR by FrMV specific primers, Lane 2: RT-PCR by PluMV specific primers, Lane 3: Duplex RT-PCR with the mixture of both the primers. **(D)** Duplex RT-PCR confirmation of single and mixed infection of PluMV and FrMV in the leaf samples collected from different trees at IARI campus. M: Marker, H: Healthy, +ve: Duplex RT-PCR from RNA extracted from the original frangipani tree, Lane 1–15: leaf samples. Fr: FrMV; Pl: PluMV.

Discussion

Temple tree was known to be infected with a tobamovirus, FrMV (Lim et al., 2010; Kumar et al., 2015). In this study, we described another tobamovirus, PluMV infecting temple tree in India. The PluMV was easily sap-transmissible to temple tree plants, *P. rubra* f. *acutifolia* and *P. rubra* f. *obtusa,* and also to many herbaceous plant such as datura, globe amaranth and tobacco. While conducting host-range study, we observed that the symptom development due to PluMV and FrMV infection was influenced by temperature (unpublished observation), as no symptoms were observed in most of these plant species below 27°C, except *N. benthamiana*, which produced mottling mosaic symptoms below 27°C, but took long incubation period for the expression of symptoms. The temperature even influenced the expression of a particular type of symptoms, for example, the inoculated *N. benthamiana* plants did not develop the whitish ring-spot and wavy whitish lines symptoms at a temperature below 27°C, but the same appeared at 30–35°C. *N. benthamiana* appears to be a suitable host for the maintenance of PluMV. Previously, similar influence of temperature on host range and symptomatology was also documented in case of FrMV infecting temple tree (Varma and Gibbs, 1978).

The comparative transmission studies of both the viruses in various plant species helped in identifying three plant species, *G. globosa, S. melongena* and *C. annuum* as important differential plant species of PluMV and FrMV. The red local spot in *G. globosa* is a diagnostic symptom of PluMV. Although, the systemic symptom developed by PluMV on *D. stramonium* could also be used as differentiating symptoms of both the viruses. The differential symptomatology observed in a particular plant species under the similar growing conditions is expected due to the difference in the genetic makeup of the two viruses, PluMV and FrMV.

The complete genome sequence revealed that PluMV had a genome structure typical to the genus, *Tobamovirus* (Adams et al., 2017). Like the subgroup-1 tobamoviruses, the MP and CP genes of PluMV were arranged in the genome without overlapping with each other. Another property of the subgroup-I tobamoviruses is that they generally infect solanaceous plant species. PluMV was originally isolated from *P. rubra* f. *acutifolia* of the family Apocynaceae. Our study showed that PluMV also infected solanaceous plant species such as *D. stramonium, N. benthamiana, N. glutinosa* and *N. tabacum*. Based on the feature of genome architecture and host biology, PluMV could be considered as a new member of the subgroup-I tobamoviruses. The genome sequence comparison of the members of the genus, *Tobamovirus* showed that PluMV was most closely related to FrMV, with only 71.4–71.6% nucleotide sequence identity. For considering a new tobamovirus species, the ICTV guideline is that the complete genome sequence of the candidate member should have less than 90% sequence identity with the recognised members (Adams et al., 2017). Further, based on the distinct phylogenetic relationships, PluMV was considered as a new tobamovirus species. The comparison of the amino acid sequences of large Rep protein of PluMV with that of FrMV showed that, irrespective of significant dis-similarities in the sequences, the major domains (methyltransferase, helicase and polymerase) of the tobamovirus were well conserved in PluMV, except, few substitutions in the helicase and polymerase domains.

Host-range study showed that temple tree was the common host of PluMV and FrMV. Both the viruses could not be readily differentiated visually by symptomatology alone on temple tree. The antiserum developed to FrMV was unable to differentiate both the viruses. Additionally, the CP based primers, designed for the detection of FrMV-Ind-1 (Kumar et al., 2015) also could not detect PluMV. The difference in the genome sequence of both the virus was utilized to develop a specific RT-PCR test for each of these viruses infecting temple tree. The primer pairs developed in this study from the most dissimilar region in the Rep gene successfully differentiated both the viruses by simplex as well as duplex RT-PCR. The RT-PCR diagnosis revealed the natural existence of PluMV alone or together with FrMV. In 2018, 3 years after our submission of the genome sequence in the NCBI database, PluMV was also found in Taiwan infecting desert rose plant (*Adenium obesum*), another ornamental plant of the family Apocynaceae (GenBank KX881422). Detection of PluMV independently in the different trees of both the species of temple tree (*P. rubra* f. *acutifolia* and *P. rubra* f. *obtusa*) in India as well as in *A. obesum* in Taiwan, provided evidence of natural existence of the new tobamovirus.

FrMV has been detected in temple tree in the different countries (Lim et al., 2010; Kumar et al., 2015; Choliq et al., 2017; Dey et al., 2020), whereas, PluMV is yet to be documented in the various parts of the World. Temple tree is commercially propagated through stem cutting. Tobamoviruses being highly contagious, both FrMV and PluMV in temple tree can easily be circulated through cuttings. The comparative host biology and molecular diagnosis presented in this study will be useful in production of virus free planting materials of temple tree. As these viruses co-infect temple tree, synergistic or antagonistic effect on the performance of temple tree needs to be investigated in further study.

Data availability statement

The datasets presented in this study can be found in online repositories. The names of the repository/repositories and accession number(s) can be found below: https://www.ncbi.nlm.nih.gov/genbank/, KJ395757.

Author contributions

AK conceptualized, designed, performed, executed the research experiments and written the manuscript. VS and AKat assisted in experimentation. BM conceptualized, guided the research experiments, and corrected the manuscript. All authors contributed to the article and approved the submitted version.

Acknowledgments

The work was carried out under the sub-project: "Novel Strategies for Molecular Diagnosis of Plant Viruses" (416501-02), awarded to BM under the Component 4 of the ICAR-World Bank funded National Agricultural Innovation Project (NAIP). The financial support from the ICAR-NAIP-Component-4 is thankfully acknowledged.

Conflict of interest

The authors declare that the research was conducted in the absence of any commercial or financial relationships that could be construed as a potential conflict of interest.

Publisher's note

All claims expressed in this article are solely those of the authors and do not necessarily represent those of their affiliated organizations, or those of the publisher, the editors and the reviewers. Any product that may be evaluated in this article, or claim that may be made by its manufacturer, is not guaranteed or endorsed by the publisher.

References

Adams, M. J., Adkins, S., Bragard, C., Gilmer, D., Li, D., Mac Farlane, S. A., et al. (2017). ICTV report consortium, ICTV virus taxonomy profile: *Virgaviridae*. *J. Gen. Virol.* 98, 1999–2000.

Adams, M. J., Antoniw, J. F., and Kreuze, J. (2009). Virgaviridae: a new family of rod-shaped plant viruses. *Arch. Virol.* 154, 1967–1972.

Alonso, E., Garcia-Luque, I., de la Cruz, A., Wicke, B., Avila-Rincbn, M. J., Serra, M. T., et al. (1991). Nucleotide sequence of the genomic RNA of pepper mild mottle virus, a resistance-breaking tobamovirus in pepper. *J. Gen. Virol.* 72, 2875–2884.

Bihani, T., Tandel, P., and Wadekar, J. (2021). Plumeria obtusa L.: a systematic review of its traditional uses, morphology, phytochemistry and pharmacology. *Phytomed. Plus.* 1, 1–14. doi: 10.1016/j.phyplu.2021.100052

Choliq, F. A., Tsang-Hai, C., and Sulistyowati, L. (2017). Molecular characterization of a rigid rod-shaped virus isolated from frangipani (Plumeria sp.) showing mosaic symptom in Taiwan. *J. Exp. Life Sci* 7, 1–6. doi: 10.21776/ub.jels.2016.007.01.01 (2017)

Deng, X. D., Fei, X. W., Huang, J. S., and Zheng, X. Q. (2000). Cloning and sequencing of the 3′-end of frangipani mosaic virus (FMV). *J. Trop. Subtrop. Bot.* 8, 185–192.

Dey, K. K., Vilez-Climent, M., and Soria, P. (2020). First report of frangipani mosaic virus infecting frangipani (Plumeria spp.) in the U.S.A. *Plant Dis.* 1566. doi: 10.1094/PDIS-09-19-2003-PDN

Francki, R. I. B., Zaitlin, M., and Grivell, C. J. (1971). An unusual strain of tobacco mosaic virus from Plumeria acutifolia. *Aust. J. Biol. Sci.* 24, 815–818.

Goldbach, R., and Wellink, J. (1988). Evolution of plus-strand RNA viruses. *Intervirol.* 29, 260–267.

Hall, T. A. (1999). Bio edit: a user-friendly biological sequence alignment editor and analysis program for windows 95/98/NT. *Nucl. Acids. Symp. Ser.* 41, 95–98.

Hilchborn, J. H., and Hills, G. J. (1965). The use of negative staining in the electron microscopic examination of plant viruses in crude extract. *Virology* 27, 528–540.

Ikea, R., Watanabe, E., Watanabe, Y., and Okada, Y. (1993). Nucleotide sequence of tobamovirus Ob which can spread systemically in N gene tobacco. *J. Gen. Virol.* 74, 1939–1944.

Kumar, A., Solanki, V., and Mandal, B. (2013). Frangipani mosaic virus and Plumeria mosaic virus: identification and comparison of two tobamovirus infecting frangipani in India, In: International Conference of Indian Virological Society (IVS) held at Amity University, Noida.

Kumar, A., Solanki, V., Verma, H. N., and Mandal, B. (2015). Characterisation and diagnosis of frangipani mosaic virus from India. *Virus Genes* 51, 310–314.

Lewandowski, D. J., and Dawson, W. O. (2000). Functions of the 126-and 183-kDa proteins of tobacco mosaic virus. *Virology* 271, 90–98.

Lim, M. A., Hong, J. S., Song, Y. S., and Ryu, K. H. (2010). The complete genome sequence and genome structure of frangipani mosaic virus. *Arch. Virol.* 155, 1543–1546.

Pagan, I., Firth, C., and Holmes, E. C. (2010). Phylogenetic analysis reveals rapid evolutionary dynamics in the plant RNA virus genus tobamovirus. *J. Mol. Evol.* 71, 298–307.

Poch, O., Sauvaget, I., Delarue, M., and Tordo, N. (1989). Identification of four conserved motifs among the RNA-dependent polymerase encoding elements. *EMBO J.* 8, 3867–3874.

Quadt, R., and Jaspars, E. M. J. (1989). RNA polymerases of plus-strand RNA viruses of plants. *Mol. Plant. Microbe. In.* 2, 219–223.

Rozanov, M. N., Koonin, E. V., and Gorbalenya, A. E. (1990). N-terminal domains of large putative NTPases of 'Sindbis-like' plant viruses share amino acid motifs and may be RNA methyltransferases. Abstracts: VIIIth International Congress of Virology (Berlin) 377.

Strauss, E. G., Levinson, R., Rice, C. M., Dalrymple, J., and Strauss, J. H. (1988). Non-structural proteins ns P3 and ns P4 of Ross River and O' Nyong-nyong viruses: sequence and comparison with those of other alphaviruses. *Virology* 164, 265–274.

Tamura, K., Stecher, G., and Kumar, S. (2021). MEGA11: molecular evolutionary genetics analysis version 11. *Mol. Bio. Evol.* 38, 3022–3027.

Varma, A., and Gibbs, A. J. (1978). CMI/AAB descriptions of plant viruses. *Netherl. J. Plant Pathol.* 77:64.

Wylie, S. J., Li, H., and Jones, M. G. K. (2013). Yellow tailflower mild mottle virus: a new tobamovirus described from *Anthocercis littorea* (Solanaceae) in Western Australia. *Arch. Virol.* 159, 791–795.

frontiers | Frontiers in Microbiology

TYPE Original Research
PUBLISHED 02 February 2023
DOI 10.3389/fmicb.2023.1046163

Check for updates

OPEN ACCESS

EDITED BY
Beilei Wu,
Institute of Plant Protection (CAAS), China

REVIEWED BY
Wenxing Liang,
Qingdao Agricultural University, China
Islam Hamim,
Bangladesh Agricultural University, Bangladesh

*CORRESPONDENCE
Fenglong Wang
✉ wangfenglong@caas.cn
Jinguang Yang
✉ yangjinguang@caas.cn

SPECIALTY SECTION
This article was submitted to Microbe and Virus Interactions with Plants, a section of the journal Frontiers in Microbiology

RECEIVED 16 September 2022
ACCEPTED 16 January 2023
PUBLISHED 02 February 2023

CITATION
Gong Y, Li Y, Liu D, Jiang L, Liang H, Wu Y, Wang F and Yang J (2023) Analysis of lysine acetylation in tomato spot wilt virus infection in *Nicotiana benthamiana*. *Front. Microbiol.* 14:1046163. doi: 10.3389/fmicb.2023.1046163

COPYRIGHT
© 2023 Gong, Li, Liu, Jiang, Liang, Wu, Wang and Yang. This is an open-access article distributed under the terms of the Creative Commons Attribution License (CC BY). The use, distribution or reproduction in other forums is permitted, provided the original author(s) and the copyright owner(s) are credited and that the original publication in this journal is cited, in accordance with accepted academic practice. No use, distribution or reproduction is permitted which does not comply with these terms.

Analysis of lysine acetylation in tomato spot wilt virus infection in *Nicotiana benthamiana*

Yanwei Gong[1], Ying Li[2], Dongyang Liu[3], Lianqiang Jiang[3], Hui Liang[3], Yuanhua Wu[1], Fenglong Wang[2]* and Jinguang Yang[2]*

[1]College of Plant Protection, Shenyang Agricultural University, Shenyang, China, [2]Key Laboratory of Tobacco Pest Monitoring, Controlling and Integrated Management, Tobacco Research Institute of Chinese Academy of Agricultural Sciences, Qingdao, China, [3]Liangshan State Company of Sichuan Province Tobacco Company, Mile, China

Introduction: Kac is a model for all acylation modification studies. Kac plays a critical role in eukaryotes and prokaryotes. It is mainly involved in six major biological functions: gene expression, signal transduction, cell development, protein conversion, metabolism, and metabolite transport.

Method: We investigated and compared the acetylation modification of proteins in healthy and tomato spot wilt virus (TSWV)-infected *Nicotiana benthamiana* leaves.

Result: We identified 3,418 acetylated lysine sites on 1962 proteins acetylation of proteins in the TSWV-infected and control groups were compared; it was observed that 408 sites on 294 proteins were upregulated and 284 sites on 219 proteins (involved in pentose phosphate, photosynthesis, and carbon fixation in photosynthesis) were downregulated after the infection. Overall, 35 conserved motifs were identified, of which xxxkxxxxx_K_ Rxxxxxxxxx represented 1,334 (31.63%) enrichment motifs and was the most common combination. Bioinformatic analysis revealed that most of the proteins with Kac sites were located in the chloroplast and cytoplasm. They were involved in biological processes, such as cellular and metabolic processes.

Discussion: In conclusion, our results revealed that Kac may participate in the regulation of TSWV infection in *N. benthamiana*.

KEYWORDS

lysine acetylation, TSWV, protein modifications, *Nicotiana benthamiana*, RBCL, post-translational

1. Introduction

In the process of gene expression, functional gene products are synthesized using genetic information to ultimately regulate cell function. As a functional product, protein is a direct and key participant in all downstream biochemical pathways (Adams et al., 2009). From genome to proteome, biological complexity significantly increases because of post-translational modifications (PTMs). The central principle of biosynthesis is PTM of proteins. In plants, sexual reproduction, vegetative growth, and response to biotic and abiotic stresses are affected by functional changes caused by the folding or addition, or removal of functional groups on proteins (Ahlquist et al., 2003; Wang and Wang, 2019). More than 400 PTMs are known (Khoury et al., 2011). Glycosylation, ubiquitination, phosphorylation, and acetylation are the common types of PTMs, whereas some other types, such as adenosine acidification are rarely reported. Acetylation is the process of adding acetyl groups to molecules through acetyltransferase (Ahlquist et al., 2003). It is reported that many proteins can undergo acetylation modification, including histone (Wang et al., 2020), p53, and tubulin (Hammond et al., 2008). According to the various acetylation sites of proteins, acetylation can be divided into three types: Nα- acetylation, lysine acetylation, and O-acetylation (Diallo et al.,

2019). In addition, protein acetylation is mainly involved in six biological functions: metabolism, protein conversion, histone/chromatin/gene expression, metabolite transport, signal transduction, and cell development cycle (Li et al., 2018).

The core histone of nucleosome is a small basic protein with conservative structure, and the tail of histone can protrude from the surface of nucleosome. Histone tails have various amino acid sites, which can exhibit completely different modifications (Phillips, 1963). Among them, histone acetylation modification was identified (Liu et al., 2021), and it was reported that it has a positive regulatory effect on transcription (Allfrey et al., 1964). Its physiological function was not identified until the last decade (Zhao and Garcia, 2015). It was reported that acetylation modification regulates histone and non-histone functions (Glozak et al., 2005; Liu et al., 2021). For example, p53 is the first reported non-histone protein with acetylation modification (Li et al., 2002), proving for the first time that Kac modification is involved in the regulation of non-histone activity. Several proteins with Kac are reported in rice, with 1,669 Kac sites on 1,024 proteins in vegetative cells and reproductive organs (Li et al., 2018) and 1,337 Kac sites on 716 proteins in the whole seedlings (Xiong et al., 2016). In addition, 2057 Kac sites were reported on 1,022 proteins in *Arabidopsis*, including many respiratory chain proteins and tricarboxylic acid cyclase (Hartl et al., 2017). With the detailed research, it was revealed that acetylation modification widely exists in eukaryotes and prokaryotes and in multiple components of cells, exhibiting diversity (Ouidir et al., 2015). It is involved in almost all biological processes, such as cell cycle regulation, cell morphology, cell metabolism, protein interaction, and enzyme activity. This modification is coordinated and regulated by histone/lysine acetyltransferases (hats/kats) and deacetylases (hdacs/kdacs). As an important means of protein function regulation, it plays an important role in defining protein structure and function (Zhang et al., 2013). However, most relevant studies are on rice and *Arabidopsis*, and only few studies have reported acetylation modification in plants from the Solanaceae family infected with tomato spot wilt virus (TSWV). Although some studies are available on Kac in plants, the effect of Kac on pathogen interactions, particularly inviral infection, and their regulation is not studied in plants (Ouidir et al., 2015; Hartl et al., 2017).

According to the classification report issued by the International Committee on Taxonomy of Viruses (ICVT), TSWV is a typical representative member of *orthotospovirus* in the *tospoviridae* family of *bunyavidales* (Zhang et al., 2013). TSWV is a newly defined genus, ranking second to TMV. The typical symptoms of this viral infection are concentric ring spots on leaves and fruits, dwarfing of some plants, distortion of young leaves, and yellowing of leaves, and long-term TSWV infection leads to the death of the whole plant (Pappu et al., 2009; Scholthof et al., 2011; Srinivasan et al., 2017). TSWV is a spherical particle wrapped in a double-layered lipid membrane with a thickness of approximately 5 mm. The diameter of the viral particle is approximately 80–120 nm. TSWV genome is composed of three single stranded genomic RNAs, which are divided into S (2,970 NT), M (4,767 NT), and L (8,913 NT) genomes according to the genomic size. Five viral proteins are expressed using negative or double sense coding strategy: L chain replicase protein RdRp (330 kDa) is responsible for regulating the replication of viral genomic RNA and the transcription of its mRNA; M-chain sense strand encodes a non-structural protein NSm (33 kDa), and the antisense encodes a glycoprotein precursor GP (127 kDa); Antisense strand of S genome encodes a non-structural protein NSs (52 kDa), and the sense strand encodes a nucleocapsid protein N (28 kDa; de Haan et al., 1991; Adkins et al., 1995; Chapman et al., 2003; Feng et al., 2020). In 2020, clones with TSWV infections were developed to study the interaction between TSWV and TSWV host (Rotenberg et al., 2015; Chen et al., 2019; Feng et al., 2020). However, to date, only a few host factors are reported that interact with TSWV coding proteins and participate in TSWV infection, and no PTMs of host proteins related to TSWV infection are reported.

In this study, using *N. benthamiana* as a model plant of Solanaceae, we investigated the changes in Kac in host proteins after TSWV infection. Overall, 4,570 peptides and 4,219 acetylated peptides were identified after LC–MS and bioinformatic analyses. This study laid a foundation for the further research on host defense in TSWV and breeding of disease-resistant species.

2. Experimental procedures

2.1. Tomato spot wilt virus inoculation and plant growth

As samples, 4-week-old *N. benthamiana* plants were selected and divided into two groups: control and treatment groups, with 3 plants in each group. The friction inoculation concentration of the treatment group was approximately 40×. The control group was treated with PBS buffer instead of TSWV. After inoculation, the plants were grown at 25°C under 16 h/8 h light/dark conditions for 7 days.

2.2. Protein extraction from *Nicotiana benthamiana*

First, 2 g leaves were collected and frozen in liquid nitrogen to retain the original composition of plant tissues. After removing the leaves form liquid nitrogen, they were quickly ground in a precooled mortar. The powder was placed in a 1.5 ml centrifuge tube containing Protease inhibitor lysate (CW2333, CW2200, CoWin Biotech, Beijing, China) and allowed to rest for 30 min at 4°C. After sufficient mixing, the suspension was centrifuged at 13,400 g at 4°Cfor 20 min. The supernatant was removed and stored at −20°C. Finally, the target proteins were dissolved in BCA working solution (prepared by mixing BCA and Cu reagent in 50: 1 ratio; it was sufficiently mixed till turbidity disappeared 37°Cfor 15–30 min (EC0001 Shandong Sparkjade Biotechnology Co., Ltd.). The absorption was measured at 562 nm using a photometer. The protein content was calculated according to the standard curve.

2.3. Database search

The Kac peptides were dissolved and separated using a reversed-phase analytical column (Acclaim PepMap RSLC C18 column, Thermo Fisher Scientific). The gradient phase composed of 2 to 10% solvent (0.1% formic acid in 98% acetonitrile) in 6 min, 10 to 20% in 45 min, 20 to 80% in 7 min and holding at 80% for at least 4 min, all at a flow rate of 250 nl/min on an UPLC system. The peptides were subjected to ESI/NSI sources followed by MS/MS in Q ExactiveTM Plus (Thermo Fisher Scientific) coupled online to UPLC. The Orbitrap was used to detect whole peptides and ion fragments at a resolution of 70,000 and 17,500, respectively, with NCE set at 30. The electrospray voltage was set at 2.0 kV. Automatic gain control (AGC) was used to prevent overfilling of the ion trap. The m/z range was from 350 to 1,800 for MS scans. The MS fixed first mass was

set at 100 m/z and LC–MS/MS analyses were conducted at Micrometer Biotech Company (Hangzhou, China). The resulting raw data were processed using MaxQuant with integrated Andromeda search engine (v.1.5.2.8). Tandem mass spectra were searched against the same database. At the same time, the peptide was cleaved with trypsin. The number of peptide deletions was controlled to be less than 4, and each peptide had 5 modifications and 5 charges. The quality error of search was approximately 10 ppm; the main search error was approximately 5 ppm, and the error of fragment ions was approximately 0.02 Da. Further, the amino methylation modification of cysteine and oxidative modification of methionine were set as fixed modifications. For the acetylation of lysine and protein N-terminal, we set it as variable modification. We set the minimum peptide length to 7 bp. The false positive rate (FDR) threshold of proteins, modification sites, and peptides was set to 1%. All other parameter values in maxquant were set to default values. The location probability of the locus was set to >0.75.

2.4. Bioinformatic analysis

The acetylated proteins identified by Gene Ontology (GO)-RRB analysis were classified into three classes using Blast2GO software: molecular function, biological process, and cell component analysis. An adjusted $p < 0.05$ was considered significant. The subcellular localization of detected proteins was analyzed using the subcellular localization prediction software Wolfpsort, and the KEGG database was used to annotate protein pathways. The results of GO, KEGG pathway, and domain analysis were considered significant at $p < 0.05$. Functional analysis of protein domains was performed using the InterProScan software based on protein sequence alignment and the InterPro[1] domain database. Motif-x software was used to analyze the amino acid composition of 21 amino acid regions in the upstream and downstream of acetylation sites of all acetylated proteins.

2.5. Protein–protein interaction network

For analyzing the interactions between proteins, we typically used the interaction gene/protein search tool (STRING) DATABASE43 and Cytoscape software (version 3.0.1) 44. When defining interaction confidence, the score was set to >0.7. All data were centrally presented only for the searched protein interaction. The dense junctions where interacting proteins appear were analyzed using a graph-theoretic clustering algorithm and a molecular complex detection (MCODE) plug-in toolkit.

2.6. Western blot analysis

The changes in the acetylated protein content after TSWV infection were detected with acetylated antibodies. The total protein extracted from plants was subjected to SDS-PAGE gel electrophoresis (precast protein plus gel, 12%, 10 wells, HEPES Tris, Yeasen, China). The separated proteins were transferred on the PVDF membrane (150 V, 40 min). The membrane was blocked with 5% BSA for 2 h and incubated with primary antibody (anti-Kac1:1500 PTM-801 PTM Biolabs, Hangzhou, China) overnight at 4°C (Actin 1:5000, ABclonal Biotechnology, Wuhan, China) and further with secondary antibody (goat anti-mouse IgG 1:10000, ABclonal Biotechnology, Wuhan, China) at room temperature for 3 h. The protein bands were visualized using Chemiluminescence imaging system (Tanon 5,200).

3. Results

3.1. Proteomic analysis of Kac peptides and proteins in tomato spot wilt virus-infected *Nicotiana benthamiana*

Compared with the control, the viral content increased exponentially in the treatment group 7 days after inoculation with TSWV, and clear symptoms of the infection were exhibited (Figure 1A). The total proteins were extracted from the leaves of *N. benthamiana* after 7 days after of TSWV infection, and their content was determined using Coomassie Brilliant Blue. The amount of acetylated protein in the control and treatment groups was determined using western blotting with pan-acetylated antibody. The results revealed that the change in acetylated protein content in *N. benthamiana* leaves infected with TSWV was significantly higher than that in the control (Figure 1B). We performed LC–MS/MS analysis of lysine-acetylated peptides (Figure 1C), exemplified by spectral signals of acetylated peptides of downregulated proteins of the ribulose-bisphosphate carboxylase large chain (Figure 1D; Supplementary Table S1). To verify the validity and accuracy of the obtained data, the quality error of the acetylated peptide and repeatability of the sample were tested (Figures 2A,B). The length of the acetylated peptide segments was analyzed; the majority of the lengths focused on ranges from 7 to 19 (Figure 2C). In summary, 2,393 proteins were identified with 4,321 acetylated lysine sites after TSWV infection. The acetylated protein levels were compared between the control and treatment groups; 408 sites were upregulated on 294 proteins, and the 284 sites were downregulated in 219 proteins when considering a change threshold of at least 1.3-fold and a $p < 0.05$ in t-test (Figure 2D; Supplementary Table S2). Of all the proteins with altered acetylation levels, 19 were involved in the carbon-fixed degradation pathway, and the acetylation levels of 6 proteins were significantly reduced, with each protein having at least one acetylation site.

3.2. Pattern analysis of acetylation sites

The characteristics and specific domains of acetylation sites were evaluated. To facilitate the future study on acetylation sites, The MOMO algorithm was set to motif-x, the minimum number of occurrences was set to 20, and the value of p threshold was 0.000001. Protein secondary structure analysis was performed using NetSurfP (Klausen et al., 2019). We used motif-x program to analyze the amino acid background of 10 to +10 on both sides of Kac site. A site-specific intensity map was generated to evaluate the significantly enriched amino acids around the acetylation sites. The concentration of amino acid frequency motifs revealed that the residues F, H, K, R, T, and N were preferentially selected at sites +1, +2, and +3, and residues A, D, G, and V were preferentially selected at sites −1, −2, and −3 (Figure 3A). However, serine residues were significantly

1 http://www.ebi.ac.uk/InterPro/

10.3389/fmicb.2023.1046163

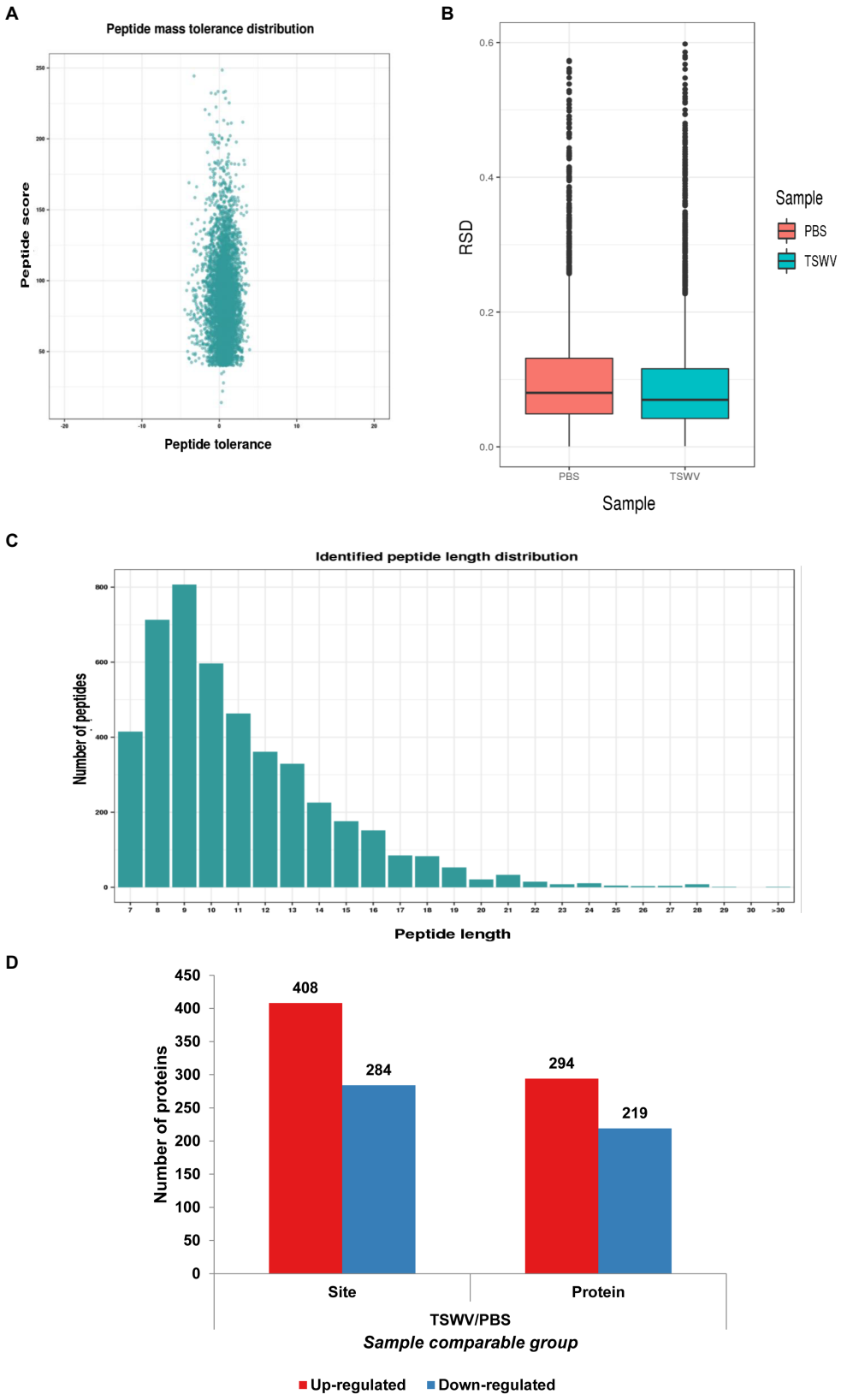

FIGURE 1
Protein acetylation in *Nicotiana benthamiana* after TSWV infection. **(A)** Photograph of *N. benthamiana* 7days after inoculation with TSWV. **(B)** Coomassie Brilliant Blue was used to control the loading amount, and pan-anti-kac antibody against Kac protein was used for Western blot analysis. **(C)** Kac proteomic and modification processing. **(D)** LC–MS/MS spectra of acetyl peptides from downregulated proteins, namely, ribulose-bisphosphate carboxylase large chains and acetyl peptide DKLNK (1) YGR with one acetylation site at K164.

10.3389/fmicb.2023.1046163

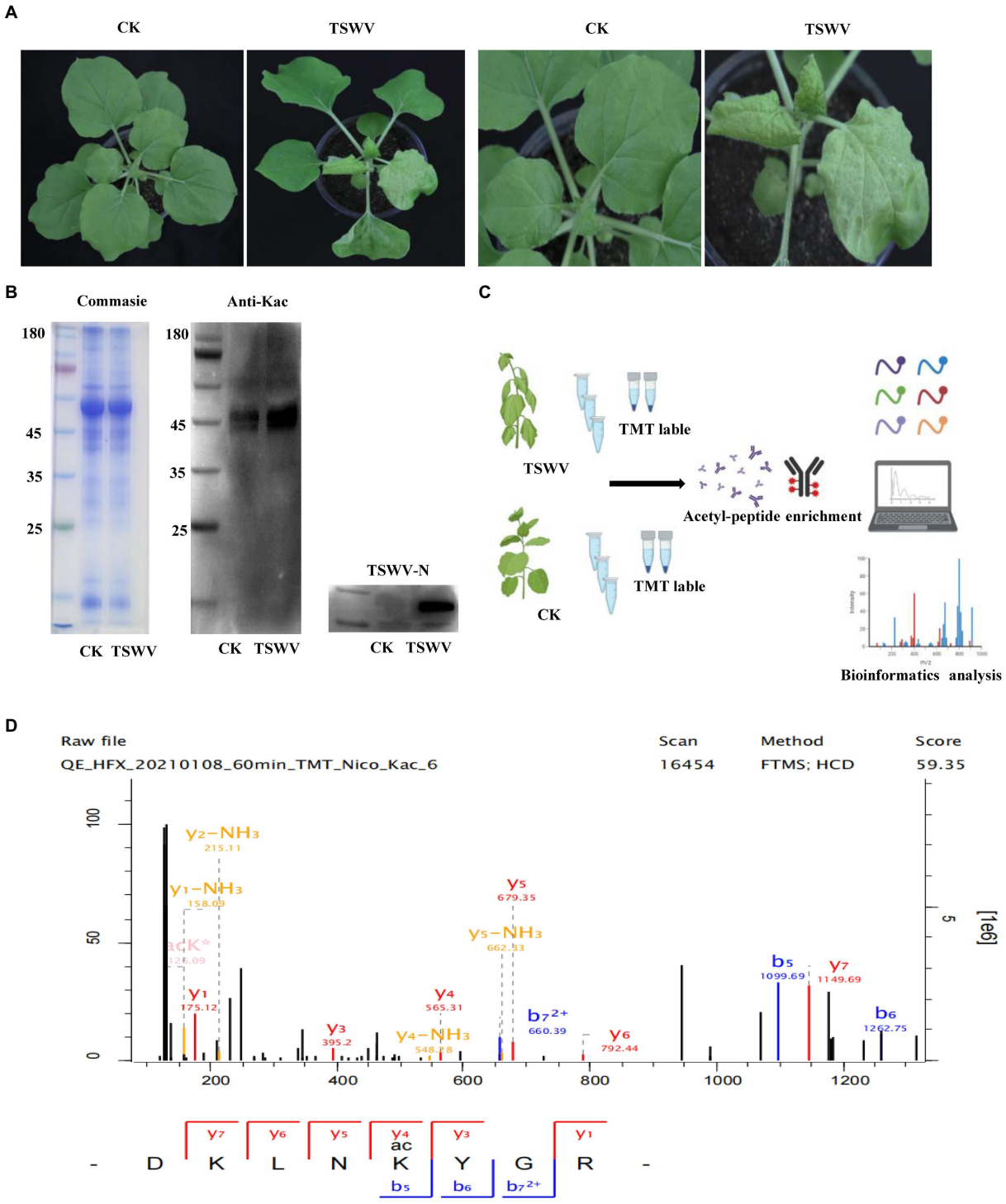

FIGURE 2
Analysis of Kac sites in *N. benthamiana*. **(A)** Quality error analysis of identified peptides. **(B)** Boxplot showing the sequence coverage of proteins that were quantified under each extraction condition. RSD, relative standard deviation efficient. **(C)** Distribution of peptide length. **(D)** The number of proteins and acetylation sites identified in the control and treatment groups.

lacking at all 20 sites around the acetylation sites. A total of 35 conservative motifs in K*A, K*R, A*K, K*K, E*K, K*NV, P*K*R, L*K*N, K*H, R*K*R, A*K*S, K*A, K*T, K*F, G*K*S, V*K*N, K*S, A*K*N, K*N, N*K*V, R*K, K*D, K*E and K*X were summarized from 4,219 acetylated peptides. Among these motifs, K*R represented 1,334 (31.63%) enriched motifs and was the most common combination (Figure 3B).

3.3. Functional distribution and subcellular localization of acetylated proteins in tomato spot wilt virus-infected *Nicotiana benthamiana*

To further classify the 1962 acetylated proteins in biological processes, cellular components, and molecular functions after TSWV

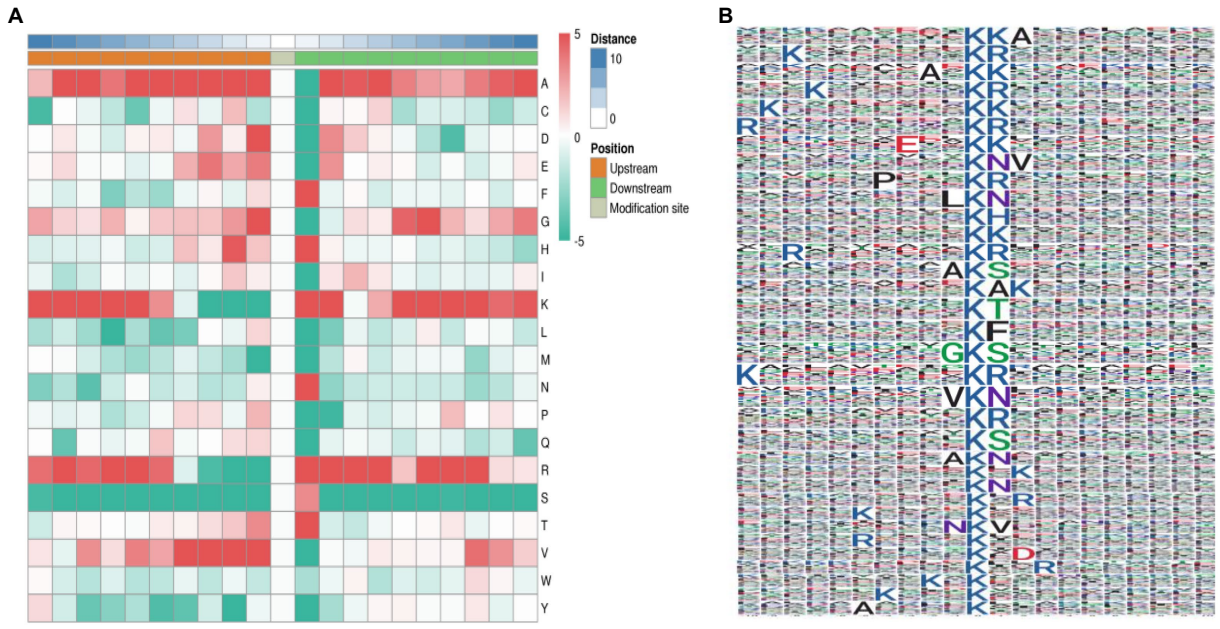

FIGURE 3
Characterization of lysine acetylation. **(A)** Heat map of the composition of common amino acids at acetylation sites. The middle white represents the Kac site, and the left and right represent the upstream and downstream amino acid residues based on Kac, respectively, with red representing tight and green representing loose. **(B)** Common acetylation motifs and conserved sites around the gene (the size of each letter corresponds to the frequency of amino acid residues at that site).

infection in *N. benthamiana*, the GO analysis was performed. The results revealed that 212 acetylated proteins were involved in metabolism, 240 in cellular processes, and 141 in response to stimulation.

Moreover 333 and 319 acetylated proteins were in the cell and intracellular, respectively, and only 82 acetylated proteins were in the protein complex. Among the proteins from molecular functional class, most acetylated proteins were associated with catalytic activity ($n = 181$) or binding ($n = 123$; Figure 4A). The results indicated that the enzyme-metabolism-related proteins might have a high probability of acetylation in TSWV-infected *N. benthamiana*. In case of subcellular localization, the most acetylated proteins were located in the chloroplast in TSWV-infected *N. benthamiana* (Figure 4B). Some of the remaining acetylation proteins were mainly located in the cytoplasm, nucleus, and plasma membrane (Supplementary Table S3).

3.4. Enrichment analysis and domain enrichment of lysine-acetylated proteins in tomato spot wilt virus-infected *Nicotiana benthamiana*

The response of acetylated proteins to TSWV infection in *N. benthamiana* was investigated based on KEGG analysis (Figure 5A). Downregulated acetylated proteins were mainly involved in the regulation of photosynthesis, carbon fixation, glyoxylic acid and dicarboxylic acid metabolism, and nitrogen metabolism (Figure 5B). Upregulated acetylated proteins were related to the regulation of biosynthesis of terpenoid skeletons, degradation of fatty acids, and protein processing in the endoplasmic reticulum (Figure 5C).

Kac was used as the preferred target for protein domain analysis using the InterPro domain database. The protein domain enrichment results revealed that 21 domains were enriched, which mainly included peroxidase, histidine kinase, DNA gyrase B, HSP90-like ATPase, and aminotransferase class III (Figure 5D). Meanwhile, the upregulated lysine-acetylated proteins included ABC transporter, peroxidase, glutathione S-transferase, and C-terminal domain cyclophilin-type peptidyl prolyl cis−trans isomerase/CLD domain (Figure 5E). Furthermore, downregulated lysine-acetylated proteins included core histone H2A/H2B/H3/H4, S1 RNA binding domain, short chain dehydrogenase, aminotransferase class III, and fructose-1,6-bisphosphatase (Figure 5F; Supplementary Table S4).

3.5. Analysis of the interaction network of acetylated proteins

To further investigate the role of Kac in TSWV infection in *N. benthamiana*, we visualized the protein–protein interaction network in a Cytoscape program using STRING database analysis. The results revealed that 155 acetylated proteins were mapped into the radiation map, and the network demonstrated how protein acetylation in various pathways was activated and mobilized in *N. benthamiana*. According to the Cytoscape program, 2 clusters of highly interconnected acetylated proteins were retrieved. The greater the density of mapping, the more the number of proteins they interacted with, indicating greater importance of proteins in the interaction network. The Internet network revealed that Kac was closely related to ribosomes and could regulate many metabolic pathways in the host (Figure 6; Supplementary Table S5).

3.6. Acetylated proteins involved in carbon fixation

In KEGG pathway enrichment analysis, a large number of acetylated proteins related to carbon fixation pathway were

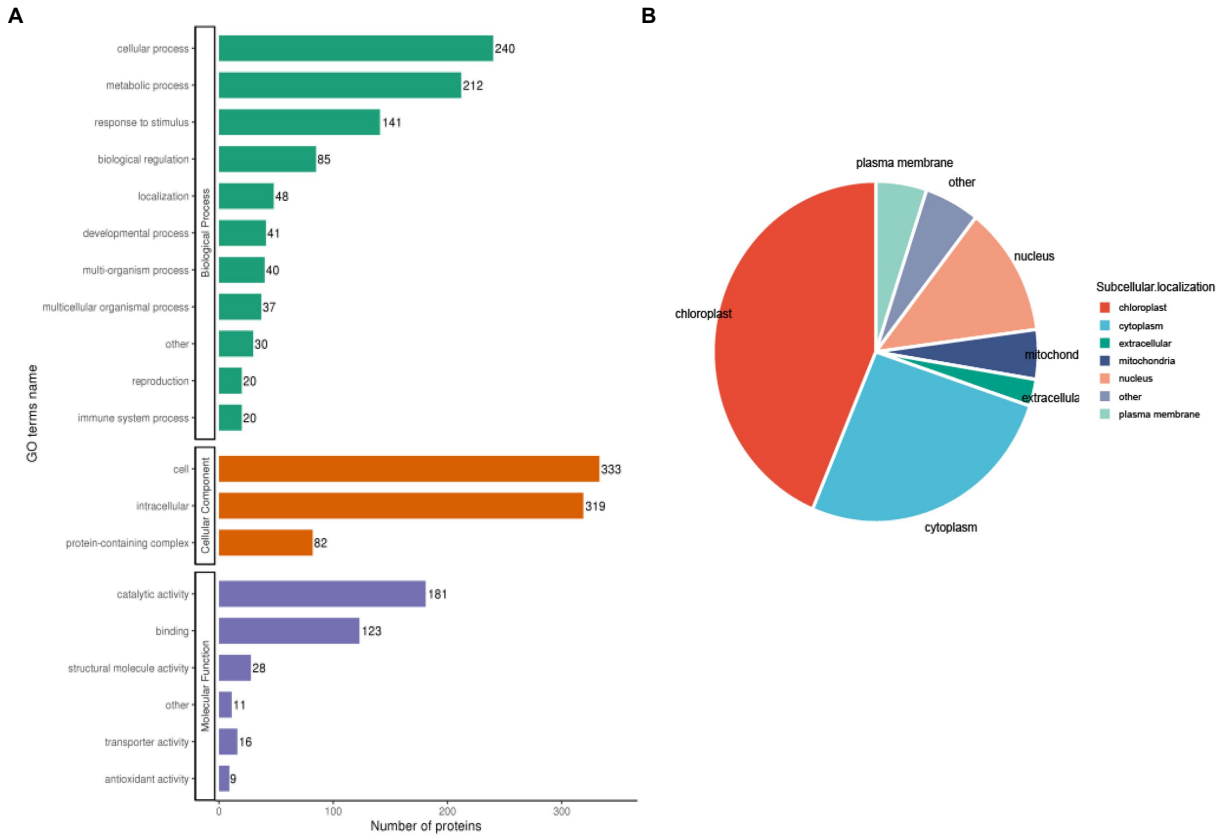

FIGURE 4
Functional distribution and subcellular localization of lysine-acetylated proteins in TSWV-infected *N. benthamiana*. **(A)** Quantitative profiles of lysine-acetylated proteins in biological processes, cellular components, and molecular functions. **(B)** The subcellular localization of lysine-acetylated protein is shown using a pie chart.

identified. Further analysis revealed that the expression of acetylated GAPDH, PPDK, pckA, MDHI, and maeb was increased and that of acetylated. Downregulated proteins PPC, Aldo, glpx sebp, tkta, NbrbcL, FBP, TPI, and gapA (which play a role in the carbon fixation pathway of photosynthesis) was decreased in *N. benthamiana* infected with TSWV (Figure 7A). It is worth noting that the change in protein acetylation after TSWV infection was inconsistent with the change in protein expression. No change was observed in the expression of all upregulated proteins, and the change in acetylation may not change the protein content (Figure 7B).

3.7. Acetylation levels of NbrbcL protein were decreased in *Nicotiana benthamiana* after tomato spot wilt virus infection

Comprehensive metabolic pathway analysis revealed that the acetylation level of NbrbcL protein in leaves infected with TSWV was lower than that in healthy leaves. The target protein structure and its acetylation site were predicted using PDB database[2] (Figure 8A). Although acetylated protein bands were detected in both TSWV-infected and healthy leaves samples subjected to western blot analysis, the acetylation level of NbrbcL protein in TSWV-infected leaves was weaker than that in healthy leaves. To explore the relationship between *NbrbcL* gene and viral infection, The silencing efficiency was determined by comparing the expression levels of NbrbcL in *TRV*:: *NbrbcL* plants and *TRV*:: *00* control plants. No phenotypic difference was observed between *TRV*:: *NbrbcL* and control plants (Figure 8B). Next, *TRV*:: *NbrbcL* and control plants were infected with TSWV virus source, and viral infection was monitored for at least 1 week. The results revealed that the viral N gene expression in *TRV*:: *NbrbcL* was significantly lower than that in *TRV:: 00* control group from 5 to 11 days after viral inoculation (Figure 8C). Western blot analysis revealed that 7 days after the inoculation, the level of viral N protein in *TRV*:: *NbrbcL* was lower than that in *TRV::00* (Figure 8D). In conclusion, *NbNbrbcL* and its acetylation may play a role in TSWV infection in *N. benthamiana*.

4. Discussion

In 1927, it was reported that acetylation significantly affects protein specificity; however, no relevant large-scale study was performed till a long time (Allfrey et al., 1964). Kac ranks first in the acylation family and is the research model of all acylation modifications. To the best of our knowledge, this is the first study to classify the acetylated proteins in *N. benthamiana*, a model plant of Solanaceae family, infected with TSWV. Here, we detected 4,321 acetylated lysine sites on 2,393 proteins. The analysis of protein–protein interaction network revealed that these modified proteins in

2 http://zhanglab.ccmb.med.umich.edu/I-TASSER/

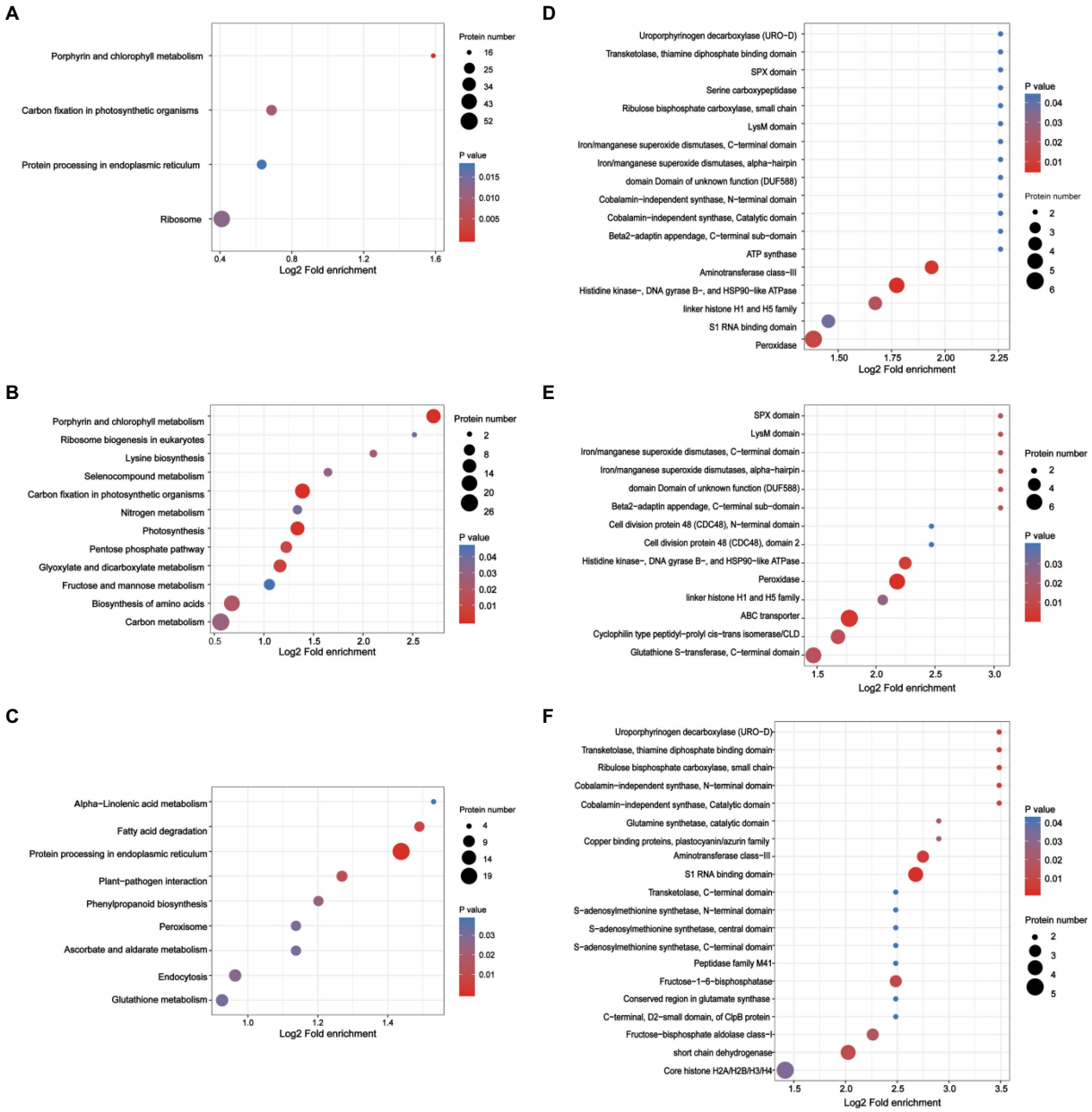

FIGURE 5
Analysis of the enrichment of lysine-acetylated proteins in *N. benthamiana* infected by TSWV. **(A)** KEGG pathway-based enrichment analysis of proteins in TSWV-infected versus uninfected plants ($p<0.05$). **(B)** KEGG pathway-based enrichment analysis of upregulated proteins in TSWV-infected versus uninfected plants ($p<0.05$). **(C)** KEGG pathway-based enrichment analysis of downregulated proteins in TSWV-infected versus uninfected plants ($p<0.05$). **(D)** Concentration analysis of protein domains in TSWV-infected versus uninfected plants. **(E)** Protein domain enrichment analysis of upregulated proteins in TSWV-infected versus uninfected plants. **(F)** Downregulated proteins in TSWV-infected versus uninfected plants.

N. benthamiana not only participate in gene expression but also play an important role in various metabolic processes. The same modified proteins can participate in one metabolic pathway and perform multiple cellular processes at the same time; they may be positively correlated in one metabolism and negatively correlated in the other (Berger, 2007; Tribus et al., 2010; Bannister and Kouzarides, 2011; Li et al., 2015). This is sufficient to demonstrate that protein acetylation may be a common phenomenon in the process of host growth, reproduction, and resistance to external infection (Imai and Guarente, 2010; Kim et al., 2012; Lu et al., 2018). These results are consistent with previous studies on acetylated proteins in liver cancer (Hu et al., 2017), breast cancer (Guo et al., 2018), strawberry (Fang et al., 2015), and *Arabidopsis* (Konig et al., 2014).

The chloroplast organelles in the mesophyll cells of higher plants represent a sun-driven metabolic factory, performing photosynthesis and carbon fixation and ultimately providing fuel for life on our planet (Kirchhoff, 2019). In this study, a large number of acetylated proteins were located in the chloroplast, cytoplasm, and nucleus, revealing that viral infection may be closely related to acetylated proteins in the three organelles. Numerous studies have reported that chloroplasts can effectively activate defensive hormone response in the process of plant pathogen interaction,

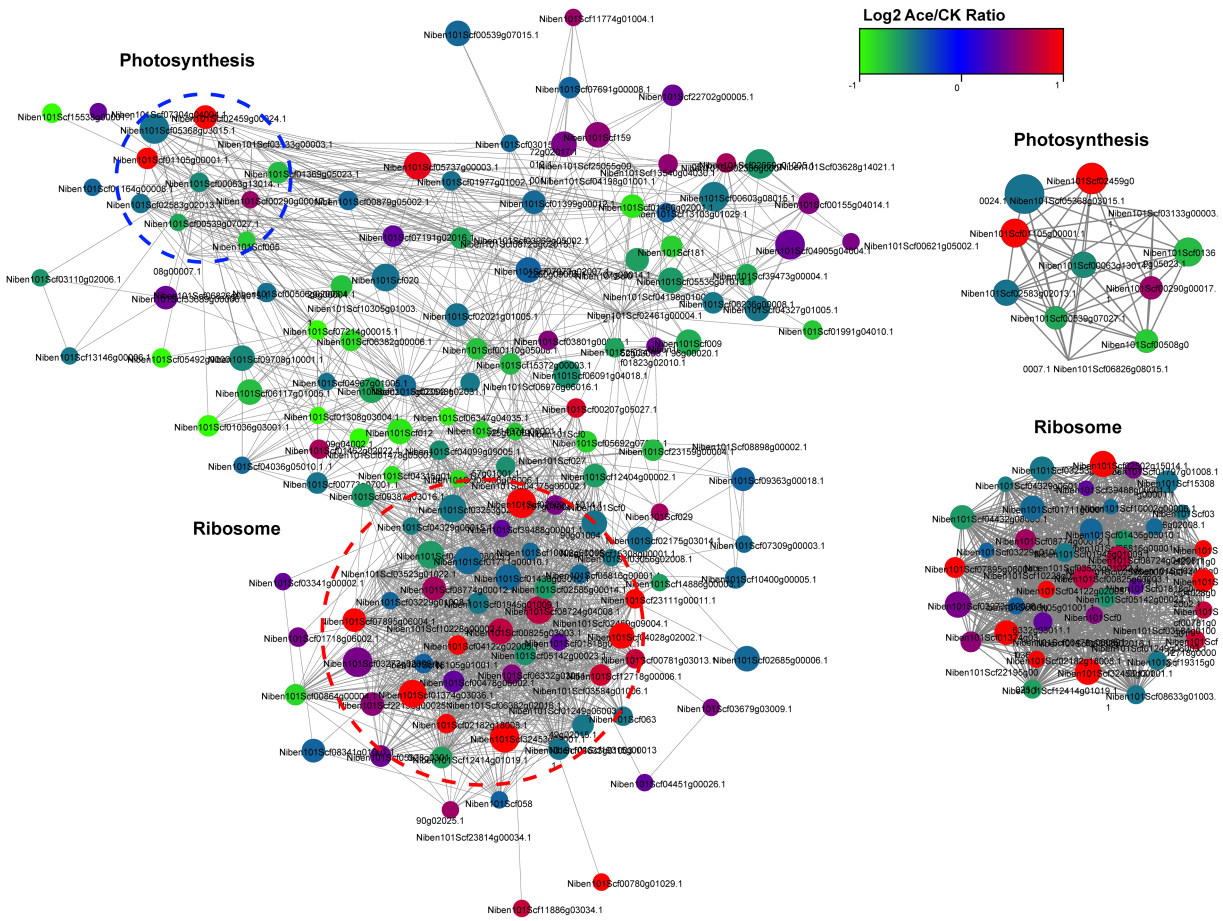

FIGURE 6
Interaction networks of differentially expressed acetylated proteins in TSWV-infected and healthy *N. benthamiana* plants.

and viral proteins located on chloroplasts can promote viral pathogenesis (Medina-Puche et al., 2020). The carbon fixation reaction in photosynthesis starts from chloroplast matrix and ends in cytoplasmic matrix. A cyclic reaction, also known as Calvin cycle, continuously consumes ATP and NADPH and fixes CO_2 to form glucose (Hirosawa et al., 2021). After the virus infects plants, it needs the help of the host to complete its own replication and proliferation. For example, when the plant defense response is activated, the C4 protein encoded by tomato yellow leaf curl virus relocates from the plasma membrane to the chloroplast, thus interfering with the biosynthesis of chloroplast-dependent antiviral salicylic acid (Wang et al., 2010). Based on these findings, we speculated that protein acetylation in photosynthesis process may play an indispensable role in viral infection.

In *N. benthamiana* leaves infected with TSWV, expression of a large number of acetylated proteins related to carbon fixation was altered, including GAPDH, PPDK, pckA, NbrbcL, FBP, TPI, and gapA. In the carbon fixation stage, green leaves absorb carbon dioxide from the environment through the pores, which cannot be directly reduced by reducing hydrogen. It must first bind to C5 (ribulose diphosphate) in plants. This process is called carbon dioxide fixation. After a carbon dioxide molecule is fixed by a C5 molecule, two C3 (12 glyceraldehyde-3-phosphate) molecules are quickly formed. Under the catalysis of relevant enzymes, C3 receives the energy released by ATP and is reduced by reducing hydrogen. NbrbcL plays an important role in this process, and the acetylation levels of NbrbcL in TSWV-infected and healthy plants were different. Therefore, we speculated that acetylated proteins may participate in carbon fixation in photosynthesis by affecting NbrbcL.

In summary, a large number of histone and non-histone lysine residues located in chloroplasts, cytoplasm, and nucleus are acetylated (Xu et al., 2021; Shvedunova and Akhtar, 2022). Some of these carbon fixation proteins may be related to viral infection and energy metabolism (Johnson, 2016). In this study, *N. benthamiana* infected with TSWV was used as the model, and acetylated proteins and their acetylation sites in it were revealed. This study broadened our understanding of Kac regulating the metabolic process and functional application in TSWV-infected *N. benthamiana*. This study on *N. benthamiana*, as a representative of plants from Solanaceae family, provided a basis for the future research on protein acetylation in plants from Solanaceae family infectec with viruses.

5. Conclusion

To the best of our knowledge, this is the first study assessing the Kac in TSWV-infected *N. benthamiana* and providing a resource for further exploration of the potential functions of Kac in the plant infections with segmented plants negative-stranded RNA viruses. The findings of this study provided insights into the function of Kac in in *N. benthamian* after sensing TSWV stages. However,further studies are needed to explore the detailed mechanism.

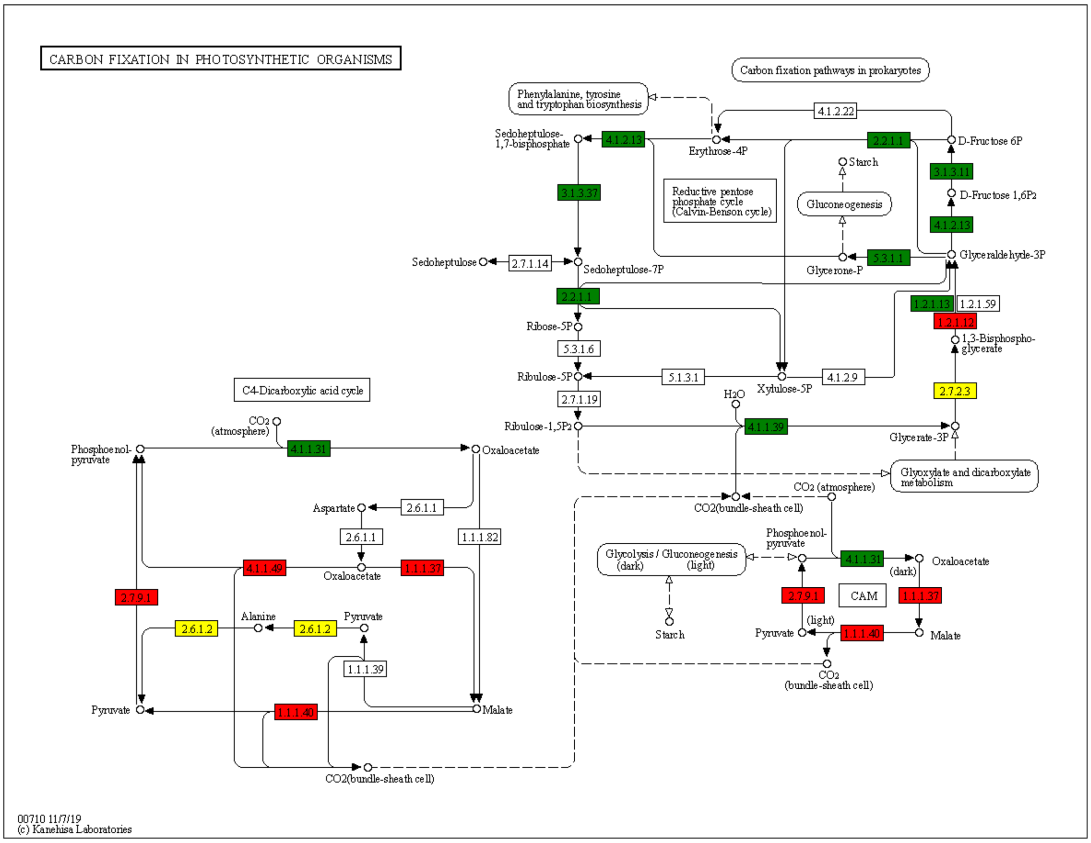

FIGURE 7
Analysis of metabolic pathways of carbon fixation. Red and green highlights are acetylated proteins that were significantly upregulated and downregulated, respectively, in the carbon fixation pathway in the treatment group compared with the control group. The yellow highlights indicate that at this point, acetylation level was upregulated and downregulated at the same time.

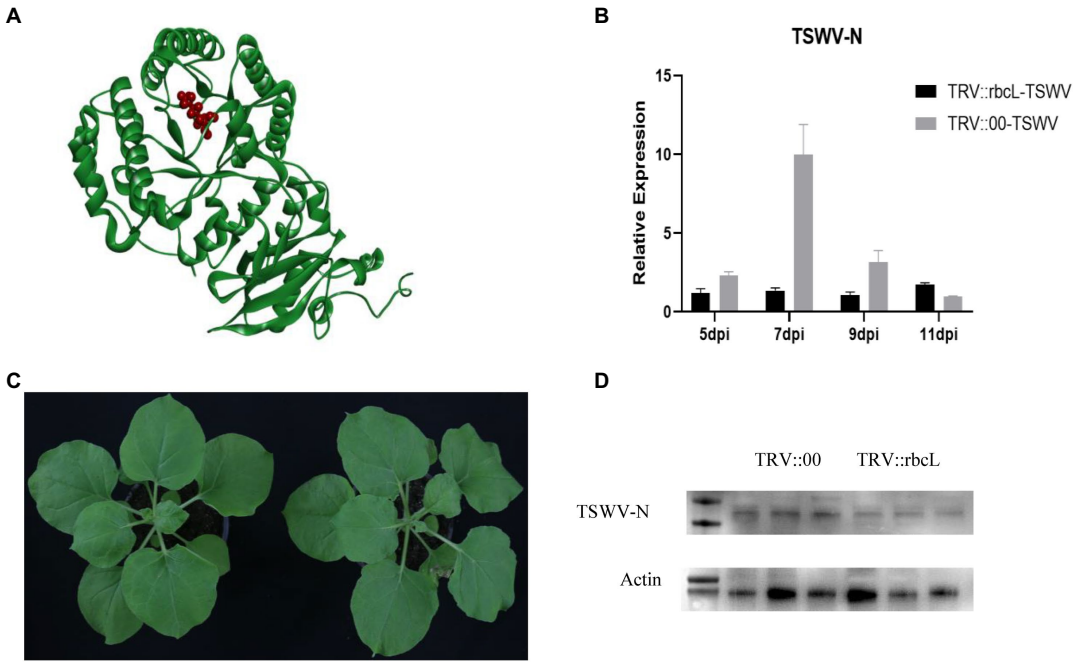

FIGURE 8
(A) Prediction of NbrbcL protein structure and acetylation site. Sites of acetylation are indicated in red. **(B)** Photographs were taken at 14days after TRV infiltration. *TRV::00* is the control. **(C)** TSWV was inoculated after silencing *NbrbcL* 14 dpi, The RNA level of viral N protein was higher compared to the control *TRV::00* inoculated TSWV at the RNA level. **(D)** Samples inoculated with TSWV for 7days were used to detect the differences in viral N expression using western blot analysis; 1–3 is TRV::00 inoculated with TSWV; 4–6 is TRV::NbrbcL inoculated with TSWV.

Data availability statement

The datasets presented in this study can be found in online repositories. The names of the repository/repositories and accession number(s) can be found in the article/Supplementary material.

Author contributions

JY and FW: conceptualization. DL: methodology. LJ: software. YG and YL: validation, formal analysis, writing-original draft preparation, and writing-review and editing. HL: investigation. YG: resources, data curation, and visualization. FW: supervision. JY: project administration and funding acquisition. All authors have read and agreed to the published version of the manuscript.

Funding

This research was funded by Shandong Provincial Natural Science Foundation Project, grant number ZR202103070049 and China National Tobacco Corporation Green Tobacco Prevention and Control Major Special Projects, grant number 110202001033(LS-02)110202101045(LS-05)110202101027(LS-02).

Conflict of interest

DL, LJ, and HL were employed by company Liangshan State Company of Sichuan Province Tobacco Company.

The remaining authors declare that the research was conducted in the absence of any commercial or financial relationships that could be construed as a potential conflict of interest.

Publisher's note

All claims expressed in this article are solely those of the authors and do not necessarily represent those of their affiliated organizations, or those of the publisher, the editors and the reviewers. Any product that may be evaluated in this article, or claim that may be made by its manufacturer, is not guaranteed or endorsed by the publisher.

Supplementary material

The Supplementary material for this article can be found online at: https://www.frontiersin.org/articles/10.3389/fmicb.2023.1046163/full#supplementary-material

References

Adams, M. J., Antoniw, J. F., and Kreuze, J. (2009). Virgaviridae: a new family of rod-shaped plant viruses. *Arch. Virol.* 154, 1967–1972. doi: 10.1007/s00705-009-0506-6

Adkins, S., Quadt, R., Choi, T. J., Ahlquist, P., and German, T. (1995). An RNA-dependent RNA polymerase activity associated with virions of tomato spotted wilt virus, a plant- and insect-infecting bunyavirus. *Virology* 207, 308–311. doi: 10.1006/viro.1995.1083

Ahlquist, P., Noueiry, A. O., Lee, W. M., Kushner, D. B., and Dye, B. T. (2003). Host factors in positive-strand RNA virus genome replication. *J. Virol.* 77, 8181–8186. doi: 10.1128/JVI.77.15.8181-8186.2003

Allfrey, V. G., Faulkner, R., and Mirsky, A. E. (1964). Acetylation and methylation of histones and their possible role in the regulation of RNA synthesis. *Proc. Natl. Acad. Sci. U. S. A.* 51, 786–794. doi: 10.1073/pnas.51.5.786

Bannister, A. J., and Kouzarides, T. (2011). Regulation of chromatin by histone modifications. *Cell Res.* 21, 381–395. doi: 10.1038/cr.2011.22

Berger, S. L. (2007). The complex language of chromatin regulation during transcription. *Nature* 447, 407–412. doi: 10.1038/nature05915

Chapman, E. J., Hilson, P., and German, T. L. (2003). Association of L protein and in vitro tomato spotted wilt virus RNA-dependent RNA polymerase activity. *Intervirology* 46, 177–181. doi: 10.1159/000071459

Chen, Y., Dessau, M., Rotenberg, D., Rasmussen, D. A., and Whitfield, A. E. (2019). Entry of bunyaviruses into plants and vectors. *Adv. Virus Res.* 104, 65–96. doi: 10.1016/bs.aivir.2019.07.001

De Haan, P., Kormelink, R., De Oliveira Resende, R., Van Poelwijk, F., Peters, D., and Goldbach, R. (1991). Tomato spotted wilt virus L RNA encodes a putative RNA polymerase. *J. Gen. Virol.* 72, 2207–2216. doi: 10.1099/0022-1317-72-9-2207

Diallo, I., Seve, M., Cunin, V., Minassian, F., Poisson, J. F., Michelland, S., et al. (2019). Current trends in protein acetylation analysis. *Expert Rev. Proteomics* 16, 139–159. doi: 10.1080/14789450.2019.1559061

Fang, X., Chen, W., Zhao, Y., Ruan, S., Zhang, H., Yan, C., et al. (2015). Global analysis of lysine acetylation in strawberry leaves. *Front. Plant Sci.* 6:739. doi: 10.3389/fpls.2015.00739

Feng, M., Cheng, R., Chen, M., Guo, R., Li, L., Feng, Z., et al. (2020). Rescue of tomato spotted wilt virus entirely from complementary DNA clones. *Proc. Natl. Acad. Sci. U. S. A.* 117, 1181–1190. doi: 10.1073/pnas.1910787117

Glozak, M. A., Sengupta, N., Zhang, X., and Seto, E. (2005). Acetylation and deacetylation of non-histone proteins. *Gene* 363, 15–23. doi: 10.1016/j.gene.2005.09.010

Guo, P., Chen, W., Li, H., Li, M., and Li, L. (2018). The histone acetylation modifications of breast cancer and their therapeutic implications. *Pathol. Oncol. Res.* 24, 807–813. doi: 10.1007/s12253-018-0433-5

Hammond, J. W., Cai, D., and Verhey, K. J. (2008). Tubulin modifications and their cellular functions. *Curr. Opin. Cell Biol.* 20, 71–76. doi: 10.1016/j.ceb.2007.11.010

Hartl, M., Fussl, M., Boersema, P. J., Jost, J. O., Kramer, K., Bakirbas, A., et al. (2017). Lysine acetylome profiling uncovers novel histone deacetylase substrate proteins in Arabidopsis. *Mol. Syst. Biol.* 13:949. doi: 10.15252/msb.20177819

Hirosawa, Y., Tada, A., Matsuura, T., Mori, I. C., Ogura, Y., Hayashi, T., et al. (2021). Salicylic acid acts antagonistically to plastid retrograde signaling by promoting the accumulation of photosynthesis-associated proteins in Arabidopsis. *Plant Cell Physiol.* 62, 1728–1744. doi: 10.1093/pcp/pcab128

Hu, H., Zhu, W., Qin, J., Chen, M., Gong, L., Li, L., et al. (2017). Acetylation of PGK1 promotes liver cancer cell proliferation and tumorigenesis. *Hepatology* 65, 515–528. doi: 10.1002/hep.28887

Imai, S., and Guarente, L. (2010). Ten years of NAD-dependent SIR2 family deacetylases: implications for metabolic diseases. *Trends Pharmacol. Sci.* 31, 212–220. doi: 10.1016/j.tips.2010.02.003

Johnson, M. P. (2016). Photosynthesis. *Essays Biochem.* 60, 255–273. doi: 10.1042/EBC20160016

Khoury, G. A., Baliban, R. C., and Floudas, C. A. (2011). Proteome-wide post-translational modification statistics: frequency analysis and curation of the swiss-prot database. *Sci. Rep.* 1:90. doi: 10.1038/srep00090

Kim, J. M., To, T. KIshida, J., Matsui, A., Kimura, H., and Seki, M. (2012). Transition of chromatin status during the process of recovery from drought stress in Arabidopsis thaliana. *Plant Cell Physiol.* 53, 847–856. doi: 10.1093/pcp/pcs053

Kirchhoff, H. (2019). Chloroplast ultrastructure in plants. *New Phytol.* 223, 565–574. doi: 10.1111/nph.15730

Klausen, M. S., Jespersen, M. C., Nielsen, H., Jensen, K. K., Jurtz, V. I., Sonderby, C. K., et al. (2019). NetSurfP-2.0: improved prediction of protein structural features by integrated deep learning. *Proteins* 87, 520–527. doi: 10.1002/prot.25674

Konig, A. C., Hartl, M., Boersema, P. J., Mann, M., and Finkemeier, I. (2014). The mitochondrial lysine acetylome of Arabidopsis. *Mitochondrion* 19 Pt B, 252–260. doi: 10.1016/j.mito.2014.03.004

Li, J., Feng, Z., Wu, J., Huang, Y., Lu, G., Zhu, M., et al. (2015). Structure and function analysis of nucleocapsid protein of tomato spotted wilt virus interacting with RNA using homology modeling. *J. Biol. Chem.* 290, 3950–3961. doi: 10.1074/jbc.M114.604678

Li, M., Luo, J., Brooks, C. L., and Gu, W. (2002). Acetylation of p53 inhibits its ubiquitination by Mdm2. *J. Biol. Chem.* 277, 50607–50611. doi: 10.1074/jbc.C200578200

Li, X., Ye, J., Ma, H., and Lu, P. (2018). Proteomic analysis of lysine acetylation provides strong evidence for involvement of acetylated proteins in plant meiosis and tapetum function. *Plant J.* 93, 142–154. doi: 10.1111/tpj.13766

Liu, M., Guo, L., Fu, Y., Huo, M., Qi, Q., and Zhao, G. (2021). Bacterial protein acetylation and its role in cellular physiology and metabolic regulation. *Biotechnol. Adv.* 53:107842. doi: 10.1016/j.biotechadv.2021.107842

Lu, Y., Xu, Q., Liu, Y., Yu, Y., Cheng, Z. Y., Zhao, Y., et al. (2018). Dynamics and functional interplay of histone lysine butyrylation, crotonylation, and acetylation in rice under starvation and submergence. *Genome Biol.* 19:144. doi: 10.1186/s13059-018-1533-y

Medina-Puche, L., Tan, H., Dogra, V., Wu, M., Rosas-Diaz, T., Wang, L., et al. (2020). A defense pathway linking plasma membrane and chloroplasts and co-opted by pathogens. *Cells* 182, 1109–1124 e25. doi: 10.1016/j.cell.2020.07.020

Ouidir, T., Cosette, P., Jouenne, T., and Hardouin, J. (2015). Proteomic profiling of lysine acetylation in Pseudomonas aeruginosa reveals the diversity of acetylated proteins. *Proteomics* 15, 2152–2157. doi: 10.1002/pmic.201500056

Pappu, H. R., Jones, R. A., and Jain, R. K. (2009). Global status of tospovirus epidemics in diverse cropping systems: successes achieved and challenges ahead. *Virus Res.* 141, 219–236. doi: 10.1016/j.virusres.2009.01.009

Phillips, D. M. (1963). The presence of acetyl groups of histones. *Biochem. J.* 87, 258–263. doi: 10.1042/bj0870258

Rotenberg, D., Jacobson, A. L., Schneweis, D. J., and Whitfield, A. E. (2015). Thrips transmission of tospoviruses. *Curr. Opin. Virol.* 15, 80–89. doi: 10.1016/j.coviro.2015.08.003

Scholthof, K. B., Adkins, S., Czosnek, H., Palukaitis, P., Jacquot, E., Hohn, T., et al. (2011). Top 10 plant viruses in molecular plant pathology. *Mol. Plant Pathol.* 12, 938–954. doi: 10.1111/j.1364-3703.2011.00752.x

Shvedunova, M., and Akhtar, A. (2022). Modulation of cellular processes by histone and non-histone protein acetylation. *Nat. Rev. Mol. Cell Biol.* 23, 329–349. doi: 10.1038/s41580-021-00441-y

Srinivasan, R., Abney, M. R., Culbreath, A. K., Kemerait, R. C., Tubbs, R. S., Monfort, W. S., et al. (2017). Three decades of managing tomato spotted wilt virus in peanut in southeastern United States. *Virus Res.* 241, 203–212. doi: 10.1016/j.virusres.2017.05.016

Tribus, M., Bauer, I., Galehr, J., Rieser, G., Trojer, P., Brosch, G., et al. (2010). A novel motif in fungal class 1 histone deacetylases is essential for growth and development of Aspergillus. *Mol. Biol. Cell* 21, 345–353. doi: 10.1091/mbc.e09-08-0750

Wang, Y., Liu, H., Liu, X., Zhang, X., Wu, J., Yuan, L., et al. (2020). Histone acetylation plays an important role in MC-LR-induced apoptosis and cycle disorder in SD rat testicular cells. *Chemosphere* 241:125073. doi: 10.1016/j.chemosphere.2019.125073

Wang, R., and Wang, G. (2019). Protein modification and autophagy activation. *Adv. Exp. Med. Biol.* 1206, 237–259. doi: 10.1007/978-981-15-0602-4_12

Wang, Q., Zhang, Y., Yang, C., Xiong, H., Lin, Y., Yao, J., et al. (2010). Acetylation of metabolic enzymes coordinates carbon source utilization and metabolic flux. *Science* 327, 1004–1007. doi: 10.1126/science.1179687

Xiong, Y., Peng, X., Cheng, Z., Liu, W., and Wang, G. L. (2016). A comprehensive catalog of the lysine-acetylation targets in rice (Oryza sativa) based on proteomic analyses. *J. Proteome* 138, 20–29. doi: 10.1016/j.jprot.2016.01.019

Xu, Q., Liu, Q., Chen, Z., Yue, Y., Liu, Y., Zhao, Y., et al. (2021). Histone deacetylases control lysine acetylation of ribosomal proteins in rice. *Nucleic Acids Res.* 49, 4613–4628. doi: 10.1093/nar/gkab244

Zhang, K., Tian, S., and Fan, E. (2013). Protein lysine acetylation analysis: current MS-based proteomic technologies. *Analyst* 138, 1628–1636. doi: 10.1039/c3an36837h

Zhao, Y., and Garcia, B. A. (2015). Comprehensive catalog of currently documented histone modifications. *Cold Spring Harb. Perspect. Biol.* 7:a025064. doi: 10.1101/cshperspect.a025064

Frontiers in Microbiology

Explores the habitable world and the potential of microbial life

The largest and most cited microbiology journal which advances our understanding of the role microbes play in addressing global challenges such as healthcare, food security, and climate change.

Discover the latest Research Topics

See more →

Frontiers

Avenue du Tribunal-Fédéral 34
1005 Lausanne, Switzerland
frontiersin.org

Contact us

+41 (0)21 510 17 00
frontiersin.org/about/contact